Titre: Title:	Second-Order Modeling for the Oxygen Uptake Kinetics in Humans
Auteur: Author:	Luis Antonio Pereira de Lima
Date:	2019
Type:	Mémoire ou thèse / Dissertation or Thesis
Référence: Citation:	Pereira de Lima, L. A. (2019). Second-Order Modeling for the Oxygen Uptake Kinetics in Humans [Thèse de doctorat, Polytechnique Montréal]. PolyPublie. https://publications.polymtl.ca/4103/

POLYTECHNIQUE MONTRÉAL

affiliée à l'Université de Montréal

Second-order modeling for the oxygen uptake kinetics in humans

LUIS ANTONIO PEREIRA DE LIMA

Institut de génie biomédical

Thèse présentée en vue de l'obtention du diplôme de *Philosophiæ Doctor*

Génie biomédical

Novembre 2019

POLYTECHNIQUE MONTRÉAL

affiliée à l'Université de Montréal

Cette thèse intitulée :

Second-order modeling for the oxygen uptake kinetics in humans

présentée par **Luis Antonio PEREIRA DE LIMA**

en vue de l'obtention du diplôme de *Philosophiæ Doctor*

a été dûment acceptée par le jury d'examen constitué de :

Aurelian VADEAN, président
Maxime RAISON, membre et directeur de recherche
Sofiane ACHICHE, membre et codirecteur de recherche
Ricardo DANTAS DE LUCAS, membre et codirecteur de recherche
Isabelle VILLEMURE, membre
Guy THIBAULT, membre externe

DEDICATION

To my parents Dora Cecilia and Laercio,

my sister Liliam, and my brother Leonardo.

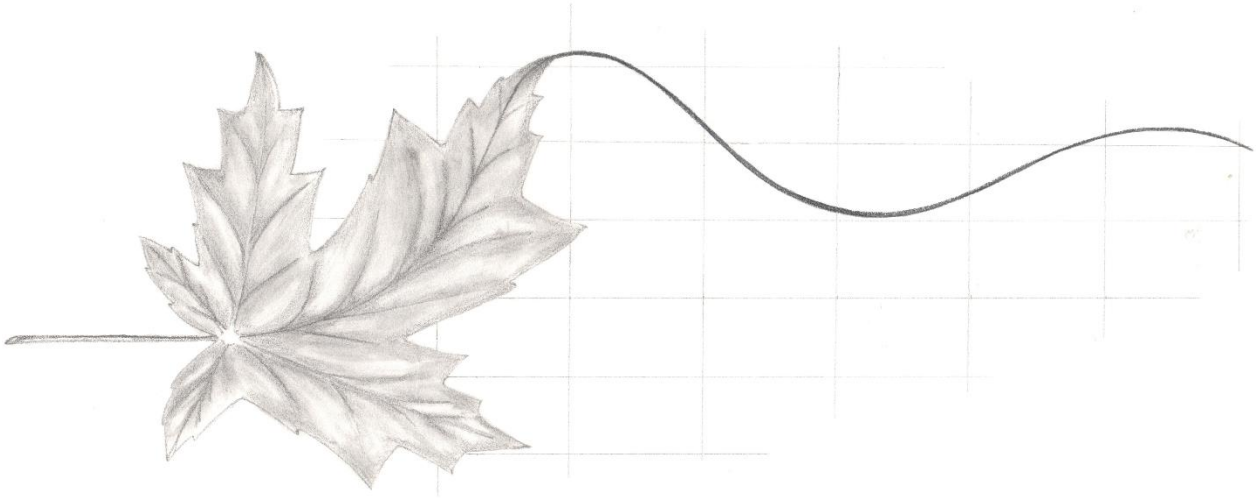

ACKNOWLEDGEMENTS

While looking back at the interactions, collaborations, and experiences accumulated during this Ph.D., I joyfully realized how long listing all the remarkable people involved would take. Although no attempt to actually name them all here will be done, there are some individuals to whom I must definitely express my deepest gratitude.

First of all, to my supervisor, Prof. Maxime Raison, for always trusting in my capacities, respecting my research management decisions and giving me the opportunity to teach twice in the GBM-6145A course. The same gratitude to my co-supervisor, Prof. Sofiane Achiche, for the experience with his Mitacs international students, for his objective guidance, and for advising me upon my arrival to a so far unknown Montreal, “not to take any big decisions during winter time.” Thanks to the valuable academic supervising and the sensibility of these two Professors, here I am, almost five winters later, finishing this Ph.D. On the Brazilian end, a sincere thank you to my co-supervisor and role model, Prof. Ricardo Dantas de Lucas, in whose physiology knowledge and attentive ears I could always rely. Thank you, Ricardo, for supporting and encouraging even the less conventional of my theories. Thank you as well to my constant friend and collaborator Augusto Mondardo Castillo, to the athletes donating massive amounts of ATP to this study, and to the colleagues from the LAEF and BioMEC laboratories, at the Federal University of Santa Catarina. Thank you Prof. Fernando Diefenthaeler for the early encouragement and support.

To my friends at the CoSIM, my appreciation for the knowledge and sense of humor always available in the room A530 (and A529). Thank you, Sana Raouafi, for the partnership during our long and caffeinated working sessions, and thank you, Mario Araya, for the existential talks during our coffee breaks. A sincere thank you to my dear friends Rafael Alencar de Paula and Prof. Samuel Bassetto, who helped me through some indoor and outdoor challenges of this Canadian experience.

In the financial aspect, a special acknowledgement to the CAPES Foundation. In that sense, I also express my gratitude to the regular Brazilian tax payer, ultimate provider of part of the resources on which I could rely for this international experience.

Finally, none of this would be built if not over the solid familiar basis founded by my parents and cultivated by my siblings. Liliam, thank you for *significantly* easing my journey. Cesar, thank you for supporting my sister’s brilliance. Leonardo, thank you for sharing your wisdom with us.

RÉSUMÉ

La consommation d'oxygène ($\dot{V}O_2$) est une mesure physiologique qui représente le taux avec lequel un individu extrait, transporte et utilise l'oxygène de l'environnement. L'étude de la cinétique du $\dot{V}O_2$ en réponse aux variations de l'intensité de travail physique (WR) peut fournir des informations précieuses sur la fonction métabolique d'un individu, dans la mesure où elle reflète la fonctionnalité et l'interaction de différents systèmes de l'organisme, tels que les systèmes cardiovasculaire, respiratoire et neuromusculaire. Outre son utilité dans la compréhension de la physiologie du corps humain, l'analyse de la cinétique du $\dot{V}O_2$ représente un levier important dans l'évaluation de la condition physique et la détection des pathologies. La pertinence des résultats de cette analyse dépend fortement du modèle adopté. Datant du début des années 1970, le modèle Multi-Exponentiel du Premier Ordre (FOME) reste l'état de l'art pour la modélisation de la réponse du $\dot{V}O_2$ à l'entrée échelon positive de la WR.

Bien que les deux ou trois exponentielles du premier ordre du modèle FOME décrivent bien les trois *phases* typiques de la réponse du $\dot{V}O_2$ à l'entrée échelon, elles restent incapables de modéliser l'oscillation connue comme le dépassement (ou l'*overshoot*) dans la cinétique du $\dot{V}O_2$ ($O\dot{V}O_2K$) au cours de la *phase II* dans certains cas. Ce patron de dépassement, très commun aux courbes du second ordre, peut être utilisé par le modèle FOME seulement en ajoutant un terme additionnel de dépassement à sa composante fondamentale. Néanmoins, cette approche est dépourvue de l'aspect physiologique et augmente le nombre de paramètres de courbe du modèle. De plus, la modélisation du premier ordre du $O\dot{V}O_2K$ pourrait mener à des évaluations erronées pour des indicateurs physiologiques importants comme le déficit en O_2, la constante de temps et l'amplitude de la composante fondamentale.

Un autre phénomène, « la composante lente du $\dot{V}O_2$ », appelée dans ce travail de recherche l'augmentation lente de la cinétique du $\dot{V}O_2$ ($\dot{V}O_2SA$), nécessite aussi l'ajout d'un terme additionnel au modèle FOME pendant la *phase III* de la réponse du $\dot{V}O_2$. Dans ce cas, le terme ajouté présume la théorie d'un délai de recrutement additionnel des fibres musculaires de type II. Grace à ce délai, le recrutement survient seulement au « début » du $\dot{V}O_2SA$, même avec une WR constant. De plus, l'ajout de la composante lente du premier ordre est limité aux transitions des

intensités supra-modérées, où la $\dot{V}O_2SA$ est présente. Pour cela, le concept d'un modèle unique de cinétique du $\dot{V}O_2$ pour l'ensemble du spectre de WR n'est pas pris en charge par le modèle FOME.

Avec l'objectif de développer et implémenter un modèle de la cinétique du $\dot{V}O_2$ pour les humains qui serait capable de représenter les réponses à l'entrée échelon positive de l'exercice pour n'importe quelle WR et indépendamment de la présence du $O\dot{V}O_2K$ ou de la $\dot{V}O_2SA$, deux modèles basés sur les courbes du second ordre sont proposés. Outre les résultats de la littérature scientifique, les données collectées pour cette étude à partir de tests de cyclergométrie avec 14 cyclistes et triathlètes bien entraînés sont utilisées pour l'appui mathématique et conceptuel des modèles proposés.

Dans le premier modèle, le *Mixed* Multi-Exponentiel (MiME), la composante fondamentale du modèle FOME, responsable de la forme de la *phase II* de la réponse du $\dot{V}O_2$ à l'échelon, est remplacée par une courbe du second ordre. Ainsi, au lieu de « corriger » la courbe du premier ordre dans le cas d'un $O\dot{V}O_2K$, le modèle MiME présente sa réponse de dépassement comme une possibilité parmi d'autres — les courbes de non-dépassement habituelles comprises — représentées à partir d'une simple adaptation des paramètres de courbe du second ordre.

Pour le deuxième modèle proposé, le terme additionnel avec un délai — utilisé pour représenter la $\dot{V}O_2SA$ dans les modèles FOME et MiME — sera supprimé. Ce modèle, construit à partir de deux composantes simultanées du second ordre (SOSC), va représenter la réponse du $\dot{V}O_2$ indépendamment de la présence du $O\dot{V}O_2K$ ou de la $\dot{V}O_2SA$. Contrairement au modèle MiME, ces différentes formes de courbe peuvent être réalisables dans la dynamique SOSC tout simplement au moyen de la modification des paramètres internes du modèle. Ainsi, l'ajout d'un terme complémentaire n'est pas nécessaire et la structure du modèle reste qualitativement inchangée pour toutes les transitions échelon de WR. La dépendance continue entre les amplitudes des composantes du modèle SOSC et la WR permet non seulement d'éliminer le problème de discontinuité présenté par le FOME et le MiME dans la transition des intensités modérées à supra-modérées, mais aussi de réinterpréter d'importants concepts physiologiques, tels que le seuil d'accumulation de lactate, la puissance critique et l'état stable maximal de lactatémie. De plus, la dynamique du SOSC permet des notions alternatives concernant les patrons du recrutement des fibres musculaires supplémentaires pendant l'exercice. Ce recrutement supplémentaire des fibres, bien que non nécessairement refusé, n'est plus obligatoire dans le modèle SOSC.

Enfin, les résultats issus de la comparaison entre la racine des erreurs quadratiques moyennes des courbes du modèle démontrent une performance d'ajustement globale nettement meilleure du SOSC par rapport au MiME et de ces deux derniers modèles par rapport au modèle FOME. Ainsi, compte tenu des résultats des analyses statistiques et conceptuelles issus de ce travail de recherche, le modèle MiME et, surtout, le modèle SOSC représentent des alternatives cohérentes et complètes pour l'amélioration de la modélisation de la cinétique du $\dot{V}O_2$ chez les humains.

ABSTRACT

The oxygen uptake ($\dot{V}O_2$) is a physiological measure that represents the rate at which an individual extracts, transports, and uses oxygen from the environment. The study of the $\dot{V}O_2$ kinetics in response to variations in exercise work rate (WR) may provide valuable information on an individual's metabolic function, as it reflects the functionality and interaction of different body systems, such as the cardiovascular, respiratory, and neuromuscular ones. Thus, in addition to enhancing the understanding of human physiology itself, the $\dot{V}O_2$ kinetics analysis represents an important tool for fitness level assessment and detection of disease conditions. Moreover, the utility and pertinence of this analysis' results are highly dependent on the appropriateness of its adopted modeling. Dating from the early 1970s, the First-Order Multi-Exponential (FOME) model remains the state-of-the-art choice for modeling the $\dot{V}O_2$ response to the WR step on-transient.

However, while the FOME's two or three first-order exponentials sufficiently describe the three *phases* of a typical $\dot{V}O_2$ step response, they fail to model the oscillation known as the overshoot in the $\dot{V}O_2$ kinetics ($O\dot{V}O_2K$) observed during *phase II* in some cases. Such an overshoot pattern, very common to second-order curves, may only be represented by the FOME model by means of the application of an overshoot add-on term to its fundamental component, an approach that lacks physiological support and increases the amount of curve parameters. Moreover, the first-order representation of $O\dot{V}O_2K$ cases may yield spurious evaluations of important physiological indicators such as the O_2 deficit and the fundamental component's time constant and amplitude.

Another phenomenon, widely know as the $\dot{V}O_2$ "slow component," and referred to in this work as the slow augmentation in the $\dot{V}O_2$ kinetics ($\dot{V}O_2SA$), also requires the incorporation of an add-on term by the FOME model, this time to *phase III* of the $\dot{V}O_2$ step response. In this case, this add-on term necessarily assumes the theory of a delayed additional recruitment of type II muscle fibers occurring only at the "onset" of the $\dot{V}O_2SA$, despite the constant WR condition. Additionally, because the incorporation of this first-order slow component add-on term is restricted to transitions to supra-moderate intensities, where the $\dot{V}O_2SA$ is considered to manifest, the concept of a single $\dot{V}O_2$ kinetics model for the whole WR spectrum is not supported by the FOME model.

With the objective of developing and implementing a comprehensive model for the $\dot{V}O_2$ kinetics in humans capable of comprising exercise step on-transient responses to any WR, regardless of the

manifestation of none, either, or both of the O$\dot{V}O_2$K and/or $\dot{V}O_2$SA phenomena, two models using second-order exponential curves are proposed in this work. In addition to results from the literature, original data collected for this study by means of cycle ergometry testing of 14 well trained cyclists and triathletes is used for the mathematical and conceptual support of these proposed models.

In the first of them, the Mixed Multi-Exponential (MiME) model, the FOME model's fundamental component is replaced by a second-order curve. Thus, instead of "fixing" the first-order curve in the O$\dot{V}O_2$K cases, the MiME presents its overshooting curve as one of the multiple shape possibilities—including the usual nonovershooting curves—achievable by a mere adaptation of the values of the two second-order solution's shape parameters. Additionally, because the O$\dot{V}O_2$K is incorporated in the second-order representation of the fundamental component, the objective detection and quantification of this phenomenon are facilitated. However, in the supra-moderate cases, the MiME will still represent the $\dot{V}O_2$SA with a first-order slow component add-on term.

In the second model proposed, the concept of a delayed add-on term to represent the $\dot{V}O_2$SA is also abandoned, and a model composed of two Second-Order Simultaneous Components (SOSC) is applied to represent $\dot{V}O_2$ step responses containing none, either, or both of the O$\dot{V}O_2$K and/or $\dot{V}O_2$SA phenomena. However, unlike in the MiME model, these shape possibilities are achievable in the SOSC dynamics exclusively by means of the numerical adaptation of the model's internal parameters, so that the conditional incorporation of add-on terms is not required and the model's structure remains qualitatively constant for step on-transients to any WR. The continuous dependence between the amplitudes of SOSC components and the WR eliminates the issue of the FOME and MiME's continuity disruption in the transition from moderate to supra-moderate intensities, allowing important physiological concepts such as the lactate threshold, the critical power, and the maximal lactate steady-state to be revisited. Moreover, alternative insights into the patterns of muscle fiber recruitment during exercise are also provided by the SOSC dynamics, and the theory of additional fiber recruitment, although not necessarily denied, is no longer mandatory.

Finally, results from the comparison between the root mean squared errors of the models' curves, demonstrate a significantly better overall fitting performance of the SOSC over the MiME, and of these two over the FOME model. Thus, considering both statistical and conceptual analyses performed in this thesis, the MiME model and, above all, the SOSC model are coherent, comprehensive alternatives for the improvement of the $\dot{V}O_2$ kinetics modeling in humans.

TABLE OF CONTENTS

LIST OF TABLES

LIST OF FIGURES

LIST OF ABBREVIATIONS

CC	$\dot{V}O_2$ response's cardiodynamic component
CI	SOSC's simultaneous component I
CI_{NOvsht}	Overdamped type CI
CI_{Ovsht}	Underdamped type CI
CII	SOSC's simultaneous component II
CII_{NOvsht}	Overdamped type CII
CP	Critical power [W]
CR	$\dot{V}O_2$ combined response of a model, equal to the sum of its components
EPOC	Excess post-exercise oxygen consumption
FC	$\dot{V}O_2$ response's fundamental component
FC_{adj}	"Adjusted FC"
$FC_{NOvshtCrit}$	SOS nature, *critically damped* type FC
FC_{FOS}	FOS nature FC
FC_{NOvsht}	SOS nature, overdamped type FC
FC_{Ovsht}	SOS nature, underdamped type FC
FC_Alt	Alternative FOS representation of the FC
FOME	First-Order Multi-Exponential (model)
FOS	First-order system
GET	Gas exchange threshold
IV	Integral volume of overshoot (obtained directly from $\dot{V}O_2$ data points)
LT	Lactate threshold
MiME	Mixed Multi-Exponential (model)
MRT	Mean response time [s]

MRT_{App}	Approximate MRT [s]
$NO\dot{V}O_2K$	Reference to the absence of $O\dot{V}O_2K$
O_2 deficit	Oxygen deficit in the $\dot{V}O_2$ kinetics
$O\dot{V}O_2K$	Overshoot in $\dot{V}O_2$ kinetics
$O\dot{V}O_2K_{SC}$	Overshoot in $\dot{V}O_2$ kinetics in the context of the SC
RMSE	Root mean squared error
SC	$\dot{V}O_2$ response's slow component
SC_{adj}	"Adjusted SC"
SOS	Second-order system
SOSC	Second-Order Simultaneous Components (model)
$\dot{V}O_2SA$	Slow augmentation in the $\dot{V}O_2$ step response
WR	Work rate

LIST OF SYMBOLS[1]

a	Exponential coefficient for the exponential evaluation of A_{CII}% [W^{-1}]
A_{CC}	Amplitude of the cardiodynamic component of the $\dot{V}O_2$ step response [$ml \cdot min^{-1}$]
A_{CC}'	Value of the CC at the instant $t = td_{FC\_Alt}$ [$ml \cdot min^{-1}$]
A_{CI}	Amplitude of the CI [$ml \cdot min^{-1}$]
A_{CI}%	Percentage contribution of the CI to the A_{CR} [%]
A_{CII}	Amplitude of the CII [$ml \cdot min^{-1}$]
A_{CII}%	Percentage contribution of the CII to the A_{CR} [%]
A_{CR}	Amplitude of the CR [$ml \cdot min^{-1}$]
A_{Decay}	Amplitude of the decay element [$ml \cdot min^{-1}$]
A_{FC}	Amplitude of the fundamental component of the $\dot{V}O_2$ step response [$ml \cdot min^{-1}$]
A_{FC_Alt}	Amplitude of the FC_Alt [$ml \cdot min^{-1}$]
A_{FC_Alt}'	"Physiologically relevant increase in $\dot{V}O_2$," equal to A_{FC} [$ml \cdot min^{-1}$]
A_{SC}	Amplitude of the slow component of the $\dot{V}O_2$ step response [$ml \cdot min^{-1}$]
A_{ref}	A_{FC} value evaluated with FC_{FOS} solution. Adopted as A_{FC} value for SOS solutions and as reference for Mp_{ref} evaluation [$ml \cdot min^{-1}$]
$A\dot{V}O_{2max}$	Amplitude of $\dot{V}O_{2max}$, equal to $\dot{V}O_{2max} - \dot{V}O_{2Baseline}$ [$ml \cdot min^{-1}$]
b	Linear coefficient for the exponential evaluation of A_{CII}% [%]
B_{III}	Linear coefficient for the "switch-on" element [$ml \cdot min^{-1} \cdot s^{-1}$]
c	Linear coefficient for the power law evaluation of A_{CII}% [$\% \cdot W^{-d}$]

[1] All units containing "[$ml \cdot min^{-1}$]" refer to the *absolute* representation of the corresponding symbol, with its *relative* version being obtained with the division by the individual's body mass (e.g., [$ml \cdot min^{-1} \cdot kg^{-1}$]).

c_{III}	Exponential coefficient for the "switch-on" element [s^{-1}]
Cp	Actual position of the mechanical system of our physiomechanical analogy [m]
Cr	Reference value for the mechanical system of our physiomechanical analogy [m]
C_{CII}	Linear coefficient for the power law evaluation of A_{CII} [$ml \cdot min^{-1} \cdot W^{-D_{CII}}$]
C_{CR}	Linear coefficient for the power law evaluation of A_{CR} [$ml \cdot min^{-1} \cdot W^{-D_{CR}}$]
d	Exponential coefficient for the power law evaluation of A_{CII}% [dimensionless]
D	Damping coefficient of a given damper [$N \cdot s \cdot m^{-1}$]
D_{CII}	Exponential coefficient for the power law evaluation of A_{CII} [dimensionless]
D_{CR}	Exponential coefficient for the power law evaluation of A_{CR} [dimensionless]
G_{CI}	Gain of the CI [$ml \cdot min^{-1} \cdot W^{-1}$]
G_{CII}	Gain of the CII [$ml \cdot min^{-1} \cdot W^{-1}$]
G_{CR}	Gain of the CR [$ml \cdot min^{-1} \cdot W^{-1}$]
G_{FC}	Gain of the FC [$ml \cdot min^{-1} \cdot W^{-1}$]
G_{SC}	Gain of the SC [$ml \cdot min^{-1} \cdot W^{-1}$]
HR	Heart rate [beats per minute, bpm]
K	Coefficient of elasticity of a given spring [$N \cdot m^{-1}$]
$K_{\_Alt}$	Ratio A_{FC_Alt}:A_{FC}, also equal to A_{FC_Alt}:A_{FC_Alt}' [dimensionless]
M	Mass of a given inertial component [kg]
Mp	Absolute $O\dot{V}O_2K$ amplitude [$ml \cdot min^{-1}$]
Mp_{ref}	Reference Mp, normalized by A_{ref} [dimensionless]
$O\dot{V}O_2K_{peak}$	$O\dot{V}O_2K$ peak value of the FC_{Ovsht} curve [$ml \cdot min^{-1}$]
$O\dot{V}O_2K_{SCpeak}$	$O\dot{V}O_2K$ peak value of the SC_{Ovsht} curve [$ml \cdot min^{-1}$]
$[O_2a]$	O_2 content of arterial blood [$ml \cdot l^{-1}$]
$[O_2v]$	O_2 content of venous blood [$ml \cdot l^{-1}$]

$\dot{Q}$	Cardiac output [$l \cdot min^{-1}$]
p_{final}	Final position of both Cr and Cp [m]
$p_{initial}$	Initial position of both Cr and Cp [m]
$PmvO_2$	Muscle microvascular O_2 pressure [Torr]
p_{peak}	Peak value of Cp [m]
$p_{0, 1, \ldots, n-1, n}$	Coefficients for the polynomial representation of $\dot{V}O_2(t)$ [$ml \cdot min^{-1} \cdot s^{-n}$]
Peak-SS	Difference between peak value and steady-state in a $\dot{V}O_2$ step transients [$ml \cdot min^{-1}$]
SV	Cardiac stroke volume [ml]
$t_{CI\_SS2\%}$	Instant when the CI curve assumes a steady-state (variation < 2% of A_{CI}) [s]
td	Hypothetical common onset time delay for the FOS-based FC and SC [s]
td_{Decay}	Onset time delay of the decay element [s]
td_{FC}	Onset time delay of the FC [s]
td_{FC_Alt}	Onset time delay of the FC_Alt [s]
td_S	Onset time delay of both CI and CII [s]
td_{SC}	Onset time delay of the slow component [s]
td_{III}	Onset time delay of the "switch-on" element [s]
t_{FC}	Time upper limit of data in FC fitting [s]
td_{ref}	td_{FC} value assessed with FC_{FOS} solution, reference for tp_{ref} evaluation [s]
tp	$O\dot{V}O_2K_{peak}$ time. Instant of $O\dot{V}O_2K_{peak}$ occurrence in the FC_{Ovsht} curve [s]
tp_{ref}	Reference *tp*, represented in terms of τ_{ref} and td_{ref} evaluated for the same data set [dimensionless]
$tp_{ref}T$	Threshold tp_{ref} value used for detection of $O\dot{V}O_2K$ containing $\dot{V}O_2$ step responses [dimensionless]
t_0	Instant of application of the step stimulus [s]

T	Time period of a square wave [s]
$T_{impulse}$	Time period of an impulse stimulus [s]
$T_{plateau}$	Time period of the plateau in a ramp wave stimulus [s]
T_{sinus}	Time period of oscillations of a sinusoidal stimulus [s]
V_{comp}	Complementary volume of O_2 (below steady-state, between FC_{Ovsht} and FC_{FOS}) [ml]
$V_{O\dot{V}O2K}$	Volume of $O\dot{V}O_2K$ below FC_{Ovsht} curve [ml]
$\dot{V}O_2$	Oxygen uptake [ml·min^{-1}]
$\dot{V}O_{2Baseline}$	$\dot{V}O_2$ average value for 60 s preceding t_0 [ml·min^{-1}]
$\dot{V}O_{2max}$	Maximal 30 s $\dot{V}O_2$ average in the incremental test [ml·min^{-1}]
WR_{LT}	WR associated with the lactate threshold [W]
WR_{MLSS}	WR associated with the maximal lactate steady-state [W]
WR_{max}	Time interpolated proportion of WR at the final step of the incremental test [W]
$WR_{\dot{V}O2max}$	WR associated with the maximal 30 s $\dot{V}O_2$ average in the incremental test [W]
[HHb]	Deoxygenated hemoglobin concentration [arb. unit]
[Lac]	Blood lactate concentration [mmol·l^{-1}]
δ	Instant when the FC starts to impose the shape of the CR [s]
ρ	Half of a $2\cdot\rho$ tolerance range around the preliminarily determined t_{FC}, adopted for the evaluation of the final t_{FC} in the context of the FOME and MiME models [s]
τ	Time constant of a FOS, referent to the time to reach 63.2% of the amplitude of its response to the step stimulus [s]
τ_{App}	Approximate time constant for FC_{NOvsht}, evaluated from its FOS approximation [s]
τ_{App_SC}	Approximate time constant for SC_{NOvsht}, evaluated from its FOS approximation [s]
τ_{Decay}	Time constant of the decay element [s]
τ_{FC_Alt}	Time constant of the FC_Alt, usually equal to τ_{FC} [s]

τ_{ref}	τ_{FC} value evaluated with FC_{FOS} solution. Adopted as reference for tp_{ref} evaluation [s]
τ_{CC}	Time constant of the FOS representation of the CC [s]
τ_{FC}	Time constant of the FOS representation of the FC [s]
τ_{SC}	Time constant of the FOS representation of the SC [s]
ω	Natural frequency of a SOS [$rad \cdot s^{-1}$]
ω_d	Damped frequency of an underdamped SOS [$rad \cdot s^{-1}$]
ω_{d_CI}	Damped frequency of the CI [$rad \cdot s^{-1}$]
ω_S	Natural frequency of both CI and CII [$rad \cdot s^{-1}$]
ζ	Damping ratio of a SOS [dimensionless]
ζ_{CI}	Damping ratio of the CI [dimensionless]
ζ_{CII}	Damping ratio of the CII [dimensionless]
40%Δ	WR equal to WR_{LT} added of 40% of the difference between WR_{LT} and $WR_{\dot{V}O2max}$ [W]
50%Δ	WR equal to WR_{LT} added of 50% of the difference between WR_{LT} and $WR_{\dot{V}O2max}$ [W]
55%LT	WR equal to 55% of WR_{LT} [W]
70%Δ	WR equal to WR_{LT} added of 70% of the difference between WR_{LT} and $WR_{\dot{V}O2max}$ [W]
70%LT	WR equal to 70% of WR_{LT} [W]
85%LT	WR equal to 85% of WR_{LT} [W]

LIST OF APPENDICES

CHAPTER 1 INTRODUCTION

1.1 Scope and overall view

The oxidative mechanism is the main source of energy on which humans depend to maintain life and work capacity [1]. The rate at which an individual extracts, transports, and uses oxygen (O_2) from the environment is defined as the oxygen uptake ($\dot{V}O_2$) [2], and is expressed in terms of volume of O_2 per time interval, either in absolute ([$ml \cdot min^{-1}$]) or relative ([$ml \cdot min^{-1} \cdot kg^{-1}$]) units, so that individuals with different body masses—and even animals from different species [3]—may have their aerobic systems compared.

The study of the *$\dot{V}O_2$ kinetics* is dedicated to the understanding of the physiological mechanisms responsible for the dynamic response of $\dot{V}O_2$ during and after physical exertion, and has been widely applied to human's exercise experiments by using ergospirometric techniques [1, 4-6]. The analysis of an individual's $\dot{V}O_2$ kinetics in response to variations in exercise intensity (or work rate, WR) may provide valuable information on his or her metabolic function, and is applicable to either healthy or unhealthy populations [5].

The importance of $\dot{V}O_2$ kinetics is mainly corroborated by its utility in both the physical activity field (fitness level assessment and training prescription) [2, 6-13] and in health related applications (disease conditions detection) [1, 4, 5, 14-32]. Additionally, pure science branches of physiology are also interested in understanding $\dot{V}O_2$ kinetics, as it reflects the very nature of interacting body systems, such as the cardiovascular, respiratory, and neuromuscular ones.

Although the fast response of the $\dot{V}O_2$ to the exercise onset has been recognized since the beginning of the twentieth century [1, 33], with its exponential nature [1, 34] remaining practically undisputed since that time, some specific phenomena continue to intrigue researchers of the field and defy the currently accepted model of $\dot{V}O_2$ kinetics. One of them, the phenomenon of the "slow component"—intentionally redefined as slow augmentation in the $\dot{V}O_2$ kinetics ($\dot{V}O_2SA$) in the present work (see Sections 2.6.2 and 7.1)—was first evidenced in the literature in the early 1960s [35, 36], and has remained in discussion since [37-45]. Another phenomenon, the overshoot in the $\dot{V}O_2$ kinetics ($O\dot{V}O_2K$), is more recent and faces intense debate regarding its nature and likely causes [12, 46-51].

Both phenomena represent basic features of the $\dot{V}O_2$ kinetics that are not completely explained by the first-order-system-based model currently accepted in the literature. Although there is wide agreement in relating the $\dot{V}O_2$SA with the recruitment of type II fibers in the active musculature [39], some issues regarding its triggering factors and delayed nature remain unresolved [38, 52-54]. In regards to the O$\dot{V}O_2$K, its modeling knowledge is still in an incipient state, as the very existence of this phenomenon as part of the $\dot{V}O_2$ system (and not an experimental collateral effect) remains a matter of debate [12, 46-49]. Moreover, as discussed in Chapters 2 and 4, the acceptance of the O$\dot{V}O_2$K as an intrinsic manifestation of the human respiratory apparatus (i.e., as part of the natural respiratory response to the exercise onset) implies, by definition [55, 56], a denial of the first-order system (FOS) basis assumed by the currently accepted $\dot{V}O_2$ kinetics modeling.

The general objective of this work is to develop and implement a comprehensive model for the $\dot{V}O_2$ kinetics in humans capable of comprising none, either, or both of the O$\dot{V}O_2$K and/or $\dot{V}O_2$SA phenomena observed in response to the step on-transient at any exercise intensity.

With this aim, the conceptual issues imposed by the use of a FOS-based representation of the $\dot{V}O_2$ kinetics are discussed prior to the presentation of possible solutions. Once these issues are exposed, two main models are proposed, tested, and compared to the current FOS-based model, one of them being of a mixed nature (comprising first- and second-order-based components), and the other one exclusively composed of second-order system (SOS) components.

1.2 The biomedical engineering approach to the $\dot{V}O_2$ kinetics modeling

Because certain aspects of the $\dot{V}O_2$ kinetics modeling concomitantly require the knowledge and tools from the physiology field (e.g., the application and interpretation of exercise testing, bioenergetics, biomechanics) and the application of engineering techniques (e.g., dynamic modeling, system identification techniques, nonlinear curve regression methods, coding), the adoption of a biomedical engineering approach becomes highly pertinent, especially due to its characteristic multi- and interdisciplinarity.

Specifically in the physiology field, this thesis's study brings new insights into the $\dot{V}O_2$ kinetics modeling that are not only innovative in terms of its fitting equations, but also presenting curve and parameters interpretations that may influence the very concepts behind the fitted data. In the

engineering aspect, besides the application of the second-order family of curves to the $\dot{V}O_2$ data, the non-traditional component separation techniques applied into the $\dot{V}O_2$ signal presented in this study are noteworthy in terms of innovation.

1.3 Structure of this thesis

Due to the particular format of the present thesis, according to which articles are incorporated to the body of the work as independent Chapters (Chapters 5 and 7), the distribution of content was optimized over the document sections in order to avoid repetition as much as possible.

An introductory chapter is dedicated to the presentation of the basic terminology regarding the $\dot{V}O_2$ kinetics, its main modeling issues, and a brief contextualization of the scope of the present thesis.

In Chapter 2, a literature review is conducted on both historical and state-of-the-art aspects of the $\dot{V}O_2$ kinetics field. Different types of exercise stimuli used in the field are presented, with a special focus on the step stimulus and its currently adopted modeling. The reader is then introduced to some characteristic phenomena observed in the $\dot{V}O_2$ response to the exercise step on-transient that defy its explanatory first-order system theory and point towards the second-order nature of the human cardiorespiratory system.

Once the limitations of the first-order system model are presented, Chapter 3 briefly defines the two modeling alternatives based on second-order systems that are explored in this work. With these models defined, this thesis's objectives and hypotheses are properly enunciated.

The methodologies adopted for the collection, pretreatment, and treatment of data are explained in Chapter 4. Details regarding the study's sample, equipment, experimental procedures, and data processing that are not covered in the subsequent chapters can be found in this part of the document.

A first model using the second-order system representation of the fundamental component of the $\dot{V}O_2$ step on-transient is presented in Chapter 5. This section is the reproduction of the article published in the *Journal of Applied Physiology* under the title *Second-order modeling for the pulmonary oxygen uptake on-kinetics: a comprehensive solution for overshooting and nonovershooting responses to exercise*, in June of 2018 [57].

Chapter 6 complements this published work, performing an investigation analogous to that of Chapter 5, this time in regards to the slow component of the $\dot{V}O_2$ on-transient. The pertinence and

the modeling advantages of a second-order representation for the slow component are also discussed in this chapter.

Chapter 7 presents the second article covering the scope of the study, entitled *Simultaneous second-order components modeling for the pulmonary oxygen uptake on-kinetics: a solution for both the overshoot and the slow augmentation phenomena*. In this paper, an enhanced second-order system-based model is presented, this time comprising two simultaneous components—in opposition to the model presented in Chapter 6, whose components start at different time instants.

In Chapter 8, the individual comparisons between the currently accepted $\dot{V}O_2$ kinetics model and each of the models proposed in Chapters 5 and 7 are resumed in the context of one single integrated analysis. Some patterns of each model's dynamics are combined under a comprehensive perspective, and some practical aspects of these models' applications are discussed.

The main aspects of the discussions developed in Chapters 5 to 8 are resumed and combined with additional insights in the general discussion presented in Chapter 9.

Chapter 10 readdresses this whole thesis work with a focus on the coverage of its objectives and hypotheses, bringing conclusive commentary on the contributions and limitations of the study, as well as potential perspectives for future work. General recommendations for the application of the proposed models and some final comments conclude both this chapter and this thesis.

CHAPTER 2 LITERATURE REVIEW

2.1 Development of the $\dot{V}O_2$ knowledge: respiration and circulation

Although the notion that the respiratory activity is vital to our survival seems intuitive, both the reasoning supporting its finality and its relationship with blood circulation have transformed over time. Believed by the ancient philosopher Empedocles (5th century BC) to be merely a means of cooling down our heart and blood, respiration only began to be associated with the transfer of crucial elements in the lungs after the proposition of the "pneumatic theory" by the physician Galen (c.130-199 AD) [1, 58]. Galen stated that a "vital spirit" was produced in the heart from the mixture between "pneuma" from the lungs and "natural spirit" from the liver (Figure 1) [1, 58, 59], and that a fuliginous waste was released back to the air through the lungs. These Greek influencers also acknowledged the important role of the circulatory system, which was believed to transport the "innate heat" (Empedocles) [1] or "vital spirit" (Galen) [1, 58] from the heart to the rest of the body.

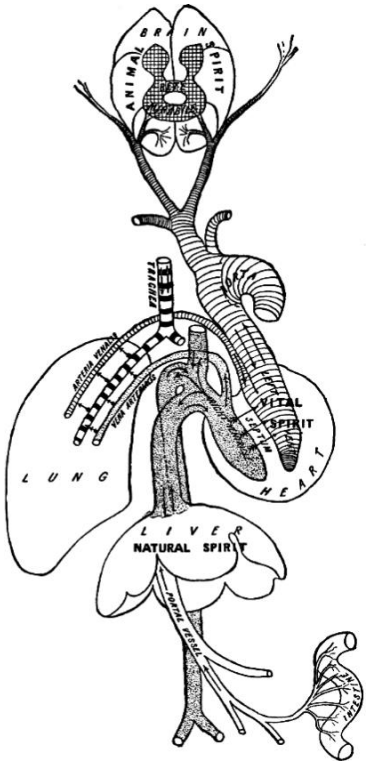

Figure 2.1 Schematic representation of the "vital spirit" formation in the heart, as idealized by the ancient physician and anatomist Galen. Reproduced with permission from [59].

Despite being the most influential anatomist of the ancient world [60], Galen did not unveil the true dynamics of cardiopulmonary circulation, believing that the blood circulation included a passage through pores on the interventricular septum [1, 58].

The real blood flow through the lungs was only identified some thousand years later, initially in the Islamic world, due to the brilliant work of the Arabian anatomist Ibn Al-Nafis (1213-1288) [1, 58-60]. However, the western world had to wait approximately three more centuries until Michael Servetus (1511-1553) and other Renascentists reproduced the findings of the Arabian physician [1, 58, 59], with a complete description of the cardiopulmonary function being published in 1628 (*Exercitatio Anatomica de Motu Cordis et Sanguinis in Animalibus*) by the English physician William Harvey (1578-1657) [1, 60]. Also in the anatomy field, the microscopist Marcello Malpighi (1628-1694) gave his contribution to the understanding of the $\dot{V}O_2$ mechanism by describing the capillaries and the alveoli structures.

The Galenian notion of a vital element obtained via respiration was reinforced in the seventeenth century with the aid of experimental methods using animals. However, only after the discoveries of oxygen (O_2) and carbon dioxide (CO_2) in the second half of the eighteenth century, was the chemist Antoine Laurent Lavoisier (1743-1794) able to experimentally conclude that respiratory combustion used the former and released the latter [1].

However, Lavoisier's erroneous notion that O_2 utilization and CO_2 production took place in the lungs would be changed due to the advances of experimental techniques occurring in the subsequent century. The blood-gas analyser constructed around 1837 by Heinrich Gustav Magnus (1802-1870), the calorimetry of an isolated muscle [von Helmholtz (1821-1894)] and whole animals [Max Rubner (1854-1932)] [1], and the O_2 and CO_2 exchange measures in exercising dogs [1] and horses [61] by Nathan Zuntz (1847-1920) and colleagues are examples of these advancements. By the last quarter of the nineteenth century, blood's role as gas transporter between the lungs and peripheral tissues was already completely established, as was the relationship between O_2 utilization and heat production [1].

In the context of this fruitful period, the German physiologist Adolf Eugen Fick (1829–1901) presented in 1870 a fundamental principle used in oxygen uptake ($\dot{V}O_2$) evaluation [62]. Originally proposed as a means of assessing the cardiac output ($\dot{Q}$), the Fick principle is represented by :

$$\dot{V}O_2(t) = \dot{Q}\left([O_2a] - [O_2v]\right) \tag{2.1}$$

In the original proposition, since $[O_2a]$ and $[O_2v]$ are, respectively, the O_2 content of arterial and venous blood at the pulmonary level, and corresponding $\dot{Q}$ to the total blood flow pumped by the heart through the lungs, the represented $\dot{V}O_2$ refers to the whole-body uptake. In that case, the blood flow represented by $\dot{Q}$ may be evaluated in terms of the cardiac stroke volume (SV) and the cardiac frequency, or heart rate (HR):

$$\dot{Q} = SV \cdot HR \tag{2.2}$$

However, Fick's principle is not restricted to the whole body $\dot{V}O_2$, but applicable to any situation where the O_2 content of a known blood flow may be measured before and after passing a given control volume, so that the O_2 uptake of a specific region (e.g., a muscle or a limb) may be evaluated.

2.2 The exponential nature of the $\dot{V}O_2$ kinetics

Once an understanding of anatomic and functional foundations regarding $\dot{V}O_2$ were unveiled, and basic instrumental and technical supports were developed, the field of the $\dot{V}O_2$ kinetics began to flourish. One fundamental method of collecting gas exchange variables during physical exertion in humans, the Douglas bag technique (Figure 2.2), was first presented in 1911 [63], by the British physiologist Claude Gordon Douglas (1882-1963).

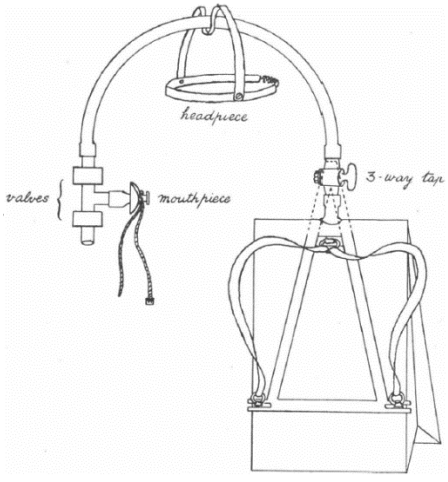

Figure 2.2 Illustrative scheme of the apparatus presented by C. G. Douglas in the *Proceedings of the Physiological Society*, in 1911. Reproduced with permission from [63].

A few years later, in 1913 at the University of Copenhagen, famous laboratory colleagues, physiologist August Krogh (1874-1949) and medical doctor Johannes Lindhard (1870-1947) [64], published the results of their experiments in humans performing exercise on-transitions on a cycle ergometer [33]. They observed the fast response of the human cardiovascular system to the exercise onset [1], remarking that:

> At the beginning of heavy work—especially in persons trained to sudden and violent exertions—there is an abrupt rise in pulmonary ventilation and heart rate. The blood flow (as indicated by the oxygen absorption in the lungs) is increased evenly but very rapidly. (Krogh and Lindhard, 1913, p. 131)

In that paper, Krogh and Lindhard not only make reference to Douglas, but also to other giants of physiology, namely John Scott Haldane (1860-1936)—Douglas' professor and collaborator, inventor of the "Haldane apparatus" for measuring O_2 and CO_2 content in air samples—and Christian Bohr (1855–1911)—father of Niels Bohr and Krogh's professor [1, 65]. Their respective descriptions of the "Haldane effect" and the "Bohr effect" were fundamental to the understanding of gas exchange and transport dynamics in living tissues [64]. At that point, the roster of contributors to the field was extensive, including names like Lorain Smith (1862-1931) and John Gillies Priestley (1880-1941), both of them Haldane's close collaborators [65], among many others.

Although Krogh and Lindhard's contributions to the field would continue to be numerous[2], their description of the $\dot{V}O_2$ response to the exercise on-transient as a simply *fast* phenomenon would be complemented by another duo of scientists. In a publication of 1923, Archibald Vivian Hill (1886-1977) and Hartley Lupton (1892-1924) published data suggesting the *exponential* nature of the $\dot{V}O_2$ response, for both the step on- and off-transients (Figure 2.3; panels A and B, respectively) [66]—see Section *2.5 Step stimulus: advantages and modelling characteristics* for a description of these step transients. In the same year, these authors were publishing specific studies about the mechanical efficiency of human movement [67], and in the following year, with the contribution of the biochemist Cyril Norman Hugh Long (1901-1970), they would report on the relationship

[2] For example, in 1920 Krogh would win a Nobel prize for the identification of the capillary recruitment in muscle during exercise [64] P. B. Raven, M. Kjaer, and Y. Hellsten, "Contributions from the Copenhagen Muscle Research Center," in *History of Exercise Physiology*, C. M. Tipton, Ed. Champaign, IL: Human Kinetics, 2014.

between $\dot{V}O_2$ and both running and walking speeds $\dot{V}O_2$ in humans (Figure 2.3; panels C and D, respectively) [34].

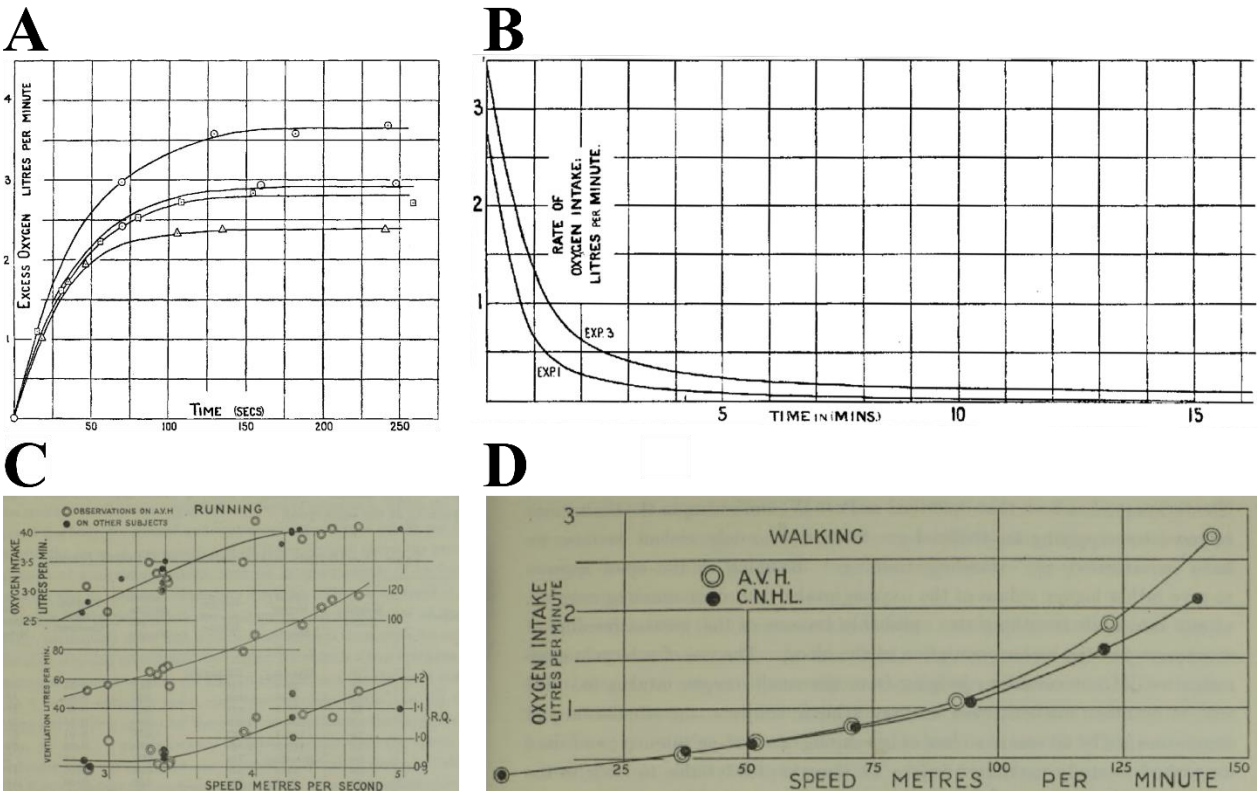

Figure 2.3 $\dot{V}O_2$ responses to the exercise step A. on- and B. off-transients; C. Oxygen uptake, ventilation, and respiratory quotient represented in function of the running speed; and D. Oxygen uptake represented in function of the walking speed; In all of the plots, some smooth, exponential-like tendency lines are suggested by the authors. Panels A and B reproduced with permission from [66]. Panels C and D reproduced with permission from [34].

In a large extent, despite minor updates, the description of the $\dot{V}O_2$ responses to the exercise provided at the beginning of the last century by Krogh, Lindhard, Hill, Long, Lupton, and some of their contemporaries has proved to be pertinent. As remarked on by Rossiter, Howe, and Ward [68], the general description of the $\dot{V}O_2$ response to the square wave stimulus (see Section *2.5 Step stimulus: advantages and modelling characteristics*) as a single first-order function was corroborated by studies published until around 1970 [68]. By that time, more specifically in the late 1960s and early 1970s, the development of technologies allowing the breath-by-breath

measurement of respiratory variables [1, 69], led to the establishment of what Jones and Poole (2005) call the "field of $\dot{V}O_2$ dynamics" [1].

This advance in measurement techniques, in association with the development of exercise testing protocols and the application of computing technologies to the treatment of ventilatory data [69, 70] allowed the brilliant Brian James Whipp (1937–2011) and Karlman Wasserman (B. 1927) to improve that mono-exponential concept into the widely adopted three-phase model[3] for the $\dot{V}O_2$ kinetics [1]. In 1972, these two researchers published a characterization of the $\dot{V}O_2$ response to the constant WR exercise at various intensities [71], describing the existence of an additional exponential component[4] manifesting at higher exercise intensities, and in collaborations with other noteworthy physiologists in the following years, contributed immensely to the methodological and theoretical improvement of the $\dot{V}O_2$ response modeling [1, 9, 73-75].

In general terms, since the establishment of this three-phase model based on first-order exponentials, studies on $\dot{V}O_2$ kinetics have investigated the influence of the exercise intensity and other conditions (e.g., hypoxia [76-80], hyperoxia [17, 19, 20, 77, 81, 82], priming exercise [83-86], nutritional [76, 87], and fitness statuses [5, 11, 32], among others) on that model's parameters. Other studies exploring the O_2 deficit [17, 85, 88], the excess post-exercise oxygen consumption (EPOC) [89, 90], the $\dot{V}O_2$SA [37-45]—which is included in the model by means of its slow component (SC)—or aspects like the linearity [91] and the on and off symmetry [50, 92] of the $\dot{V}O_2$ kinetics, have largely relied on this FOS-based model. As further discussed in this work, two specific phenomena, namely the aforementioned O$\dot{V}O_2$K and $\dot{V}O_2$SA, have been challenging the very FOS nature of the $\dot{V}O_2$ response to exercise.

---

[3] As will be discussed in Section *2.5.1 First-Order Multi-Exponential model*, this model is a composition of two or three exponentials, each one characterizing the response of a first-order system to the transition in exercise intensity.

[4] This component, latter defined as the as the "slow component," had already been reported in at least two other publications: one in 1961 ([35] P.-O. Astrand and B. Saltin, "Oxygen uptake during the first minutes of heavy muscular exercise," *Journal of Applied Physiology*, vol. 16, no. 6, pp. 971-976, 1961.), as remarked by Gaesser and Pole (1996), and another in 1966 ([72] N. I. Volkov, V. N. Cheremisinov, and E. N. Ruzumovskii, "Oxygen exchange in man during muscular activity," presented at the Oxygen regime of the organism and its regulation (Symposyum, translated from Russian), Kiev, 1966.), as remarked by Whipp and Wasserman (1972) themselves.

2.3 Muscle fiber types, O_2 utilization, and $\dot{V}O_2$ kinetics

Ultimately, the $\dot{V}O_2$ reflects the rate at which the O_2 is transported from the environment air to the cellular mitochondria and used within these organelles for the oxidative phosphorylation—the biochemical process responsible for the aerobic turnover of ATP. Thus, the actual O_2 utilization results from a chain of steps composing the whole pathway of this gas in the human body, including its extraction from the air in the lungs, its transportation via circulatory system (where the cardiac output plays a fundamental role), and its diffusion in the tissues [1] (mainly the exercising muscles).

But while the muscles of a given region of the body are oxygenated by the same macrovascular system (forming one muscular compartment, in opposition to the extra muscular region), pools of fibers sharing similar anatomic and histochemical characteristics may also be considered as different compartments[5]. Such characteristics have a direct influence on these muscle compartments' ability to use the O_2 provided to them [93].

In general terms, the type I muscle fibers are more adapted to the aerobic energy pathway due to characteristics such as their mitochondrial and capillary densities, as well as the activity of oxidative enzymes, which are higher in these fibers than in other fiber types, namely the types IIA and IIX. The type I (or "slow-twitch") fibers are more adapted to slow contraction velocities and lower loads, offering a lower tension cost and higher resistance to fatigue. On the other end, type II (or "fast-twitch") fibers are generally less efficient (with both higher ATP cost of force generation [94] and higher $\dot{V}O_2$ cost per ATP resynthesis [95]) but more adapted to faster contractions and higher force generation, with this specialization being more prominent in the type IIX than in the IIA ones [93].

As expected, these muscle fiber's specificities may influence the $\dot{V}O_2$ kinetics responses, as the participation of the different muscle fiber types change for different individuals [39] and exercise conditions such as the WRs [88, 93, 96] and the contraction velocity [42, 97, 98]). An example of

---

[5] The structure composed of intra and extra muscular compartments is briefly commented in Sections *5.1.2 Physiomechanical analogy* and further explored in Section *7.4.2 Physiological coherence of the SOSC model*.

this influence involves the recruitment of type II fibers and the etiology of the $\dot{V}O_2$SA phenomenon [39, 41, 42, 88, 96-99], discussed in details in Sections 2.6.2 and 7.1.

2.4 The importance of the $\dot{V}O_2$ kinetics

2.4.1 Physical activity related uses of the $\dot{V}O_2$ Kinetics

For physical activity related purposes, measures of O_2 uptake may provide important exercise intensity references used in prescription and assessment of training methods [2, 6-10]. One good example is the gas exchange threshold (GET), which determines the transition between two important exercise domains (see Section *2.5.2 Exercise domains and the First-Order Multi-Exponential representation of the observed step* responses) and is a less invasive estimation of the widely used lactate threshold (LT) [6, 9, 15, 100, 101].

Another important cardiorespiratory index is the maximal oxygen uptake ($\dot{V}O_{2max}$), defined by Basset and Howley (2000) as "the highest rate at which oxygen can be taken up and utilized by the body during severe exercise" [2], or by Jones and Poole (2005) simply as "the maximum $\dot{V}O_2$ attained during for example an incremental test to exhaustion" [1]. The $\dot{V}O_{2max}$ is considered one of the main physiological variables available, being not only used for evaluation of cardiorespiratory fitness and exercise prescription [2], but also considered a determining factor for high intensity exercise tolerance [10, 11, 13].

While certain physiological references like the GET and the $\dot{V}O_{2max}$ are evaluated by means of incremental tests, where ventilatory values are obtained for a range of different WRs, some other indexes of high relevance are those represented by the parameters of the FOS exponential used for modeling the $\dot{V}O_2$ response to a constant WR (see Section 2.4.4). This is the case for the amplitude A_{FC} or the sum of amplitudes A_{FC} + A_{SC} (see Figure 2.6), which represent the additional cost of oxygen above baseline values required for a given physical task (e.g., a given cycling power output or running speed), and may provide information about the efficiency of the aerobic mechanism and, ultimately, of the entire physiological and biomechanical apparatus. Another useful FOS parameter is the time constant τ, which indicates the speed of the augmentation of the $\dot{V}O_2$ response to a new required level, reflecting the responsivity of the individual to the aerobic exercise.

In addition, some other variables may be obtained from the FOS response curve and its parameters. Two examples are the O_2 deficit, which estimates the energy obtained via the anaerobic metabolism on certain exercise conditions [1, 85, 88], and the aforementioned EPOC [89, 90], which reflects the aerobic metabolism in the period following the cessation of the physical activity. Section *2.5* provides a more detailed presentation of the FOS curve parameters and its derived variables.

In any case, all the aforementioned $\dot{V}O_2$ related indexes represent useful evaluation tools, as they reflect fitness status, training adaptations to exercise, and serve as a reference for accessing the efficiency of training protocols [7, 8, 10-13].

2.4.2 Health related uses of $\dot{V}O_2$ kinetics

Regarding the utilization of $\dot{V}O_2$ information in clinical investigation, many of the index [102] used for fitness level assessment of athletes (e.g., $\dot{V}O_{2max}$, A_{FC}, τ) are also useful for the evaluation of patients, suggesting or detecting possible dysfunctions of their respiratory, cardiovascular, and neuromuscular systems [1, 4, 5, 14-32]. Like in the physical activity context, the use of $\dot{V}O_2$ related variables as a diagnostic aid in the clinical context relies on reference values for comparison, either obtained from previous tests performed on the same patient, or from directive tables corrected for the individual's population (e.g., age and sex).

In a 2005 publication, Jones and Poole [1] remark on the augmentation of the publications in the $\dot{V}O_2$ kinetics thematic since the late 1970s:

> Measurement of $\dot{V}O_2$ kinetics has become an important tool in the evaluation of the extent of a dysfunction and in some instances the mechanism behind that dysfunction in many major chronic disease conditions. (Jones and Poole, 2005, p. 17)

The authors also present a table with fourteen examples of chronic disease conditions that may be evaluated using $\dot{V}O_2$ kinetics measurements (see [1], p. 19), amongst which cystic fibrosis [20], coronary artery disease [21], mitral stenosis [22, 23], chronic heart failure [24], atrial fibrillation [25], dilated cardiomyopathy [26], HIV [103], peripheral arterial disease [28], spinal cord injury [29, 30], chronic fatigue syndrome [31], and prolonged immobility [32].

More recent examples of publications relating $\dot{V}O_2$ kinetics evaluations and chronic conditions are also numerous, like those assessing pulmonary hypertension [77], chronic obstructive pulmonary disease [104-107], type 2 diabetes [108], congenital hearth disease [109], amongst many other.

2.4.3 The importance of a proper modeling for the $\dot{V}O_2$ kinetics

At least two different aspects justify the constant search for improvements in the models used for the $\dot{V}O_2$ kinetics. A more pragmatic one relies on the usefulness of $\dot{V}O_2$ kinetics as a tool for health or physical activity-oriented purposes, which is highly dependent on the existence of a proper model to fit data and extract valuable information from it. Because the use of indexes extracted directly or indirectly from the curve's parameters require the model to be an appropriate one, adopting an equivocated model is assuming unrealistic references for $\dot{V}O_2$ kinetics evaluations.

Moreover, leaving aside the use of $\dot{V}O_2$ kinetics in health or physical activity applications, and considering only the scientific interest in understanding the O_2 uptake system itself, the model to be adopted by the researcher is still very important. In a majority of cases, experimental interventions—and the subsequent interpretations of results—are strongly dictated by a given adopted model, since it is believed to reflect the underlying dynamics of the process under investigation.

2.4.4 Input functions used in $\dot{V}O_2$ kinetics studies

Considering that $\dot{V}O_2$ kinetics addresses the dynamic behavior of oxygen uptake in response to some physical exertion [1], the qualitative and quantitative characteristics of the input function applied to the studied subject (i.e., the type of stimulus) become naturally important.

In order to identify or simply describe some features of the O_2 uptake system of humans, a variety of input functions have been used in $\dot{V}O_2$ kinetics studies [1, 5, 50, 80, 82, 92, 110-119]. Table 2.1 lists examples of this type of study, associating it with the class of applied stimuli and the chosen approach, namely the time or frequency domain analyses. Such stimuli are applied by means of alterations in the exercise intensity during a given activity, the variation of the speed of a treadmill or the load of a cycle ergometer being two common examples of this type of WR manipulation.

As grouped in Table 2.1, the normally used input functions may be derived from four main classes, namely the step, the ramp, the impulse, and the sinusoidal stimuli (Figure 2.4; curves on panels A, E, G, and H, respectively).

Step stimulus: The most used class of stimuli is the step-like entry (Figure 2.4.A), where a sudden change in WR is applied at a given time t_0. In the case of a simple increase in the WR, the step-

stimulus will cause the so-called on-transient of the ventilatory response [12, 46-48]. In addition, some studies also analyze the response caused by a subsequent decrease in the WR, also referred to as the off-transient [80, 92, 110, 113]. Figure 2.4.B illustrates a set of on- and off-transients step entries forming a generic "square wave" of duration T imposed at the instant t_0. Following the same pattern, other studies apply not only a single, but a sequence (or train) of square waves to the individuals (Figure 2.4.C), where the time intervals T_1, T_2, …, T_n may be constant [47, 50] or varying [80, 116, 119].

Table 2.1 Main classes of input functions and their variations used in $\dot{V}O_2$ kinetics studies

Main classes of input functions and its variations	Panel on Figure 2.4	Publications (by approach)*	
		Time domain	Frequency domain
Step			
On-transient only	A	[12, 46-48]	
Square wave (on- or off-transients)	B	[92, 110, 113]	
Sequence of square waves	C	[1, 5, 47, 50, 80, 82, 92, 110-118]	[20] †
Incremental step pattern	D	[6, 12, 47, 50, 112, 118]	
Ramp			
Incremental ramp pattern	E	[111, 112]	
Ramp wave (on- or off-transients)	F	[92, 113]	
Sequence of triangular pulses	F	[114]	
Impulse (and sequence of impulses)	G	[110]	[80, 92, 119, 120]
Sinusoidal	H		[82, 92, 117, 118, 120]

*Non-exhaustive list; †In the real experimental context, the impulses applied in some studies [80, 92, 119, 120] may be interpreted as a sequence of very short square waves. However, these cases were assigned as impulses for differentiation purposes. See *Impulse stimulus* below for details.

Additionally, the step stimuli may be combined as described on Figure 2.4.D to compose the widely used incremental step pattern [6, 12, 47, 50, 112, 118], which is very useful for determining ventilatory and lactate thresholds, as well as the $\dot{V}O_{2max}$ value, especially when extended until subject's volitional fatigue.

Ramp stimulus: Another class of stimuli often found in physiology studies is the ramp-like entry. Comprised of a constant increase of WR from a given instant t_0 on (Figure 2.4.E), this pattern may

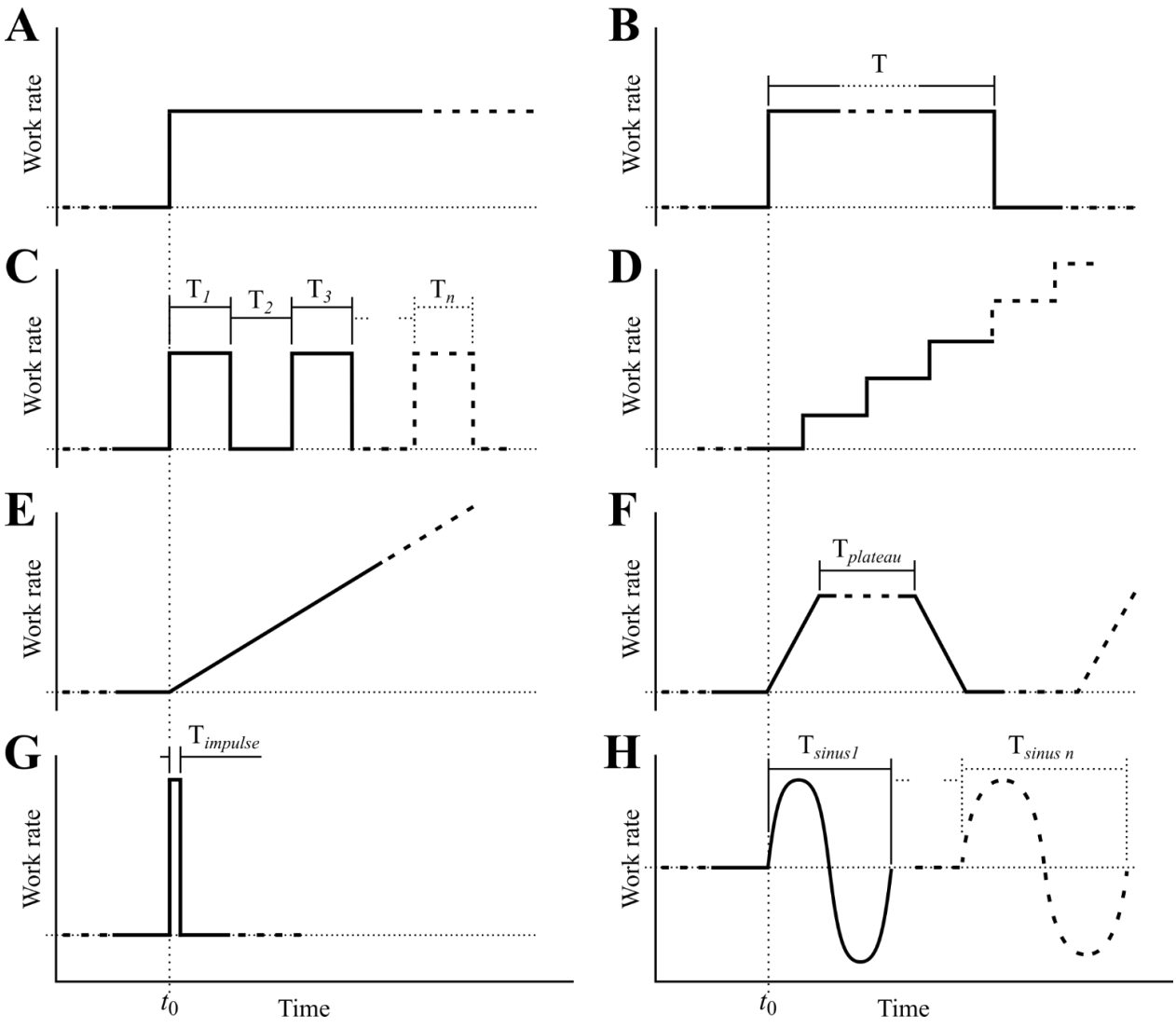

Figure 2.4 Input functions commonly used in $\dot{V}O_2$ kinetics studies. See text for details.

also be sustained until individual's fatigue during an incremental ramp test, usually for assessment of ventilatory thresholds and $\dot{V}O_{2max}$ [111, 112]. Alternatively, like the square wave test, the on- and off-transients in response to the ramp stimulus may also be studied by means of the application of a "ramp wave" (Figure 2.4.F) [92, 113], which may become a "triangular pulse" in the case of $T_{plateau} = 0$, and may also be repeated in a sequential manner [114].

Impulse stimulus: A different class of input functions found in $\dot{V}O_2$ kinetics studies is the impulse-like stimulus [80, 92, 110, 119, 120], which is, ideally, an instantaneous peak in the input's amplitude. However, since the ideal impulse is not feasible in a real experimental context [55], the

actually implemented impulse may be interpreted as a very short square wave applied at an instant $t = t_0$ (Figure 2.4.G), with values for $T_{impulse}$ lasting up to around 10 to 15 seconds.

Sinusoidal stimulus: Finally, sinusoidal patterns have also been used as input functions in ventilatory experiments (Figure 2.4.H), where the function period T_{sinus} is usually manipulated and the complete stimulus may last for *n* periods [82, 92, 117, 118, 120].

2.5 Step stimulus: advantages and modelling characteristics

Despite the variety of stimuli that may be applied in studies involving $\dot{V}O_2$ kinetics, a clear majority of studies assuming the time rather than the frequency domain approach is observed in literature. This preference may be due not only to the difficulties involving data collection for the frequency approach (see Section *4.2.6 Additional considerations on the experimental protocol*), but also to the practicalities involving stimuli such as the ramp and step types. More specifically, the researchers' recurrent choice for the step stimulus and its correlated entries (e.g., the incremental step test and square waves) is highly supported by the advantages of such type of stimulus, namely:

- the step stimulus is technically easy to apply, especially due to its simple shape (i.e., a simple sudden change in WR) and low quantity of describing input parameters;
- the $\dot{V}O_2$ response to the step stimulus has been the most well-characterized and modeled type of response, which provides an abundance of references and sources for comparison values;
- it is in response to the step stimulus that the $O\dot{V}O_2K$ and $\dot{V}O_2SA$ have been observed and described by specific literature, obliging any model attempting to explain these controversial phenomena to contemplate the $\dot{V}O_2$ step response; and
- step stimuli are largely used in system identification studies, since their responses, depending on the case, may provide useful information (e.g., order of a system, rise time, settling time, stability and ringing characteristics, overshoot features etc.) [55, 56].

In general terms, the step stimulus consists of a sudden change in WR from one constant level to another. The so-called on-transient is characterized by a change from a lower level, usually a baseline value, to a higher one (Figure 2.5.A), whereas the opposite change characterizes an off-transient (Figure 2.5.B).

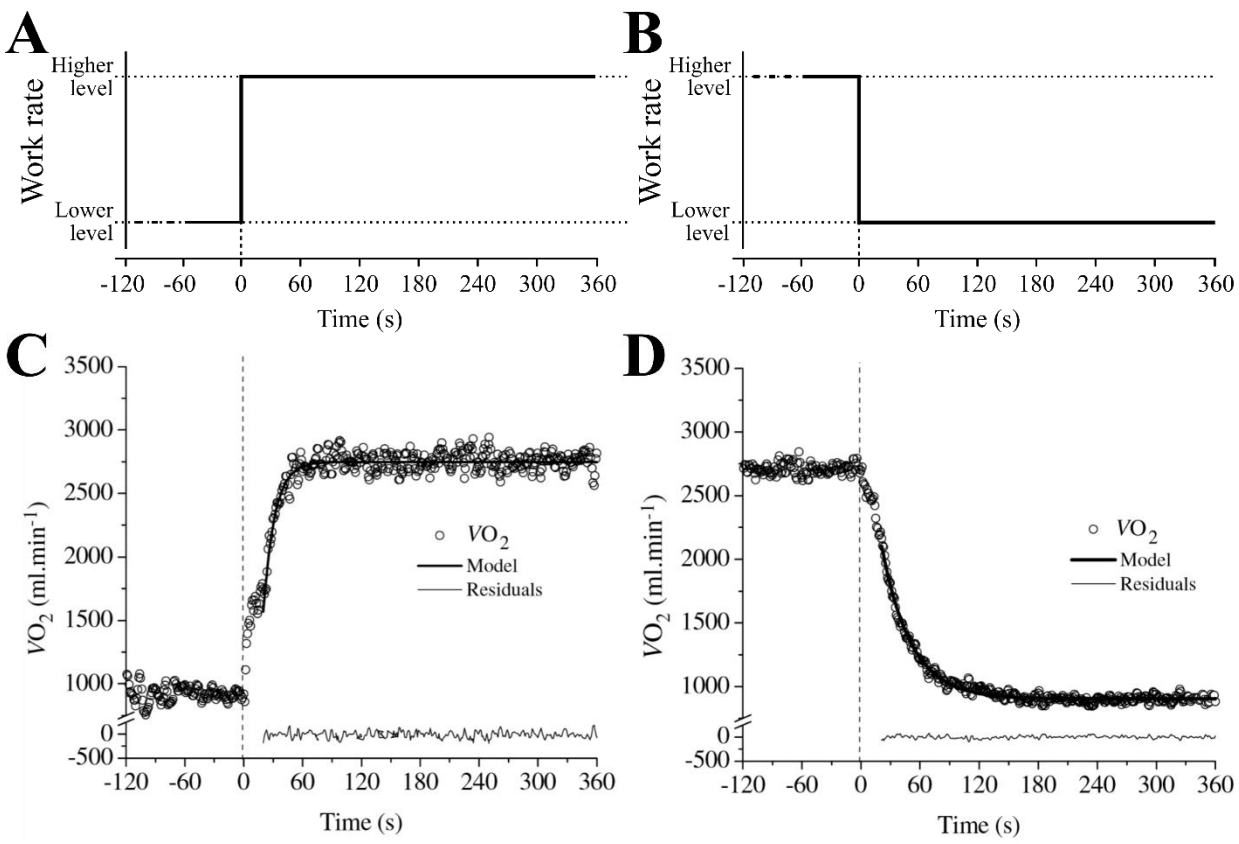

Figure 2.5 A and B. WR step on- and off-transients, respectively; C and D. averaged $\dot{V}O_2$ responses to the step on- and off-transients. Panels C and D reproduced with permission from [50].

The bold solid lines in panels C and D (see "Model")—adapted from Kilding et al. [50]—of Figure 2.5 describe a FOS approximation for averaged $\dot{V}O_2$ data (circles) collected in response to WR step on- and off-transients, respectively. This representation, composed of a single first-order exponential, is not so different from the tendency line patterns proposed by Lupton and Hill back in 1923 [66] (Figure 2.3.A-B). As the next section will demonstrate, despite some modifications, such as the incorporation of onset time delays and additional components, the notion that the first-order exponential pattern would be adequate to describe human $\dot{V}O_2$ kinetics in response to step stimuli has remained practically intact until the present days.

2.5.1 First-Order Multi-Exponential model

Although the ascending part of the response in Figure 2.5 is only partially fitted, it is currently agreed upon that the entire response to the step on-transient stimulus may be described using one

or two additional exponential curves (also based upon FOS responses), which composes the three-phase model developed from early propositions presented by Whipp and Wasserman in 1972 [71].

Despite differences in its formulation (see Appendix A), this model is always composed of three *phases* and comprises two or three first-order exponential components [1, 71, 74, 88], being thus generally defined in this thesis as the First-Order Multi-Exponential (FOME) model. In Figure 2.6, the FOME model is depicted under the representation adopted in this thesis.

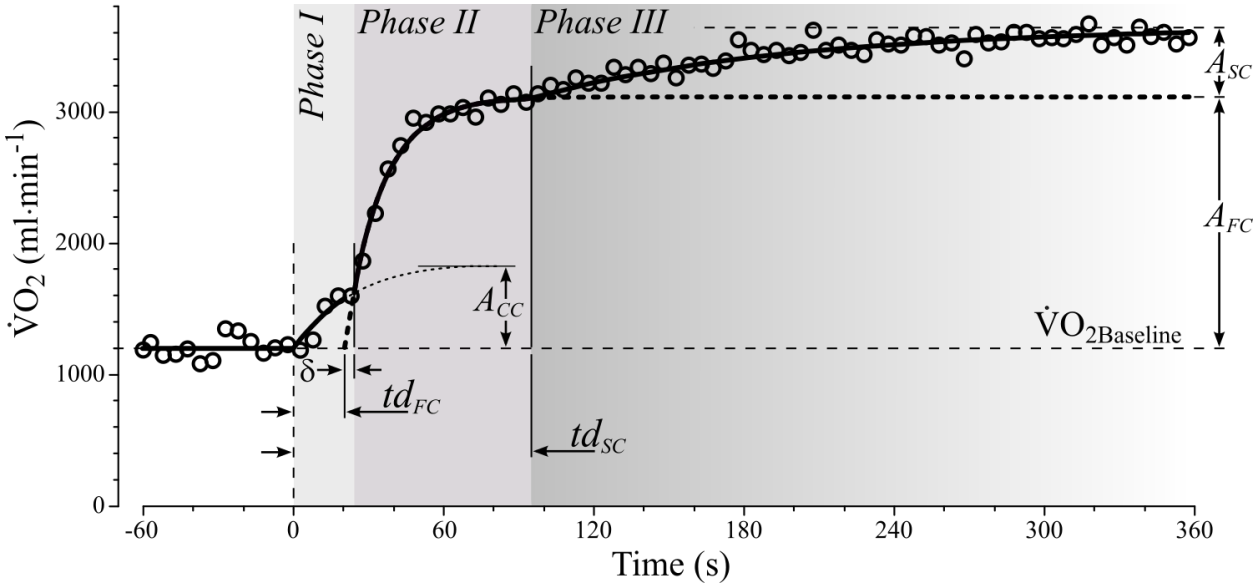

Figure 2.6 Combined response of the FOME model for the exercise step on-transient. See text for details.

The combined response curve (continuous line) is formed by an arrangement of first-order components, each one corresponding to a specific physiological mechanism acting on the $\dot{V}O_2$ kinetics: the cardiodynamic component (CC), the fundamental component (FC)—sometimes referred as primary or fast component—and the slow component (SC) [1, 4, 88, 101, 121].

In mathematical terms, the multi-exponential curve above becomes:

$$\begin{aligned}\dot{V}O_2(t) = \dot{V}O_{2Baseline} &+ A_{CC}\left\{1-\exp\left[\frac{-t}{\tau_{CC}}\right]\right\}_{0\le t<td_{FC}+\delta} \\ &+ A_{FC}\left\{1-\exp\left[\frac{-(t-td_{FC})}{\tau_{FC}}\right]\right\}_{t\ge td_{FC}+\delta} + A_{SC}\left\{1-\exp\left[\frac{-(t-td_{SC})}{\tau_{SC}}\right]\right\}_{t\ge td_{SC}>td_{FC}}\end{aligned}, \qquad (2.3)$$

where A_{CC}, A_{FC}, and A_{SC} are the amplitudes and τ_{CC}, τ_{FC}, and τ_{SC} are the time constants of the cardiodynamic, fundamental, and slow components, respectively. In addition, td_{FC} and td_{SC} are the time delays of FC and SC, respectively, and $\dot{V}O_{2Baseline}$ is the constant term for the initial, or baseline, O_2 uptake.

An important remark is that the increase in $\dot{V}O_2$ represented by the CC is conditioned only to the so-called *phase I* of the $\dot{V}O_2$ response, a limited transition period when the blood initially resting on the venous bed is pumped through the lungs after a rapid increase in cardiac output, at the very beginning of the WR transition [74, 122] (see equation 2.1).

Additionally, depending on the representation adopted for the FOME model (see Appendix A), the end of *phase I* may or may not coincide with the onset of the FC component (i.e., with $t = td_{FC}$). For the representation adopted in Figure 2.6 and equation 2.3, the end of *phase I*, is precisely set at $t = td_{FC} + \delta$, which marks the instant when the CC no longer represents the shape of the combined response. This representation, however, is only an approximation of the pulmonary $\dot{V}O_2$ data during the transition from the CC to the FC, making any concern regarding the precise ending instant of *phase I* irrelevant. Thus, the δ term will be disregarded in this thesis for further representations of the FOME and other models. Such a simplification, in any case, not only contributes to the clarity of the model, but also has no impact on the fitting performance evaluations, since the *phase I* is usually removed from the data sets in $\dot{V}O_2$ modeling studies (e.g., [4, 47, 48, 50, 123]), and so will be in this thesis (see Section *5.2.3 Curve-fitting procedures* and Appendix A).

At the end of *phase I* (around 20 s after the exercise onset [122]), the FC—considered the best representation of muscle O_2 uptake [122]—begins to actually determine the shape of the $\dot{V}O_2$ response. This period during which the FC will present its major increase towards stabilization is called the *phase II* of the $\dot{V}O_2$ step response.

Finally, during the so-called *phase III* of the $\dot{V}O_2$ step response, two situations may be observed (see Section *2.5.2*; next paragraph). In the absence of a third exponential, *phase III* will correspond to the steady-state of the FC. Alternatively, this phase may contain the SC, which is added to the combined response at $t = td_{SC}$ [1, 88, 121], and is believed to reflect the additional recruitment of muscle fibers, mostly of type II [39, 41, 42, 88, 96-99].

2.5.2 Exercise domains and the First-Order Multi-Exponential representation of the observed step responses

To cope with the variety of shapes observed for the complete $\dot{V}O_2$ responses to the step on-transient, the FOME model presents different compositions throughout the possible WR spectrum. In other words, the presence of two or three components in addition to the initial $\dot{V}O_2$ value is conditioned by the intensity and duration of the exercise at the higher level WR of the step, which is, in turn, associated with the different exercise domains [1, 10, 101, 121, 124, 125].

Figure 2.7 depicts a general description of the FOME-based $\dot{V}O_2$ step response to different exercise intensities, and reflects a compilation of different representations adopted by authors such as Jones and Poole [1], Burnley and Jones [10], Whipp and Rossiter [101], Wilkerson et al. [121], amongst others.

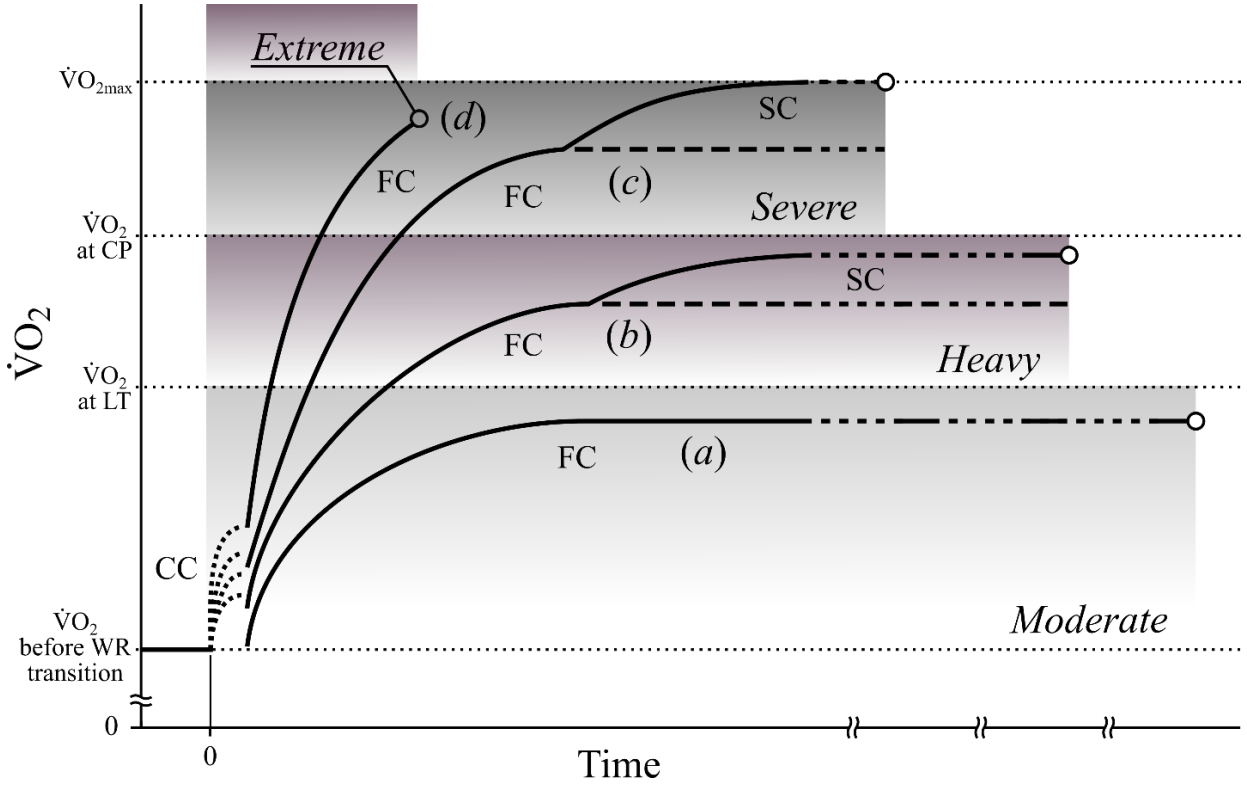

Figure 2.7 $\dot{V}O_2$ responses to step stimulus at different exercise domains, as represented by the FOME model. In addition to the intuitive concept that the time to fatigue (*circles*) will be longer for exercises at lower intensities [10], important qualitative differences are observed for each WR domain (*moderate*, *heavy*, *severe*, and *extreme*). See text for further information.

Although transitory, the first exponential term represented by the CC (Figure 2.7; dotted line) is always considered present in the $\dot{V}O_2$ step on-transient response, despite being often left out of fitting procedures. In this case, the data referent to the initial seconds (15 to 25 s) after t_0 is simply ignored in the mathematical regressions of the FC and SC curves.

The FC is also present in the FOME step responses representation at all WRs, although an asymptotic steady-state at $\dot{V}O_{2Baseline} + A_{FC}$ (Figure 2.6) is only observable for WRs within the moderate domain (Figure 2.7; curve *a*). The upper limit of this domain, however, may be defined differently by some authors. In the studies from Whipp and Rossiter [101], and Burnley and Jones [10], and Hill et al. [124], for example, it is defined as the WR corresponding to the lactate threshold (LT; see Section *4.2.3 Incremental step test*), with the same criteria being adopted in the present work. In some other studies, such as those from Jones and Poole [1] or Wilkerson et al. [121], the upper limit of the moderate domain is defined as the WR corresponding to the GET.

Whereas in the moderate domain the O_2 uptake stabilizes at the asymptote of the FOME model's FC, at supra-LT intensities the $\dot{V}O_2$ response may present different behaviors. One possibility is its increase until the stabilization of the $\dot{V}O_2$SA phenomenon, which in the FOME model representation, occurs at $\dot{V}O_{2Baseline} + A_{FC} + A_{SC}$ (Figure 2.6). This stabilization is only possible for WRs below or equal to the individual's critical power (CP), defined as the asymptote of the exercise power-duration curve [126] and considered to be the upper limit of the heavy exercise domain [1, 10, 101, 121, 124, 125] (Figure 2.7; curve *b*). Briefly, the CP corresponds to the WR value at the asymptote of the individual's exercise intensity vs. duration curve [10, 125].

For WRs above the CP, the continued $\dot{V}O_2$SA precludes the FOME's SC from reaching its asymptotic stability, and given enough exercise time, the individual may achieve his $\dot{V}O_{2max}$ (Figure 2.7; curve *c*), which defines the severe exercise domain [1, 10, 121, 124, 125]. Finally, in the exercise domain referred to as extreme [124][6], the WRs are so intense that fatigue will cause

[6] See [101] B. J. Whipp and H. B. Rossiter, "The kinetics of oxygen uptake: Physiological inferences from the parameters," in *Oxygen uptake kinetics in sport, exercise and medicine*, vol. 1, A. M. Jones and D. C. Poole, Eds. New York, USA: Taylor & Francis, 2005, pp. 62-94. B. J. Whipp and H. B. Rossiter, "The kinetics of oxygen uptake: Physiological inferences from the parameters," in Oxygen uptake kinetics in sport, exercise and medicine, vol. 1, A.

the individual to cease the exercise before $\dot{V}O_{2max}$ is achieved (Figure 2.7; curve *d*), and the $\dot{V}O_2$SA (or SC, in the FOME context) will not be evident [10].

2.6 Inconsistencies of the first-order representation for the $\dot{V}O_2$ kinetics

Since its publication in the early 1970s, the FOME representation has been the predominant model in studies investigating the human $\dot{V}O_2$ step response. Nevertheless, at least two phenomena may bring controversy to this first-order-based modeling choice, namely the O$\dot{V}O_2$K [12, 46-51] and the $\dot{V}O_2$SA) [35-45].

2.6.1 The phenomenon of the overshoot in the $\dot{V}O_2$ kinetics

The first-order nature of the FOME model imposes a very specific qualitative behavior to each of its components: a fast initial rise rate that is continually smoothed, causing $\dot{V}O_2$ values within each component to achieve, in an asymptotic fashion, its own steady-state level (i.e., the amplitudes A_{CC}, A_{FC}, or A_{SC} in Figure 2.6) [49, 55, 127]. Thus, although the variation in $\dot{V}O_2$ values from one time instant to the next is constantly reduced, it is still constantly positive.

In this context, any component presenting an overshoot above its own steady-state level (see examples of Figure 2.8; or *grey line* in Figure 5.1) constitutes an inconsistency for the FOS model, for this behaviour requires a negative variation in the $\dot{V}O_2$ values. Notwithstanding such a conceptual constraint, the phenomenon of O$\dot{V}O_2$K has been observed in the FC (during the *phase II*) of FOME's step on-transient responses [12, 46-51] (Figure 2.8). The literature dedicated to this topic indicates that the O$\dot{V}O_2$K is observed in step on-transitions to (i) relatively low intensities [12, 46-51, 57], not necessarily [57], however most commonly within the moderate exercise domain [48, 57]; (ii) in fit individuals, such as athletes or very active subjects [12, 46-48, 50, 51, 57]; and (iii) more often and more pronouncedly during cycling rather than running [47].

Additionally, in one study applying an endurance training to cyclists (approximately 13 h per week during 5 months) [12], the general observed pattern was of the increase in the O$\dot{V}O_2$K magnitude

---

M. Jones and D. C. Poole, Eds. New York, USA: Taylor & Francis, 2005, pp. 62-94 for an alternative scheme for the supra-CP exercise intensity domains.

(measured as the difference *Peak-SS*; see Section *5.1.1 Overshooting behavior and the second-order model*)—mainly due to a decrease in the post-training $\dot{V}O_2$ steady-state levels—and an anticipation of the $\dot{V}O_2$ peak occurrence, i.e., a faster kinetics.

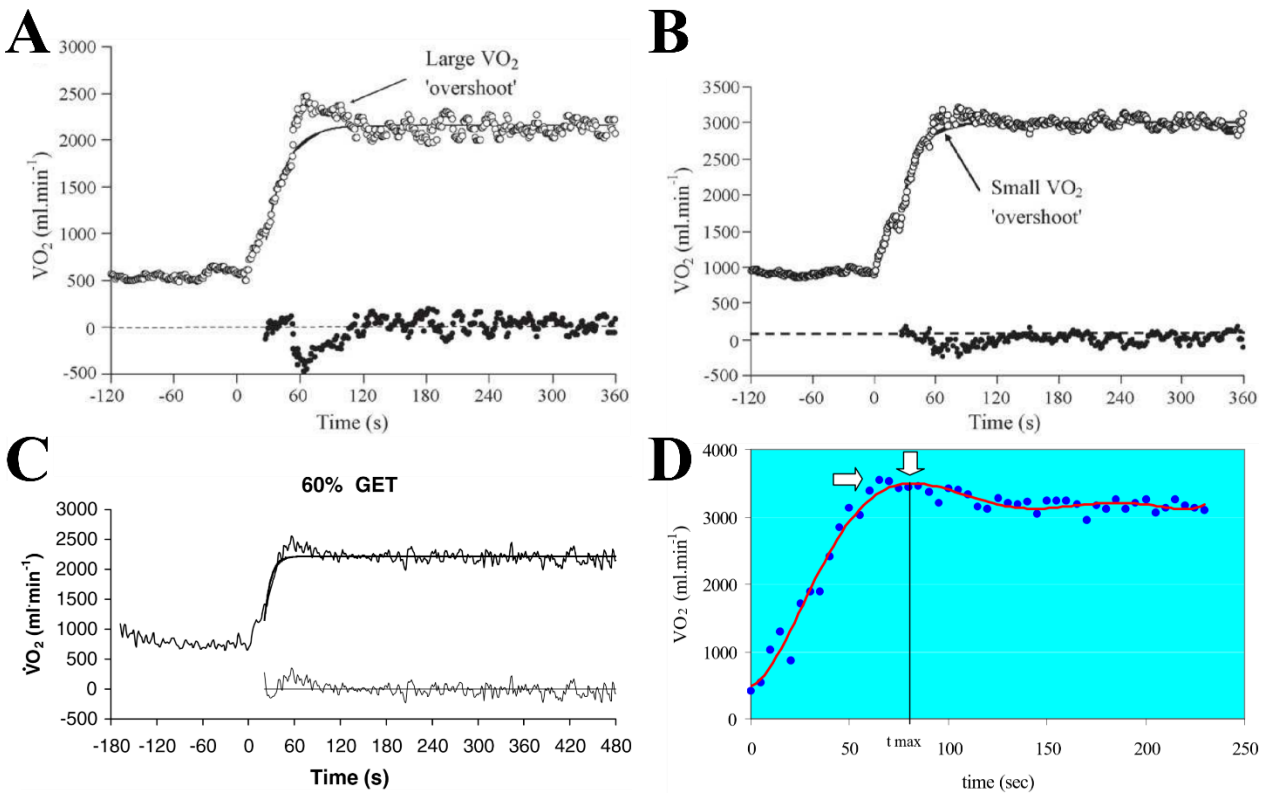

Figure 2.8 The O$\dot{V}O_2$K phenomenon observed $\dot{V}O_2$ step responses during: A. cycling, and B. running at 80% of GET intensity, and C. cycling at 60% of GET intensity. Error plots represent the difference between data points and the first-order FC (solid line); D. the O$\dot{V}O_2$K phenomenon as first depicted in a journal paper, with data fitted by using a polynomial function (equation 2.5). See text for details. Sources: panels A and B reproduced with permission from [47]; panel C reproduced with permission from [48]; and panel D reproduced with permission from [46].

Examination of the error plots obtained with the first-order exponential curve (Figure 2.8.A-C) denotes the inadequacy of this solution in fitting data containing O$\dot{V}O_2$K manifestations, which have already been remarked on by diverse authors [46-49, 51, 57]. Such an inadequacy may lead not only to unsatisfactory fittings in the overshooting region and its surroundings, but also to poor estimations of the O_2 deficit [46-48, 51, 57], τ_{FC} [47, 48, 51, 57], and A_{FC} [47, 48] (see Section *5.3.2 Mixed Multi-Exponential versus First-Order Multi-Exponential models*).

In the face of this modeling inconvenience intrinsic to the fist-order solution, the use of a higher order model is a convenient alternative. As presented by the *Physiomechanical analogy* [57] developed in Section 5.1.2, the SOS family of curves is a conceptual extension of the FOS solutions that is able to assume either overshooting or nonovershooting shapes [55, 56], while still respecting the control systems approach and the exponential nature of the $\dot{V}O_2$ response to exercise.

Origin of the O$\dot{V}O_2$K phenomenon. Speculations regarding the O$\dot{V}O_2$K causes are numerous [49], with some of them attributing this "additional" O_2 uptake above the steady-state level to:

- the activation of accessory muscles, such as those from trunk and higher limbs [46], or the respiratory ones [48];
- the acceleration of lower limbs and pedals at the beginning of the step stimulus [46], although not applicable in studies where a constant pedaling cadence was maintained from the baseline until the end of the step—which is the case of this thesis's investigation;
- a temporary reduction in muscle [5, 47, 48, 128] or movement [50] efficiency at the beginning of the step, due to an "excessive" recruitment of fibers [5, 47, 50, 128] or other metabolic factors [47, 48];
- an overshoot in the HR causing, via the logic described by Fick's principle (see equations 2.1 and 2.2), an overshoot in the pulmonary $\dot{V}O_2$. This theory, however, is discredited by the fact that HR overshoots were not always present in concomitance with O$\dot{V}O_2$K observations [47, 48, 128];
- a muscle $\dot{V}O_2$ kinetics faster than the muscle blood flow [47, 48], which could cause an O$\dot{V}O_2$K in the $\dot{V}O_2$ measured at the pulmonary level, in an effect that Kilding and Jones [47] called a "secondary cardiodynamic phase";
- a sudden increase in the muscular perfusion [46]; and
- other methodological and experimental causes [47, 48, 50].

In another line of thought, also mentioned in [49], Kilding and Jones [47] assume the possibility that the O$\dot{V}O_2$K may actually be an expression of the control dynamics controlling the oxidative phosphorylation. These authors hypothesise that adaptations to resistance training could cause the

mitochondrial respiration control to be influenced by metabolites other than those associated with ATP hydrolysis, which could allow behaviors no longer typical of a FOS dynamics and thus, allow manifestations such as the O$\dot{V}O_2$K [47].

First-order modeling for the O$\dot{V}O_2$K phenomenon. In the first journal paper describing the O$\dot{V}O_2$K [46] (previously published as a thesis chapter [102]), Hoogeveen and Keizer proposed a modeling solution that incremented the usual FOME structure by adding a "switch-on" element to its first-order FC (Figure 2.9.A; curves *III* and *I*, respectively). However, this solution's fitting performance would not actually be tested before the study from Dale and Glaister [51] (Figure 2.9; "*Model 2*").

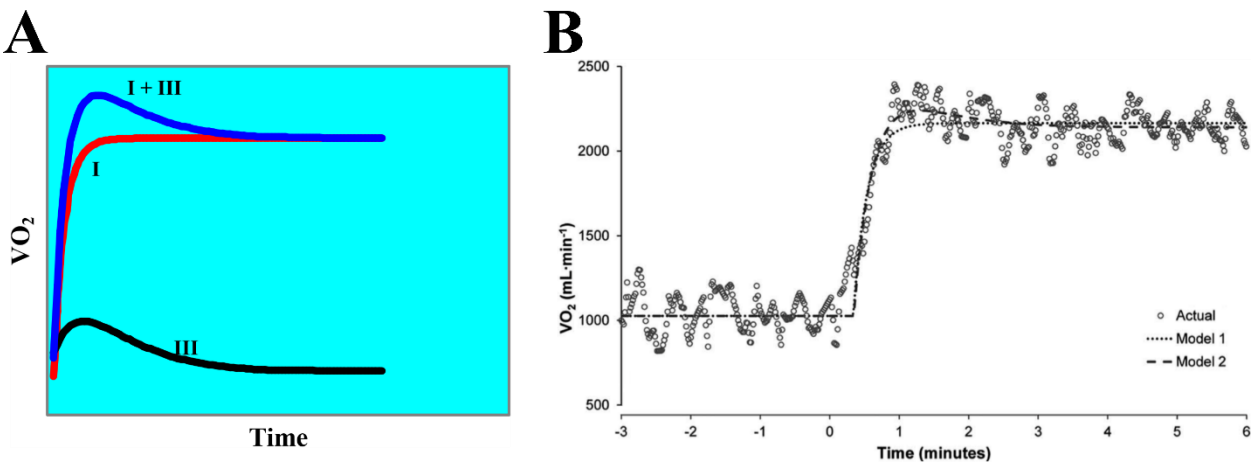

Figure 2.9 Alternative modeling for the O$\dot{V}O_2$K phenomenon A. as originally presented by Hoogeveen and Keizer [46]; and B. as applied by Dale and Glaister [51]. See text for details. Panel A reproduced with permission from [46]; Panel B adapted with permission from [51].

Equation 2.4 describes this solution, without including the cardiodynamic phase nor the SC[7]:

$$\dot{V}O_2(t) = \dot{V}O_{2Baseline} + \underbrace{A_{FC}\left\{1-\exp\left[\frac{-(t-td_{FC})}{\tau_{FC}}\right]\right\}_{t \geq td_{FC}}}_{\text{Curve I: first-order FC}} + \underbrace{B_{III}\left\{(t-td_{III})\ \exp\left[-(t-td_{III})\,c_{III}\right]\right\}_{t \geq td_{III}}}_{\text{Curve III: switch-on element}} \quad (2.4)$$

[7] In the original papers, the authors do not explicitly mention the condition for the switch-on element activation (i.e., $t \geq td_{III}$), which was included in the present work for clarity purposes.

Although the parameters of curve *III* (B_{III}, td_{III}, and c_{III}) are independent from those of curve *I*, the first-order exponential (Figure 2.9.B; "*Model 1*") has to be previously obtained from data where a 90-s period of a possible $O\dot{V}O_2K$ is left out of the regression. Only then, with A_{FC}, td_{FC}, and τ_{FC} already evaluated and kept constant, the curve III parameters may be obtained from the whole data set. Such a methodological measure is necessary to ensure a plausible steady-state of the combined response (i.e., curve *I* + *III* in Figure 2.9.A; or "*Model 2*," in Figure 2.9.B) instead of an excessively long and non-realistic decrease over time (i.e., for $t \rightarrow +\infty$) caused by the component *III* [51]. Moreover, while the addition of *curve III* to the FOME model is also possible when the $O\dot{V}O_2K$ is not present [51], it is important to consider that this will unnecessarily (i) add curve parameters to the model; and (ii) jeopardize the original *curve I* fitting due to the removal of the 90-s data period previous to its evaluation.

Alternatively, due to the unavailability of computational programs to implement the solution in equation 2.4 pointed out by Hoogeveen and Keizer [46] at the time of its presentation, these authors proposed a sixth-degree polynomial solution (equation 2.5 and Figure 2.8.D) to model overshooting and nonovershooting $\dot{V}O_2$ step responses:

$$\dot{V}O_2(t) = p_6 \cdot t^6 + p_5 \cdot t^5 + p_4 \cdot t^4 + p_3 \cdot t^3 + p_2 \cdot t^2 + p_1 \cdot t + p_0 \quad (2.5)$$

However, not only is any physiological basis claimed for this modeling solution [49], but it also fails to achieve a steady-state condition beyond the limits of the fitted data, for its polynomial nature will necessarily lead its values to positive or negative infinite for $t \rightarrow +\infty$.

Finally, adopting the same strategy of modeling of the $O\dot{V}O_2K$ by incrementing the conventional first-order solution with an add-on element, Koppo et al. [48] propose the addition of a mono-exponential decay term to the first-order FC. This representation is described in equation 2.6, where neither the cardiodynamic phase or the SC are included[8]:

[8] In the original paper, the authors do not explicitly mention the condition for the decay element activation (i.e., $t \geq td_{Decay}$), which was included in the present work for clarity purposes. See also legend of Figure 2.10.

$$\dot{V}O_2(t) = \dot{V}O_{2Baseline} + \underbrace{A_{FC}\left\{1 - \exp\left[\frac{-(t - td_{FC})}{\tau_{FC}}\right]\right\}_{t \geq td_{FC}}}_{\textit{First-order FC}} + \underbrace{A_{Decay}\left\{\exp\left[\frac{-(t - td_{Decay})}{\tau_{Decay}}\right]\right\}_{t \geq td_{Decay}}}_{\textit{Decay element}} \quad (2.6)$$

As remarked on by de Lima [49], this decay term is analogous to that used in many studies modeling the $\dot{V}O_2$ step off-transient (e.g., [50, 83, 90, 110]). In this case, however, no regression curve nor further details of this model's application are available. Moreover, considering that this decay element begins at a higher $\dot{V}O_2$ level than it ends, the manner how the three addends of equation 2.3 (described on Figure 2.10) may be combined in order to reproduce a smooth and overshooting response remains unclear.

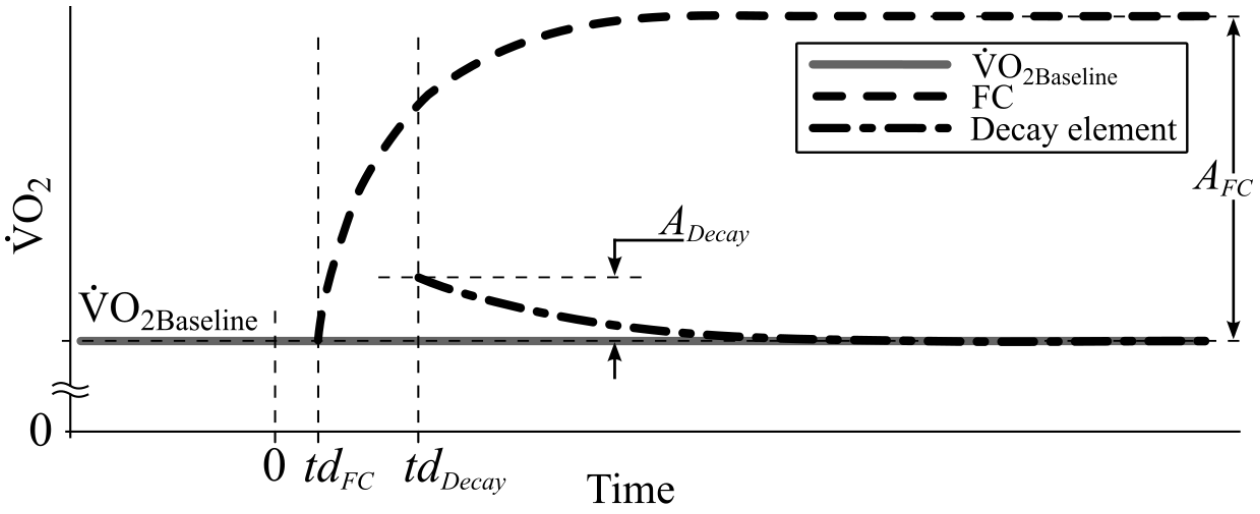

Figure 2.10 Three elements composing the model proposed by Koppo et al. [48] for overshooting $\dot{V}O_2$ responses. This representation where the decay element is (i) only activated for $t \geq td_{Decay}$, (ii) referenced above the $\dot{V}O_{2Baseline}$, and (iii) with $td_{Decay} \geq td_{FC}$ was not explicitly mentioned by the original authors, being adopted in the present work for clarity purposes.

In Chapter 5, both the switch-on and the decay elements are referred as cases of the *overshoot term* added to the FOME model to cope with $\dot{V}O_2$ step responses containing the O$\dot{V}O_2$K phenomenon. Thus, the models represented by equations 2.4 and 2.6 are referred to in Table 7.1 as "FOME/*overshoot term*" model.

In any case, regardless of the alternative model proposed, all these authors comment on the inadequacy of the FOS-based solutions in modeling overshooting $\dot{V}O_2$ responses [49]. In addition

to inadequate estimations of the O_2 deficit [46-48, 51, 57] and the τ_{FC} [47, 48, 51, 57], the $\dot{V}O_2$ values presented by the FOS exponentials tend to be underestimated at the beginning of the responses [48] and overestimated around the FC's steady-state region [47, 48].

Further discussions regarding the O$\dot{V}O_2$K phenomenon and the issues regarding its first-order representation are available in Chapters 5 to 9.

2.6.2 The phenomenon of the slow augmentation in the $\dot{V}O_2$ kinetics and the slow component onset time delay

When the step transition is performed to the heavy or severe domains, a slow rise in $\dot{V}O_2$ values is often observable 3 min or so after this transition [1, 35, 36, 91]. In some cases, this slow rise may start as early as 90-180 s after the WR transition [10], like noticeable around t = 95 s in Figure 2.6.

As explained in Section *7.1*, a differentiation must be made between this phenomenon itself—in this work referred to as the $\dot{V}O_2$SA—and its modeling under the specific perspective of the FOME model, that is, the SC. Additionally, as remarked by Gaesser and Poole [36], this phenomenon must not be confused with the "O_2 drift" [36]—also referred to as "$\dot{V}O_2$ drift" [129, 130] or "cardiovascular drift" [130]—observed after one hour or more of exercise and not usually associated with an augmentation of blood lactate concentration [36], unlike the $\dot{V}O_2$SA [39, 41, 96, 98, 99]. Due to the adoption of the FOME model and, consequently, the use of the SC for modeling the $\dot{V}O_2$SA, the literature has been referring to this phenomenon by using the homonymous denomination of "slow component" in $\dot{V}O_2$ kinetics [1, 37-45, 91].

Origin of the $\dot{V}O_2$SA phenomenon. In general terms, the etiology of the $\dot{V}O_2$SA is assumed to be related with indicators of type II fibers recruitment in the exercising muscles [39, 41, 42, 88, 96-99]. The pattern of this recruitment, however, is still under debate [8, 38, 52-54, 131-133], despite its direct implications to the structure of the $\dot{V}O_2$ kinetics model being assumed. While the physiological aspects of this recruitment are discussed in details in Chapter 7, the mathematical issue regarding the FOS-based representation of the $\dot{V}O_2$SA and the delayed nature of the SC is presented below.

First-order modeling for the $\dot{V}O_2$SA phenomenon. Although the first-order representation of the $\dot{V}O_2$SA may not represent *per se* a modeling issue (see Chapter 5), the arrangement between the

FOS-based exponential components required by the FOME model in order to reproduce the "protuberance" (or "bump") observed in $\dot{V}O_2$ step responses manifesting this phenomenon (Figure 2.11.A; combined response, CR) may be a source of controversy.

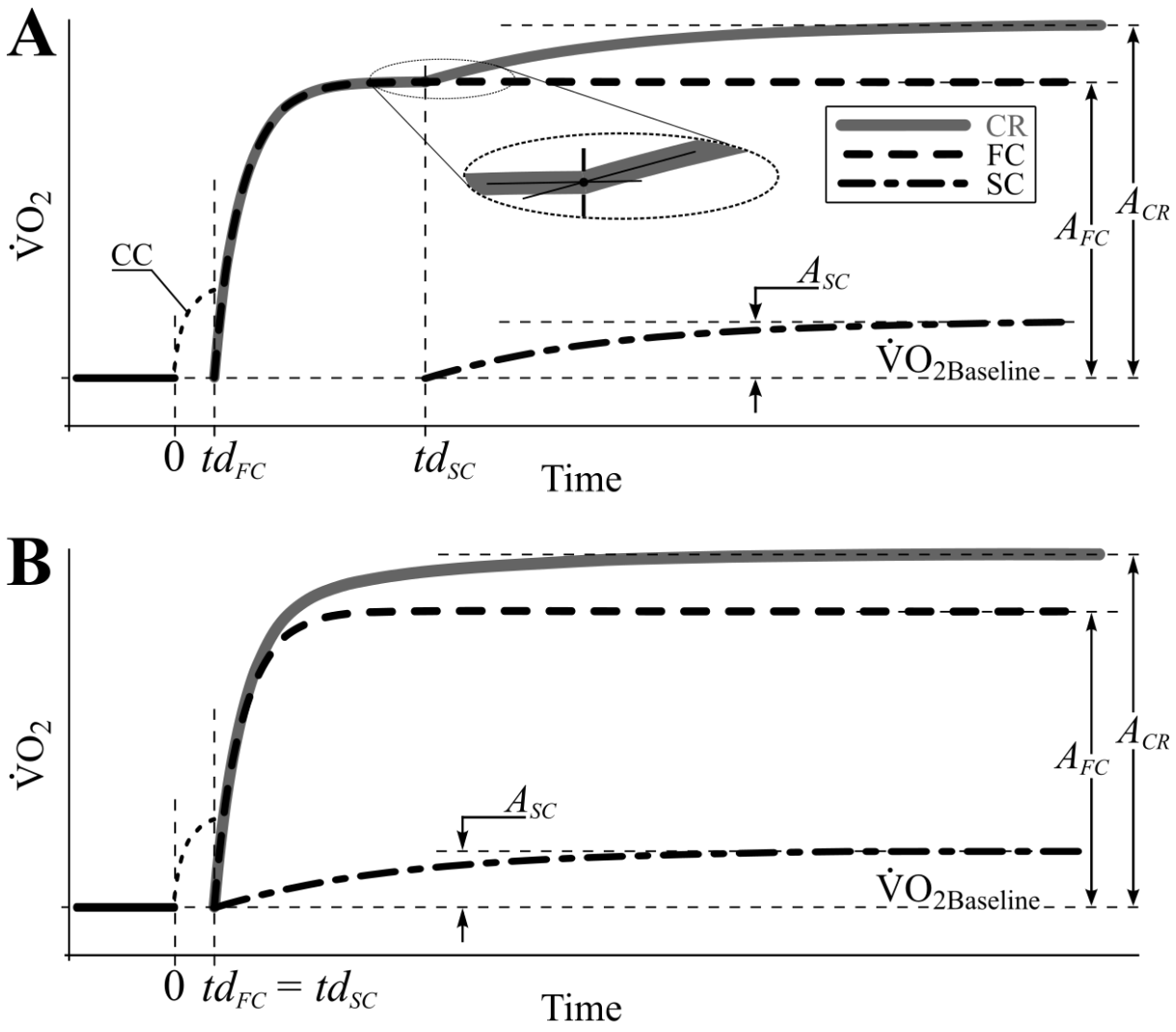

Figure 2.11 Representations of $\dot{V}O_2$ combined responses to the step stimulus formed by a FC summed to either A. a delayed SC or B. a simultaneous SC.

From the inspection of Figure 2.11, it becomes evident that the accentuated increase in $\dot{V}O_2$ values observed at the beginning of the $\dot{V}O_2$SA (see detail on Figure 2.11.A) is only possible for the FOME model if the td_{SC} is greater than the td_{FC}, and not for a model with both first-order-based FC and SC starting at the same time (i.e., $td_{SC} = td_{FC}$, as in Figure 2.11.B)—See Appendix B for a mathematical proof of this assertion.

Conceptually speaking, the FOME model relies on the assumption that the physiological events causing the SC present an onset delay much longer than those causing the FC. Such an assumption, however, may not be adequate in terms of its physiological background [8, 45, 53, 134-136] (see Chapter 7), and when combined with the results from studies demonstrating poorer fitting performances for the model with simultaneous rather than non-simultaneous first-order components [88, 91], it exposes the dilemma inherent to the FOS-based modeling of the $\dot{V}O_2SA$ phenomenon.

In Chapter 7, these conceptual issues of assuming a delayed SC are readdressed, with a model based upon second-order components being presented and proven to offer a better fitting performance than that of the FOME model. Conveniently, the assumption of a delayed nature for the physiological causes of the $\dot{V}O_2SA$ is not required by this alternative model.

CHAPTER 3 OBJECTIVES AND HYPOTHESES

3.1 Models proposed in this study

In this thesis, two models for the $\dot{V}O_2$ kinetics in humans are presented as alternatives for the currently accepted FOME modeling (Figure 3.1; top panel), namely the Mixed Multi-Exponential (MiME) model and the Second-Order Simultaneous Components (SOSC) model, generally depicted in the middle and bottom panels of Figure 3.1, respectively.

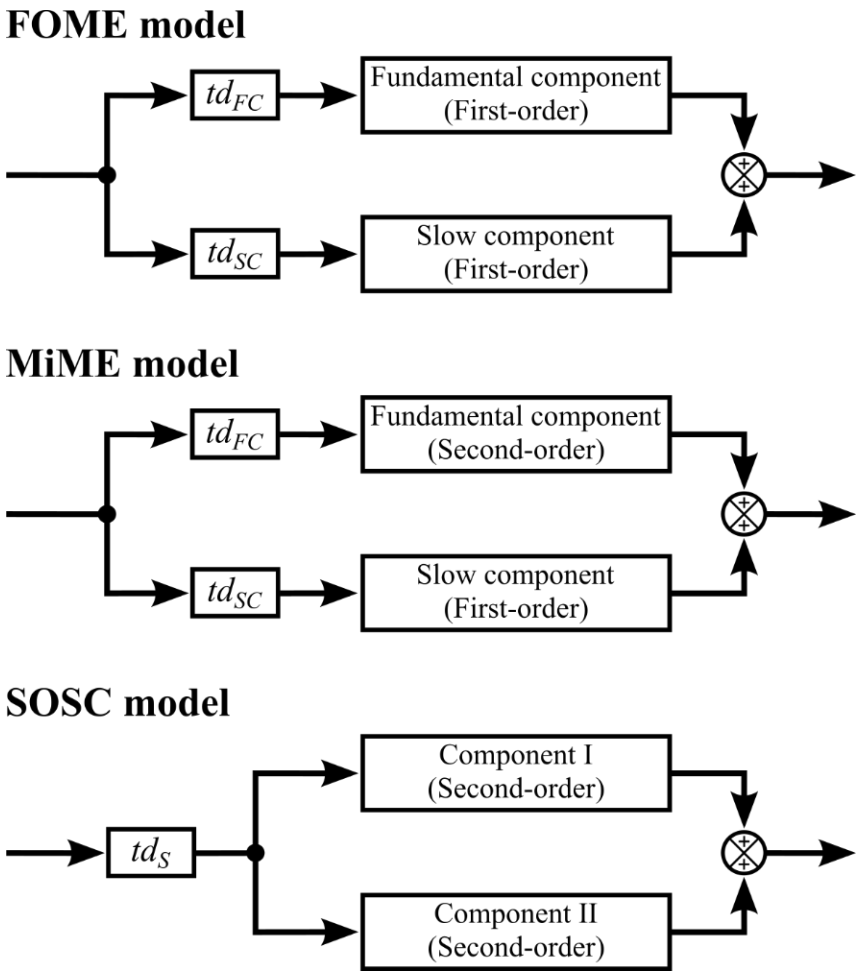

Figure 3.1 Block diagrams of the First-Order Multi-Exponential (FOME) model (top), the Mixed Multi-Exponential (MiME) model (middle), and the Second-Order Simultaneous Components (SOSC) model (bottom) proposed in this work. The cardiodynamic component (here suppressed for clarity purposes) occurs at the beginning of all three described models, and is represented by a first-order exponential. See text bellow for details.

A complete description comprising the composition, mathematical formulations, mechanistic bases, and evaluation methodologies of the MiME and SOSC models are presented in Chapters 5 and 7, respectively, with Chapters 6 and 8 complementing this characterization.

Very briefly, the MiME model is composed of: a transitory initial FOS-based cardiodynamic component, starting at $t = t_0$; a SOS-based fundamental component (FC), delayed by a time period td_{FC}; and a not always present slow component (SC), represented by another FOS exponential that, when manifested, starts after an onset time delay td_{SC}. In all cases, $td_{SC} > td_{FC} \geq t_0$.

As for the SOSC model, it is composed of a transitory initial FOS-based cardiodynamic component, starting at $t = t_0$, and of two SOS-based components I and II (CI and CII, respectively), always present and simultaneously starting after an onset time delay $td_S \geq t_0$.

In face of the exposed issues associated with the widely accepted FOME model, and considering the potentiality of the SOS-based solutions in modeling particularly "unexpected" data behaviors, this study's fundamental research question is formulated as follows: "Is the oxygen uptake kinetics in humans in better agreement with a second-order system model than with the currently adopted first-order system theory?"

3.2 Objectives and hypotheses

The answer to this research question is obtained by means of the accomplishment of the *general* and *specific objectives* defined below (Sections *3.2.1* and *3.2.2*), supported in quantitative terms by the testing of *hypotheses 1* and *2* (Section *3.2.3*).

3.2.1 General objective

To develop and implement a comprehensive model for the $\dot{V}O_2$ kinetics in humans capable of comprising none, either, or both of the O$\dot{V}O_2$K and/or $\dot{V}O_2$SA phenomena observed in response to the step on-transient at any exercise intensity.

3.2.2 Specific objectives

Specific objective 1: To implement the MiME model for the $\dot{V}O_2$ kinetics in humans;

Specific objective 2: To define and implement an objective methodology for detecting and quantifying the O$\dot{V}O_2$K phenomenon in step on-transient responses;

Specific objective 3: To implement the SOSC model for the $\dot{V}O_2$ kinetics in humans; and

Specific objective 4: To compare the performances of the FOME, MiME, and SOSC models for fitting and describing $\dot{V}O_2$ step on-transient responses at all exercise intensities, containing none, either, or both of the O$\dot{V}O_2$K and/or $\dot{V}O_2$SA phenomena.

3.2.3 Hypotheses

Hypothesis 1: The MiME model presents a better overall fitting performance than that of the FOME model for $\dot{V}O_2$ step responses at all WRs, either containing or not containing the O$\dot{V}O_2$K phenomenon.

Hypothesis 2: The SOSC model presents a better overall fitting performance than that of the FOME model for $\dot{V}O_2$ step responses at all WRs, containing none, either, or both of the O$\dot{V}O_2$K and/or $\dot{V}O_2$SA phenomena.

3.2.4 Coverage of objectives and hypotheses

The accomplishment of this thesis's *general objective* results from the coverage of its four *specific objectives*. *Specific objectives 1* and *2* are covered in Chapter 5 and complemented in Chapter 6. *Specific objective 3* is covered in Chapter 7, while *specific objective 4* is covered in its whole by the association of Chapters 5 to 9.

Hypotheses 1 and *2* are tested in Chapters 5 and 7, respectively. Additional analyses presented in Chapters 6 and 8 corroborate the confirmation of both *hypotheses 1* and *2*.

A more detailed description of the coverage of the objectives and hypotheses defined above is available in Section *10.1 Objectives accomplishment and hypotheses testing*.

CHAPTER 4 METHODOLOGY

4.1 Content of the methodology chapter

As explained in the introduction of this thesis, the format by articles of the document prescribe the concentration of relevant content in those chapters intended to the publication as independent scientific papers. In this context, the purpose of the present chapter is to complement the methodological sections of these articles with any specific information, images, and technical details that are not in accordance with the conciseness preconized by scientific journals.

4.2 Sample, equipment, and experimental procedures

The data collection stage of this study was performed during the first trimester of 2016, in the Physical Effort Laboratory (Laboratório de Esforço Físico, LAEF; Figure 4.1), located at the Sports Centre of the Federal University of Santa Catarina (UFSC, Brazil). All experimental procedures described in this work were approved by the UFSC's Ethics Committee for Research with Human Beings, under the process number 51223015.0.0000.0121.

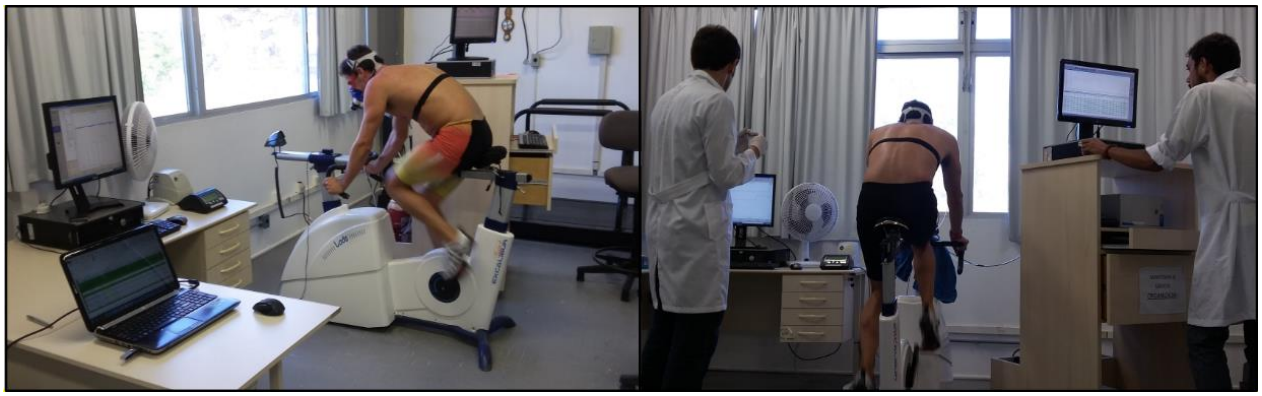

Figure 4.1: The Physical Effort Laboratory facilities at the UFSC, Brazil

Every subject has been informed about any discomfort and risk related to the tests and has signed an Informed Consent Form. Additionally, an individualized summary report containing the results from the incremental step test (Section *4.2.3 Incremental step test*) was provided to each participant as a courtesy feedback (see Appendix C for an example of the report and Appendix D for its version in English).

The fundamental information regarding the sample of the study, the equipment used, the experimental procedures, and the data processing are available in the *Materials and methods* Sections of Chapters 5 and 7. Nevertheless, for contextualization and complementation purposes, this methodology subsection presents additional information about these topics' aspects.

4.2.1 Sample

The experimental sample was composed of 14 well-trained cyclists (mountain and/or road bikers) and triathletes with no history of serious injury, and at least three years of cycling background. While data from the 14 subjects is considered in Chapters 5 to 7, a sub-group of seven subjects is defined in Chapter 7 and used in Chapters 7 and 8.

4.2.2 Equipment

Electromagnetically braked cycle ergometer. Excalibur Sport (Figure 4.2), from Lode Medical Technology (Groningen, The Netherlands) [137]. This equipment allowed the imposition of a customized workload protocol and an accurate reproduction of the athlete's personal bicycle configuration (pedal model, seat and handle bars positions) in the testing context.

Figure 4.2 Electromagnetically braked cycle ergometer Lode Excalibur. Adapted with permission from [137].

Moreover, although the athletes could avoid variations in their pedaling frequency (i.e., cadence) by monitoring it in a feedback display, the cycle ergometer was used in its constant workload mode, where the power imposed by the athlete to move the pedals remains as designed in the protocol—via compensations in the resistant torque—regardless of reasonable cadence variations.

Respiratory gas analyser: Quark CPET (Figure 4.3), from Cosmed (Rome, Italy) [138]. The quick response from the bidirectional turbine flow meter, combined with paramagnetic and nondispersive infrared sensors for measurements of O_2 and CO_2 contents, respectively [139], provided a breath-by-breath evaluation of respiratory variables. Additionally, the anatomical mouth and nose mask connected to the analysis unit by a sampling tube and a connection cable of reduced diameters ensured satisfactory comfort and freedom of movement for the subjects.

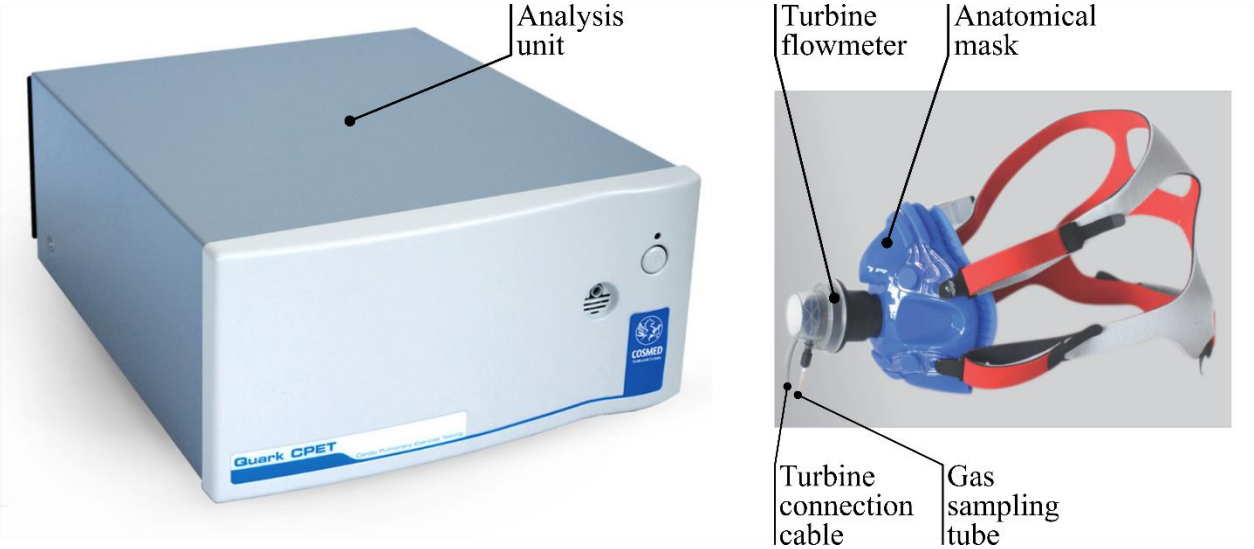

Figure 4.3: Respiratory gas analyser Cosmed CPET, composed of the analysis unit (*left*) and the sampling set (*right*). Adapted with permission from [138].

Biochemistry Analyzer. Blood lactate concentration ([Lac]) evaluations were performed in an YSI 2700 Select (Yellow Springs, USA) [140] (Figure 4.4.A), with the equipment's automatic self-calibration protocol being executed before every round of measurements.

Heart rate monitor. The Polar DataLink system **(**Kempele, Finland) [141], composed of a chest strap sensor (see Figure 4.6.B) wirelessly connected to an USB reception module, was used for registering the time course of the hearth rate (HR) data in a computer.

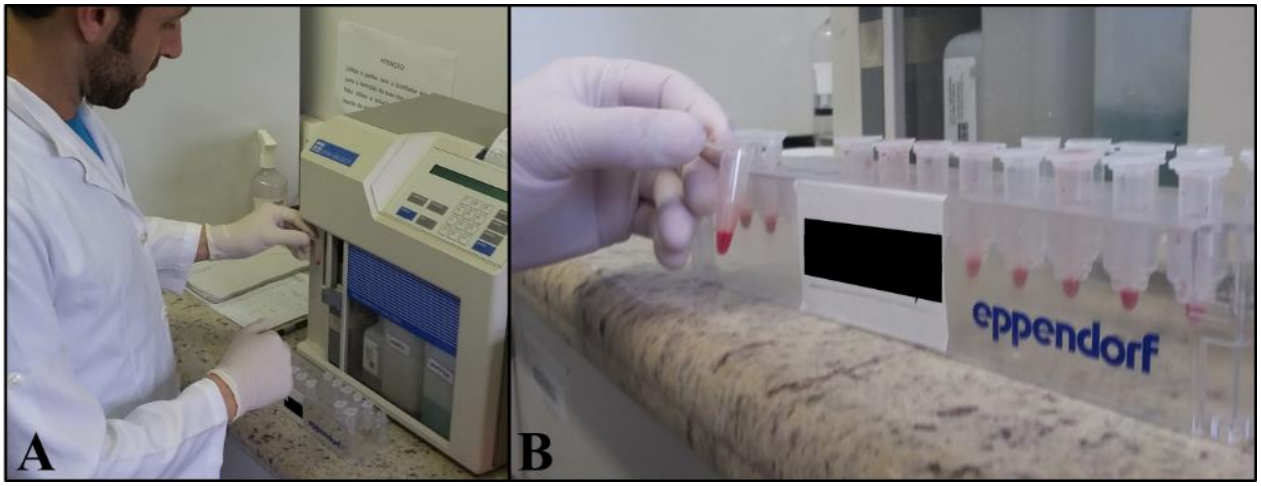

Figure 4.4: A. Evaluation of [Lac] in the Biochemistry Analyzer YSI 2700 Select; B. Detail of the blood samples in the Epperndorf tubes.

Stadiometer. A $5 \cdot 10^{-4}$ m resolution stadiometer Sanny ES2020 (São Bernardo do Campo, Brazil) [142] was used to measure the stature of each subject.

Weighing scale. Every subject's body mass was measured with a 0.1 kg resolution digital Sohenle weighing scale (Nassau, Germany) [143].

4.2.3 Incremental step test

Performed in the first visit to the laboratory, the incremental step testing protocol started with an unloaded warm up period of three minutes, during which the subject could chose his preferred cadence. As described in Figure 4.5, the test continued with subsequent step increments of 25 W, each one lasting for three minutes to ensure satisfactory stability of the [Lac] at its end [144]. The test was completed when the subject could no longer maintain the chosen cadence, despite intense verbal motivation from the researchers. Right after the end of the test, the subjects selected a very low WR at which they remained for an active recovery period of at least three minutes.

Lactate threshold. A 25-µl blood sample was collected from the subject's earlobe during the last 20 seconds of each step with a glass capillary tube pre-calibrated with heparin (Figure 4.6.A-B). Each sample was diluted in 50 µL of a sodium fluoride solution (at 1%) in an Eppendorf tube [145] prior to biochemical analysis (Figure 4.4.B and Figure 4.6.B).

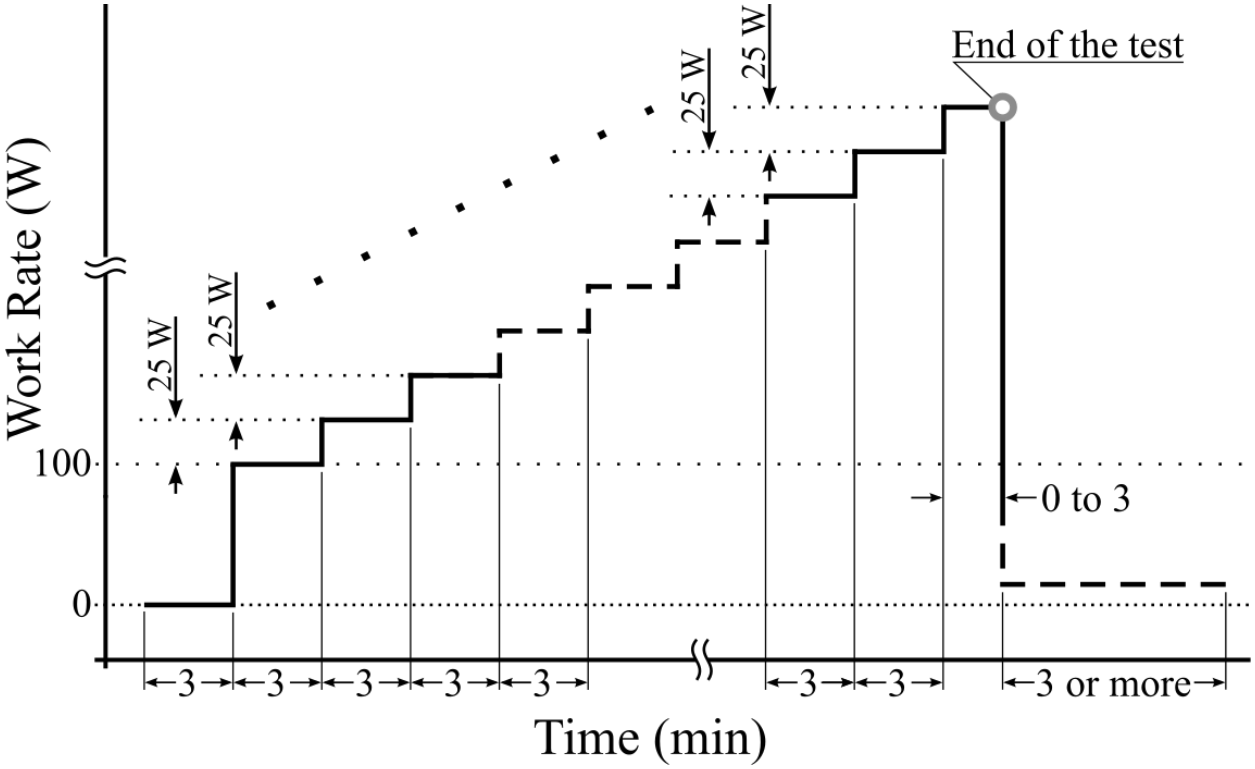

Figure 4.5: Incremental step test protocol applied during the first visit of each subject.

Figure 4.6: A. Blood sampling from the subject's earlobe; B. Glass capillary and Epperndorf tubes.

The typical behavior of the [Lac] values attained at the end of each stage is depicted in Figure 4.7.A. With the aid of plots generated in MATLAB (The MathWorks Inc., Natick, USA), the

intensity referent to the subject's LT (WR_{LT}) was set at the maximal WR preceding an evident blood lactate accumulation above baseline [144, 146]—e.g., the WR_{LT} of 175 W in Figure 4.7.A.

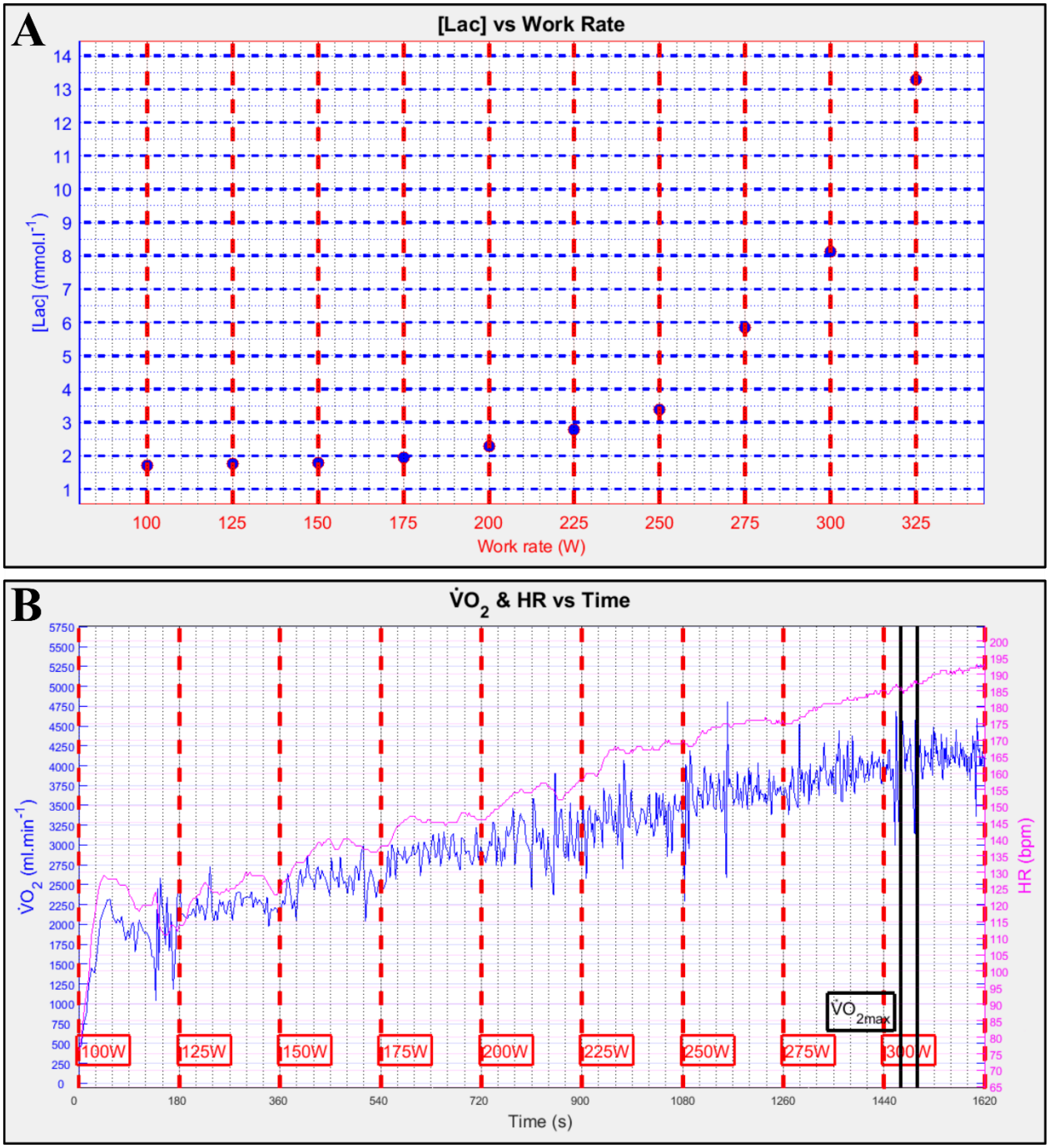

Figure 4.7: Plots from a MATLAB inspection and evaluation routine showing A. the [Lac] values at the end of each WR stage, and B. the timecourses of $\dot{V}O_2$ and HR during the incremental step test for *subject 6*. Similar plots for *subject 13* are available in Appendices C and D.

Maximal oxygen uptake. The $\dot{V}O_{2max}$, evaluated as the highest 30-s mean $\dot{V}O_2$ value observed during the test, and the $WR_{\dot{V}O2max}$, set as the smallest WR at which the $\dot{V}O_{2max}$ occurred, were automatically extracted for every subject, as depicted in Figure 4.7.B. Whenever an individual reached his $\dot{V}O_{2max}$ during a WR stage terminated before the intended 3-min duration, his $WR_{\dot{V}O2max}$ was estimated proportionally to the time sustained at that intensity by means of a linear interpolation between the WR of the incomplete step and that of the previous one.

Maximal work rate. Because some individuals may be able to continue the incremental test until reaching a WR higher than that at which his $\dot{V}O_{2max}$ was observed, the highest exercise intensity attained at the step incremental test (WR_{max}) was also registered. For tests terminated before the completion of a given step, the same interpolative procedure adopted for the $\dot{V}O_{2max}$ was followed.

4.2.4 Square wave tests

Once the WR_{LT} and $WR_{\dot{V}O2max}$ values for a given subject were identified, a special set of three different protocols could be personalized for the athlete so the relative physiological effort would be similar for every individual. Figure 5.4 provides a graphic description of these protocols, each one performed in the second through fourth visits to the laboratory in randomized order. In total, a set of 13 square waves were applied in order to cover all domains of exercise intensity at which a $\dot{V}O_2$ steady-state is observable, namely:

Moderate intensity domain. Three square waves at each of three intensities, respectively referent to 55, 70 and 85% of the WR_{LT} (55%LT, 70%LT, and 85%LT, respectively). The application of these moderate intensities is justified by the tendency of the O$\dot{V}O_2$K phenomenon to occur at sub-LT WRs (see Section *2.6.1 The phenomenon of the overshoot in the $\dot{V}O2$ kinetics* for details). Additionally, the use of different sub-LT WRs aimed to provide information about the O$\dot{V}O_2$K characteristics and to test our proposed models at different exercise intensities.

Heavy intensity domain. Two square waves at an intensity referent to the WR_{LT} added by 40% of the difference between the WR_{LT} and the $WR_{\dot{V}O2max}$ (40%Δ). The application of this supra-LT intensity was aimed at obtaining data that manifested the $\dot{V}O_2$SA phenomenon. Moreover, in association with the transitions to the severe exercise domain (see next paragraph), these heavy transitions could provide a broader characterization and modeling of the $\dot{V}O_2$SA phenomenon.

Severe intensity domain. Two square waves at an intensity referent to the WR_{LT} added by 70% of the difference between the WR_{LT} and the $WR_{\dot{V}O2max}$ (70%Δ). The application of this WR greater than the 40%Δ one was chosen not only to complement the characterization and modeling of the $\dot{V}O_2$SA throughout different WRs, but also to ensure the observation of this phenomenon for at least one WR, since its amplitude is found to be more pronounced at higher than at lower supra-LT step stimuli [36, 71].

4.2.5 Pretreatment of data and curve regressions

For every subject, each group of equal intensity square waves was divided into a pair of step responses (i.e., on- and off-transients), with the step on-transients being considered from t_0 – 60 s to the end of the higher level WR, that is, t_0 + 360 s for the sub-LT WRs, and t_0 + 900 s for the supra-LT ones. By means of specifically designed routines and interface tools coded in MATLAB, clearly errant breaths—caused by coughing, sighing, swallowing, or talking—and points distancing more than four standard deviations (SD) from the local means were removed from data—with SD and means calculated using two points to the left and to the right of the evaluated value [48]. The remaining breath-by-breath points were linearly interpolated to generate a $\dot{V}O_2$ value for each entire second (Figure 4.8; *blue* plots). Subsequently, data from trials at the same WR were time aligned, merged, and averaged into one single response (Figure 4.8; *green* plots).

Finally, the points of each of these combined data sets were regrouped in 5-s bins, with the time reference set at the center of the bin interval to avoid time shift distortions (e.g., the mean $\dot{V}O_2$ value of seconds 26 to 30 was set at t = 28 s).

After this pretreatment stage, the optimal parameters for all solutions presented in Chapters 5 to 8 were obtained by iterative routines specifically coded in MATLAB. The regression curves for these solutions were obtained with the non-linear least squares technique based in the Gauss-Newton method.

In Chapters 5 to 7, the equations of each proposed solution used in the regressions are presented together with the physiological contextualization of their parameters. Additionally, these chapters describe the manner in which these solutions' curves are combined to compose the complete responses of the FOME, MiME, and SOSC models.

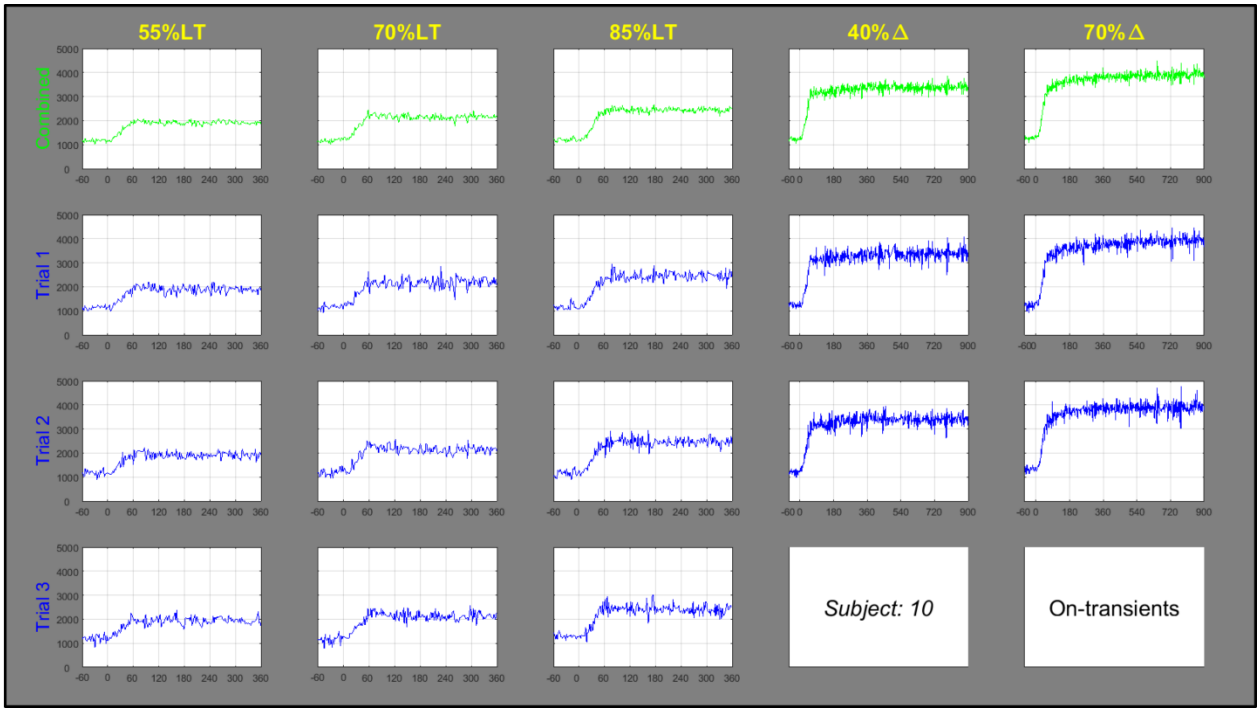

Figure 4.8: Output from the pretreatment code containing "clean" data sets from each trial (*blue* plots) and the average responses for each WR tested (*green* plots).

4.2.6 Additional considerations on the experimental protocol

The choice for the step stimulus has been justified in Section *2.5 Step stimulus: advantages and modelling characteristics.* However, the orientation of this study's experimental protocol towards the time domain analysis of $\dot{V}O_2$ responses is also motivated by inconveniences found in the frequency domain approach. Modeling and methodological issues intrinsic to the application periodic functions such as the sinusoidal input may discourage the adoption of this approach in the context of $\dot{V}O_2$ kinetics, namely:

System linearity and time-variance. The classic frequency approach applied in $\dot{V}O_2$ studies assumes the time-invariance and the linearity of the stimulated system [92, 117, 118, 120]. However, the complete response of the SOSC model (Chapters 7 and 8) is composed of two components whose individual gains do not vary linearly with the amplitude of the WR (see Section *7.2.1 The Second-Order Simultaneous Components model*). A possible solution for this inconvenient is the restriction of the WR input to a range strictly below the WR_{LT}, where the non-linear aspect of the SOSC model is less important (see *Sub-LT intensities* in Section *7.4.1*) and a

reasonable linearity is accepted for the FOME [54, 82, 118, 120] and MiME [57] models. In that case, however, the characterization of these models for the whole WR spectrum is not possible.

Moreover, even if a linearity region is assumed beyond the moderate domain, the FOME and MiME models would still be affected by a time-variance issue in the case, for instance, of a sinusoidal stimulus, since the system is deeply altered by the mandatory "activation" of the SC whenever the WR surpassed the WR_{LT} value (and vice-versa). This issue becomes even more complex due to the fact that, even at constant a WR, the SC is only considered present after $t = td_{SC}$ (Figure 2.6), making unclear, in the case of a varying WR, when to incorporate it to the model.

Extension of the experimental period. The large amount of laboratory visits required from each subject may not be feasible for a sample formed by high-level athletes, whose training schedules are necessarily affected by the data collection sessions. A combination of three methodological issues is the cause of this inconvenient:

- Considering the low signal-to-noise ratio of $\dot{V}O_2$ measures, two or more responses to a same stimulus (i.e., to a same frequency) must be collected for each subject, so then a more robust average response may be obtained;
- When imposing a sequence of sinusoidal exciting waves for frequency analysis, it is a common practice to discard the first entire cycle to avoid transitory effects; and
- A satisfactory frequency domain analysis should cover a certain range of frequencies (gathering enough data for the proper elaboration of Nyquist diagrams or Bode plots). Reference studies have used up to five [92, 120] or even six [117, 118] non-zero frequencies values.

These aspects taken together may cause, in some cases, the necessity of up to seven [118] or eight [117] laboratory visits from each individual.

4.3 Resources

The development of the present research work was possible thanks to the financial support provided by the CAPES Foundation (Ministry of Education, Brazil), under the scope of the Science without Borders Program (process number 13546/13-9).

CHAPTER 5 ARTICLE 1: SECOND-ORDER MODELING FOR THE PULMONARY OXYGEN UPTAKE ON-KINETICS: A COMPREHENSIVE SOLUTION FOR OVERSHOOTING AND NONOVERSHOOTING RESPONSES TO EXERCISE

Luis A. P. de Lima[a,b], Maxime Raison[a], Sofiane Achiche[a], and Ricardo D. de Lucas[c]

[a]*Mechanical Engineering Department, Polytechnique Montréal, Quebec, Canada;* [b]*CAPES Foundation (Brazilian Ministry of Education), Brasília, Distrito Federal, Brazil; and* [c]*Sports Centre, Federal University of Santa Catarina, Florianópolis, Santa Catarina, Brazil*

Journal of Applied Physiology. Submitted 12 February 2018; accepted in final form 7 June 2018.

de Lima LAP, Raison M, Achiche S, de Lucas RD. Second-order modeling for the pulmonary oxygen uptake on-kinetics: a comprehensive solution for overshooting and nonovershooting responses to exercise. *J Appl Physiol* 125: 1315–1328, 2018. First published June 14, 2018; doi:10.1152/japplphysiol.00147.2018.[9]—The human oxygen uptake ($\dot{V}O_2$) response to step-like increases in work rate is currently modeled by a First-Order System Multi-Exponential (FOME) arrangement. Because of their first-order nature, none of FOME model's exponentials is able to model an overshoot in the oxygen uptake kinetics ($O\dot{V}O_2K$). Nevertheless, $O\dot{V}O_2K$ phenomena are observed in the fundamental component of trained individuals' step responses. We hypothesized that a Mixed Multi-Exponential (MiME) model, where the fundamental component is modeled with a second- instead of a first-order system, would present a better overall performance than that of the traditional FOME model in fitting $\dot{V}O_2$ on-kinetics at all work rates, either presenting or not $O\dot{V}O_2K$. Fourteen well-trained male cyclists performed three step on-transitions at each of three work rates below their individual lactate thresholds' work rate (WR_{LT}), and two step on-transitions at each of two exercise intensities above WR_{LT}. Averaged responses for each work rate were fitted

[9] Address for reprint requests and other correspondence: L. A. Pereira de Lima, Doctoral Program in Biomedical Engineering, Mechanical Engineering Dept. of Polytechnique, Montréal, 2500, Chemin de Polytechnique, H3T1J4 Montreal, QC, Canada (e-mail: luis.delima@polymtl.ca).

with MiME and FOME models. Root mean squared errors were used for comparisons between fitting performances. Additionally, a methodology for detecting and quantifying O$\dot{V}O_2$K phenomena is proposed. Second-order solutions performed better ($P < 0.000$) than the first-order exponential when the O$\dot{V}O_2$K was present, and did not differ statistically ($P = 0.973$) in its absence. O$\dot{V}O_2$K occurrences were observed below and, for the first time, above WR_{LT} (88 and 7%, respectively). We concluded that the MiME model is more adequate and comprehensive than the FOME model in explaining $\dot{V}O_2$ step on-transient responses, considering cases with or without O$\dot{V}O_2$K altogether.

NEW & NOTEWORTHY To our knowledge, this is the first study applying second-order system equations to model $\dot{V}O_2$ on-kinetics, which is useful for both mathematical representation and physiological understanding of the overshoot phenomenon manifesting in the fundamental components of some step responses. Moreover, an objective methodology for detecting and quantifying this overshoot that considers data from the whole response is proposed. Finally, this is the first work detecting overshoot occurrences outside the moderate domain of exercise.

Modeling; oxygen uptake kinetics; overshoot; second order; $\dot{V}O_2$.

5.1 Introduction

The exponential nature of the transient behavior of pulmonary oxygen uptake ($\dot{V}O_2$) responses in exercising individuals has been recognized since 1913 [33]. However, only since the 1970s has a special interest for the analysis in both time [110, 113] and frequency domains [82, 118, 120, 147] been clearly reported in the studies investigating the dynamics inherent to the human body's respiratory system, specially due to the breath-by-breath measurement advent. Following system identification techniques [55, 148, 149], these studies on $\dot{V}O_2$ kinetics make use of different types of Work Rate (WR; see Glossary for definition of other parameters[10]) manipulation as input stimuli to exercising subjects, such as altering the resistance load on a cycle-ergometer or the running speed on a treadmill.

[10] Glossary of abbreviations appears at the end of this chapter.

The WR step on-transient is the most used type of stimulus, where a sudden increase in WR from a lower level to a higher one is applied at a given time t_0. For the response to the step stimulus, researchers have been favoring models based upon first-order systems (FOS) dynamics, the *First*-Order Multi-Exponential model (or FOME model, as defined in the present paper) being the most accepted [1, 91, 150]. FOME's expression describing the shape of the entire response is composed by a baseline value ($\dot{V}O_{2Baseline}$), and by the cardiodynamic, the fundamental (FC), and the slow components:

$$\begin{aligned}\dot{V}O_2(t) = \dot{V}O_{2Baseline} + \left[\text{Cardiodynamic Component}(t)\right]_{0 \le t < td_{FC}}, \\ + \left[\text{FC}(t)\right]_{t \ge td_{FC}} + \left[\text{Slow Component}(t)\right]_{t \ge td_{SC}}\end{aligned} \quad (5.1)$$

where the FC is the FOS function FC_{FOS} defined by

$$FC_{FOS}(t) = A_{FC}\left\{1 - \exp\left[\frac{-(t - td_{FC})}{\tau_{FC}}\right]\right\}_{t \ge td_{FC}}, \quad (5.2)$$

and where A_{FC} is the amplitude, and τ_{FC} is the time constant of the FC (see Figure 5.1; dashed curve). The instant t_0 is set to zero, and the onset time delay values td_{FC} and td_{SC} define the instants when the FC and the slow component, respectively, start to contribute to the response. It should be noted that a slow component only appears at exercises above WR_{LT}, i.e., the WR associated with the individual's lactate threshold (LT) [1, 91, 150].

5.1.1 Overshooting behavior and the second-order model

Whereas first-order exponentials face no apparent issues in modeling step response's cardiodynamic or slow components, specific behaviors of the FC preclude the indiscriminate application of the FC_{FOS} expression. Although conceptually inconceivable for the any first-order curve [55, 56], the phenomenon of the overshoot in the $\dot{V}O_2$ kinetics ($O\dot{V}O_2K$), where the O_2 uptake values oscillate above their steady-state reference (Figure 5.1; *grey* curve), has been reported by some studies in the FC of step on-transients responses [12, 46-48, 50].

Literature reported $O\dot{V}O_2K$'s magnitude, evaluated as the difference between the highest data value in the transient phase and that of the steady-state (*Peak-SS*), ranges from 111 [47] to 336 ml·min^{-1} [48], with the peak point between ~45 and ~120 or ~140 s after t_0 in some studies [47, 48], or between 65 and 90 s in another [46].

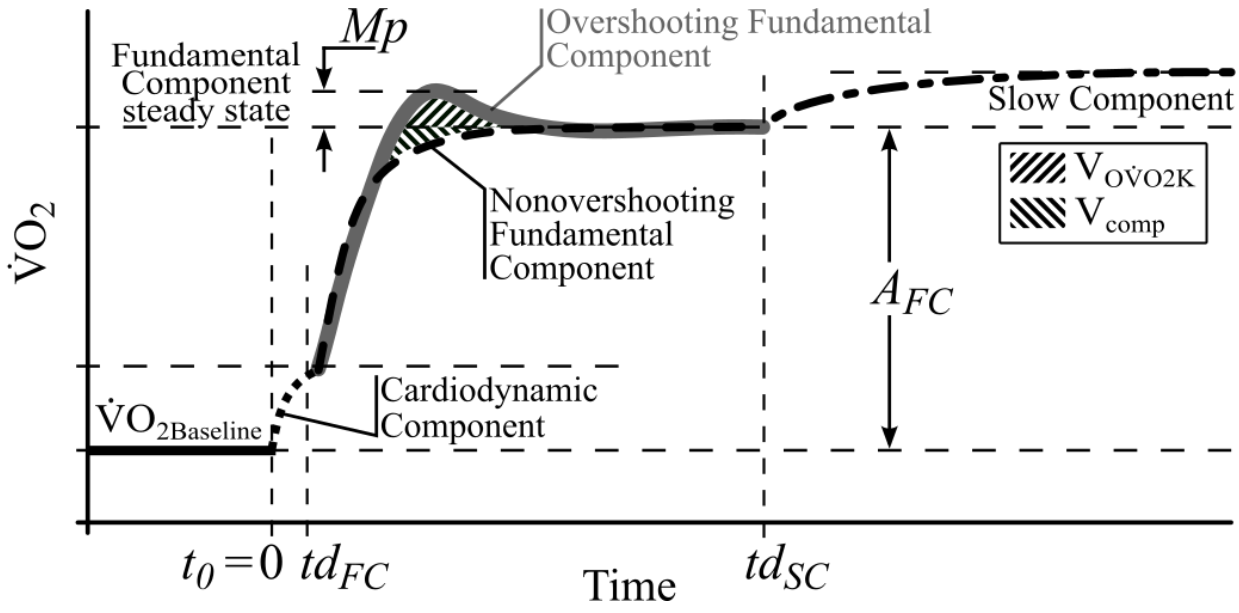

Figure 5.1 Possibly observed $\dot{V}O_2$ responses to the work rate step on-transient, with the overshoot phenomenon either present (*grey* line) or absent (dashed line) in the fundamental component. Other figure's elements are explained in the text.

Articles specifically addressing the $O\dot{V}O_2K$ report that this phenomenon is manifested mainly by trained rather than sedentary individuals [12, 46-48], more frequently at lower WRs [12, 48], and more prevalently in cycling than in running exercise [47]. Regardless of its still debated cause, the repeated $O\dot{V}O_2K$ occurrences under these well-identified conditions, combined with the increase of the *Peak-SS* magnitude and the anticipation of its peak occurrence in response to an endurance training period [12], discredit any suggested artifactual, incidental nature of the $O\dot{V}O_2K$.

In the modeling aspect, as detailed exposed in the following sections, either overshooting or nonovershooting patterns may be properly described by an exponential associated with the step responses of a second-order system (SOS) [55, 56]; so that an alternative to cope with a possible overshooting FC in equation 5.1 could be its replacement with a SOS-based addend.

The resulting Mixed Multi-Exponential (MiME) model, combining the FOS for the cardiodynamic and slow components, with the SOS for the FC, should be flexible enough to describe both overshooting and nonovershooting $\dot{V}O_2$ step responses. The hypothesis of the present study was that the MiME model would present a better overall performance than that of the traditional FOME model in fitting $\dot{V}O_2$ step responses at all WRs, either containing or not containing the $O\dot{V}O_2K$

phenomenon. Additionally, a methodology for detecting the occurrence of the O$\dot{V}O_2$K phenomenon—thus indicating, among SOS solution types, the one suitable to each situation—is proposed as an auxiliary tool for the MiME model application.

5.1.2 Physiomechanical analogy

Considered separately, each of the exponential components composing the FOME model (Figure 5.1) represents itself the time response (output) of a single FOS excited by a step-like stimulus (input) applied to the WR. By analogy, it is possible to find SOS' time responses induced by step stimuli in a variety of contexts, such as electrical circuits or mechanical arrangements [55, 56]. In this paper, due to mechanical systems' visual and intuitive aspects, we use a physiomechanical analogy to illustrate the $\dot{V}O_2$ kinetics in humans and help present our proposed SOS modeling.

For the classical spring-damper FOS described in Figure 5.2, Cr arrow indicates the input signal, or reference value, while the Cp value is the output value, or actual position of the system. Figure 5.2.A represents the system in resting condition (Cr and Cp at $p_{initial}$), similarly to that of $\dot{V}O_2 = \dot{V}O_{2Baseline}$ (output) for the WR at its Lower Level (input) before t_0 on Figure 5.1.

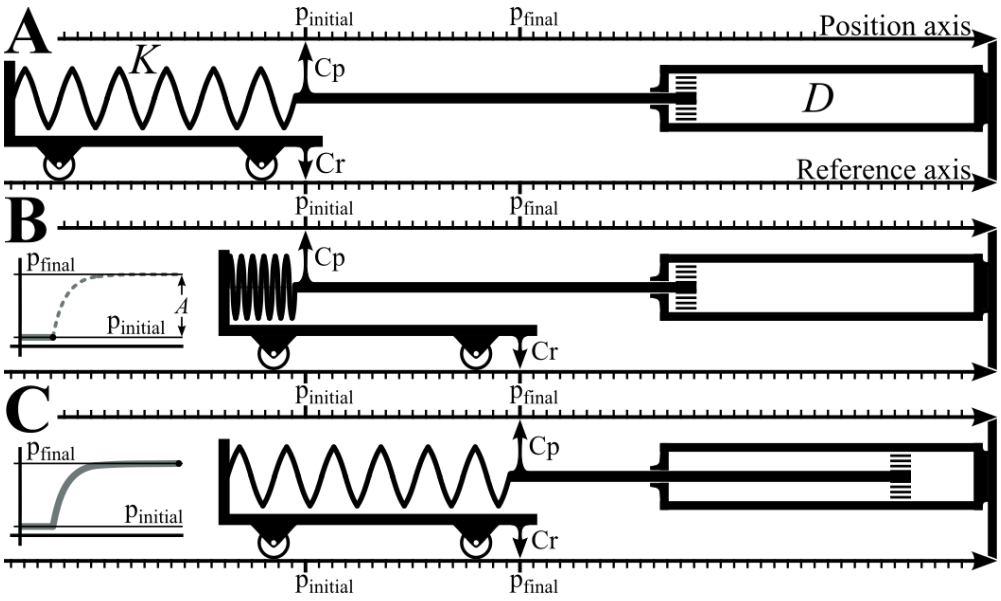

Figure 5.2 Three states of a spring-damper FOS excited by a step stimulus: A. resting condition; B. immediately after the imposition of a step stimulus; and C. asymptotically approaching p_{final} (steady-state reference value). See text for further details.

With the imposition of a sudden, step-like alteration in Cr from $p_{initial}$ to p_{final} (Figure 5.2.B), the tensioned spring (coefficient of elasticity *K*) will move Cp towards that newly set reference. This movement, however, will face a resistance from the damper (damping coefficient *D*), causing Cp to approach p_{final} in an asymptotical manner (Figure 5.2.C), exactly as each first-order $\dot{V}O_2$ component approaches its own steady-state "reference."

In the context of our physiomechanical analogy,[11] the concept of a general *K* coefficient comprises all "responsive" factors related to $\dot{V}O_2$ kinetics' acceleration (such as cardiac debit capacity, degree of vascularization, O_2 availability, or oxidative enzymes content), assuming a higher "value" as such factor are increased. Inversely, the coefficient *D* may comprise those factors imposing a continuously hindering effect on $\dot{V}O_2$ kinetics, such as a cardiopulmonary condition or the use of β-blockers.

Resuming the mechanical first-order configuration of Figure 5.2, an overshoot in Cp, i.e., the attainment of a value in the Position axis beyond p_{final}, is clearly impossible, for there is no force causing the spring to extend beyond its natural resting length. By analogy, it is also impossible for a single FOS component of $\dot{V}O_2$ to reach values above its own steady-state (Figure 5.1; *grey* curve).

In this case, the adoption of a SOS model seems more adequate to describe a possible overshoot in the step response. In our mechanical example, a SOS is obtained by adding an inertial element (mass *M*) to the arrangement, as described on Figure 5.3. Conveniently, depending on the values of *M*, *K* and *D*, the SOS may or may not present an overshoot in its step response.

Starting at the resting condition (Figure 5.3.A), the imposition of a step stimulus (Figure 5.3.B) will still cause the compressed spring to push the embolus to the right. In this case, however, a

---

[11] The definitions of τ, ζ and ω below [55] K. Ogata, "Transient and Steady-State Response Analyses," in *Modern Control Engineering*, K. Ogata, Ed. Fourth ed. Upper Saddle River, New Jersey: Prentice Hall, 2002, pp. 219-336, [56] N. S. Nise, "Time Response," in *Control systems engineering*, N. S. Nise, Ed. Hoboken, New Jersey: J. Wiley & Sons, 2015, pp. 157-298. provide useful insight on the influence of increasing or decreasing the relative importance of coefficients *K*, *D* and *M* over the system's kinetics in both mechanical and physiological contexts:

$$\tau = \frac{D}{K}, \quad \zeta = \frac{D}{2\sqrt{MK}}, \quad \text{and} \quad \omega = \sqrt{\frac{K}{M}}$$

resistant inertial force (acceleration of *M*) will add up to the damper's resistance, changing the whole kinetics of Cp from t_0 on (graph on Figure 5.3.B).

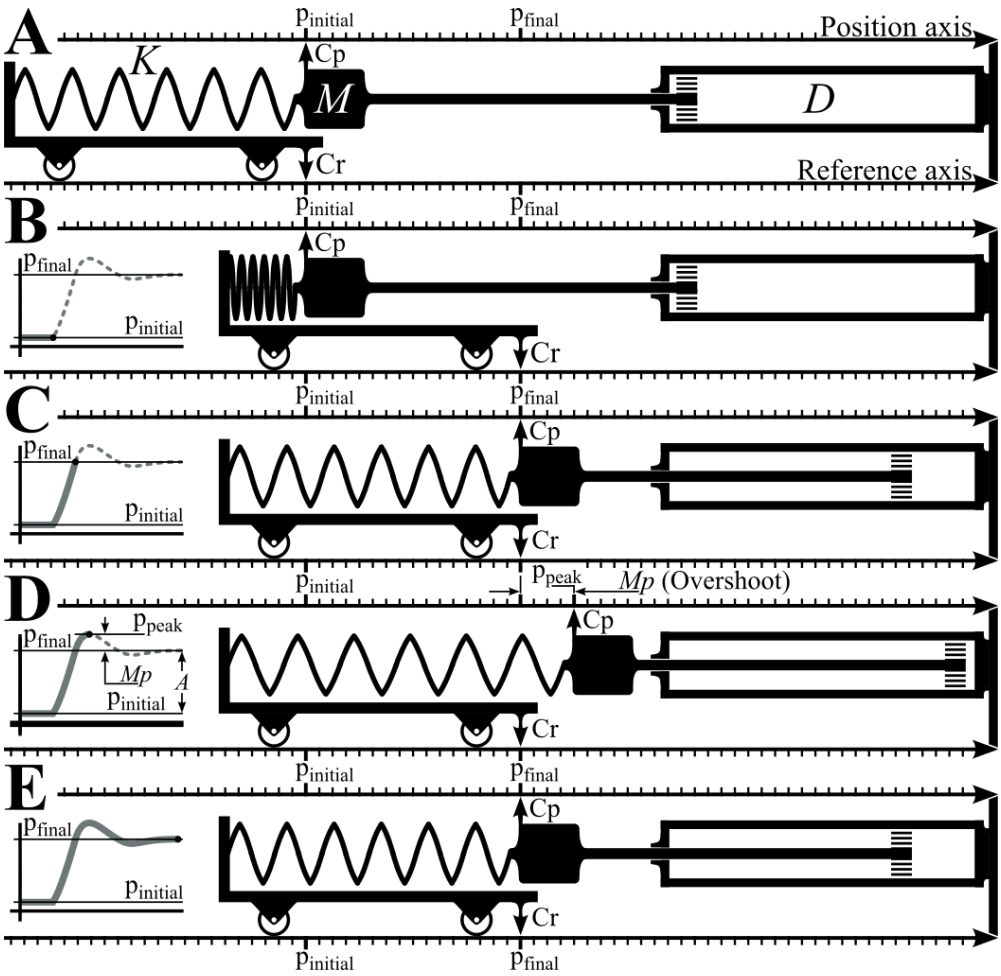

Figure 5.3 Five states of a mass-spring-damper SOS excited by a step stimulus: A. resting condition; B. immediately after the imposition of a step stimulus; C. reaching and in the imminence of overshooting p_{final} due to momentum of mass *M*; D. reaching p_{peak} and inverting displacement sense of Cp; and E. oscillating around p_{final} in a damped fashion. See text for further details.

The overshooting condition arises if *D* is not sufficiently large, i.e., if the SOS is *underdamped*, so the mass *M* will still present momentum when Cp reaches p_{final} (Figure 5.3.C). In that case, Cp will continue to increase beyond p_{final}, being then decelerated by both the spring (now longer than its nominal, resting length) and the damper until its maximal value in the position axis (p_{peak}; Figure

5.3.D) is reached. Subsequently, Cp will follow an oscillatory pattern around p_{final} (Figure 5.3.E), with several overshoots of decreasing amplitudes occurring as the movement is continuously attenuated by the damper. Alternatively, if *D* is large enough in relation to *M* and *K*, thus configuring either an overdamped or a critically damped SOS type, Cp will not overshoot, and will approach p_{final} asymptotically, similarly to a FOS.

Following the physiomechanical analogy, the set of inertial-like behaviors caused by a given coefficient *M* might find a parallel, at the metabolic level, in the transitory effect caused by hormones/metabolites release on both enzymatic activity and vessel diameters in response to WR alterations, and/or in the internal muscle temperature rising. At a more generalist physiological level, this inertial-like manifestation may be related with inter-compartmental differences of O_2 buffering an extraction in its transport chain.

We remark that our concept of inertia is borrowed from Mechanics in its complete sense. More than simply imposing a hampering effect to the '$\dot{V}O_2$ movement' (wrongly associated with a dissipative action), a *true inertia* also implies an amassing effect: just as the accelerated mass on Figure 5.3 may accumulate momentum, eventually contributing to the system's movement (thereby allowing possible oscillations beyond the reference p_{final}), these physiological effects associated with the coefficient *M*, once "activated," may temporarily support $\dot{V}O_2$ levels above the FC's steady-state.

5.2 Materials and methods

5.2.1 Sample and data collection

Fourteen well-trained male athletes (triathletes, mountain and road bikers) with a minimum of three years of cycling experience participated in the study. Prior to data collection, written informed consent was obtained in accordance with the institutional Ethical Committee. Each subject was tested on four different visits, with a minimal 48 hours interval. Athletes were instructed to avoid extreme efforts and to maintain their nutritional routines during the testing period. To avoid biases related to the circadian cycle, large differences in the time of the tests were avoided for any given subject.

All tests were performed on a laboratory cycle ergometer (Lode Excalibur Sport; Lode Medical

Technology, Groningen, The Netherlands). Gas exchange variables were measured with a gas analyzer (Quark CPET; Cosmed, Rome, Italy) using breath-by-breath sampling technology, and the blood lactate concentration ([Lac]) was assessed by a biochemistry analyzer (YSI 2700 Select; Yellow Springs, USA).

First visit: incremental step protocol. On the first visit, every subject had his stature and body mass measured. A customized 'bike fitting' procedure enhanced comfort and allowed reproduction of the athlete's actual position on the cycle ergometer. An incremental step test followed, with the WR starting at 100 W after a 0 W warming up period, and increasing 25 W every third minute. The protocol was terminated when the subject could no longer sustain the cycling cadence he had chosen at the beginning of the test. Table 5.1 displays general information about the study sample.

Table 5.1 Overall characterization of the sample

Characteristics	Mean ± SD
General	
Age, yr	32.5 ± 7.5
Body Mass, kg	68.9 ± 6.6
Stature, cm	172.9 ± 6.7
Absolute $\dot{V}O_{2max}$, $ml \cdot min^{-1}$	4294 ± 429
Relative $\dot{V}O_{2max}$, $ml \cdot min^{-1} \cdot kg^{-1}$	62.6 ± 6.0
Chosen testing cadence ($revolutions \cdot min^{-1}$)	91 ± 4
Cycling experience, yr	9.9 ± 6.6
WR	
Absolute WR_{max}*, W	313 ± 37
Relative WR_{max}*, $W \cdot kg^{-1}$	4.6 ± 0.5
$WR_{\dot{V}O2max}$, W	311 ± 37
WR_{LT}, W	174 ± 23
55%LT, W	96 ± 12
70%LT, W	122 ± 16
85%LT, W	148 ± 19
40%Δ, W	229 ± 27
70%Δ, W	270 ± 32

*WR_{max} is the time interpolated proportion of the WR at the highest step attained in the incremental step test; see text for other variables.

During the last 20 seconds of each step, a 25-µl blood sample was collected from the subject's earlobe for [Lac] assessment. The individualized analysis of [Lac] data allowed identifying the

WR_{LT} of each subject, considered as the exercise intensity immediately before the start of accumulation of blood lactate above baseline values.

From $\dot{V}O_2$ analysis, it was possible to assess the WR relative to the maximal $\dot{V}O_2$ value ($WR_{\dot{V}O2max}$), defined as the maximal average of a 30 s period of data. Both WR_{LT} and $WR_{\dot{V}O2max}$ individual values were used as references to define the intensities (i.e., WRs) performed within the intended intensity domains.

Second to fourth visits: square wave protocols. For each of the second to fourth visits, every subject performed, in randomized order, one of the three square wave protocols depicted in Figure 5.4.A–C. We sought to avoid priming exercise induced biases by optimizing the distribution of tested WRs (lower first) and/or by reproducing literature preconized recovery times [47, 50, 84, 151, 152]. In total, every subject performed three square waves at each of the three selected sub-LT intensities (moderate intensity domain), namely at 55%, 70%, and 85% of WR_{LT}, i.e., 55%LT, 70%LT and 85%LT, respectively. Additionally, the subjects performed two square waves at each of the two selected supra-LT intensities, corresponding to the WR_{LT} added of 40% (heavy intensity domain) and 70% (severe intensity domain) of the difference between WR_{LT} and $WR_{\dot{V}O2max}$ (40%Δ and 70%Δ, respectively).

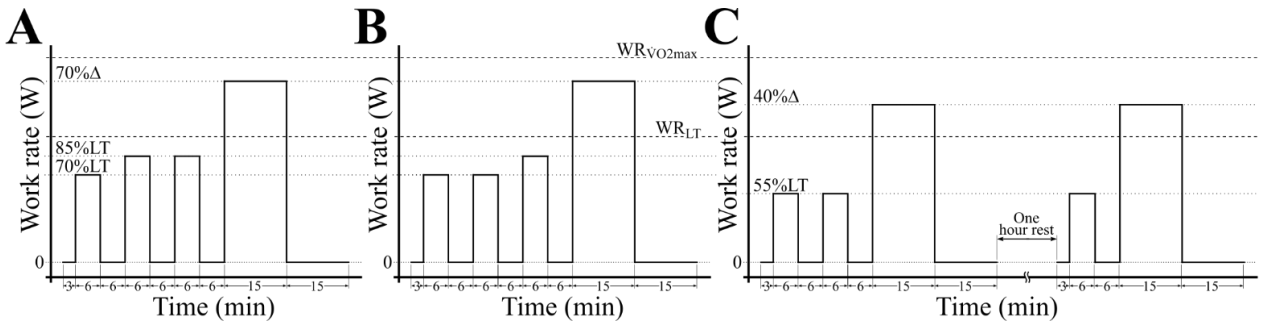

Figure 5.4 A to C: three different square wave protocols performed by each subject in randomized order

Pretreatment of data. Breath-by-breath $\dot{V}O_2$ data from gas analyzer's output files were processed with specifically designed computational codes in MATLAB (The MathWorks Inc., Natick, USA). After selecting every on-transient data between $t_0 = -60$ s and the end of the square wave, each set of $\dot{V}O_2$ values was visually inspected for clearly errant breaths (e.g., coughing, sighing, swallowing, talking). A mathematical inspection was also applied, eliminating any point distancing

more than four standard deviations from the local mean evaluated from its four surrounding values [48].

Remaining points were linearly interpolated for each entire second and, for every WR, the three sub-LT or the two supra-LT responses were time aligned, merged and averaged into a single data set [4, 47, 48]. Points were then grouped into 5-s bins [4], (with time values located at the center of each averaging window, to avoid time shift distortions), which were finally used for curve fitting.

5.2.2 Second-order modeling of the fundamental component

Accordingly to the behavior of the step response's FC, the FC(t) term in the MiME modeling of equation 5.1 may be assigned one of the three possible SOS types, namely, the underdamped, overdamped, or critically damped cases; in our study, they are referred as FC_{Ovsht}, FC_{NOvsht} or $FC_{NOvshtCrit}$, respectively, and formulated as [55]

$$FC_{Ovsht}(t) = A_{FC}\left\{1-\exp(-\zeta\,\omega\,t)\left[\cos(\omega_d\,t)+\frac{\zeta}{\sqrt{1-\zeta^2}}\sin(\omega_d\,t)\right]\right\}_{t\,\geq\,0} \tag{5.3}$$

for $0 \leq \zeta < 1$

$$FC_{NOvshtCrit}(t) = A_{FC}\left[1-\exp(-\omega\,t)\,(1+\omega\,t)\right]_{t\,\geq\,0} \tag{5.4}$$

for $\zeta = 1$

$$FC_{NOvsht}(t) = A_{FC}\left\{1+\frac{\exp\left[-(\zeta+\sqrt{\zeta^2-1})\,\omega\,t\right]}{2\sqrt{\zeta^2-1}(\zeta+\sqrt{\zeta^2-1})}-\frac{\exp\left[-(\zeta-\sqrt{\zeta^2-1})\,\omega\,t\right]}{2\sqrt{\zeta^2-1}(\zeta-\sqrt{\zeta^2-1})}\right\}_{t\,\geq\,0} \tag{5.5}$$

for $\zeta > 1$

In any of them, the introduction of a time delay is possible by the mere replacement of each term t on the right side of the equation with $(t - td_{FC})$, being the $t \geq 0$ requisite accordingly corrected to $t \geq td_{FC}$.

A noteworthy feature of these SOS functions is that their shapes are not given by the τ_{FC} value, but

by two other parameters of the system, namely:

Damping ratio (ζ), a dimensionless value inversely proportional to the speed of the individual's $\dot{V}O_2$ kinetics that indicates the type of SOS solution, being the FC_{Ovsht}, the $FC_{NOvshtCrit}$ and the FC_{NOvsht} respectively associated to $0 \leq \zeta < 1$, $\zeta = 1$ and $\zeta > 1$ [55, 56];

Natural frequency (ω), measured in $rad \cdot s^{-1}$, and directly proportional to the speed of the individual's $\dot{V}O_2$ kinetics. Specifically in the FC_{Ovsht} (equation 5.3), although the variable ω may be used without restrictions, the actually observed oscillations around the steady-state value present a damped frequency (ω_d) defined by [55]:

$$\omega_d = \omega \sqrt{1-\zeta^2} \tag{5.6}$$

Two alternative parameters are the *natural* and the *damped periods* of the system (respectively $2\pi \cdot \omega^{-1}$ and $2\pi \cdot \omega_d^{-1}$). Similarly to τ_{FC}, these periods may constitute convenient kinetics' indicators, for they are also measured in seconds, and also inversely proportional to the speed of the $\dot{V}O_2$ response. However, following the praxis of Control theory in SOS curves representation, the frequency-based approach was retained in our study.

5.2.3 Curve-fitting procedures

Despite the increased complexity of the SOS formulas (equations 5.3 to 5.5) in comparison to the classic FOS solution in equation 5.2, the computational regression method implemented in MATLAB for the former—nonlinear least squares—is the same commonly adopted for the latter. Moreover, some useful properties of these SOS curves allow very good initial parameter estimates[12], which favor the convergence of subsequent iterations and facilitate its use in

[12] For the FC_{Ovsht}, a simple preliminary analysis of data points may provide good estimations for both *tp* and *Mp* values (Figure 5.5). Numerical regression methods may benefit from these estimations by using adequate initial ω and ζ obtained by means of equation 5.8 and the relationships below [55] K. Ogata, "Transient and Steady-State Response Analyses," in *Modern Control Engineering*, K. Ogata, Ed. Fourth ed. Upper Saddle River, New Jersey: Prentice Hall, 2002, pp. 219-336, [56] N. S. Nise, "Time Response," in *Control systems engineering*, N. S. Nise, Ed. Hoboken, New Jersey: J. Wiley & Sons, 2015, pp. 157-298.:

conventional regression software.

Individual A_{FC}, τ_{FC}, and td_{FC} values were preliminarily assessed for each data set by the equation 5.1 considering only the first-order FC—i.e., $\dot{V}O_2(t) = \dot{V}O_{2Baseline} + FC_{FOS}(t)$— and used as reference (respectively referred as A_{ref}, τ_{ref}, and td_{ref}; Figure 5.5) for subsequent analyses. For all tested second-order FC expressions (equations 5.3 to 5.5), A_{FC} was fixed as A_{ref}. $\dot{V}O_{2Baseline}$ was evaluated as the average value for the 60 s preceding t_0 [47, 153] (Figure 5.5). Any interference of the cardiodynamic component was avoided by eliminating the first 20 s of data after t_0 [4, 47, 48, 50, 123], with data being included until instant $t = t_{FC}$.

For sub-LT steps, t_{FC} was set at 240 s to highlight the transitory phase of the FC (Figure 5.5.A). For supra-LT intensities, the instant t_{FC} corresponded to the latest moment when the FC apparently suffered no influence from the eventually manifesting slow component (Figure 5.55.B). As already described in other studies [13, 153], determination of supra-LT t_{FC} followed the analysis of the changes in equation 5.2 exponential regression results (e.g., regression's chi-squared, τ_{FC} and its 95% confidence interval, and plotted residuals) as data points were systematically included in the fitting interval. Four unidentifiable t_{FC} values (WR = 40%Δ) were set at 240 s.

5.2.4 Overshoot detection using the FC_{Ovsht} solution

Because FC_{Ovsht} is only applicable for overshooting cases, whereas $FC_{NOvshtCrit}$ and FC_{NOvsht} are exclusive to nonovershooting responses, an objective criterion to detect the $O\dot{V}O_2K$ occurrence in a data set was required.

In other studies addressing the subject [12, 46-48, 50], any $O\dot{V}O_2K$ occurrence was simply

---

$$\omega = \pi / \left[\left(tp - td_{FC} \right) \sqrt{1 - \zeta^2} \right], \; td_{FC} \text{ from } FC_{Ovsht}$$

$$\zeta = -\ln\left(Mp_{ref} \right) / \sqrt{\ln\left(Mp_{ref} \right) + \pi^2}$$

In the FC_{NOvsht} case, useful preliminary information about ω and ζ values are also available: FC_{NOvsht} solution's FOS-like behavior allows its FOS approximation, yielding the concept of an "approximate" τ (τ_{App}) often comparable to τ_{FC}:

$$\tau_{App} = \left[\omega \left(\zeta - \sqrt{\zeta^2 - 1} \right) \right]^{-1} \approx \tau_{FC}$$

confirmed by the presence of $\dot{V}O_2$ values above the steady-state level. A more conservative and robust criterion based on the overall behavior of data is proposed in this study to avoid the influence of punctual and/or random data oscillations.

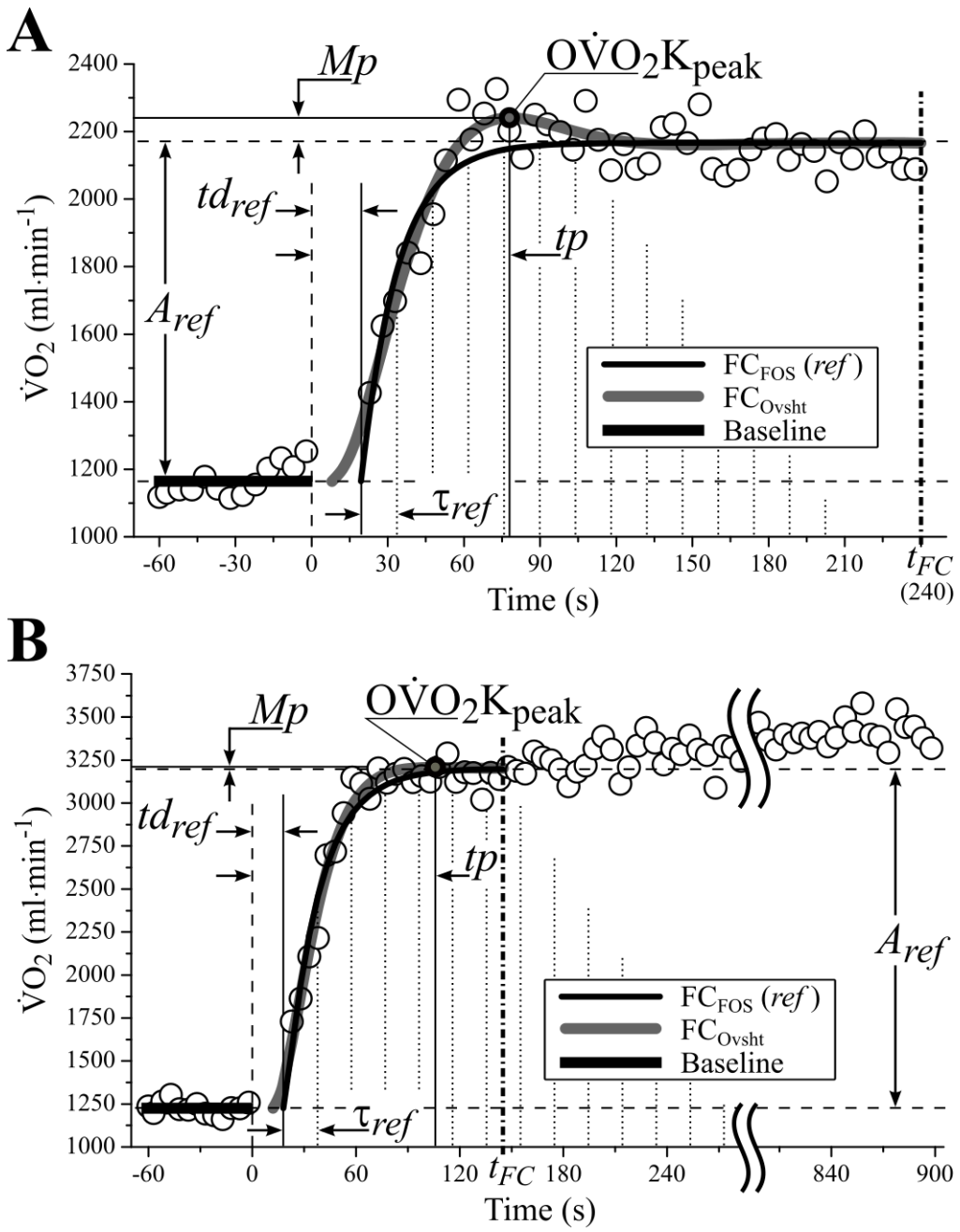

Figure 5.5 Illustrative example of overshoot detection procedure in the FC of A. sub-LT, and B. supra-LT intensities. The parameters A_{ref}, τ_{ref} and td_{ref} from the FOS modeling are used as references (*ref*) for the SOS solutions' regressions and analyses (see text for details).

This innovative criterion (further explained in the Appendix E) was mainly developed with basis on two characteristic values of the FC_{Ovsht} curve, namely the *tp* (instant of occurrence of $O\dot{V}O_2K_{peak}$, the maximal value of the evaluated FC_{Ovsht} curve), and *Mp* (absolute $O\dot{V}O_2K$ amplitude; difference between $O\dot{V}O_2K_{peak}$ and A_{ref}), both represented on Figure 5.5. To account for amplitude and kinetics differences between individuals and WRs, each *tp* and *Mp* were represented in terms of their own subject's FOS model, respectively producing the reference *tp* (tp_{ref}) and the reference *Mp* (Mp_{ref}) values, as follows:

$$tp_{ref} = \frac{tp - td_{ref}}{\tau_{ref}} \tag{5.7}$$

$$Mp_{ref} = \frac{Mp}{A_{ref}} \tag{5.8}$$

Finally, overshooting occurrences were objectively identified by comparing the obtained tp_{ref} values with a fixed threshold ($tp_{ref}T$) equal to five. An $O\dot{V}O_2K$ was confirmed for every data set converging to a FC_{Ovsht} with a valid ζ value ($\zeta \in \mathbb{R} \mid 0 \leq \zeta < 1$) and a $tp_{ref} \leq 5$.

5.2.5 Statistical analyses

For both overshooting ($O\dot{V}O_2K$) and nonovershooting ($NO\dot{V}O_2K$) groups of data sets, goodness of fit comparisons between the models was based on the root mean squared error (RMSE) values from least squares regressions. The choice for RMSE allowed a fair comparison between tested solutions, since it compensates for their different quantities of fitting parameters (i.e., degrees of freedom).

In $O\dot{V}O_2K$ cases, a paired Student's t-test was used for comparison between FC_{FOS} and FC_{Ovsht}, whereas in $NO\dot{V}O_2K$ cases a repeated measures ANOVA including results from FC_{FOS}, $FC_{NOvshtCrit}$ and FC_{NOvsht} solutions was applied, with *post-hoc* Tukey's test for honest significant difference complementing the analysis. Residual analysis complemented the goodness of fit assessment.

Variations in Mp_{ref} and tp_{ref} mean values at each sub-LT WR were examined by the same procedure applied on $NO\dot{V}O_2K$ cases. Significance for tests was set at $P < 0.05$, and all data sets presented normality at $P > 0.20$, as examined by Kolmogorov–Smirnov tests. All statistical tests were performed with the STATISTICA 13.1 package (The Dell Inc., Round Rock, USA).

5.3 Results and discussion

5.3.1 Overshoot detection and quantification

Despite of the restrictive O$\dot{V}O_2$K detection criteria adopted in our study, the occurrence of this phenomenon remained remarkably high (see Table 5.2, bottom), most likely due to the reproduction of its known propitious conditions, i.e., trained individuals [12, 46-48] performing low WR step transitions [12, 48] in cycling exercise [47]. The consistently high O$\dot{V}O_2$K occurrence at sub-LT WRs may indicate a natural tendency of the O_2 uptake system to overshoot when the WR is still low, thus far from the individual's maximal capability. Furthermore, when the WR was increased above WR_{LT}, thus approaching $WR_{\dot{V}O2max}$, the O$\dot{V}O_2$K occurrence was markedly reduced, especially at the highest tested WR (70%Δ), where O$\dot{V}O_2$K cases were absent (Table 5.2).

Regardless of the WR, however, none of the nonovershooting conditions observed, namely tp_{ref} > 5 or FC_{Ovsht} model's lack of convergence, did necessarily reflect the actual absence of O$\dot{V}O_2$K. Instead, one alternative scenario is that where the *Mp* magnitude of any possibly existing O$\dot{V}O_2$K was equivalent to or smaller than the measurement noise, either inducing the regression method to wrongly situate it in the time scale, yielding overly elevated, unrealistically late *tp* and tp_{ref} values; or simply making this phenomenon undetectable, causing convergence failure of the FC_{Ovsht} solution. In any case, the objectivity of our O$\dot{V}O_2$K detection criterion was conserved by assigning the NO$\dot{V}O_2$K classification even for such possibly false negative cases.

Overshoot below the lactate threshold intensity. Restraining the analysis to the moderate domain, where the O$\dot{V}O_2$K incidence is consistently high, the pattern followed by tp_{ref} and Mp_{ref} (Table 5.2, bottom; and Figure 5.6), and by its respective non-transformed versions *tp* and *Mp* (Table 5.2, *top*) may provide valuable information about the FC_{Ovsht} solution's linearity.

According to SOS' theory, *tp* is expected to be invariant for any step input magnitude WR within a given linear range of analysis [55, 56]. The absence of significant differences ($P = 0.12$) between *tp* mean values in the ANOVA considering the 10 subjects with O$\dot{V}O_2$K at all sub-LT WRs (see Table 5.2) is not only coherent with SOS' properties, but also with the linearity assumed for the FOS modeling of $\dot{V}O_2$ kinetics in the moderate domain [54, 82, 118, 120]. Conveniently, the transformation of *tp* into tp_{ref} left the analogous ANOVA result practically unaffected ($P = 0.11$; Figure 5.6, hollow circles).

Table 5.2 Overshoot indicators obtained from the regressions with the FC_{Ovsht} solution

Absolute values	*tp*, s					*Mp*, ml·min^{-1}				
Subject	55%LT	70%LT	85%LT	40%Δ	70%Δ	55%LT	70%LT	85%LT	40%Δ	70%Δ
1	*63.7*	*69.4*	*69.4*	N-C	720.1	*86.2*	*29.9*	*9.1*	N-C	0.0
2	*70.9*	*74.0*	*73.7*	1123.9	N-C	*45.2*	*77.4*	*72.5*	0.0	N-C
3	140.0	*100.7*	145.9	N-C	N-C	1.1	*25.6*	0.3	N-C	N-C
4	*74.2*	*65.2*	842.5	*72.5*	1210.2	*61.2*	*25.6*	0.0	*16.8*	0.0
5	*112.6*	*88.2*	*91.7*	2399.0	1413.7	*18.5*	*3.8*	*16.0*	0.0	0.0
6	*76.6*	*65.0*	*73.4*	556.0	124.2	*20.7*	*71.6*	*48.9*	0.0	0.0
7	*74.6*	*77.4*	*106.2*	N-C	1875.1	*31.2*	*41.9*	*12.5*	N-C	0.0
8	*112.5*	219.6	*91.7*	865.3	2193.2	*17.0*	0.0	*9.5*	0.0	0.0
9	*88.9*	*91.2*	668.4	4721.0	351.9	*18.3*	*16.3*	0.0	0.0	0.0
10	*78.3*	*78.4*	*90.6*	*104.4*	886.9	*53.7*	*74.4*	*15.7*	*6.8*	0.0
11	*69.1*	*86.9*	*78.1*	N-C	1335.6	*66.9*	*9.6*	*73.6*	N-C	0.0
12	*78.8*	*72.2*	*81.9*	2345.6	2291.8	*112.9*	*73.0*	*68.0*	0.0	0.0
13	*69.5*	*90.2*	*89.0*	940.0	2378.6	*36.9*	*51.8*	*43.7*	0.0	0.0
14	*94.1*	*88.3*	*116.4*	N-C	N-C	*15.0*	*50.5*	*9.2*	N-C	N-C
Mean ± SD	*81.8 ± 15.8*	*80.6 ± 11.2*	*87.5 ± 14.4*	*88.4 ± 22.5*	—	*44.9 ± 30.4*	*42.4 ± 26.1*	*34.4 ± 27.4*	*11.8 ± 7.0*	—
All WRs	Mean ± SD = *83.3 ± 14.0*					Mean ± SD = *39.4 ± 27.7*				

Relative Values	tp_{ref} (dimensionless)					Mp_{ref} (dimensionless)				
Subject	55%LT	70%LT	85%LT	40%Δ	70%Δ	55%LT	70%LT	85%LT	40%Δ	70%Δ
1	*3.83*	*4.46*	*4.28*	N-C	56.02	*0.101*	*0.028*	*0.006*	N-C	<0.00
2	*4.17*	*4.58*	*4.23*	44.39	N-C	*0.050*	*0.068*	*0.053*	<0.001	N-C
3	5.14	*3.83*	5.92	N-C	N-C	0.002	*0.030*	<0.001	N-C	N-C
4	*4.15*	*3.63*	47.97	*4.17*	69.43	*0.089*	*0.031*	<0.001	*0.009*	<0.00
5	*4.15*	*4.26*	*4.35*	110.12	50.80	*0.019*	*0.003*	*0.010*	<0.001	<0.00
6	*3.88*	*3.93*	*3.96*	31.79	7.83	*0.025*	*0.066*	*0.036*	<0.001	<0.00
7	*3.77*	*3.64*	*4.10*	N-C	75.24	*0.056*	*0.055*	*0.012*	N-C	<0.00
8	*4.21*	9.43	*4.25*	39.95	95.89	*0.018*	<0.001	*0.007*	<0.001	<0.00
9	*4.46*	*3.86*	33.76	282.86	22.61	*0.028*	*0.019*	<0.001	<0.001	<0.00
10	*4.17*	*4.08*	*4.14*	*4.47*	38.34	*0.071*	*0.074*	*0.013*	*0.003*	<0.00
11	*4.82*	*4.68*	*4.44*	N-C	54.49	*0.076*	*0.008*	*0.048*	N-C	<0.00
12	*3.65*	*4.13*	*3.91*	96.37	102.49	*0.107*	*0.048*	*0.037*	<0.001	<0.00
13	*4.06*	*4.07*	*4.15*	42.22	79.88	*0.053*	*0.053*	*0.034*	<0.001	<0.00
14	*4.00*	*4.25*	*4.47*	N-C	N-C	*0.017*	*0.043*	*0.006*	N-C	N-C
Mean ± SD	*4.10 ± 0.31*	*4.11 ± 0.33*	*4.21 ± 0.18*	*4.32 ± 0.21*	—	*0.055 ± 0.032*	*0.040 ± 0.023*	*0.024 ± 0.018*	*0.006 ± 0.004*	—
All WRs	Mean ± SD = *4.14 ± 0.28*					Mean ± SD = *0.039 ± 0.028*				

$O\dot{V}O_2K$ cases	55%LT	70%LT	85%LT	40%Δ	70%Δ
n (% of 14)	13 (92.9%)	13 (92.9%)	11 (78.6%)	2 (14.3%)	0 (0.0%)
sub-/supra-LT	37 $O\dot{V}O_2K$ cases (88.1% of 42 sub-LT cases)			2 $O\dot{V}O_2K$ cases (7.1% of 28 supra-LT cases)	
All WRs	39 $O\dot{V}O_2K$ cases (55.7% of all 70 cases)				

Values in italic are exclusive to $O\dot{V}O_2K$ containing cases, i.e., those datasets yielding a convergent FC_{Ovsht} solution with a satisfactory ζ value ($\zeta \in \mathbb{R} \mid 0 \leq \zeta < 1$), and $tp_{ref} > tp_{ref}T = 5$; N-C: No convergent FC_{Ovsht} solution satisfying ζ's requirements could be found (see Appendix E for details).

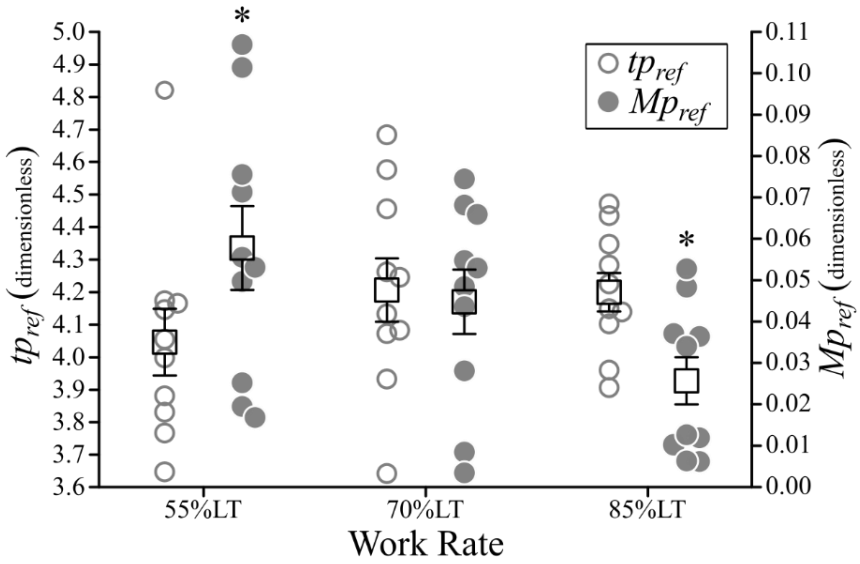

Figure 5.6 Profiles of tp_{ref} (left axis, hollow circles) and Mp_{ref} (right axis, solid circles) for the 10 selected subjects with O$\dot{V}O_2$K at all sub-LT WRs; Whiskers are mean value ± 1·SD; *Significant difference between Mp_{ref} mean values (P = 0.03; *post-hoc* test, P = 0.02). No significant difference between tp_{ref} mean values (P = 0.11).

Furthermore, the sub-LT within-subject variation, evaluated as the difference between a given individual's maximal and minimal values, divided by the latter, was markedly reduced after the transformation from *tp* to tp_{ref}, with respective mean values changing from 19.8% to 8.8% (n = 13). This equalizing effect of reducing *tp*'s within-subject variation, combined with the aforementioned unaltered ANOVA results, corroborate both the pertinence and the convenience of the tp_{ref} approach in the FC_{Ovsht} context.

Another parameter expected to be invariant along WRs according to the SOS linearity concept is the Mp_{ref}. However, repeated measures ANOVA performed along sub-LT WRs reveals a significant difference between Mp_{ref} mean values (P = 0.03; n = 10; Figure 5.6, solid circles), which was found to be exclusively between 55%LT and 85%LT (*post-hoc* test, P = 0.02), thus only between the two extremes of the moderate domain spectrum. One likely explanation for the apparent loss of linearity in Mp_{ref} may be the intrinsically reduced magnitude of *Mp* (see equation 5.8). Due to the reduced signal-to-noise ratio characteristic of breath-by-breath $\dot{V}O_2$ measures at low WRs, the often modest *Mp* values (ranging in our study between 3.8 and 112.9 ml·min^{-1} for the O$\dot{V}O_2$K cases) are more likely to be affected by noise. This low '*Mp*-to-noise' biasing effect acting on *Mp* is propagated to Mp_{ref}.

Linearity conjectures left aside, both O$\dot{V}O_2$K's incidence and magnitude related observations of our study remain in agreement with the specific literature, according to which overshoots in the FC of $\dot{V}O_2$ responses to step are seemingly more frequent and pronounced at lower WRs, with this pattern being observed even within the moderate domain [12, 47, 48].

To quantify the O$\dot{V}O_2$K phenomenon, two other magnitude indicators alternative to *Mp* and Mp_{ref} have already been proposed by Koppo et al. [48], and adopted by Kilding and Jones [47], namely the integral volume of the overshoot above the steady-state and below the real $\dot{V}O_2$ data points (*IV*); and the already mentioned *Peak-SS*. However, while the *Peak-SS* is particularly subject to punctual data extremes, the computation of *IV* is highly dependent on the interval considered, i.e., the point beyond which given data values above steady-state are no longer considered as overshooting points.

In this sense, the use of *Mp* and/or Mp_{ref} is a more robust alternative for *Peak-SS*, for it considers the whole data set via the FC_{Ovsht} regression curve. Similarly, but as an alternative to *IV*, the use of the FC_{Ovsht} regression curve—rather than the actual $\dot{V}O_2$ data—as the upper limit for evaluation of the integral volume of O_2 above steady-state is proposed, defining the $V_{O\dot{V}O2K}$ (Figure 5.1). In the $V_{O\dot{V}O2K}$ case, it is important to remark that even those O_2 volumes referent to the second and subsequent oscillations above steady-state (omitted in Figure 5.1 due to its minute magnitudes) are considered in the evaluation. Moreover, no ending point is required since oscillations' magnitudes tend to zero for larger *t* values.

Overshoot above the lactate threshold intensity. To our knowledge, this is the first time that an O$\dot{V}O_2$K was observed beyond the moderate domain of exercise. Thus, a special attention is devoted to the two cases detected, both at the 40%Δ intensity (Table 5.2, subjects 4 and 10). Despite of their modest *Mp* and Mp_{ref} values, these data sets not only present reasonable *tp* values, but would be also included in the overshooting category according to criteria adopted by previous studies where a quantitative evaluation of O$\dot{V}O_2$K events was also attempted [47, 48].

For comparison purposes, the two alternative O$\dot{V}O_2$K magnitude indicators proposed (*Peak-SS* and *IV*) were evaluated on our supra-LT overshooting data. Specific data processing conditions from the original studies [47, 48] were reproduced to the best of our possibilities, such as the 1 s linear interpolation of data, or the *IV* evaluation between 55 and 140 s after t_0—the same interval used

for the highest WR evaluated in Koppo et al. [48].

The obtained *Peak-SS* values for subjects 4 and 10 (271 and 289 ml·min^{-1}, respectively) are similar to those previously reported in the literature, and its occurrence instants (at t = 62 and 74 s, respectively) lie within the normally observed intervals [47, 48]. As for *IV*, the 78 ml of O_2 obtained by subject 4 is equivalent to the lowest values normally attained in the moderate domain [47, 48], while the relative importance of the 29 ml obtained by subject 10 remains unclear. In any case, the evaluated *Peak-SS* and *IV* values indicate a congruence between the tp_{ref}-based criterion and the available literature data in confirming O$\dot{V}O_2$K cases. These two overshooting $\dot{V}O_2$ step responses above WR_{LT} bring to discussion the role of the LT—or, alternatively, that of the Gas Exchange Threshold—as a reference for the O$\dot{V}O_2$K investigation.

No longer confined to the moderate domain of exercise, the O$\dot{V}O_2$K events may demonstrate a more continuous loss of magnitude (due to nonlinearities and/or increments on ζ) throughout the whole WR spectrum than that associated with a limiting value such as the WR_{LT}. Nevertheless, such a punctual drop in the quantity of detected O$\dot{V}O_2$K cases would still be acceptable, as it could coincide with the point at which *Mp*'s magnitude becomes as low as that of the measurement noise, jeopardizing the *tp* identification and, ultimately, the O$\dot{V}O_2$K detection.

Instead of an intermediate limiting threshold like the WR_{LT}, a conceptually proper reference for the O$\dot{V}O_2$K occurrence may be the actual ceiling of the respiratory system, represented by the $WR_{\dot{V}O2max}$, although any overshooting likely ceases long before the WR reaches this far. In any case, the proportion of the $WR_{\dot{V}O2max}$ where most of the O$\dot{V}O_2$K occurrences cease may still coincide with the vicinity of WR_{LT}, which was found between 50 and 61 % of $WR_{\dot{V}O2max}$ for our sample.

5.3.2 Mixed Multi-Exponential versus First-Order Multi-Exponential models

As hypothesized, the MiME model presented a better overall fitting performance for $\dot{V}O_2$ on-kinetics in comparison with the FOME model at all WRs, regardless of the O$\dot{V}O_2$K phenomenon manifestation.

Comparisons within NO$\dot{V}O_2$K cases. RMSE values from the FC_{FOS} were compared with those from the nonovershooting SOS variations, namely the $FC_{NOvshtCrit}$ and the FC_{NOvsht} (Table 5.3, top panel).

Three combinations of data sets were analyzed: two comprising either only the sub- or the supra-LT intensities, and another one testing all WRs at once. In all combinations, no significant differences were found between FC_{FOS} and FC_{NOvsht} solutions, denoting similar goodness of fit for $NO\dot{V}O_2K$ cases. The $FC_{NOvshtCrit}$ solution performed significantly worse than the FC_{FOS} according to the ANOVAs comprising all WRs and only supra-LT cases. In comparison to the FC_{NOvsht}, the $FC_{NOvshtCrit}$ also proved significantly worse for the supra-LT condition.

Comparisons within $O\dot{V}O_2K$ cases. Pairwise comparisons between RMSE mean values from FC_{FOS} and FC_{Ovsht} demonstrated a better goodness of fit of the latter for all sub-LT intensities, taken either separately or combined (Table 5.3, bottom panel).

Table 5.3 Comparisons between mean RMSE values from the FC_{FOS} and the second-order proposed solutions

$NO\dot{V}O_2K$ cases	FC_{FOS}	$FC_{NOvshtCrit}$	FC_{NOvsht}
All sub-LT (P = 0.24; n = 5)	62.3 ± 7.7	61.4 ± 7.9	62.0 ± 8.0
All supra-LT (P < 0.01; n = 26)	98.8 ± 5.0*	101.3 ± 5.0*†	99.1 ± 5.2†
All WRs (P = 0.02; n = 31)	92.9 ± 5.0*	94.9 ± 5.1*	93.1 ± 5.1
$O\dot{V}O_2K$ cases‡	FC_{FOS}	vs.	FC_{Ovsht}
All sub-LT (P = 0.000; n = 37)	90.5 ± 28.1		84.3 ± 28.9
55%LT (P = 0.003; n = 13)	79.2 ± 19.7		73.0 ± 19.9
70%LT (P = 0.000; n = 13)	93.6 ± 31.4		87.2 ± 32.9
85%LT (P = 0.000; n = 11)	100.3 ± 30.4		94.2 ± 30.8
All WRs (P = 0.000; n = 39)	90.9 ± 27.5		84.4 ± 28.1

Root mean squared error (RMSE) values are expressed as means ± SD ($ml \cdot min^{-1}$). *Significant differences between FC_{FOS} and $FC_{NOvshtCrit}$ solutions. †Significant differences between $FC_{NOvshtCrit}$ and FC_{NOvsht} solutions. ‡Significant differences for all compared WR groups.

When the analysis comprised the two supra-LT $O\dot{V}O_2K$ cases, thus covering all WRs, the significant difference favoring the FC_{Ovsht} option persisted.

Parameters, curve shaping, and underlying phenomena. For any given family of SOS curves sharing identical values for ω and *td* (or at least very similar, to a certain extent), the $FC_{NOvshtCrit}$ type represents the fastest rise towards the steady-state value achievable without the occurrence of an $O\dot{V}O_2K$ [55, 56]. This particular intermediate condition between FC_{NOvsht} and FC_{Ovsht} SOS types is imposed to the $FC_{NOvshtCrit}$ by its $\zeta = 1$ constraint, and explains why this solution is not suitable

for O$\dot{V}O_2$K cases, and why it tends to perform worse than both FC_{FOS} (which has even fewer degrees of freedom) and FC_{NOvsht} for NO$\dot{V}O_2$K cases (Table 5.3, *top*).

Considering the poor fitting performance of the $FC_{NOvshtCrit}$, and for being it so specific a solution ($\zeta = 1$), we have discarded it as a fitting option for NO$\dot{V}O_2$K cases in the following analyses. Moreover, if required by the data points, both FC_{NOvsht} and FC_{Ovsht} solutions may still yield ζ values that, if not exactly equal to one, are very close, tending to that value (e.g., 1.01 or 0.99, respectively).

Once ζ is allowed to be greater than one, the SOS model assumes the FC_{NOvsht} shape, which is flexible enough to adapt to a wider range of $\dot{V}O_2$ nonovershooting data patterns, and not only to the specific steepness referent to $\zeta = 1$. Oppositely, the $\zeta < 1$ in the FC_{Ovsht} allows the exponential not only to overshoot its steady-state value, but also to approach it in a steeper fashion, as the curve crosses it towards the O$\dot{V}O_2K_{peak}$. Figure 5.7.A and Figure 5.7.B, depict representative examples of respectively NO$\dot{V}O_2$K and O$\dot{V}O_2$K data sets fitted by FC_{FOS} and adequate SOS solutions. Visual inspection of errors distributions around the estimated curves reveals a general fitting superiority of the SOS in comparison with the FOS model.

Although both first- and second-order exponentials tend to equalize as time progresses towards the FC's steady-state, exclusive features of the SOS curves enhance their fitting performance in three noteworthy regions within the transitory phase of the response (Figure 5.7.A-B), namely: 1) the initial rise of the response; 2) the rapid increase preceding the O$\dot{V}O_2$K (i.e., immediately before the first attainment of the steady-state value); and 3) the first overshooting region of data.

The better adjustment of SOS curves to data already in the first considered points (Figure 5.7.A-B, *region 1*; between t = 21 and roughly 35 s), which was generally noticeable in the majority of our regressions, reflects the advantage of the initial upward concavity, an absent feature in the FOS responses. By allowing the response curve to begin its rise earlier and more smoothly, the SOS curves' initial upward concavity not only better fits the initial data of the responses, but also brings more coherence to the FC modeling: *1)* because it allows shorter td_{FC} values than those obtained with the FOS model (see Figure 5.7.A-B, and the consistently shorter td_{FC} values both NO$\dot{V}O_2$K and, especially, for O$\dot{V}O_2$K cases; Table 5.4), which is in better accord with the expected muscles-to-lung blood flow transit time; and *2)* because the intuitive concept of a smoother increase from

$\dot{V}O_{2Baseline}$ seems more adequate to a physiological response of a system where pulmonary blood inflow rises with contributions from different body regions.

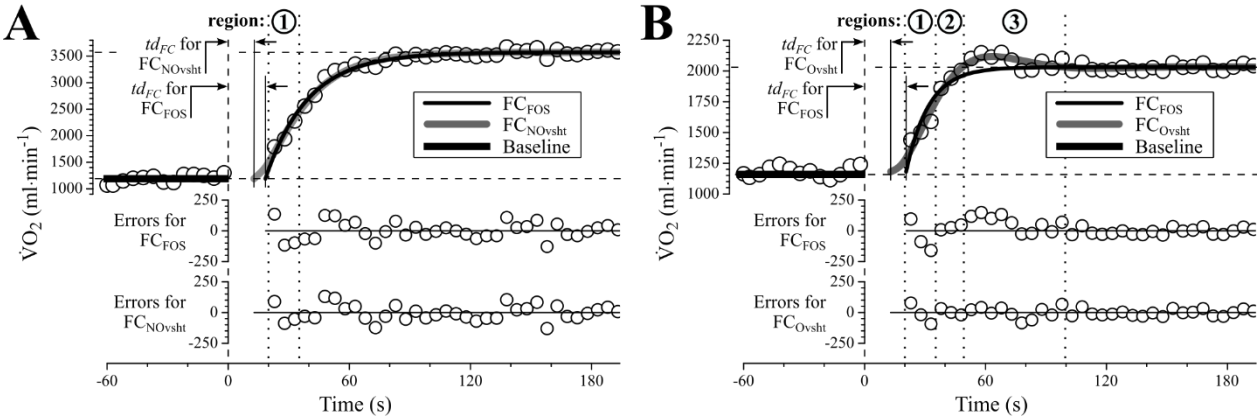

Figure 5.7 Representative examples of FC's data regression comparing the FC_{FOS} with both the FC_{NOvsht} and FC_{Ovsht} solutions. Plots of errors around fitted curves illustrate a superior adequacy of SOS solutions (MiME model) in three identifiable regions: A. in the NO$\dot{V}O_2$K context, the smooth rising of data in *region 1* is better fitted by the initial upward concavity of FC_{NOvsht} curve (which also allows a shorter td_{FC}); B. in the O$\dot{V}O_2$K context, in addition to the same advantages experienced by the FC_{NOvsht} curve in *region 1*, the FC_{Ovsht} curve also presents a better fit to both the rapidly increasing values in *region 2*, and the overshooting data on *region 3*. Note: For comparison purposes, plots of errors in panel A are augmented to the same scale of plots in panel B. See text for further commentaries.

Furthermore, in the case of a real mechanical arrangement, every component of our FOS analogy on Figure 5.2 would actually present some mass, rendering the FOS-like behavior an idealistic simplification. Likewise, factors associated with O_2 transport and utilization may present inertial attributes in the real physiological context, in line with the "metabolic inertia" of the oxidative mechanism described by Grassi [154]. As already discussed, the "true inertia" concept, possibly acting at the metabolic level, is not only in accordance with a smooth initial increase, but also with possible oscillations around the reference final condition.

However, in the less specific assessment of $\dot{V}O_2$ responses allowed by measures performed at the pulmonary level, the explanation for the overshooting pattern evidenced on *regions 2* and *3* (Figure 5.7.B) may also involve various stages of the O_2 transport chain, possibly reflecting a muscle O_2 utilization-supply mismatch, (see *Further evidence of second-order system's features*). In these

overshooting cases, regardless of the physiological mechanism involved, the FC_{Ovsht} variation of the SOS benefits from both its ability to rapidly increase and cross the steady-state line (*region 2*), and from the subsequent oscillating pattern, which allows the proper fitting of the $O\dot{V}O_2K$ phenomenon itself (*region 3*). Indeed, the affinity between FC_{Ovsht} solution's features and the $O\dot{V}O_2K$ data patterns in *regions 2* and *3* is in agreement with the fact that fitter individuals are those presenting overshooting step responses: in the SOS perspective, the $O\dot{V}O_2K$ may be, rather than an isolated or abnormal phenomenon, a natural consequence of an accelerated $\dot{V}O_2$ kinetics. Alternatively, once a curve is not allowed to surpass its steady-state value (FC_{FOS}, $FC_{NOvshtCrit}$ and FC_{NOvsht} solutions), it will be deformed towards *region 2* when attempting to comprise some rapidly rising data, or to *region 3*, when attempting to comprise a possible $O\dot{V}O_2K$, likely hindering its overall fitting performance.

Although the FC_{FOS} may be able to adapt to overshooting cases by yielding a reduced τ_{FC} and, depending on data in *region 1*, a longer td_{FC}, this model remains inadequate in qualitative, by simplistically ignoring the $O\dot{V}O_2K$, and quantitative aspects, by providing unrealistic parameters. As remarked by previous studies [46-48], fitting overshooting data with a FC_{FOS} could lead to spurious $\dot{V}O_2$ kinetics' results, including an A_{FC} above the actual FC steady-state [47], an inappropriately fast τ_{FC} [47, 48], and an inadequate O_2 deficit [46-48]. In our study (Table 5.4, *top*), the values of mean response time (MRT, equal to FC_{FOS}'s $td_{FC} + \tau_{FC}$) obtained by the FC_{FOS} when fitting $O\dot{V}OK$ cases, if not inadequate, are at least clearly shorter that those of $NO\dot{V}OK$ cases, mostly due to its shorter τ_{FC} values. However, when only $NO\dot{V}OK$ cases are considered (Table 5.4; *left*), the τ_{FC} values are not so different from the τ_{App} estimated by the FC_{NOvsht} solution (see Footnote 12). In this case, the differences between MRT and the approximate mean response time (MRT_{App}, equal to FC_{NOvsht}'s $td_{FC} + \tau_{App}$) are due mostly to the aforementioned shorter time delays allowed by the SOS curves—the FC_{NOvsht} solution, in that case.

In regard to the O_2 deficit, while a reduction in its value in the FC_{FOS} curve results from a steeper response related to a shorter τ_{FC}, a similar left-upwards shift is easily obtainable in a SOS curve by increasing ω and/or reducing ζ. Thus, being the $O\dot{V}O_2K$ associated with the decrease in ζ's value ($\zeta < 1$), this phenomenon may represent an advantage of the FC_{Ovsht} curve over nonovershooting shapes also in terms of O_2 deficit reduction.

Table 5.4 $\dot{V}O_2$ on-kinetics parameters obtained from least squares regressions for FC_{FOS}, FC_{NOvsht} and FC_{Ovsht} solutions

		NO$\dot{V}O_2$K cases						O$\dot{V}O_2$K cases*				
	WR	55%LT	70%LT	85%LT	40%Δ	70%Δ	All WRs	55%LT	70%LT	85%LT	40%Δ	All WRs
	Sample size	n = 1	n = 1	n = 3	n = 12	n = 14	n = 31	n = 13	n = 13	n = 11	n = 2	n = 39
First-Order System		FC_{FOS}						FC_{FOS}				
	td_{FC}, s	13.5 —	18.7 —	18.9 ± 1.2	15.6 ± 3.2	16.6 ± 2.8	16.4 ± 2.9	18.4 ± 3.2	18.6 ± 2.9	17.8 ± 2.7	19.8 ± 0.6	18.4 ± 2.8
	τ_{FC}, s	24.6 —	21.3 —	19.3 ± 2.2	24.2 ± 6.0	23.1 ± 6.7	23.1 ± 5.9	15.5 ± 4.2	15.1 ± 3.3	16.5 ± 3.7	15.8 ± 4.6	15.7 ± 3.7
	MRT†, s	38.1 —	40.0 —	38.2 ± 1.2	39.7 ± 5.1	39.7 ± 4.4	39.6 ± 4.3	33.9 ± 3.4	33.8 ± 3.0	34.4 ± 2.2	35.6 ± 4.0	34.1 ± 2.9
Second-Order System		FC_{NOvsht}						FC_{Ovsht}				
	td_{FC}, s	3.2 —	11.5 —	13.7 ± 3.6	11.8 ± 3.2	13.2 ± 4.8	12.3 ± 4.3	6.9 ± 5.7	8.2 ± 5.3	7.6 ± 4.5	7.8 ± 1.8	7.8 ± 5.1
	ζ (dimensionless)	1.02 —	1.02 —	1.19 ± 0.21	2.25 ± 1.55	2.46 ± 1.91	2.16 ± 1.64	0.69 ± 0.08	0.73 ± 0.07	0.78 ± 0.07	0.85 ± 0.03	0.74 ± 0.08
	ω, rad·s^{-1}	0.061 —	0.074 —	0.103 ± 0.037	0.177 ± 0.147	0.212 ± 0.185	0.179 ± 0.157	0.062 ± 0.011	0.067 ± 0.015	0.067 ± 0.016	0.084 ± 0.019	0.066 ± 0.015
	ω_d ‡, rad·s^{-1}	—	—	—	—	—	—	0.044 ± 0.010	0.045 ± 0.009	0.041 ± 0.009	0.044 ± 0.014	0.044 ± 0.009
	τ_{App}§, s	20.4 —	16.7 —	17.1 ± 0.4	23.2 ± 6.3	22.3 ± 7.1	21.9 ± 6.4	—	—	—	—	—
	MRT_{App}§, s	23.6 —	28.2 —	30.8 ± 3.4	35.0 ± 6.0	35.4 ± 5.8	34.2 ± 6.0	—	—	—	—	—

Values are mean ± SD; *No O$\dot{V}O_2$K cases observed at 70%Δ; †MRT = FC_{FOS}'s td_{FC} + τ_{FC}; ‡The concept of ω_d does not apply to the FC_{NOvsht} solution; §The variable τ_{App} derives from the FOS approximation of FC_{NOvsht} (see Footnote 12), and MRT_{App} = FC_{NOvsht}'s td_{FC} + τ_{App}.

Even without mentioning the SOS modeling, the idea that the O_2 volume surplus represented by *IV*, equivalently to the $V_{O\dot{V}O2K}$ (Figure 5.1), may constitute a "payback" for the O_2 deficit already at the beginning of exercise has already been proposed [46-48]. Moreover, it should be remarked that not only the $V_{O\dot{V}O2K}$ represents an important supplementary O_2 uptake comprised by the FC_{Ovsht} solution. A similar "O_2 complement" is already identifiable below the steady-state value, in the V_{comp} volume evaluated between the FC_{Ovsht} and the FC_{FOS} curves (Figure 5.1), which is concentrated in *regions 2* and *3* of the overshooting response (Figure 5.7.B). Further investigation of the influence of $V_{O\dot{V}O2K}$ and V_{comp} in the O_2 deficit and/or debt (off-transient) may contribute to this payback conjecture.

Second-order system parameters. In addition to the already commented shortness of td_{FC}, other features presented by SOS parameters may denote strong coherence with the actual physiological phenomenon involving the FC. The consistently similar mean values obtained for FC_{Ovsht} regressions' td_{FC}, ζ, ω and ω_d at different WRs (Table 5.4) corroborates both the robustness and pertinence of this solution, for such recurring values may be more likely due to data attributes than accidental.

To a lesser extent, results for the FC_{NOvsht} solution present a similar behavior, differing from the FC_{Ovsht} by greater SD values and less uniform means obtained for parameters ζ and ω at different WRs (Table 5.4). One explanation for these different variances in ζ and ω results may be the interaction between the regression method used and the features of either FC_{Ovsht} or FC_{NOvsht} curves. In the FC_{Ovsht} case, the least squares mechanism is benefited already from its first iteration by somewhat accurate ζ and ω initial estimates provided by data in *region 3* (Figure 5.7.B)—which contains valuable preliminary information about *tp* and *Mp* values (see Footnote 12). In addition, the curvy shape of FC_{Ovsht} may benefit from fitting references of points in *regions 2* and *3* to improve parameters convergence during computational iterations.

In opposition, the combination of the less curvy FC_{NOvsht} solution's shape with the less oscillating $NO\dot{V}O_2K$ data naturally offers reduced resources to numerical regression methods. Because very similar FC_{NOvsht} curve shapes may be achieved through different combinations of ζ and ω values, the detection of an optimal pair of these parameters is only accurate enough to satisfactorily select a range of equivalently suitable values. Within this range, the narrower selection of a particularly optimal ζ-ω pair becomes susceptible to fortuitous numerical precision and convergence related

factors, so that further optimization—even improved by the reference of τ_{FC} (Footnote 12)—is limited. Therefore, the shape of a FC_{NOvsht} response allows a less constrained trade-off between ζ and ω values, which may interfere with an otherwise noticeable repeatability pattern in the results obtained for these parameters.

Nevertheless, FC_{NOvsht} solution's ζ and ω mean values remained within the same orders of magnitude (1 and 0.01, respectively) obtained for the FC_{Ovsht} solution. Furthermore, the fact that neither ζ nor ω mean values present a substantial magnitude variation between WRs despite of their numerical freedom in the FC_{NOvsht} context (with $\zeta > 1$ being the only restriction) also supports the pertinence of the SOS model for nonovershooting FCs.

Moreover, as further applications of SOS to $\dot{V}O_2$ kinetics point towards reference values for a physiologically acceptable ω for humans (possibly around 0.06 or 0.07 $rad \cdot s^{-1}$, considering the tendency in the less biased results from the FC_{Ovsht} solution; Table 5.4), or as a better characterization of FC_{NOvsht} cases is established, this parameter ambiguity may be ruled out.

First- and second-order system parameters. Thus far, the prevalence of the FOS model as the fitting standard for the FC of the step response was largely justifiable by the difficulties in detecting and, ultimately, in recognizing inertial-like features of $\dot{V}O_2$ data. While any possible smooth initial increase is hidden by the cardiodynamic component in pulmonary $\dot{V}O_2$ uptake measures, the oscillatory pattern around the steady-state value (of which the $O\dot{V}O_2K$ composes a first and more pronounced oscillation) is often either absent or comparable to measure noise in magnitude.

However, despite of its important implications and advantages, the adoption of SOS' concepts must not imply a summary abandonment of the currently accepted FOS theory, for the former constitutes an extension of the latter. Instead, this transition between models may benefit from references provided by the extensively characterized FOS's td_{FC}, τ_{FC} and MRT (used in tp_{ref} and/or in the comparison with τ_{App} and MRT_{App}), and A_{FC} (used in Mp_{ref} and adopted as A_{ref} for all SOS solutions). Concomitantly, further applications of the SOS model may gather additional information about what may be the reasonable (i.e., physiological) ranges of values for SOS' td_{FC}, ω and ζ in the $\dot{V}O_2$ kinetics context.

5.3.3 Mixed Multi-Exponential model: Physiological relevance

Further evidence of second-order system's features. Going beyond pulmonary $\dot{V}O_2$ measurements,

where the cardiodynamic component pre-empts an accurate fitting of FC's early stage, data regarding O_2 utilization at the muscular level, such as deoxygenated hemoglobin concentration ([HHb]), muscle microvascular O_2 pressure ($PmvO_2$) or muscle $\dot{V}O_2$ itself, may also present some of SOS-like features.

Although not stressed by the study's author, a smooth initial increase (i.e., upward concavity) is observable in the maximal and submaximal muscle $\dot{V}O_2$ responses of an isolated *in situ* dog gastrocnemius preparation (see bottom panels in Figure 2 from Grassi [155]).

Moreover, at the onset of submaximal cycling exercise, [HHb] kinetics of *vastus lateralis* may present not only a smooth initial increase (also not mentioned by the authors, but noticeable in the plots of Bailey et al. [7] and Wilkerson et al. [123]), but even a clear overshoot in healthy [7, 123] and type II diabetic [123, 156] individuals. Additionally, a similar overshoot in muscle O_2 uptake at the beginning of the exercise was also observed via $PmvO_2$ kinetics measured in the spinotrapezius muscle of type II diabetic rats [157].

These peripheral transient peaks of O_2 extraction indicated by both [HHb] and $PmvO_2$ kinetics have been attributed to a mismatch caused by a reduction in the O_2 delivery-to-use ratio at the mitochondrial level, especially in the vascular limited condition associated with type II diabetes [123, 156, 157].

In a broader view, these overshooting phenomena at different stages of the O_2 transport chain seem to be always associated with a condition where intracellular $\dot{V}O_2$ experiences an increase of its relative importance in relation to the aerobic supply provided by blood flow. This mismatch between skeletal muscle O_2 utilization and supply may result from the increment of the former, e.g., via endurance training, and/or from the impairment of the latter, e.g., due to some vascular condition, creating an unusual contextual similarity between the opposite statuses of very fit and unhealthy individuals. Another observation in accordance with this scenario is that both $\dot{V}O_2$ [12] and [HHb] (see illustrative example on top of Figure 3 from Bailey et al. [7]) responses to step stimulus have presented more pronounced overshoots and faster kinetics after an endurance training period.

Once considered the association between the $O\dot{V}O_2K$ with an O_2 utilization-supply mismatch in the skeletal muscle, a possible explanation for this oscillation around steady-state value in pulmonary measures is that it would reflect a 'wave' of low O_2 content blood arriving at the lungs

after the overshooting extraction at the peripheral level. In this case, the origins of the transitory increment of pulmonary $\dot{V}O_2$ in the overshoot situation would be similar to those of the cardiodynamic component. Moreover, given the role of blood flow in Fick's equation [1], some influence of the cardiac kinetics on O$\dot{V}O_2$K events might be suggested. However, although already observed, heart rate overshoots are not consistently present in all O$\dot{V}O_2$K cases [46-48].

Therefore, further studies comparing pulmonary and muscular $\dot{V}O_2$ kinetics (including comparisons between pulmonary and muscular ω and ζ values), concomitantly with measures such as the heart rate, cardiac stroke volume, and the peripheral blood flow during O$\dot{V}O_2$K episodes may be needed.

Mixed Multi-Exponential model and the overshoot. Even though the O$\dot{V}O_2$K is a phenomenon so far observed only in specific conditions [12, 46-48, 50], and regardless of its unprecedented appearance in supra-LT intensities here reported, its undeniable existence in the moderate domain of exercise [12, 46-48, 50] reveals *per se* a conceptual conflict within the FOME model. In both physiological and numerical approaches, such a conflict is ruled out by the adoption of a SOS representation for the FC, naturally expanding the FOME model into the more comprehensive MiME formulation.

Illustrated by the dynamics between '*physiological forcing, damping and (truly) inertial*' elements, and modelled by the SOS family of curves, nonovershooting and overshooting behaviors, rather than seen as qualitatively unrelated cases, are unified under the logic of a continuum from a more to a less damped system (i.e., from a less to a more fit status). By means of variations in parameters ω and ζ, $\dot{V}O_2$ step responses either manifesting or not manifesting an O$\dot{V}O_2$K are coherently explainable by the unified SOS modeling.

At the same time that important concepts such as the O_2 deficit, the relationship between the speed of increment in the response and the individual's fitness level, and the exponential nature of the curve remain valid in the MiME model, they are coherently related to the O$\dot{V}O_2$K advent and to other features of the SOS curves. The incorporation of these features as *intrinsic characteristics* of the response—instead of incidental phenomena—brings flexibility and accuracy to the assessment of kinetic indicators (e.g., curve parameters estimation, or the O_2 deficit evaluation). Additionally, as the MiME model supports both a representation of and a methodology for detecting and quantifying O$\dot{V}O_2$K phenomena, new insights on the mechanisms modulating the $\dot{V}O_2$ kinetics to

WR variations may be allowed.

Finally, the shape similarities between the SOS curves and the actual behaviors of muscle $\dot{V}O_2$ represent strong motivation for the adoption of such modeling, especially in regards to the FC of the pulmonary $\dot{V}O_2$ step response.

5.4 Conclusion

Regarding the $\dot{V}O_2$ fundamental component, the comprehensiveness and pertinence of the second-order modeling is three times corroborated: by the better goodness of fit in hitherto unexplained O$\dot{V}O_2$K cases; by the better comprehension of underlying factors involved in the overshoot occurrence; and by the possibility of representing NO$\dot{V}O_2$K cases without losses in comparison to first-order system's fitting ability and physiological reasoning.

Therefore, considering both fundamental and slow components together, the hybrid—or mixed—nature of the MiME model presented here emerges as the optimal trade-off between the best of both first- and second-order systems' features for the modeling of $\dot{V}O_2$ on-kinetics in humans.

5.5 Glossary

A_{FC}	Amplitude of the fundamental component of $\dot{V}O_2$ step response
A_{ref}	A_{FC} value evaluated with FC_{FOS} solution. Adopted as A_{FC} value for SOS solutions and as reference for Mp_{ref} evaluation
Cp	Actual position of the mechanical system of our physiomechanical analogy
Cr	Reference value for the mechanical system of our physiomechanical analogy
D	Damping coefficient of a given damper
FC	$\dot{V}O_2$ response's fundamental component
$FC_{NOvshtCrit}$	SOS nature, *critically damped* type FC
FC_{FOS}	FOS nature FC
FC_{NOvsht}	SOS nature, overdamped type FC
FC_{Ovsht}	SOS nature, underdamped type FC

FOME	First-Order Multi-Exponential (model)
FOS	First-order system
[HHb]	Deoxygenated hemoglobin concentration
IV	Integral volume of overshoot (obtained directly from $\dot{V}O_2$ data points)
K	Coefficient of elasticity of a given spring
[Lac]	Blood lactate concentration
LT	Lactate threshold
M	Mass of a given inertial component
MiME	Mixed Multi-Exponential (model)
Mp	Absolute $O\dot{V}O_2K$ amplitude
Mp_{ref}	Reference *Mp*, normalized by A_{ref}
MRT	Mean response time (FC_{FOS}'s $td_{FC} + \tau_{FC}$)
MRT_{App}	Approximate MRT (FC_{NOvsht}'s $td_{FC} + \tau_{App}$)
$NO\dot{V}O_2K$	Reference to the absence of $O\dot{V}O_2K$
$O\dot{V}O_2K$	Overshoot in $\dot{V}O_2$ kinetics
$O\dot{V}O_2K_{peak}$	$O\dot{V}O_2K$ peak value of the FC_{Ovsht} curve
Peak-SS	Difference between step transient's $\dot{V}O_2$ data peak value and that of steady-state
p_{final}	Final position of both Cr and Cp
$p_{initial}$	Initial position of both Cr and Cp
$PmvO_2$	Muscle microvascular O_2 pressure
p_{peak}	Peak value of Cp
RMSE	Root mean squared error
SOS	Second-order system
τ_{App}	Approximate time constant for FC_{NOvsht}, evaluated from its FOS approximation

τ_{ref}	τ_{FC} value evaluated with FC_{FOS} solution. Adopted as reference for tp_{ref} evaluation
τ_{FC}	Onset time delay of the FC
td_{FC}	Onset time delay of the FC
td_{SC}	Onset time delay of the slow component
t_{FC}	Time upper limit of data in FC fitting
td_{ref}	td_{FC} value assessed with FC_{FOS} solution. Adopted as reference for tp_{ref} evaluation
tp	$O\dot{V}O_2K_{peak}$ time. Instant of $O\dot{V}O_2K_{peak}$ occurrence in the FC_{Ovsht} curve
tp_{ref}	Reference tp, represented in terms of τ_{ref} and td_{ref} evaluated for the same data set
$tp_{ref}T$	Threshold tp_{ref} value used for detection of $O\dot{V}O_2K$ containing $\dot{V}O_2$ step responses
t_0	Instant of application of the step stimulus
V_{comp}	Complementary volume of O_2 (below steady-state, between FC_{Ovsht} and FC_{FOS})
$V_{O\dot{V}O2K}$	Volume of $O\dot{V}O_2K$ below FC_{Ovsht} curve
$\dot{V}O_2$	Oxygen uptake
$\dot{V}O_{2Baseline}$	$\dot{V}O_2$ average value for 60 s preceding t_0
$\dot{V}O_{2max}$	Maximal 30 s $\dot{V}O_2$ average in the incremental test
ω	Natural frequency of a SOS
ω_d	Damped frequency of an underdamped SOS
WR	Work rate
WR_{LT}	WR associated with the lactate threshold
WR_{max}	Time interpolated proportion of WR at the final step of the incremental step test
$WR_{\dot{V}O2max}$	WR associated with the maximal 30 s $\dot{V}O_2$ average in the incremental test
ζ	Damping ratio of a SOS
40%Δ	WR equal to WR_{LT} added of 40% of the difference between WR_{LT} and $WR_{\dot{V}O2max}$
55%LT	WR equal to 55% of WR_{LT}

70%Δ WR equal to WR_{LT} added of 70% of the difference between WR_{LT} and $WR_{\dot{V}O2max}$

70%LT WR equal to 70% of WR_{LT}

85%LT WR equal to 85% of WR_{LT}

5.6 Acknowledgements

The authors thank A. M. Castillo for valuable contribution during the data acquisition process, P. C. do Nascimento Salvador and LAEF's staff for their technical support, as well as all the athletes volunteering in this study for their time and effort.

5.7 Grants

This study and ongoing research are possible thanks to the financial support provided by CAPES Foundation (Ministry of Education, Brazil) under the scope of the Science without Borders Program (process 13546/13-9).

5.8 Disclosures

No conflicts of interest, financial or otherwise, are declared by the authors.

5.9 Author contributions

L.A.P.d.L., M.R., S.A., and R.D.d.L. conceived and designed research; L.A.P.d.L. and R.D.d.L. performed experiments; L.A.P.d.L. analyzed data; L.A.P.d.L. interpreted results of experiments; L.A.P.d.L. prepared figures; L.A.P.d.L., M.R., S.A., and R.D.d.L. drafted manuscript; L.A.P.d.L., M.R., S.A., and R.D.d.L. edited and revised manuscript; L.A.P.d.L., M.R., S.A., and R.D.d.L. approved final version of manuscript.

CHAPTER 6 COMPLEMENT TO ARTICLE 1: SECOND-ORDER MODELING FOR THE SLOW COMPONENT OF THE PULMONARY OXYGEN UPTAKE ON-KINETICS

6.1 Introduction

While the MiME model presented in the previous chapter enhanced the representation of the FC by means of the second-order family of solutions, it still retained the FOME model's first-order representation of the SC. More than a mere simplification, this choice was based upon both the absence of reports of overshooting SCs in the literature and, as it will be presented, by the lack of impact brought by the second-order solutions to the representation of the SC.

In the present chapter, the utilization of the SOS-based modeling for the SC is tested and discussed, and the overshoot detection and quantification methodology using the FC_{Ovsht} solution applied to the FC in the article 1 is reproduced in the context of the SC. For a conceptual differentiation between the already defined $O\dot{V}O_2K$ phenomenon—observable in some FCs—and any overshoot possibly observed in the SC, we will refer to the former as the $O\dot{V}O_2K_{SC}$.

6.2 Materials and methods

6.2.1 Isolation of the slow component data set

At supra-LT intensities, the SC data set was isolated by subtracting the extrapolated FC curve (dashed section of FC_{FOS} curve; Figure 6.1) from the actually measured $\dot{V}O_2$ data from $t > t_{FC}$ until the end of the step (see Section *5.2.3 Curve-fitting procedures* for details about the t_{FC} evaluation). The choice for subtracting the FC_{FOS} from the measured $\dot{V}O_2$ data instead of the second-order alternative representations of the FC (i.e., the FC_{Ovsht}, FC_{NOvsht}, or $FC_{NOvshtCrit}$ solutions) is justified by the fact that, for $t > t_{FC}$, the difference between the FC_{FOS} curve and the SOS alternatives was negligible. In fact, all FC solutions, when evaluated at $t > t_{FC}$, yielded values lying within a 1% range from their final steady-state reference (i.e., $\dot{V}O_{2Baseline} + A_{FC} \pm 1\%$ of A_{FC}), causing their isolated SC data sets to be extremely similar to each other. Moreover, while any of the FC solutions could be equivalently used for the SC isolation, the FC_{FOS} was chosen with the purpose of providing a comparison somehow conservative in favor of the FOME model.

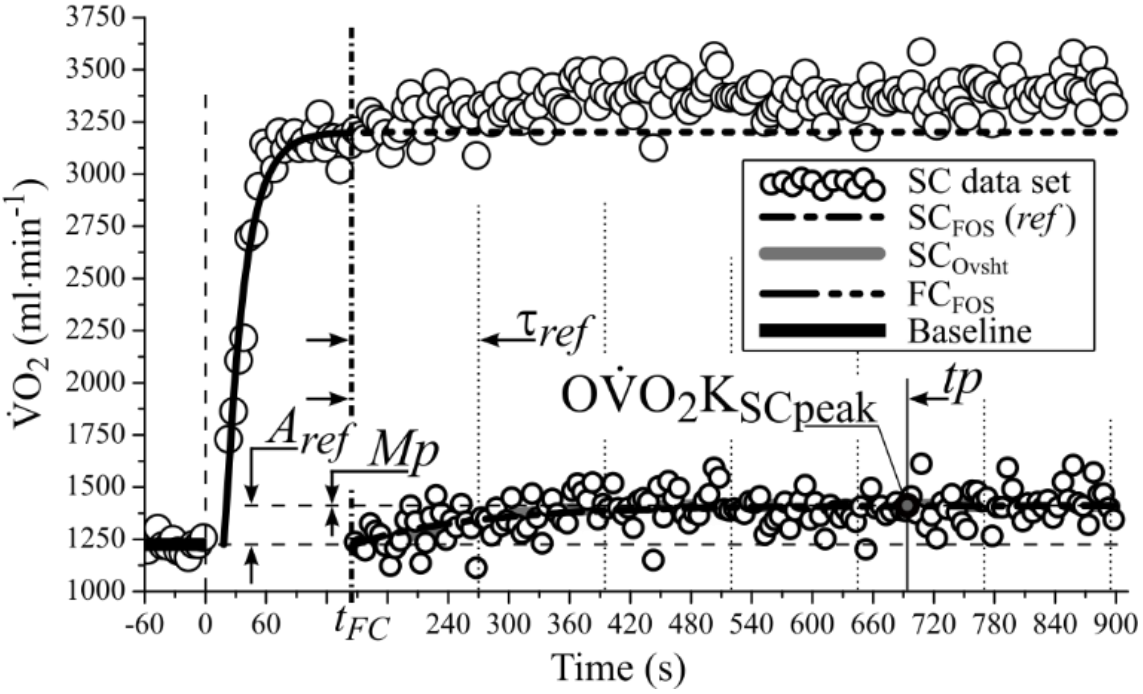

Figure 6.1 Isolation and fitting of the SC data set at supra-LT intensities. Note: The represented *Mp* of this particular subject (0.05 ml·min^{-1}) is not noticeable in the plotted scale.

6.2.2 Underdamped second-order system for overshoot detection and quantification

For the quantification and detection of the $O\dot{V}O_2K_{SC}$ phenomenon, the methodology used for the FC was reproduced (see Section *5.2.4 Overshoot detection using the FCOvsht solution*). For the reference values tp_{ref} and Mp_{ref} (equations 5.7 and 5.8, respectively), the adopted A_{ref} and τ_{ref} parameters were those obtained from the FOS approximation of the SC data set (Figure 6.1), i.e., the A_{SC} and τ_{SC} values, respectively, from the SC_{FOS} described bellow:

$$SC_{FOS}(t) = A_{SC}\left[1 - \exp\left(\frac{-(t - t_{FC})}{\tau_{SC}}\right)\right]_{t \geq t_{FC}} \quad (6.1)$$

In regards to the analogy with the use of equation 5.2 in the FC context, the only required adaptations are the replacement of A_{FC} with the SC's amplitude A_{SC}, the use of the time constant τ_{SC} instead of τ_{FC}, and the use of the previously determined t_{FC} instead of td_{FC}. These same replacements with A_{SC} and t_{FC} were repeated for the evaluation of the proposed SOS solutions, where the equations 5.3 to 5.5 were adapted, being redefined as SC_{Ovsht}, $SC_{NOvshtCrit}$, or SC_{NOvsht}, respectively.

$$SC_{Ovsht}(t) = A_{SC}\left\{1-\exp\left[-\zeta\,\omega\,(t-t_{FC})\right]\left\{\cos\left[\omega_d\,(t-t_{FC})\right]+\frac{\zeta}{\sqrt{1-\zeta^2}}\sin\left[\omega_d\,(t-t_{FC})\right]\right\}\right\}_{t\,\geq\,t_{FC}} \quad (6.2)$$

for $0 \leq \zeta < 1$

$$SC_{NOvshtCrit}(t) = A_{SC}\left\{1-\exp\left[-\omega\,(t-t_{FC})\right](1+\omega\,(t-t_{FC})\right\}_{t\,\geq\,t_{FC}} \quad (6.3)$$

for $\zeta = 1$

$$SC_{NOvsht}(t) = A_{SC}\left\{1+\frac{\exp\left[-\omega\,(\zeta+\sqrt{\zeta^2-1})\,(t-t_{FC})\right]}{2\sqrt{\zeta^2-1}(\zeta+\sqrt{\zeta^2-1})}-\frac{\exp\left[-\omega\,(\zeta-\sqrt{\zeta^2-1})\,(t-t_{FC})\right]}{2\sqrt{\zeta^2-1}(\zeta-\sqrt{\zeta^2-1})}\right\}_{t\,\geq\,t_{FC}} \quad (6.4)$$

for $\zeta > 1$

For simplification purposes, the parameters ζ, ω, and ω_d were kept under the same denomination from the FC context, although new and independent values were calculated for the SC.

Table 6.1 brings the $O\dot{V}O_2K_{SC}$ indicators for the 24 successfully isolated SC data sets. Amongst the 12 satisfactorily convergent regression results obtained with the SC_{Ovsht} solution, only five data sets were considered as candidates for $O\dot{V}O_2K_{SC}$ cases by meeting the requirement of a valid ζ value ($\zeta \in \mathbb{R} \mid 0 \leq \zeta < 1$) and a $tp_{ref} \leq tp_{ref}T = 5$.

The reduced convergence rate represented by the six convergent cases (25% of the 24 available SC data sets), with only five "potentially" overshooting results (i.e., $tp_{ref} \leq 5$) and only two presenting *Mp* values above the 1 ml·min^{-1} mark may be a reflection of either the naturally low magnitude of any possible $O\dot{V}O_2K_{SC}$, or simply the absence of this phenomenon in the SC context.

6.2.3 Comparison between first- and second-order solutions: root mean squared errors

The same goodness of fit evaluation based upon the RMSE values used in the FC analysis was applied to the SC for comparisons between the FOS and the SOS proposed solutions (see Section *4.2.4 Statistical analyses*). Again, the comparisons were performed within two different groups,

namely the $NO\dot{V}O_2K_{SC}$, where the SC_{FOS} was compared to both the SC_{NOvsht} and the $SC_{NOvshtCrit}$ solutions, and the $O\dot{V}O_2K_{SC}$ group, with the SC_{FOS} being compared to the SC_{Ovsht} solution.

Table 6.1 Overshoot indicators obtained from the regressions with the SC_{Ovsht} solution

	Absolute Values				Relative Values			
	tp, s		*Mp*, ml·min^{-1}		tp_{ref} (dimensionless)		Mp_{ref} (dimensionless)	
Subject	40%Δ	70%Δ	40%Δ	70%Δ	40%Δ	70%Δ	40%Δ	70%Δ
1	N-C	238.0	N-C	0.0	N-C	8.39	N-C	<0.001
2	X	N-C	X	N-C	X	N-C	X	N-C
3	N-C	N-C	N-C	N-C	N-C	N-C	N-C	N-C
4	N-C	N-C	N-C	N-C	N-C	N-C	N-C	N-C
5	X	N-C	X	N-C	X	N-C	X	N-C
6	*185.9*	N-C	*0.1*	N-C	*4.55*	N-C	*<0.001*	N-C
7	*113.0*	*133.9*	*19.6*	*3.8*	*3.30*	*3.63*	*0.168*	*0.017*
8	N-C	N-C	N-C	N-C	N-C	N-C	N-C	N-C
9	N-C	N-C	N-C	N-C	N-C	N-C	N-C	N-C
10	*549.3*	N-C	*0.1*	N-C	*4.40*	N-C	*<0.001*	N-C
11	X	N-C	X	N-C	X	N-C	X	N-C
12	N-C	N-C	N-C	N-C	N-C	N-C	N-C	N-C
13	*781.8*	N-C	*0.7*	N-C	*3.25*	N-C	*0.006*	N-C
14	X	N-C	X	N-C	X	N-C	X	N-C
Mean ± SD	*407.5 ± 272.0*	*133.9* —	*5.1 ± 8.4*	*3.8* —	*3.87 ± 0.61*	*3.63* —	*0.044 ± 0.083*	*0.017* —
All supra-LT Mean ± SD	4.14 ± 0.28		4.14 ± 0.28		0.039 ± 0.028		0.039 ± 0.028	

Values in italic are exclusive to $O\dot{V}O_2K_{SC}$ containing cases, i.e., those datasets yielding a convergent FC_{Ovsht} solution with a satisfactory ζ value ($\zeta \in \mathbb{R} \mid 0 \leq \zeta < 1$), and $tp_{ref} > tp_{ref}T = 5$; N-C: No convergent SC_{Ovsht} solution satisfying ζ's requirements could be found (see Appendix E for details); X: Cases where the SC data set was not available due to unidentifiable t_{FC} instants.

Table 6.2 Comparisons between mean RMSE values from the SC_{FOS} and the second-order proposed solutions

$NO\dot{V}O_2K_{SC}$ cases	SC_{FOS}	$SC_{NOvshtCrit}$	SC_{NOvsht}
All supra-LT ($P < 0.0002$; $n = 19$)	105.1 ± 34.5	108.6 ± 33.3*	107.5 ± 34.4*
40%Δ ($P = 0.10$; $n = 6$)	95.2 ± 31.3	99.9 ± 30.8	97.8 ± 30.6
70%Δ ($P < 0.001$; $n = 13$)	109.7 ± 36.2	112.6 ± 34.8*	111.9 ± 36.2*
$O\dot{V}O_2K_{SC}$ cases	SC_{FOS}	vs.	SC_{Ovsht}
All supra-LT ($P = 0.18$; $n = 5$)	125.3 ± 44.7		125.5 ± 44.7
40%Δ ($P = 0.37$; $n = 4$)	111.3 ± 36.9		111.5 ± 36.9
70%Δ ($n = 1$)	181.1		181.5

Root mean squared error (RMSE) values are expressed as means ± SD (ml·min^{-1}). *Significantly different from the SC_{FOS} solution.

In the $NO\dot{V}O_2K_{SC}$ situation (Table 6.2, *top*; ANOVA results), the FOS and both SOS suitable options remained statistically equivalent at the 40%Δ intensity. The same equivalence was demonstrated between the $SC_{NOvshtCrit}$ and the SC_{NOvsht} in the comparisons at either 70%Δ (*post-hoc* test, $P = 0.59$) or including all supra-WRs (*post-hoc* test, $P = 0.30$), conditions where a significantly better performance of the FOS was observed.

For the $O\dot{V}O_2K_{SC}$ cases, the SC_{Ovsht} solution did not alter the RMSE mean values significantly from the SC_{FOS} model, as shown by paired Student's t-test reported in Table 6.2 (bottom).

6.2.4 Comparison between FOME and MiME models: limitation of the fixed slow component's time delay

As explained previously, the fact that the definition of the instant t_{FC} in both FOME and MiME models occurs before the actual regressions on the FC and SC data sets (see Section *5.2.3 Curve-fitting procedures*) imposes an important difference between the obtention of these two components' parameters.

In the context of the FC component, the impact of reasonable variations in the location of t_{FC} is merely the inclusion or exclusion of points in the data set close to this component's steady-state region (thus, further from the transitory phase), which does not influence the curve parameters evaluation in a substantial manner. As for the SC context however, where the pre-defined t_{FC} is already the component's onset time delay itself (td_{SC}), a possibly late td_{SC} causes the initial increase of the SC to appear too steep, and vice-versa. Moreover, it is noteworthy that the condition of an erroneously late td_{SC} specifically punishes the SOS modeling due to its tendency to start less abruptly (with its upward concavity).

Although not attempted in the present work, one possible approach might be useful to rule out or at least reduce the influence of the pre-fixed t_{FC} on the SC's curve parameters: the introduction of a $2 \cdot \rho$ tolerance range for td_{SC} around the pre-determined t_{FC} (i.e., $t_{FC} - \rho \leq td_{SC} \leq t_{FC} + \rho$). This strategy could at the same time compensate for the limited accuracy of t_{FC}'s evaluation and allow the FOS and SOS solutions to freely fit themselves into the initial region of the SC.

In regards to the other parameters presented on Table 6.3, the magnitude order obtained for ω and ω_d was generally smaller than that observed in the FC. Moreover, values of ζ higher than those

from the FC are in accordance with the slower, less oxidative nature of the type II fibers associated with the SC [39].

Table 6.3 $\dot{V}O_2$ on-kinetics parameters obtained from least squares regressions for SC_{FOS}, SC_{NOvsht} and SC_{Ovsht} solutions

	$NO\dot{V}O_2K_{SC}$ cases			$O\dot{V}O_2K_{SC}$ cases		
WR	40%Δ	70%Δ	All supra-LT	40%Δ	70%Δ	All supra-LT
Sample size	n = 6	n = 13	n = 19	n = 4	n = 1	n = 5
$td_{SC} = t_{FC}$, s	194.2 ± 64.0	170.8 ± 52.7	178.2 ± 55.8	183.7 ± 32.2	145.0 —	176.0 ± 32.9
First-Order System	SC_{FOS}			SC_{FOS}		
τ_{SC}, s	166.1 ± 123.2	134.1 ± 84.7	144.2 ± 96.1	110.2 ± 96.3	36.9 —	95.5 ± 89.6
Second-Order System	SC_{NOvsht}			SC_{Ovsht}		
ζ (dimensionless)	3.05 ± 2.6	5.74 ± 3.38	4.89 ± 3.33	0.80 ± 0.21	0.79 —	0.80 ± 0.18
ω, rad·s^{-1}	0.031 ± 0.017	0.088 ± 0.065	0.070 ± 0.060	0.070 ± 0.060	0.03 —	0.027 ± 0.015
ω_d *, rad·s^{-1}	—	—	—	0.014 ± 0.011	0.023 —	0.016 ± 0.011
τ_{App_SC}†, s	176.9 ± 111.3	148.3 ± 82.3	157.4 ± 90.3	—	—	—

Values are mean ± SD; *The concept of ω_d does not apply to the SC_{NOvsht} solution; †The variable τ_{App_SC} derives from the FOS approximation of SC_{NOvsht} (in analogy to the variable τ_{App} evaluated in the FC context, as described in the Footnote 12).

Additionally, the larger relative importance of the SD values observed in the SC, especially in the ζ for $NO\dot{V}O_2K_{SC}$ cases, may also be explained by the less oxidative nature of these fibers. In the context of a low signal-to-noise ratio caused by the modest A_{SC} magnitudes (mean ± SD = 287 ± 127 ml·min^{-1} for the $NO\dot{V}O_2K_{SC}$, and 165 ± 44 ml·min^{-1} for the $O\dot{V}O_2K_{SC}$ cases), the difficulties in accurately evaluating these parameters may be increased.

Finally, while in the FC context the τ_{FC} and MRT tended to be longer than their second-order approximations (i.e., τ_{App} and MRT_{App}, respectively; Table 5.4), the opposite tendency is observed

for the SC regarding the τ_{SC} and τ_{App_SC}[13] (Table 6.3). This effect may be numerically explained by the τ_{App} formula in Footnote 12, which imposes an increasing relative sensitivity to ω in comparison to ζ values for the SC conditions (namely greater ζ and smaller ω). However, while these numerical aspects may cause the second-order approximation of the SC_{FOS} to be less valid, it is also intuitive that the subtle features of the SC's transitory phase may not be properly detected in that reduced signal-to-noise ratio context by either the first- or the second-order solutions, reducing the likelihood of a similarity between τ_{SC} and τ_{App_SC} values.

6.3 Conclusion

The overall superior fitting performance of the SC_{FOS} in the $NO\dot{V}O_2K_{SC}$ situations, combined with the equivalence between SC_{FOS} and SC_{Ovsht} for the possibly overshooting data sets (Table 6.2) do not justify the abandonment of the more succinct FOS formulation for the SC, at least when a pre-fixed td_{SC} is used.

Once again, the convenience of a model mixing both FOS and SOS proposed in the MiME model is corroborated for the case where a second component is added to a first one after a different onset time delay (i.e., $td_{SC} \neq td_{FC}$). In the next two chapters, a new model whose components are simultaneously activated and participating throughout the whole $\dot{V}O_2$ response will be presented, analyzed, and discussed.

---

[13] Since both FOME and MiME models use the same td_{SC}, the MRT and MRT_{App} values would be respectively calculated, in the SC context, as $td_{SC} + \tau_{SC}$ and $td_{SC} + \tau_{App\_SC}$. Thus, the comparison between MRT and MRT_{App} values performed in the FC analysis (see Table 5.4) was not reproduced for the SC. Instead, the more direct comparison between τ_{SC} and τ_{App_SC} was performed, as shown on Table 6.3.

CHAPTER 7 ARTICLE 2: SECOND-ORDER SIMULTANEOUS COMPONENTS MODEL FOR THE OVERSHOOT AND "SLOW COMPONENT" IN $\dot{V}O_2$ KINETICS

Luis A. P. de Lima[a,b], Sofiane Achiche[a], Ricardo D. de Lucas[c], and Maxime Raison[a]

[a]*Mechanical Engineering Department, Polytechnique Montréal, Quebec, Canada;* [b]*CAPES Foundation (Brazilian Ministry of Education), Brasília, Distrito Federal, Brazil; and* [c]*Sports Centre, Federal University of Santa Catarina, Florianópolis, Santa Catarina, Brazil*

Respiratory Physiology & Neurobiology. Submitted 16 October 2019.

The human oxygen uptake responses to exercise step on-transients present different shapes depending on the overshoot and/or the "slow component" manifestations. The conventional First-Order Multi-Exponential (FOME) model incorporates delayed add-on terms to comprise these phenomena, increasing parameters quantity, requiring a delayed recruitment of type II fibers to explain the "slow component," and not offering a unified structure for different individuals and intensity domains. We hypothesized that a model composed of two Second-Order Simultaneous Components (SOSC) would present a better overall fitting performance than the FOME. Fourteen well-trained male cyclists performed repeated step on-transitions to moderate, heavy, and severe cycling intensities, whose responses were fitted with FOME and SOSC models. The SOSC presented significantly smaller ($p < 0.05$) root mean squared errors for moderate, supra-moderate, and all intensities together. Combined with conceptual analyses, these findings suggest the SOSC as a comprehensive alternative to the FOME model, explaining all oxygen uptake step responses with as many parameters and without delayed add-on components.

KEYWORDS: Second-order system; $\dot{V}O_2$; oxygen uptake kinetics; overshoot; slow component; mathematical modelling.

HIGHLIGHTS

- Model for $\dot{V}O_2$ step response composed of two second-order simultaneous components.
- Comprises responses with none, either, or both the overshoot and "slow component."
- Does not require the delayed recruitment of fibers to explain the "slow component."

- Describes the $\dot{V}O_2$ step on-transient to any exercise intensity.
- Overall goodness-of-fit superior to that of first-order multi-exponential model.

7.1 Introduction

In response to the work rate (WR) step on-transient, the most used model for the $\dot{V}O_2$ kinetics is the First-order Multi-exponential (FOME). After the transitory cardiodynamic component, this model is composed of a fundamental component (FC) and, for intensities above the lactate threshold WR (WR_{LT}), of a delayed slow component (SC) [1, 121]. As shown in equation 7.1, both FC and SC present independent onset time delays (td_{FC} and td_{SC}), amplitudes (A_{FC} and A_{SC}), and time constants (τ_{FC} and τ_{SC}).

$$\dot{V}O_2(t) = \dot{V}O_{2Baseline} + \left[\begin{matrix}\text{Cardiodynamic}\\ \text{Component}(t)\end{matrix}\right]_{0 \le t < td_{FC}} + A_{FC}\left[1-\exp\left(\frac{-(t-td_{FC})}{\tau_{FC}}\right)\right]_{t \ge td_{FC}} + A_{SC}\left[1-\exp\left(\frac{-(t-td_{FC})}{\tau_{FC}}\right)\right]_{t \ge td_{SC}} \quad (7.1)$$

Motivated by the inability of the FOME model to describe the $\dot{V}O_2$ overshoot ($O\dot{V}O_2K$) above the FC's steady-state observed in some step on-transient responses [12, 46-48, 50, 51, 57], we have recently proposed a Mixed Multi-Exponential (MiME) model [57], whose FC is represented by a second-order curve. Thus, its FC shape is no longer defined by τ_{FC}, but by two other parameters conveniently adaptable to reproduce either overshooting or nonovershooting responses [55, 56]. Alternative modeling attempts aggregate an *overshoot term* to the FOME model in $O\dot{V}O_2K$ cases [46, 48, 51], which add three new parameters to the response (Table 7.1).

Another add-on term is the SC, whose "activation" in FOME or MiME models is conditioned to the occurrence of the "slow component" phenomenon—a slow rise in $\dot{V}O_2$ values usually observed at supra-LT intensities [1, 91], referred to as the $\dot{V}O_2$ slow augmentation ($\dot{V}O_2SA$) in our work to avoid nomenclature ambiguity with the SC. Despite considerable consensus in associating the $\dot{V}O_2SA$ with the participation of type II fibers in the exercising muscles [39, 41, 42, 88, 96-99], their recruitment regimen is still debated [38, 52-54, 133, 158, 159]. Moreover, not only the existence of differently delayed phases in $\dot{V}O_2$ kinetics is questioned [8, 45, 134-136], but the $\dot{V}O_2SA$ is observable in conditions where all muscle fiber types are recruited simultaneously [53].

Nevertheless, both FOME and MiME may only model the $\dot{V}O_2SA$ by adopting a delayed SC. Attempts to represent $\dot{V}O_2$ pulmonary responses with two simultaneous first-order components ($td_{SC} = td_{FC}$) performed poorer than the FOME model [91].

Table 7.1 Comparison between quantities of components and parameters used in different models for the $\dot{V}O_2$ kinetics

	Phenomena observed in the data set			
Model	None	O$\dot{V}O_2$K	$\dot{V}O_2$SA	O$\dot{V}O_2$K and $\dot{V}O_2$SA
FOME*	FC (3)	FC (3)	FC + SC† (6)	FC + SC† (6)
FOME*/*overshoot term*‡	FC (3)	FC + overshoot term† (6)	FC + SC† (6)	FC +overshoot term† + SC† (9)
MiME§	FC (4)	FC (4)	FC + SC† (7)	FC + SC† (7)
SOSC	CI + CII (6)	CI + CII (6)	CI + CII (6)	CI + CII (6)

The cardiodynamic component was omitted, for its present in all the compared models. Values between parenthesis indicate the quantity of parameters required by the model. *FOME's FC is first-order, thus unable to present an overshooting behaviour. †Add-on term introduced accordingly with data characteristics. ‡The *Overshoot term* proposed in [46, 51] is different from that in [48], although both present three parameters; §Same structure as FOME, however assuming a second-order FC [57].

The hypothesis of the present study was that a Second-Order Simultaneous Components (SOSC) model (Table 7.1, last row) would present a better overall fitting performance than the FOME model in fitting $\dot{V}O_2$ step responses at all WRs, containing none, either, or both of the O$\dot{V}O_2$K and $\dot{V}O_2$SA phenomena.

7.2 Materials and methods

7.2.1 The Second-Order Simultaneous Components model

The combined response (CR) of the SOSC model is composed of two second-order curves starting after a common time delay td_S, namely the Component I (CI) and the Component II (CII). The general formulation of the SOSC model response to the exercise step on-transient applied at $t = 0$ is:

$$\dot{V}O_2(t) = \dot{V}O_{2Baseline} + \begin{bmatrix} \text{Cardiodynamic} \\ \text{Component}(t) \end{bmatrix}_{0 \le t < td_{FC}} + \left[\text{CI}(t) + \text{CII}(t)\right]_{t \ge td_S} , \qquad (7.2)$$

with a baseline value ($\dot{V}O_{2Baseline}$) being added of a cardiodynamic component (Figure 7.1.A) until around $t = td_S$, when the CR shape assumes the shape of the sum CI + CII.

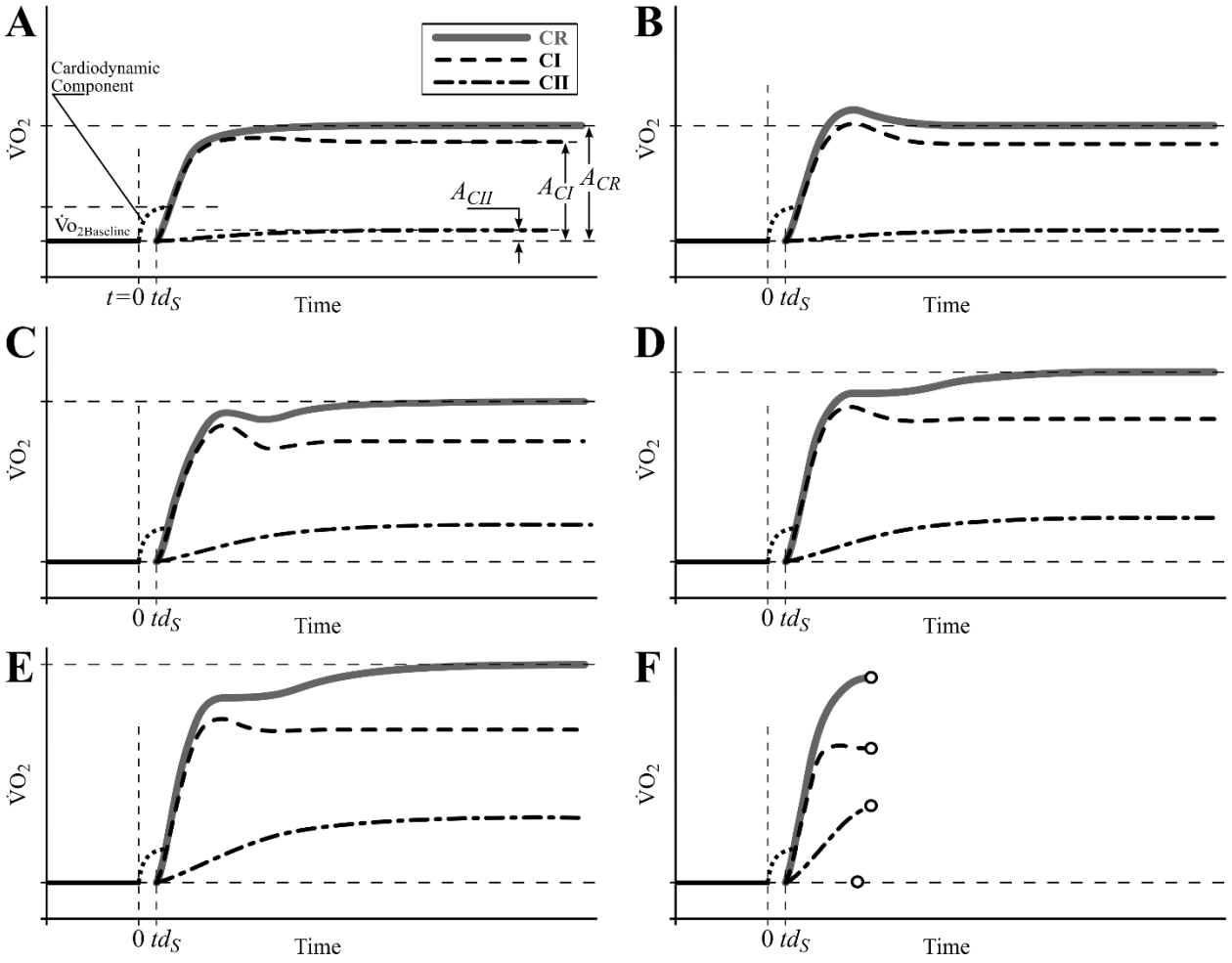

Figure 7.1 Six qualitative configurations of the $\dot{V}O_2$ step response comprised by the SOSC model. In all cases, the CR is formed by adding two components starting at the same time delay td_S to the baseline value, namely CI and CII (A to F). For clarity, the reference for CI and CII is set as the $\dot{V}O_{2Baseline}$ instead of zero in the $\dot{V}O_2$ axis. A_{CR} is equal to $A_{CI} + A_{CII}$. See text for details.

Second-order system modeling. First-order models constitute very idealistic approximations of real systems, since inertia-like elements are always present (see *physiomechanical analogy* in [57]), with higher-than-one models being often adopted despite the added parameters. The shape of a second-order step response is defined by two parameters, namely the natural frequency (ω) and the damping ratio (ζ). For each type of second-order system, a different formulation must be used: the *underdamped* type ($0 \leq \zeta < 1$) is the only one accepting the overshooting behaviour, whereas the *critically damped* ($\zeta = 1$) and the *overdamped* ($\zeta > 1$) types describe nonovershooting curves [55, 56]. As adopted in [57], the formulation for the *critically damped* case was disregarded, for the

specific ζ = 1 condition is satisfactorily approached by the *underdamped* (ζ = 0.999) or the *overdamped* (ζ = 1.001) solutions. In the SOSC formulation, the CI may be modelled by an *underdamped* (CI_{Ovsht}) or an *overdamped* (CI_{NOvsht}) curve, respectively represented by equation 7.3 or 7.5, while the CII is always represented by the *overdamped* curve (CII_{NOvsht}) in equation 7.5:

$$CI_{Ovsht}(t) = A_{CI}\left\{1-\exp\left[-\zeta_{CI}\,\omega_S\,(t-td_S)\right]\left[\cos\left(\omega_{d\_CI}\,(t-td_S)\right)+\frac{\zeta_{CI}}{\sqrt{1-\zeta_{CI}{}^2}}\sin\left(\omega_{d\_CI}\,(t-td_S)\right)\right]\right\}_{t\,\geq\,td_S} \quad , (7.3)$$

for $0 \leq \zeta_{CI} < 1$

where CI's damped frequency (ω_{d_CI}) is given by

$$\omega_{d\_CI} = \omega_S\sqrt{1-\zeta_{CI}{}^2} \quad , \qquad (7.4)$$

for $0 \leq \zeta_{CI} < 1$

and

$$CI_{NOvsht}(t), CII_{NOvsht}(t) = A\left[1+\frac{\exp\left[-(\zeta+\sqrt{\zeta^2-1})\,\omega_S\,(t-td_S)\right]}{2\sqrt{\zeta^2-1}(\zeta+\sqrt{\zeta^2-1})}-\frac{\exp\left[-(\zeta-\sqrt{\zeta^2-1})\,\omega_S\,(t-td_S)\right]}{2\sqrt{\zeta^2-1}(\zeta-\sqrt{\zeta^2-1})}\right]_{t\,\geq\,td_S} \quad , (7.5)$$

for $\zeta > 1$

where ζ represents the damping ratios ζ_{CI} or ζ_{CII}, respectively for CI or CII, and *A* may assume either A_{CI} or A_{CII} values, i.e., the respective amplitudes of CI and CII. The natural frequency ω_S and time onset delay td_S is the same for both SOSC model components.

7.2.2 SOSC model and the exercise intensity spectrum

The SOSC model configuration allows its CR to cover the exercise intensity spectrum by assuming a variety of shapes comprising none, either, or both of the $\dot{V}O_2$SA and O$\dot{V}O_2$K phenomena (Figure 7.1). In Figure 7.1.A, the summation of a slightly overshooting CI (or even a possibly nonovershooting CI) with a minute CII results in the typical CR of the moderate domain, containing neither the $\dot{V}O_2$SA nor the O$\dot{V}O_2$K. For fitter individuals, where the CR may manifest an O$\dot{V}O_2$K, the CI will present a more pronounced overshooting behaviour (Figure 7.1.B). This is the case of O$\dot{V}O_2$K containing responses, more often reported in the moderate exercise domain [12, 46-48, 50, 51, 57].

As the WR increases beyond the moderate domain (Figure 7.1.C-F), the magnitudes of both components will also increase, allowing the CR curve to adapt to the higher $\dot{V}O_2$ demand. However, the percentage contribution of the CII to the CR (A_{CII}%) will increase more than that of CI (A_{CI}%), causing the $\dot{V}O_2$SA phenomenon to become increasingly more evident, at the same time that the O$\dot{V}O_2$K will tend to disappear in the CR.

Figure 7.1.C describes the less usual situation where both $\dot{V}O_2$SA and O$\dot{V}O_2$K are concomitantly present in the observed response, which is more likely to occur in the lower limits of the heavy domain of exercise (see [57] for the first reports of these occurrences). Regardless of the occurrence of Figure 7.1.C situation, the continued increase of the step WR magnitude illustrated from Figure 7.1.D to Figure 7.1.E will cause both the relative importance of the CII and the magnitude of the $\dot{V}O_2$SA to increase accordingly, leaving no noticeable O$\dot{V}O_2$K manifestation in the net response. Eventually, either or both CI or/and CII will find their physiological limits, establishing the ceiling ($\dot{V}O_{2max}$) of the CR attained at the severe exercise domain (Figure 7.1.E). Finally, the premature fatigue at the extreme exercise domain [124] will preclude the SOSC components from fully developing (Figure 7.1.F).

7.2.3 Sample, experimental procedures and data pre-treatment

The data sets analysed were the same collected by de Lima et al. [57], from a sample composed of fourteen well-trained male endurance athletes from cycling and triathlon backgrounds, with the following characteristics (mean ± SD): 32.5 ± 7.5 years old; body mass: 68.9 ± 6.6 kg; $\dot{V}O_{2max}$: 62.6 ± 6.0 ml·min^{-1}·kg^{-1}; WR at $\dot{V}O_{2max}$: 311 ± 37 W; WR_{LT}: 174 ± 23 W; and 9.9 ± 6.6 (minimum of three) years of cycling experience. Written informed consent was obtained in accordance with institutional ethical committee rules.

In a first visit, each subject underwent anthropometric measurements, a “bike fitting,” and a maximal incremental step test of constant pedalling cadence starting at 100 W, with a 25 W step every third minute (Lode Excalibur Sport; Lode Medical Technology, Groningen, The Netherlands). Blood was sampled from the subject’s earlobe at the end of each step for blood lactate concentration assessment (YSI 2700 Select; Yellow Springs, USA) and WR_{LT} evaluation. Breath-by-breath gas exchange measurements (Quark CPET; Cosmed, Rome, Italy) allowed the assessment of $\dot{V}O_{2max}$ (maximal 30 s $\dot{V}O_2$ average in the incremental test) and its respective WR.

A minimum interval of 48 hours was allowed before each of the subsequent three visits, whereby every athlete performed a total of 13 step on-transients, covering five WRs as follows:

Sub-LT intensities. Three 6 min. square waves at each of the three moderate intensities of 55%, 70% or 85% of WR_{LT}, respectively denominated 55%LT, 70%LT and 85%LT;

Supra-LT intensities. Two 15 min. square waves at each of two supra-LT WRs, one at the heavy and another at the severe exercise domains, corresponding to the WR_{LT} added of respectively 40% (40%Δ) or 70% (70%Δ) of the difference between WR_{LT} and the WR of $\dot{V}O_{2max}$ added of respectively 40% and 70% of the difference between WR_{LT} and the WR of $\dot{V}O_{2max}$.

Each step on-transient response data was pre-treated by a computational code developed in MATLAB (The MathWorks Inc., Natick, USA). Clearly errant breaths were visually removed, and every point distancing more than four standard deviations from the mean of its four surrounding data values was automatically removed [48]. Inspected data points were linearly interpolated to generate one point per entire second. Responses to the same WR of each individual were time aligned and averaged into a single data set [4, 47, 48], whose data points represented each a 5-s bin [4].

7.2.4 Curve fitting procedures

For all models, the value adopted for $\dot{V}O_{2Baseline}$ (equations 7.1 and 7.2) was the average of the 60 s preceding the step transition [47, 153]. The first 20 s of the step response data, roughly corresponding to the cardiodynamic component, were ignored [4, 47, 48, 50, 123].

FOME methodology: The formulations and the fitting procedures for these models have been extensively discussed in our previous work [57]. Very briefly, the amplitude of the FC (A_{FC}) adopted in the MiME model is that obtained by the first-order exponential from the FOME model, while the amplitude of the SC (A_{SC}) is obtained with the first-order step response in both models. For supra-LT intensities, the td_{SC} was defined with an iterative analysis of the fitting indicators from the first-order regressions for the FC (e.g., chi-squared, τ_{FC} and its 95% confidence interval, and plotted residuals), as already adopted in previous studies [13, 153].

SOSC methodology: Whilst the FOME model rely on the premise that a single component is present between td_{FC} and td_{SC}, the SOSC model has to deal with the issue of the complete superposition of CI and CII (Figure 7.1). Thus, we developed an iterative decomposing method in MATLAB to find

the optimal CI and CII curves. This recursive mechanism (Figure 7.2; dashed contour) was applied by systematically assigning different values to A_{CII}% (ranging from 0 to 100%, with resolution of 1%). For each A_{CII}%, a pair of A_{CII} and A_{CI} values was calculated as proportions of A_{CR} (A_{CR} is also the sum of FOME model's A_{FC} and A_{SC}), and different td_S values were tried ($0 \leq td_S \leq 25$ s; resolution of 0.1 s). For each combination of A_{CII}% and td_S, the iteration cycle of *steps A*-to-*F* was repeated until the RMSE value obtained for the CR was no longer improved (i.e., less than 0.001% of variation), as described below:

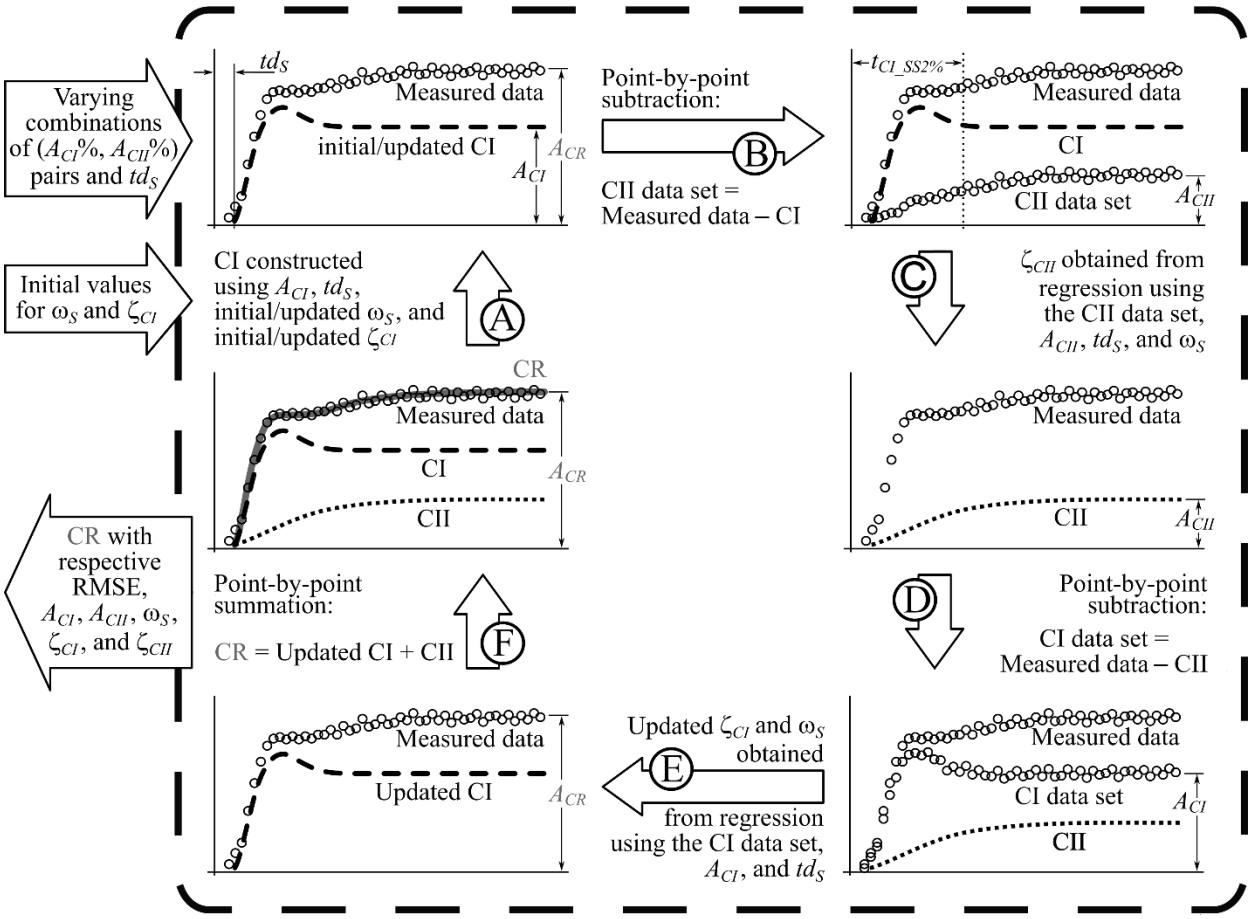

Figure 7.2 Representation of the SOSC model's evaluation methodology. See *SOSC methodology* for a detailed description.

A. a CI curve is evaluated at each 5-s bin time point by plugging the amplitude A_{CI} [where $A_{CI} = A_{CR} \cdot A_{CI}\% = A_{CR} \cdot (100 - A_{CII}\%)$], and specific initial values of ω_S and ζ_{CI} into equation 7.3 or 7.5;

B. with the CI curve constructed, a possible CII data set is "isolated" by means of a simple point-by-point subtraction of the CI from the measured $\dot{V}O_2$ response, i.e., CII data set = Measured data – CI;

C. a regression is performed by fitting the equation 7.5 into the CII data set, with A_{CII} and the same ω_S of CI. A ζ_{CII} value is obtained and thus, an estimation of CII;

D. a CI data set is then "isolated" by subtracting the estimate CII from the measured data;

E. an updated estimation of CI is obtained by the regression to equation 7.5 using the CI data set and A_{CI}. The new ζ_{CI} obtained becomes the updated ζ_{CI}, and the updated ω_S is evaluated as the mean value between the newly obtained and the precedent ω_S values; and

F. the CR candidate is obtained by simply summing up the CI and the updated CII;

At this point, CR's goodness of fit is assessed, and if a new iteration is required, the initial values of ζ_{CI} and ω_S used in *step A* are replaced with the updated ones. After all combinations of (A_{CI}%, A_{CII}%) pairs and td_S have been tested, the parameters set yielding the smallest RMSE was selected.

In order to have good initial estimates for the parameters ω_S and ζ_{CI} of each subject to be used in the *step A* of the first iteration, we used those values obtained for the CI_{Ovsht} or CI_{NOvsht} alone (whichever yielded the better fit) applied to the lowest WR available, i.e., 55%LT. The reasoning behind this approach is that, at such low intensities, the contribution of the CII is still small, so that CI is a good approximation of the CR curve. In other words, the lower the WR, the more the CR approaches a "pure" CI situation. In any case, as remarked during our numerical trials, once these parameters' initial estimates were maintained within physiological limits, they did not influence its final convergence values. Moreover, in the first two iterations of the *A-F cycle*, the CII data set in the regression of *step C* was only considered from $t = t_{CI\_SS2\%}$ onward (dotted vertical line; Figure 7.2), i.e., the instant when the CI enters an steady-state with a variation smaller than 2% of A_{CI}, given by [55, 56]:

$$t_{CI\_SS2\%} = td_S + \frac{4}{\omega_S \, \zeta_{CI}} \tag{7.6}$$

In practical terms, the first two iterations used a part of the CII data set where the CI curve was practically equal to A_{CI} (for $t < t_{CI\_SS2\%}$, CII data set ≈ Measured data – A_{CI}), which reduced dramatically the influence of the initial ω_S and ζ_{CI} values in the final results.

Sub-LT intensities. Due to the $\dot{V}O_2SA$ absence below the WR_{LT}, the CII contribution to the CR is expected to be negligible or, at least, not necessarily detectable by our methodology alone. In that case, the A_{CII}% was inferred from the extrapolation of an exponential decay towards the WR of zero Watts (Figure 7.3). Thus, for every subject at each of the sub-LT intensities, the iterative method of Figure 7.2 was applied only for the specifically determined A_{CII}%.

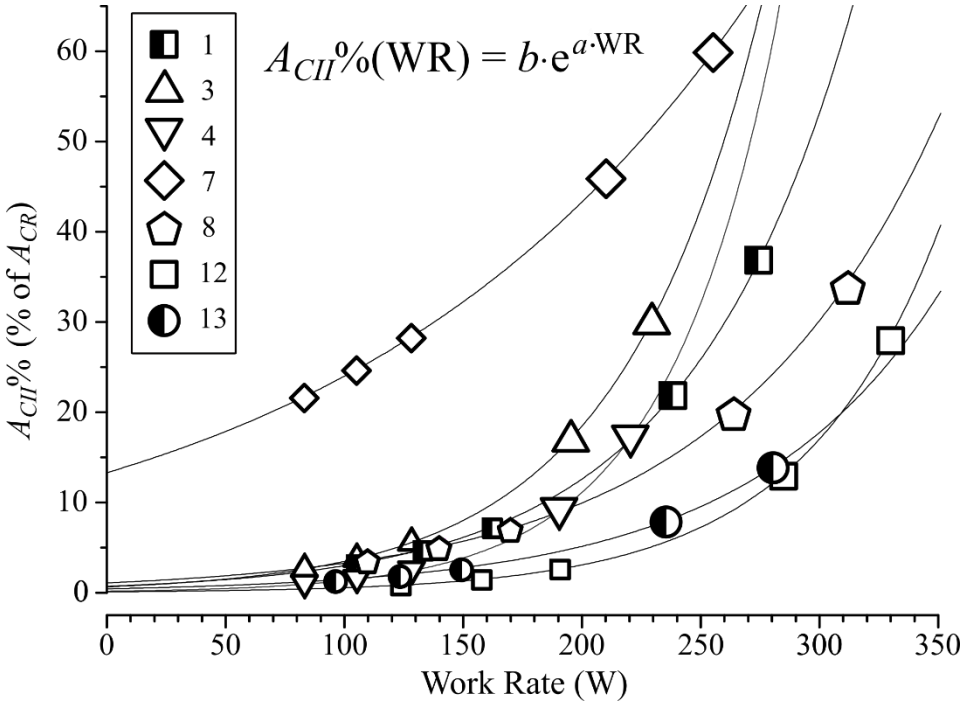

Figure 7.3 A_{CII}% values for sub-LT intensities (*small markers*) predicted from the extrapolation using the exponential obtained with the supra-LT data (*large markers*). A pair of parameters *a* and *b* (see general equation in the figure) was evaluated for every subject.

7.2.5 Statistical analyses

SOSC and FOME models had their fitting performances assessed by means of the root mean squared error (RMSE) values compensated for the different number of parameters present in their equations, with residual analysis complementing the goodness of fit assessment. Paired Student's *t*-tests or repeated measures ANOVA (with post hoc Tukey's test for honest significant difference) were used for comparisons between two or multiple variables, respectively. Whenever normality and homoscedasticity of data required a nonparametric test, Wilcoxon matched pairs test or Friedman ANOVA were applied. In all tests, significance was accepted for $p < 0.05$. All statistical tests used the software package STATISTICA 13.1 (The Dell Inc., Round Rock, USA).

7.3 Results

7.3.1 Convergence analysis of the SOSC model at supra-LT intensities

The typical pattern for the RMSE results along the different A_{CII}% values is illustrated in Figure 7.4.A, where a smooth "V" pattern was defined around the optimal value. This was the case of 23 (CONV group) out of the 28 supra-LT tested data sets. However, in five cases (*subjects 2, 5, 11* and *14* at 40%Δ, and *subject 11* at 70%Δ; nonCONV group) the RMSE discontinuously varied within a very narrow amplitude (2.2 ± 2.1 ml·min^{-1}), failing to present a sharply defined A_{CII}% optimal value (Figure 7.4.B). Coherently, these particular four 40%Δ cases were the same ones to which the FOME and MiME models' methodology failed to identify the beginning of the SC, showing that, regardless of the modeling used, the characterization of certain less evident $\dot{V}O_2$SA is intrinsically less obvious. Moreover, these five "optimal" A_{CII}% values were all equal to or greater than 80% (Figure 7.4.C), which seems unrealistic in terms of a slow-twitch fibers' contribution to the net $\dot{V}O_2$.

A peculiarity was presented by *subjects 6, 9* and *10*, to whom the A_{CII}% was greater at 40%Δ than at 70%Δ (see descending slopes on Figure 7.4.C). Nevertheless, the overall tendency of the CONV group, where A_{CII}% values went from 24.6 ± 14.9% at 40%Δ to 29.8 ± 12.0% at 70%Δ, agrees with the augmented relative contribution of CII at higher intensities expected for the SOSC model. Due to this peculiarity, we defined a sub-group CONV+ formed exclusively by subjects whose data sets presented a positive variation of A_{CII}% values from 40%Δ to 70%Δ (Figure 7.4.C).

7.3.2 RMSE comparisons

The paired comparison between the fit errors from both models' CRs (Table 7.2) presented significant differences for most of the tested conditions, with the SOSC model always presenting lower RMSE mean values than those from the FOME model.

The overshooting version of the CI (equation 7.3) was predominant, with only four cases at 40%Δ (*subjects 1, 3, 12* and *13*), four cases at 70%Δ (*subjects 2, 4, 10* and *13*), and only one sub-LT case (*subject 4* at 85%LT) showing better fit performances with the use of the CI_{NOvsht} rather than the CI_{Ovsht}. All parameters and descriptive variables obtained for the tested models in the CONV+ group are presented in Table 7.3.

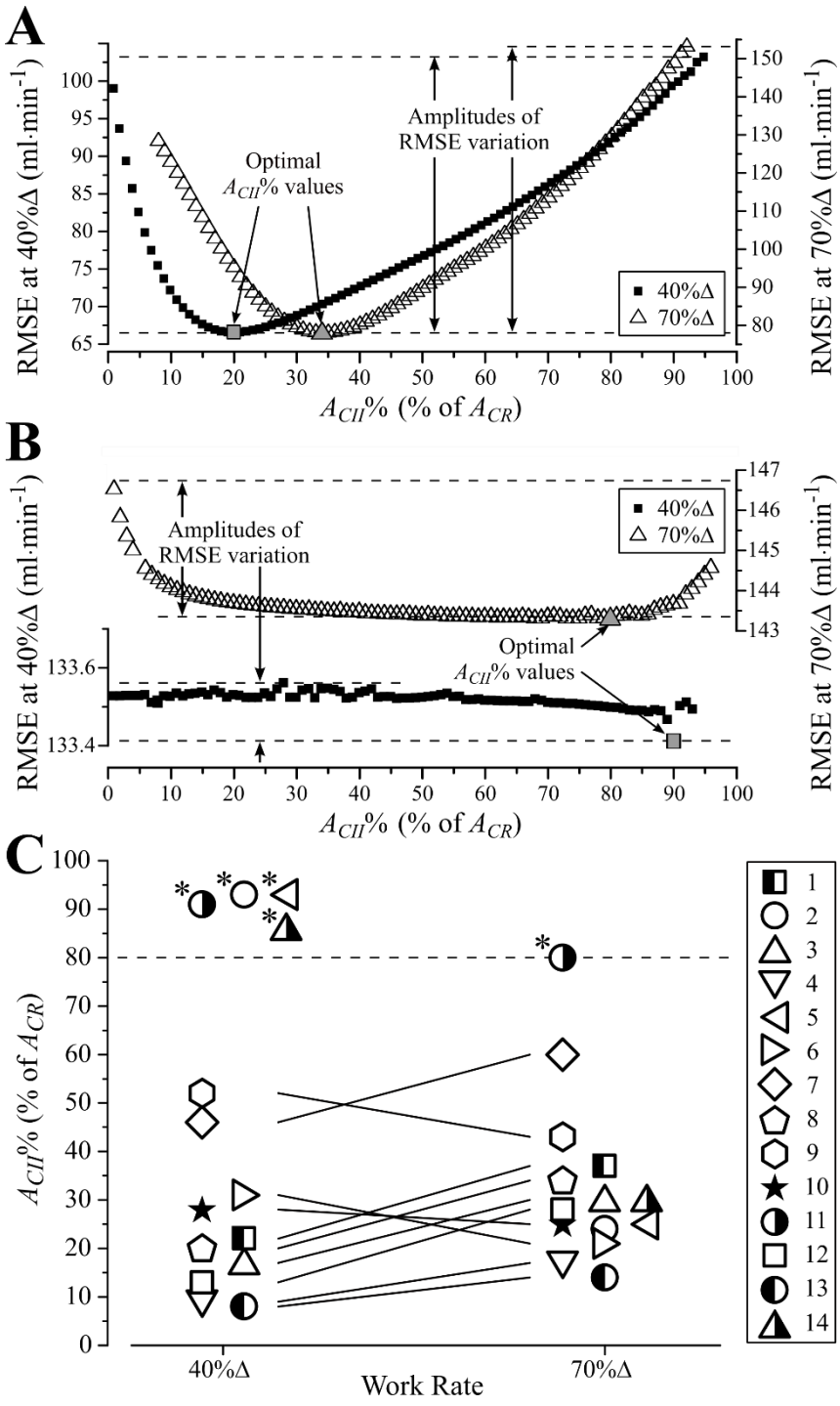

Figure 7.4 A. Typical smooth "V" pattern obtained for the RMSE values in 82% of the supra-LT data sets evaluated with the SOSC model's methodology; B. Example of inconclusive RMSE pattern found for the five data sets of the nonCONV group; and C. A_{CII}% values presented by the 28 supra-LT data sets (C). *Cases from the nonCONV group. CONV+ group contains *subjects 1*, *3*, *4*, *7*, *8*, *12*, and *13*.

Table 7.2 Comparisons between mean RMSE values from SOSC and FOME models

Model	FOME	SOSC
CONV group		
All supra-LT WRs (P = 0.002; n = 23)	105.5 ± 33.9	104.3 ± 34.7*
40%Δ (P = 0.032; n = 10)	99.7 ± 28.4	98.4 ± 29.2*
70%Δ (P = 0.034; n = 13)	110.0 ± 38.1	108.8 ± 38.9*
CONV+ group		
All WRs (P = 0.000; n = 35)	97.7 ± 32.7	94.6 ± 33.5*
All sub-LT WRs (P = 0.000; n = 21)	82.6 ± 22.3	78.1 ± 20.8*
55%LT (P = 0.053; n = 7)	77.2 ± 21.0	72.4 ± 19.5
70%LT (P = 0.006; n = 7)	84.1 ± 25.8	79.1 ± 23.4*
85%LT (P = 0.088; n = 7)	86.4 ± 22.5	82.8 ± 21.2
All supra-LT WRs (P = 0.009; n = 14)	120.5 ± 33.3	119.4 ± 34.2*
40%Δ (P = 0.034; n = 7)	109.7 ± 28.3	108.5 ± 29.1*
70%Δ (P = 0.139; n = 7)	131.3 ± 36.4	130.2 ± 37.6

RMSE values are mean ± SD (ml·min^{-1}); *Significantly different from FOME model.

7.4 Discussion

7.4.1 Curve characteristics and fitting aspects

Supra-LT intensities. In the cases where the O$\dot{V}O_2$K did not occur and the onset of the $\dot{V}O_2$SA was not evident (e.g., *subject 8* at 70%Δ; Figure 7.5), the somewhat "plain" measured response allowed the SOSC model to present its optimal fittings using mildly overshooting CI_{Ovsht} curves (equation 7.3), or, as for the nine cases mentioned above, even using the CI_{NOvsht} formula (equation 7.5).

In the case depicted in Figure 7.5, the smooth increase of SOSC's CR resulted in fit errors more evenly and closely distributed around zero than those from the FOME, especially in the middle of the transitory phase (around t = 90 s), and close to $t = td_{SC}$ (Figure 7.5; *amplified region*). This may be explained by two artificialities imposed by the FOME methodology, namely: performing two independent fits with different portions of the data set for the FC and SC; and forcing a break point into the CR curve at a given instant td_{SC}, when an imposed SC must start rising. Oppositely, the SOSC model takes advantage of the flexibility of our recursive fitting methodology involving two simultaneous components and comprising the whole data set at each iteration.

For nonovershooting cases presenting more apparent $\dot{V}O_2$SA (Figure 7.6.A-B), the SOSC fitting

Table 7.3 $\dot{V}O_2$ on-kinetics parameters and variables from the models at all tested intensities (CONV+ group)

WR	55%LT	70%LT	85%LT	40%Δ	70%Δ
FOME					
td_{FC}, s	17.7 ± 2.8	18.6 ± 3.4	18.2 ± 3.2	16.0 ± 3.7	16.7 ± 2.7
τ_{FC}, s	16.6 ± 5.2	16.2 ± 4.6	17.6 ± 3.8	23.2 ± 7.2[ab]	23.3 ± 7.2[ab]
td_{SC}, s	—	—	—	210.0 ± 46.5	167.9 ± 35.5[e]
τ_{SC}, s	—	—	—	176.4 ± 116.5	152.1 ± 103.1
A_{FC}, ml·min^{-1}	777 ± 176	1037 ± 267[a]	1342 ± 267[ab]	2189 ± 411[abc]	2458 ± 355[abcd]
A_{SC}, ml·min^{-1}	—	—	—	174 ± 56	312 ± 115[e]
A_{SC}%, % of A_{CR}	—	—	—	7.3 ± 1.4	11.1 ± 3.1[e]
G_{FC}, ml·min^{-1}·W^{-1}	7.90 ± 0.66	8.26 ± 0.75	8.87 ± 0.55[a]	9.58 ± 1.72[ab]	9.09 ± 1.30[ab]
G_{SC}, ml·min^{-1}·W^{-1}	—	—	—	0.77 ± 0.26	1.16 ± 0.47[e]
SOSC					
td_S, s	5.7 ± 4.6	7.8 ± 5.7	9.2 ± 6.0	12.0 ± 2.5[a]	11.5 ± 5.4[a]
ω_S, rad·s^{-1}	0.057 ± 0.010	0.064 ± 0.017	0.075 ± 0.031	0.116 ± 0.079[ab]	0.099 ± 0.036[ab]
ζ_{CI} (dimensionless)	0.62 ± 0.12	0.67 ± 0.13	0.79 ± 0.22[a]	1.13 ± 0.40[ab]	1.02 ± 0.43[ab]
ω_{d_CI}, rad·s^{-1}[f]	0.044 ± 0.011	0.046 ± 0.012	0.045 ± 0.012 (6)	0.046 ± 0.011 (3)	0.049 ± 0.023 (5)
ζ_{CII} (dimensionless)	72.44 ± 88.68	32.12 ± 46.83	4.25 ± 3.17[ab]	11.70 ± 6.00[c]	9.78 ± 8.93
A_{CI}, ml·min^{-1}	745 ± 198	981 ± 295[a]	1245 ± 317[ab]	1927 ± 532[abc]	1921 ± 552[abc]
A_{CII}, ml·min^{-1}	32 ± 41	56 ± 62[a]	97 ± 93[ab]	436 ± 235[abc]	848 ± 342[abcd]
A_{CII}%, % of A_{CR}	4.9 ± 7.5	6.2 ± 8.3[a]	8.0 ± 9.2[ab]	19.3 ± 12.9[abc]	31.4 ± 15.2[abcd]
G_{CI}, ml·min^{-1}·W^{-1}	7.54 ± 1.08	7.77 ± 1.18	8.19 ± 1.18	8.29 ± 1.71	7.12 ± 1.99[d]
G_{CII}, ml·min^{-1}·W^{-1}	0.36 ± 0.50	0.48 ± 0.60[a]	0.68 ± 0.75[ab]	1.90 ± 1.09[abc]	3.12 ± 1.23[abcd]
All models					
$\dot{V}O_{2Baseline}$, ml·min^{-1}	1108 ± 81	1110 ± 74	1098 ± 88	1133 ± 61	1145 ± 102
A_{CR}, ml·min^{-1}	777 ± 176	1037 ± 267[a]	1342 ± 267[ab]	2363 ± 454[abc]	2770 ± 423[abcd]
G_{CR}, ml·min^{-1}·W^{-1}	7.90 ± 0.66	8.26 ± 0.75	8.87 ± 0.55[a]	10.19 ± 0.75[abc]	10.24 ± 0.94[abc]
WR, W	98 ± 16	124 ± 21[a]	151 ± 25[ab]	231 ± 35[abc]	271 ± 41[abcd]

Values are mean ± SD; n = 7 for each tested WR, except where indicated between parenthesis; [a,b,c,d] Significantly different from 55%LT, 70%LT, 85%LT and 40%Δ, respectively (Post hoc test); [e] Significantly different from 40%Δ (Paired tests); [f] Values between parenthesis indicate the quantity of CI_{Ovsht} cases, since the concept of ω_d do not apply to the *overdamped* solution, i.e., when CI is represented by CI_{NOvsht} (equation 7.5).

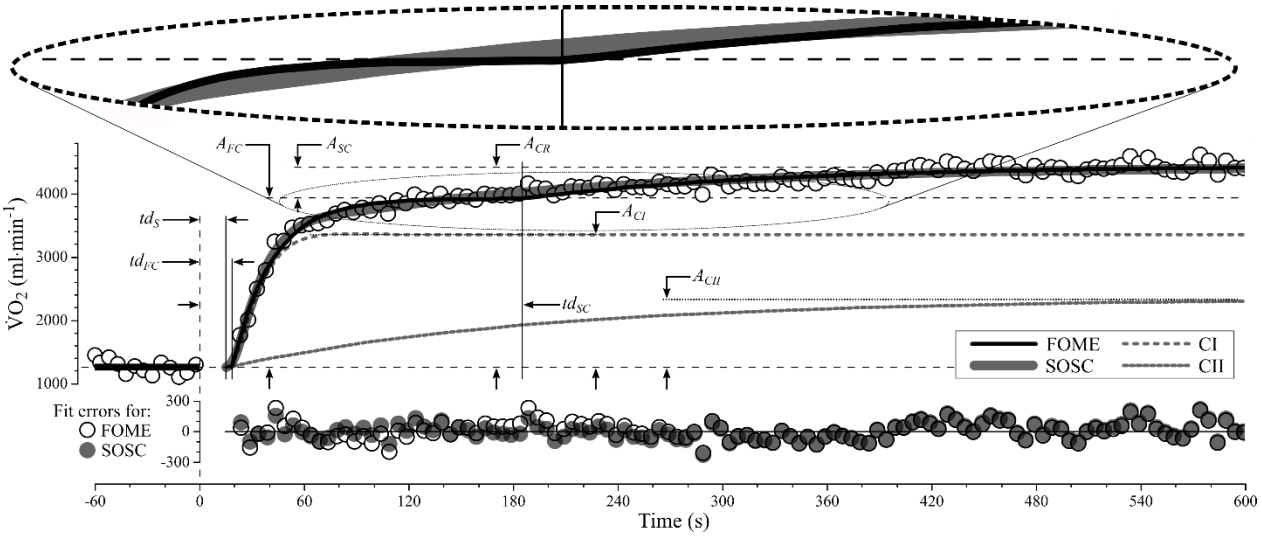

Figure 7.5 SOSC and FOME curves for *subject 8* at the 70%Δ intensity. The optimal CR for the SOSC model was obtained at an A_{CII}% of 34 (see Figure 7.4.A), i.e., an amplitude A_{CII} corresponding to 34% of A_{CR}.

advantages become even more evident, as its CR not only converged to the usually expected shape whereby either or both the O$\dot{V}O_2$K and/or $\dot{V}O_2$SA features are preserved, but also presented slightly better fit error profiles. This was also the case for the two supra-LT O$\dot{V}O_2$K cases found in our data sets (one of them depicted in Figure 7.6.6C), in which the O$\dot{V}O_2$K was not comprised by the FOME model. Additionally, the FOME model presented some poorer fitting results in the instants preceding $t = td_{SC}$ (e.g., *amplified region* of Figure 7.6.C), where the constraint of having a FC converging to the amplitude A_{FC} forced the FOME curves to pass by this intermediate asymptote, while the SOSC response could more freely "dive" below this value, for this would not compromise its fit at the remaining data points. Finally, the smooth abandon of the $\dot{V}O_{2Baseline}$ allowed by the initial upward concavity characteristic of second-order curves explains the SOSC's shorter onset time delays (Table 7.3) and smaller errors right after t = 20 s (Figures 7.5 to 7.7).

Sub-LT intensities. Under the SOSC's logic of a CII that fades at lower intensities, the difference between its CR and the CI is expected to be reduced in the moderate intensity domain. Figure 7.7.A-B illustrate such effect, with the CI being almost entirely responsible for the SOSC's CR shape. As for the FOME model in sub-LT conditions, its poorer fitting performance (Table 7.2) is mostly explained by the presence of the O$\dot{V}O_2$K phenomenon (e.g., Figure 7.7.A) in 17 of the 21 CONV+ cases.

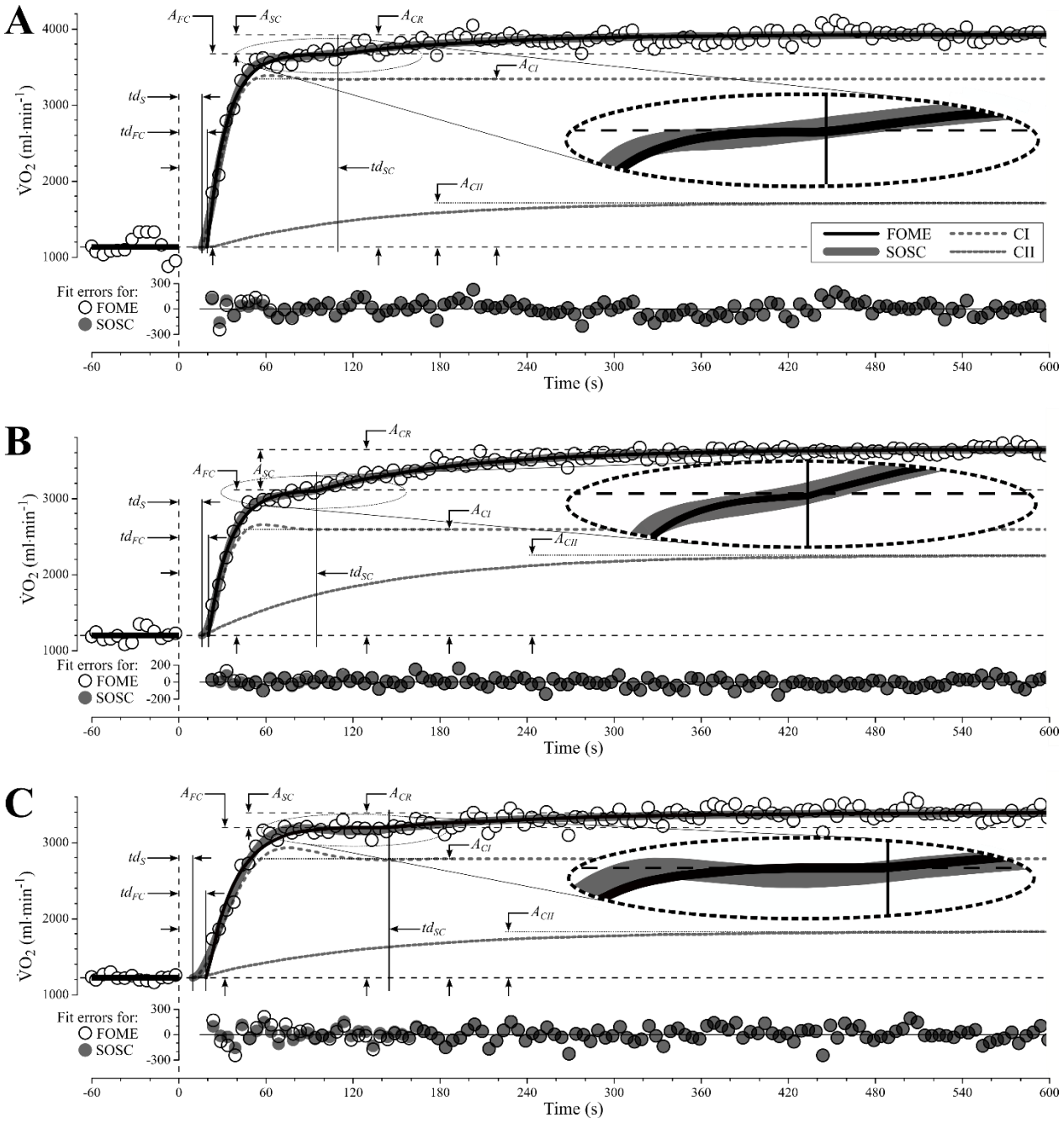

Figure 7.6 Representative examples of SOSC and FOME curves: A. *subject 6* at the 70%Δ intensity, where the absence of the O$\dot{V}O_2$K and a reduced $\dot{V}O_2$SA cause the two models to be very similar, with a slight superiority of the SOSC model at the first minute of the response; B. *subject 9* at 70%Δ, where the more pronounced $\dot{V}O_2$SA was thoroughly represented by the SOSC model, retaining the expected curve shape from the FOME model; and C. *subject 10* at 40%Δ, one of the two cases manifesting both the O$\dot{V}O_2$K and the $\dot{V}O_2$SA phenomena in [57]; In the three illustrated cases, the plots of errors around the fitted curves indicate the SOSC's consistently good fitting performance, with local advantages in comparison to the FOME model especially evident in the vicinity of td_{SC} (*amplified regions*).

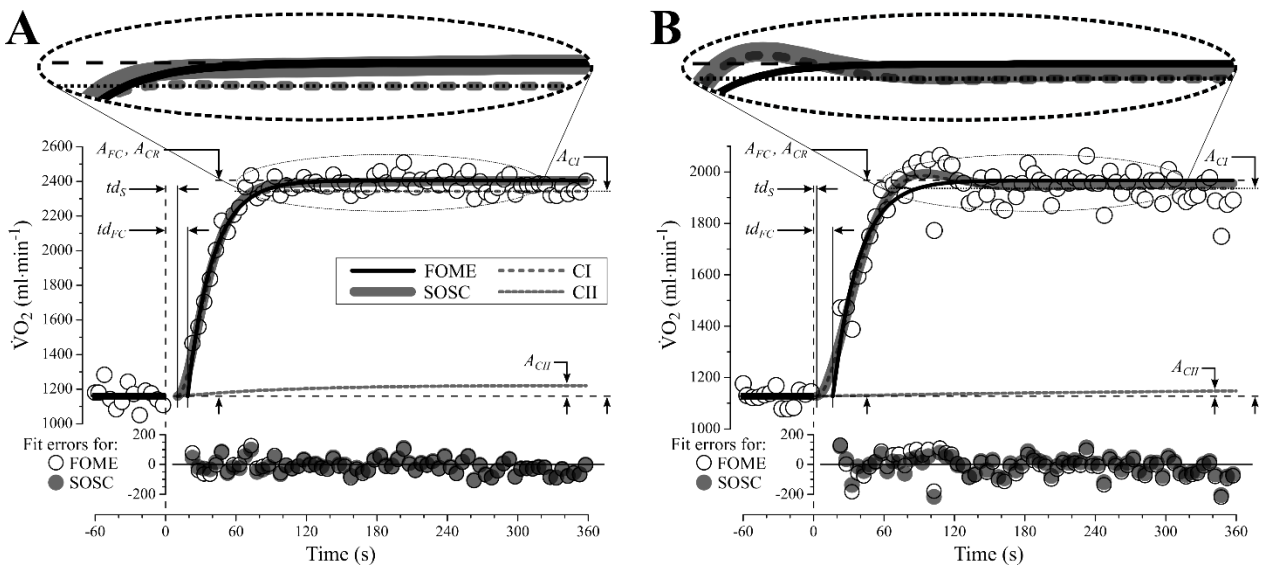

Figure 7.7 Representative examples of SOSC and FOME curves at 70%LT: A. *subject 8*, one of the four cases without an O$\dot{V}O_2$K. A mild plateau followed by a $\dot{V}O_2$SA-like rise is noticeable in the SOSC curve; and B. *subject 3*, with a noticeable O$\dot{V}O_2$K well represented by the SOSC curve and also followed by a mild $\dot{V}O_2$SA-like rise towards the A_{CR} asymptote; Despite magnitude differences, an overshooting CI is present in both cases (see *amplified regions*).

7.4.2 Physiological coherence of the SOSC model

One strong aspect of the SOSC model is that, despite the possibility of assuming two independent ω values for CI and CII, significantly better fittings are obtained by adopting a common ω_S shared by CI and CII. More than reducing the quantity of model parameters, this single ω_S may suggest the concept of a natural frequency of the "human $\dot{V}O_2$ mechanism" that could reflect the interaction between the respiratory and circulatory systems and/or between central and peripheral regions of the circulatory system alone—similarly to the computational model of "muscle and 'rest-of-body' compartments" proposed by Barstow et al. [161]. Such common ω_S, that may vary from one intensity to another (e.g., due to differences in heart rate, muscle perfusion, or pulmonary gas exchange)[14] would represent the time course of muscle oxygen supply, while the difference

[14] When different exercise intensities are compared, it is noteworthy the ω_{d_CI} stability throughout the entire WR spectrum (Table 7.3), likely because its evaluation formula (equation 7.4) comprises concomitantly the evaluation of both ω_S and ζ_{CI}.

between ζ_{CI} and ζ_{CII} would be due to the intrinsic features (e.g. biochemical) of each muscle fiber type that affect the efficiency of oxygen utilization. The tight variation of ζ_{CI} values around the value of one (Table 7.3) agrees with fast and responsive CI that, due to the high oxidative capacity of type I fibers, is often overshooting or on the verge of doing so. Oppositely, the ζ_{CII} values consistently much greater than one are coherent with the slower CII mechanism, less specialized in the oxidative activity, but offering the advantages of force and/or speed generation from the type II fibers, even if at the expenses of the system's net efficiency (see G_{CR} ascending values; Table 7.3).

This may be the underlying message from studies associating more pronounced $\dot{V}O_2SA$ relative contributions in the $\dot{V}O_2$ net response with higher percentage of type II fibers in the working muscles [39], with higher blood lactate concentration situations [39, 41, 96, 98, 99], higher exercise intensities [88, 96], and higher pedalling cadences—thus, higher contraction velocity [42, 97, 98]. In studies applying step tests [97, 98], the increase of both A_{FC} and A_{SC} observed at the higher cadences for a same WR have been attributed to the augmented recruitment of fast-twitch fibers. While this expected increment in A_{SC} alone does not affect the delayed SC theory, the increase in A_{FC} suggests the presence of a type II fiber-related contribution manifesting before td_{FC}. This early contribution, that in the FOME model might be wrongly attributed to the FC, would be trivially explained by the SOSC dynamics of larger CIIs at higher cadences.

A similar perspective may explain the smaller A_{SC}, and the larger gain and τ values of the fundamental phase obtained for heavy WR step transitions when initiating from a moderate rather than an unloaded cycling baseline [133], considered by the authors as a possible effect of the greater recruitment of higher-order fibers (i.e., approaching a type II) already "at (or close to)" the WR transition, and thus, refuting the relationship between the $\dot{V}O_2SA$ and the progressive recruitment of these fibers.

In fact, the debate about whether type II fibers are recruited under a time-progressive regimen or already at the beginning of the exercise [38, 52-54, 133, 158, 159] becomes pointless if the aforementioned association between these fibers and the $\dot{V}O_2SA$ is considered in the FOME model context, where the $\dot{V}O_2SA$ is represented by the necessarily delayed SC.

Instead of assuming that type I fibers are initially stressed to their limit and an additional fast-twitch pool is only recruited after $t = td_{SC}$, the SOSC logic prioritizes the "original purpose" of each fiber

type, using the efficient slow-twitch fibers for the main portion of the work generation and recruiting their stronger and faster type II counterparts “on demand,” as required by the instantaneous WR. Such strategy has been recently corroborated by the predominance of type I and II fibers recruitment at respectively, low and high power outputs found in the model of the cortically stimulated muscle [162].

In terms of aerobic efficiency of force production, the use of a muscle pool composed of type II fibers—with both higher ATP cost of force generation [94], and higher $\dot{V}O_2$ cost per ATP resynthesis [95] than the type I—already at the beginning of the exercise may not seem appealing. However, when a given WR must be delivered already at the first seconds of the exercise, with power generation requiring certain levels of speed and/or force of contraction, delaying the recruitment of eventually necessary type II fibers does not appear convenient.

A fundamental aspect of our model, however, is that it does not ignore the effect of fatigue nor its relationship with the loss in muscle efficiency and the $\dot{V}O_2$SA phenomenon [158, 163, 164]. Instead, it actually considers that such effect may take place within the CI and/or CII respective fiber pools, gradually starting already at the exercise onset and being more evident in the CII (e.g., causing a greater ζ_{CII} than ζ_{CI}) due to the greater susceptibility of type II fibers to fatigue. Corroborating this possibility, studies involving all-out cycling tests in humans [159], or electrically stimulated animal preparations [53] demonstrate that a same pool of fibers may manifest $\dot{V}O_2$SA-like increases for a constant WR independently of additional fiber recruitment.

7.4.3 SOSC curve shape formation

The combination of a fast-rising CI with a belated rise of the CII may cause different scenarios. For nonovershooting or slightly overshooting CIs (Figures 7.5 and 7.7.A), the CR will simply present an initial upward concavity followed by a slope reduction, with the final increase towards stabilisation being more (Figure 7.5) or less (Figure 7.7.A) pronounced accordingly with the CII profile. For CIs presenting more pronounced overshoots, the CII interference may be: barely noticeable, allowing the CI’s overshoot to be almost entirely revealed in the O$\dot{V}O_2$K (Figure 7.7.B); important enough to cause a clearly defined $\dot{V}O_2$SA but not enough to preclude the O$\dot{V}O_2$K manifestation in the CR (Figure 7.6.C); or so pronounced that only a plateau (Figure 7.6.A) or a small slope attenuation (Figure 7.6.B) can be seen in the CR before the $\dot{V}O_2$SA.

Such flexible SOSC dynamics releases the $\dot{V}O_2$ kinetics modeling from the notion of a transition WR sharply associated with the LT—or with the similar WR values at the gas exchange or the ventilatory thresholds [9, 101]. The $\dot{V}O_2$SA-like drifts reported in step responses below the ventilatory threshold [160], the similar $\dot{V}O_2$SA cases observed in our sub-LT SOSC curves, and some supra-LT cases combining both O$\dot{V}O_2$K and $\dot{V}O_2$SA occurrences [57] suggest that these phenomena are not mutually exclusive. Instead, they seem to have a common origin explained by the interaction between CI and CII.

In methodological terms, the advantage of the SOSC model lies on the concomitant optimization of both of its components, with the CR overall performance being evaluated at each iteration. In opposition, the FOME and procedure of previously defining td_{SC} in order exclude the portion of data influenced by the SC from the FC regression is a segmentation that may jeopardize the fitting process in its whole. The narrow variation range of td_S and td_{FC} in opposition to the wide fluctuation of td_{SC} (Table 7.3) may indicate the artificiality of this imposed SC.

7.4.4 Potentiality of the SOSC model

Due to its first-order nature, not only the FOME model requires different components' onsets time delays (td_{SC} longer than td_{FC}) to represent the $\dot{V}O_2$SA [91], but also its incapacity of comprising the O$\dot{V}O_2$K [57] requires the incorporation of another add-on term to its formulation whenever this phenomenon is present. Alternatively, without losing coherence with fundamental findings from the literature regarding the $\dot{V}O_2$SA and the O$\dot{V}O_2$K, the SOSC model may provide a comprehensive explanation for the diverse $\dot{V}O_2$ response shapes of the whole WR spectrum while maintaining its composition qualitatively identical for any individual and all exercise domains. The dynamics of a G_{CII} growing faster than G_{CI} in response to the WR augmentation explains the concomitant and opposite tendencies of the $\dot{V}O_2$SA and O$\dot{V}O_2$K phenomena (Figure 7.1), namely a reduction in both magnitude and incidence of the O$\dot{V}O_2$K as the exercise intensity increases towards the $WR_{LT,}$ concatenated with the insurgence, from around the WR_{LT} onward, of an increasingly more prominent $\dot{V}O_2$SA as the exercise intensity continues to rise.

Regarding the SOSC implementation, the apparent complexity of two concomitant second-order exponentials is sorted out by a completely automatic fitting methodology, avoiding highly subjective steps such as the definition of the td_{SC} in the FOME model. Moreover, even if the

magnitude of the errors involving pulmonary $\dot{V}O_2$ measurements raise doubt about the better goodness-of-fit statistically demonstrated by the SOSC model in comparison with the FOME, our results indicate that these models' fitting performances are *at least equivalent*.

7.4.5 Conclusions

Thus, considering these implementation aspects and the conceptual advantage of representing $\dot{V}O_2$ step response (i) by using as many parameters as the FOME model, (ii) without aggregating any add-on components of conditional existence, and (iii) without assuming a time lapse between the recruitment of different pools of fiber types during constant WR exercise, we propose the SOSC model as an adequate and comprehensive alternative for explaining $\dot{V}O_2$ responses to the step on-transient in humans at any exercise intensity, regardless of the presence of the O$\dot{V}O_2$K and/or the $\dot{V}O_2$SA phenomena.

7.5 Acknowledgements

We thank AM Castillo for his support in the data acquisition process, and for their dedication, the athletes volunteering in our study.

7.6 Funding

This work was supported by the CAPES Foundation (Ministry of Education, Brazil) under the scope of the Science without Borders Program [process number 13546/13-9].

7.7 Abbreviations and symbols

A_{CI}	Amplitude of the CI
A_{CI}%	Percentage contribution of the CI to the A_{CR}
A_{CII}	Amplitude of the CII
A_{CII}%	Percentage contribution of the CII to the A_{CR}
A_{CR}	Amplitude of the CR
A_{FC}	Amplitude of the Fundamental Component
A_{SC}	Amplitude of the Slow Component

CI	SOSC's simultaneous component I
CI_{NOvsht}	*Overdamped* representation of the CI
CI_{Ovsht}	*Underdamped* representation of the CI
CII	SOSC's simultaneous component II
CII_{NOvsht}	*Overdamped* representation of the CII
CR	$\dot{V}O_2$ combined response of a model
FC	Fundamental component
FOME	First-Order Multi-Exponential (model)
G_{CI}	Gain of the CI (A_{CI} / WR)
G_{CII}	Gain of the CII (A_{CII} / WR)
G_{CR}	Gain of the CR (A_{CR} / WR)
G_{FC}	Gain of the FC (A_{FC} / WR)
G_{SC}	Gain of the SC (A_{SC} / WR)
LT	Lactate threshold
MiME	Mixed Multi-Exponential (model)
$O\dot{V}O_2K$	Overshoot in $\dot{V}O_2$ kinetics
RMSE	Root mean squared error
SC	Slow component;
SOSC	Second-Order Simultaneous Components (model)
$t_{CI\_SS2\%}$	Instant when the CI curve assumes a steady-state (variation < 2% of A_{CI})
td_{FC}	Onset time delay of the FC
td_S	Onset time delay of both CI and CII
td_{SC}	Onset time delay of the slow component
$\dot{V}O_{2Baseline}$	$\dot{V}O_2$ average value for the 60 s preceding the step onset

$\dot{V}O_2SA$	Slow augmentation in the $\dot{V}O_2$ step response
ω	Natural frequency of a second-order system
ω_{d_CI}	Damped frequency of CI;
ω_S	SOSC's ω, common to both CI and CII
WR	Work rate
WR_{LT}	WR associated with the lactate threshold
$WR\dot{V}O_{2max}$	WR associated with the maximal 30 s $\dot{V}O_2$ average in the incremental test
τ_{FC}	Time constant of the first-order representation of the FC
τ_{SC}	Time constant of the SC
ζ	Damping ratio of a second-order system
ζ_{CI}	Damping ratio of the CI
ζ_{CII}	Damping ratio of the CII
40%Δ	WR equal to WR_{LT} added of 40% of the difference between WR_{LT} and $WR\dot{V}O_{2max}$
55%LT	WR equal to 55% of WR_{LT}
70%Δ	WR equal to WR_{LT} added of 70% of the difference between WR_{LT} and $WR\dot{V}O_{2max}$
70%LT	WR equal to 70% of WR_{LT}
85%LT	WR equal to 85% of WR_{LT}

CHAPTER 8 SOSC, MIME, AND FOME MODELS: COMPARISON AND OVERVIEW

The purpose of this chapter is to complement the comparisons between the FOME model and either the MiME or the SOSC models performed separately in Chapters 5 and 7, respectively. After the addition of the MiME curves, Figures 7.5 to 7.7 are revisited in their colored version (for enhanced distinction between curves) as Figures 8.1 to 8.3. To avoid repetition, only aspects regarding the comparison with the MiME curves, therefore omitted in Chapter 7, are commented on. In regards to the comparison between the parameters and variables, a more complete version of Table 7.3 including data from the three tested models and separated into the CONV and CONV+ groups is available in Appendix F (Table F.2).

8.1 Comparison between FOME, MiME, and SOSC curves at different WRs

8.1.1 RMSE comparisons

General tendency. ANOVAs comparing the RMSE mean values from the three tested models (Table 8.1) demonstrated a worse fitting performance of the FOME model for the majority of the tested conditions, with the SOSC model always presenting significantly lower values than either or both the FOME and MiME models.

Table 8.1 Comparisons between mean RMSE values from SOSC, MiME, and FOME models

Model	SOSC	MiME	FOME
All WRs (P = 0.00; n = 35)	94.6 ± 33.5	95.5 ± 33.5	97.7 ± 32.7*
All sub-LT (P = 0.00; n = 21)	78.1 ± 20.8	78.7 ± 21.0	82.6 ± 22.3*†
55%LT (P = 0.01; n = 7)	72.4 ± 19.5	72.5 ± 19.2	77.2 ± 21.0*†
70%LT (P = 0.00; n = 7)	79.1 ± 23.4	80.5 ± 23.6	84.1 ± 25.8*†
85%LT (P = 0.04; n = 7)	82.8 ± 21.2	83.2 ± 21.6	86.4 ± 22.5*
All supra-LT (P = 0.00; n = 14)	119.4 ± 34.2	120.6 ± 33.5*	120.5 ± 33.3*
40%Δ (P = 0.01; n = 7)	108.5 ± 29.1	109.6 ± 28.6*	109.7 ± 28.3*
70%Δ (P = 0.04; n = 7)	130.2 ± 37.6	131.6 ± 36.5*	131.3 ± 36.4

RMSE values are mean ± SD (ml·min^{-1}); *Significantly different from SOSC model; †Significantly different from MiME model.

Models with non-simultaneous main components: FOME and MiME. At none of the tested supra-LT conditions was a significant difference ever observed between the mean RMSE values from MiME and FOME curves (Table 8.1; Post hoc $P > 0.77$ for any supra-LT scenarios), marking a

similarity between these models at higher WRs. In fact, this similarity already becomes noticeable at the upper bounds of the moderate domain (Table 8.1; 85%LT, Post hoc $P = 0.078$).

Models using second-order solutions: MiME and SOSC. The direct comparisons between the MiME and SOSC responses failed to demonstrate a significant difference between these models at intensities below the WR_{LT} (Table 8.1; Post hoc $P > 0.34$ for any sub-LT scenarios), where both models exclusively use SOS-based curves. As the WR is increased (causing the CII's participation in the SOSC model to become important, and the SC to emerge in the MiME context, as discussed bellow), this equivalence between the MiME and SOSC models did not persist (Table 8.1; Post hoc $P < 0.037$ for any supra-LT scenarios).

8.1.2 Curve shape characteristics and fitting aspects

In addition to the generalist quantitative analysis provided by the mean RMSE comparisons, some specific curve shape features and analyses of individual examples at lower and higher intensities may add insights into the models' curves comparison:

Sub-LT intensities. The logic of a fading importance of CII at lower intensities, presented in the Section *7.4.1 Curve characteristics and fitting aspects* as an explanation for the similarity between the SOSC's CR and CI in the moderate domain, is also applicable to the similarity between the MiME and SOSC curves observed in all sub-LT responses (illustrated by Figure 8.1.A-B).

In this case, however, two other contributing factors should be considered in addition to the modest CII magnitudes: since both MiME and SOSC models use the same second-order formulas to represent their FC or CI curves (equations 5.3 or 5.5 for the FC, and equations 7.3 or 7.5 for the CI), and considering that no SC is added to the MiME curve below the WR_{LT}, it is expected that, at lower WRs, the SOSC and MiME combined responses will be quite similar.

Supra-LT intensities. With the augmentation of the WR, the consequent diminution in the relative amplitude Mp_{ref} of the $O\dot{V}O_2K$ and the eventual vanishment of this phenomenon (see Table 5.2 and Figure 5.6) will reduce the differences between the FOME and either the MiME or SOSC models. However, this effect is only evident in the comparisons with the FOME model due to its inability to comprise $O\dot{V}O_2K$-related features. Therefore, another factor(s) may be responsible for the increasing difference between the MiME and SOSC models—both capable of fitting overshooting responses—observed with the increase of the test WR.

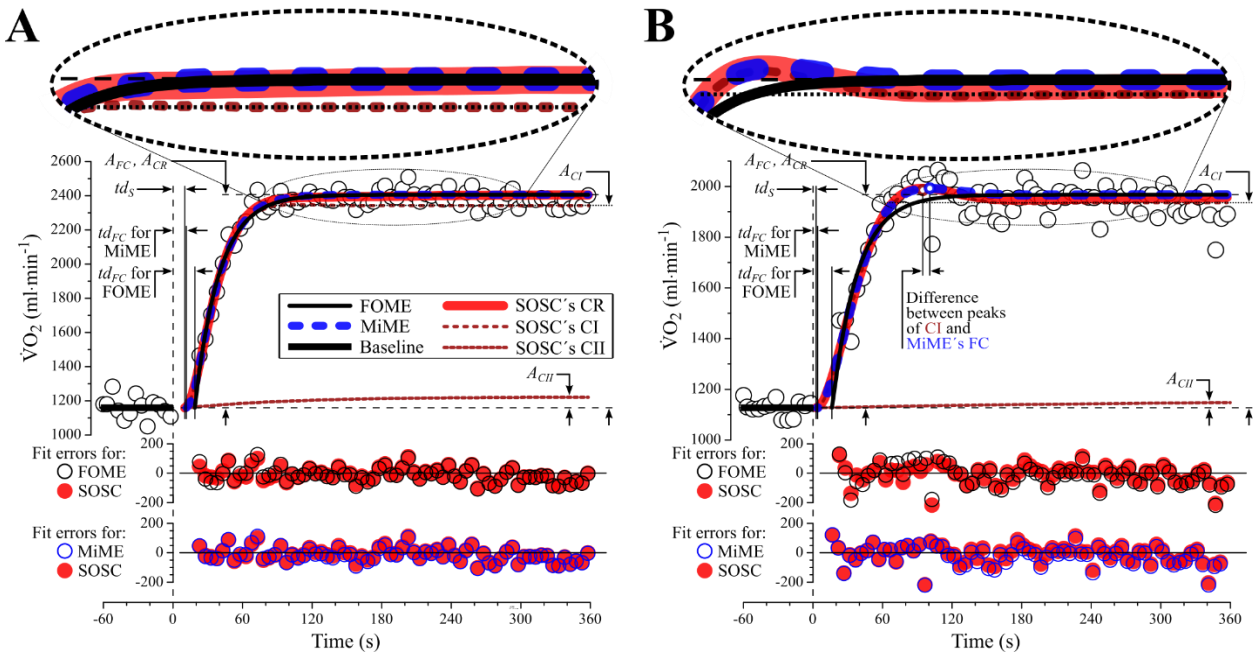

Figure 8.1 SOSC, MiME, and FOME curves for tests at 70%LT. The modest CII magnitudes cause both MiME and SOSC curves to be very similar, as demonstrated by the superposition of their fitting error plots. A. even in the absence of an O$\dot{V}O_2$K, the SOS-based curves could still fit the pronouncedly rising $\dot{V}O_2$ values in the first 80 s of this response better than the FOME model. B. Although both MiME and SOSC curves may represent well the evident O$\dot{V}O_2$K, the combination of CI and CII allows the former to oscillate more freely than the latter after $t \approx 120$ s. See this chapter's text and *7.4.1 Curve characteristics and fitting aspects* (especially in the legend for Figure 7.7) for further information.

In this context, one fundamental difference between the ways that the SOSC and MiME responses are composed may explain the superiority of the former over the latter in fitting the more complex $\dot{V}O_2$ data measured at higher WR step transitions: the already discussed artificiality of performing independent regressions for the FC and SC data sets (see *7.4.1 Curve characteristics and fitting aspects*), which are joined at an inflexion point forced into the CR at $t = td_{SC}$. Figure 8.2 illustrates a case where this inflexion point forced into both FOME and MiME models induces a plateau in their FCs, leading to a poor fitting of the otherwise smoothly ascending data (better represented by the SOSC's CR; see *amplified region*) not only in the vicinity of $t = t_{FC}$, but also around $t = 90$ s.

However, even when the $\dot{V}O_2$SA is more evident, like in the cases depicted in Figure 8.3.A-C, the imposition of a mandatory inflexion "check point" at $t = t_{FC}$ may still be problematic, not only for

"wasting" one valuable degree of freedom by fixing the parameter td_{SC} before the SC regression itself (see Section *6.2.4 Comparison between FOME and MiME models: limitation of the fixed slow component's time delay*), but also for limiting the FC's ability to adjust to some more subtle data characteristics, as discussed below.

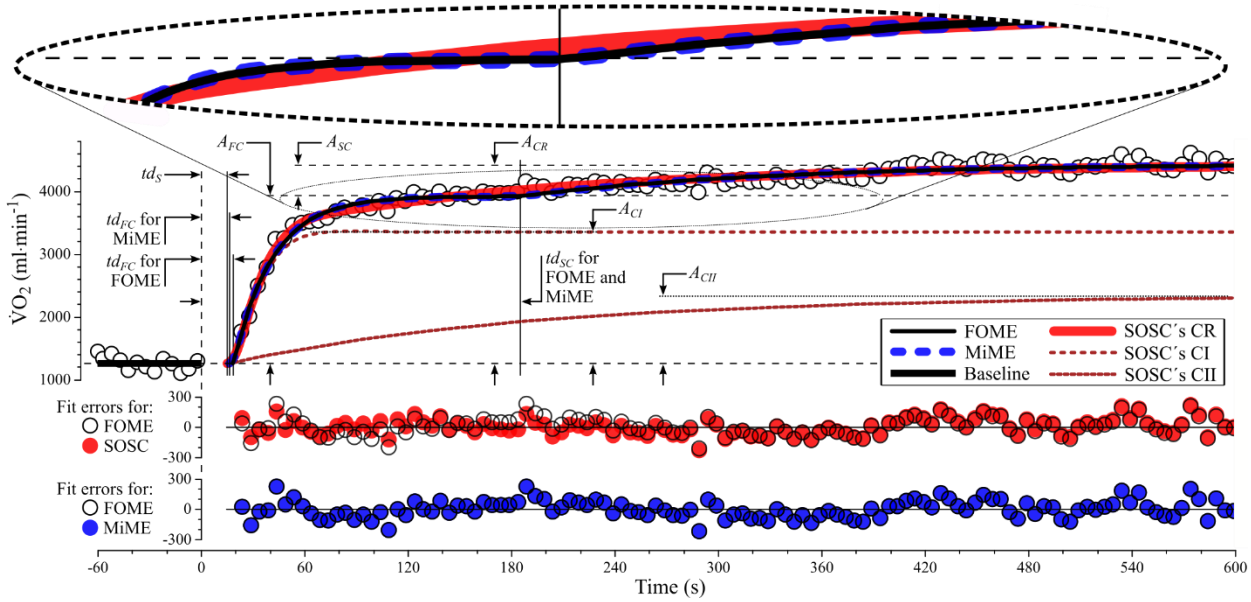

Figure 8.2 SOSC, MiME and FOME curves at 70%Δ. Details available in this chapter's text and Section *7.4.1 Curve characteristics and fitting aspects* (especially in the legend for Figure 7.5).

8.2 Characteristics and advantages of the SOSC model internal dynamics

The dynamics between the SOSC's components in the CR composition and its relationship with the representation of both O$\dot{V}O_2$K and $\dot{V}O_2$SA phenomena are discussed in Section *7.4.2 Physiological coherence of the* SOSC model

One strong aspect of the SOSC model is that, despite the possibility of assuming two independent ω values for CI and CII, significantly better fittings are obtained by adopting a common ωS shared by CI and CII. More than reducing the quantity of model parameters, this single ωS may suggest the concept of a natural frequency of the "human V̇O2 mechanism" that could reflect the interaction between the respiratory and circulatory systems and/or between central and peripheral regions of the circulatory system alone—similarly to the computational model of "muscle and 'rest-of-body' compartments" proposed by Barstow et al. [161]. Such common ωS, that may vary from one intensity to another (e.g., due to differences in heart rate, muscle perfusion, or pulmonary gas

exchange) would represent the time course of muscle oxygen supply, while the difference between ζCI and ζCII would be due to the intrinsic features (e.g. biochemical) of each muscle fiber type that affect the efficiency of oxygen utilization. The tight variation of ζCI values around the value of one (Table 7.3) agrees with fast and responsive CI that, due to the high oxidative capacity of type I fibers, is often overshooting or on the verge of doing so. Oppositely, the ζCII values consistently much greater than one are coherent with the slower CII mechanism, less specialized in the oxidative activity, but offering the advantages of force and/or speed generation from the type II fibers, even if at the expenses of the system's net efficiency (see *GCR* ascending values; Table 7.3).

This may be the underlying message from studies associating more pronounced V̇O2SA relative contributions in the V̇O2 net response with higher percentage of type II fibers in the working muscles [39], with higher blood lactate concentration situations [39, 41, 96, 98, 99], higher exercise intensities [88, 96], and higher pedalling cadences—thus, higher contraction velocity [42, 97, 98]. In studies applying step tests [97, 98], the increase of both *AFC* and *ASC* observed at the higher cadences for a same WR have been attributed to the augmented recruitment of fast-twitch fibers. While this expected increment in *ASC* alone does not affect the delayed SC theory, the increase in *AFC* suggests the presence of a type II fiber-related contribution manifesting before *tdFC*. This early contribution, that in the FOME model might be wrongly attributed to the FC, would be trivially explained by the SOSC dynamics of larger CIIs at higher cadences.

A similar perspective may explain the smaller *A*SC, and the larger gain and τ values of the fundamental phase obtained for heavy WR step transitions when initiating from a moderate rather than an unloaded cycling baseline [133], considered by the authors as a possible effect of the greater recruitment of higher-order fibers (i.e., approaching a type II) already "at (or close to)" the WR transition, and thus, refuting the relationship between the V̇O2SA and the progressive recruitment of these fibers.

In fact, the debate about whether type II fibers are recruited under a time-progressive regimen or already at the beginning of the exercise [38, 52-54, 133, 158, 159] becomes pointless if the aforementioned association between these fibers and the V̇O2SA is considered in the FOME model context, where the V̇O2SA is represented by the necessarily delayed SC.

Instead of assuming that type I fibers are initially stressed to their limit and an additional fast-twitch pool is only recruited after $t = tdSC$, the SOSC logic prioritizes the "original purpose" of each fiber

type, using the efficient slow-twitch fibers for the main portion of the work generation and recruiting their stronger and faster type II counterparts “on demand,” as required by the instantaneous WR. Such strategy has been recently corroborated by the predominance of type I and II fibers recruitment at respectively, low and high power outputs found in the model of the cortically stimulated muscle [162].

In terms of aerobic efficiency of force production, the use of a muscle pool composed of type II fibers—with both higher ATP cost of force generation [94], and higher V̇O2 cost per ATP resynthesis [95] than the type I—already at the beginning of the exercise may not seem appealing. However, when a given WR must be delivered already at the first seconds of the exercise, with power generation requiring certain levels of speed and/or force of contraction, delaying the recruitment of eventually necessary type II fibers does not appear convenient.

A fundamental aspect of our model, however, is that it does not ignore the effect of fatigue nor its relationship with the loss in muscle efficiency and the V̇O2SA phenomenon [158, 163, 164]. Instead, it actually considers that such effect may take place within the CI and/or CII respective fiber pools, gradually starting already at the exercise onset and being more evident in the CII (e.g., causing a greater ζCII than ζCI) due to the greater susceptibility of type II fibers to fatigue. Corroborating this possibility, studies involving all-out cycling tests in humans [159], or electrically stimulated animal preparations [53] demonstrate that a same pool of fibers may manifest V̇O2SA-like increases for a constant WR independently of additional fiber recruitment.

SOSC curve shape formation. However, some additional considerations including not only the SOSC and FOME, but also the MiME curves must be made.

Although the aforementioned drawback of the segmentation into FC and SC and the imposed inflexion point between them may be less problematic to the MiME than to the FOME model due to the ability of the former’s FC to oscillate above and below its asymptote before stabilization, it is still an important disadvantage in comparison with the SOSC model. While in the simultaneous components’ dynamics of SOSC methodology all of its six parameters are somehow available for concomitant adaptations and always considering the whole fit of the CR, the FOME and MiME’s

flexibility is limited to either the FC or SC parameters in different sections of the data set, and not simultaneously[15].

This can be noticed, for example, in the superior complexity of shapes presented by the SOSC curves in the "junction" region between the FC and SC (*amplified regions* of Figure 8.3). Especially when the coexistence of the $\dot{V}O_2SA$ and $O\dot{V}O_2K$ phenomena requires a particularly flexible CR (Figure 8.3.C), the SOSC's combination of a highly oscillating and overshooting CI_{Ovsht} (equation 7.3) with a much-damped CII_{NOvsht} (equation 7.5) seems to be a convenient composition. In fact, this combination is also present in the less complex cases of Figures 8.1.A-B, 8.2, and 8.3.A-B, where the CI is also represented by the CI_{Ovsht} solution.

Although the shape of the SOSC's CR is formed at any point by the sum of CI and CII, the most intense interaction between these components' shapes occurs in this "inflective region"—i.e., the aforementioned "junction" region, in the context of the FOME and MiME models, roughly in the center of the *amplified regions* of Figures 8.1 to 8.3.

Before this inflective region, the CI tends to dictate the shape of the CR in the cases of modest CIIs (Figure 8.1). Moreover, in the cases presenting the $O\dot{V}O_2K$ phenomenon, the overshooting CI_{Ovsht} solution becomes a requirement (Figures 8.1.B and 8.3.C). The better performance of the CI_{Ovsht} rather than the CI_{NOvsht} solution in 95% of the sub-LT cases (CONV+ group), where the occurrence of the $O\dot{V}O_2K$ phenomenon was more often observed, in contrast to the 43% found for the supra-LT cases (CONV+ group; 65% if considering the CONV group), is in accordance with this assertion (see Section *7.3.2 RMSE comparisons*). Oppositely, after the inflective region, where the CII is approximately stable around its steady-state value, the $\dot{V}O_2SA$ will basically reflect the more (Figures 8.2 and 8.3) or less (Figure 8.1) pronounced rise of CII.

---

[15] This poor usage of t_{FC} in the SC combined with the modeling using non-simultaneous components may be the reason why the MiME and FOME models, despite using respectively one more or the same number of parameters than the SOSC model at supra-LT intensities (see Table 7.1), still provide significantly greater RMSE values.

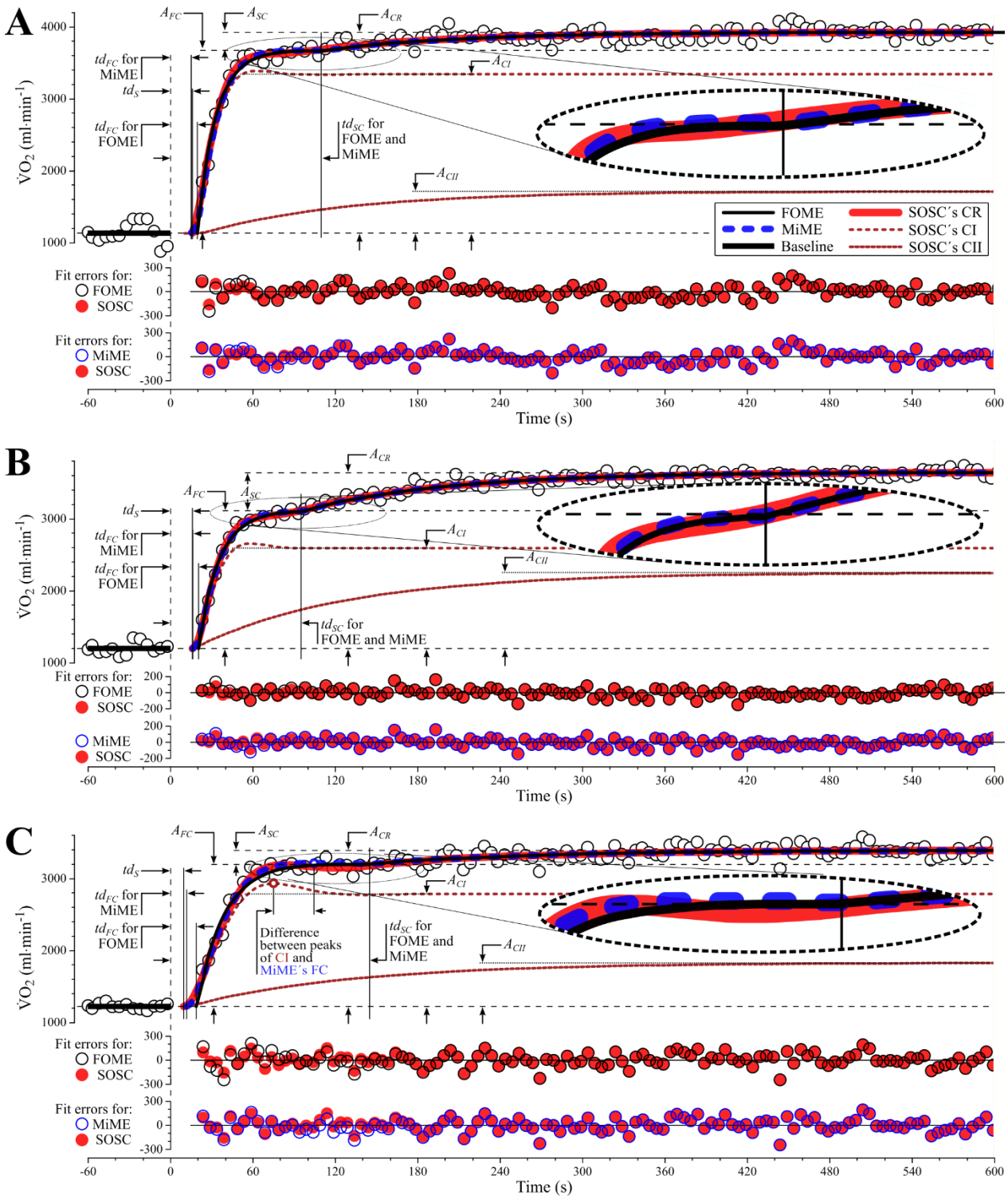

Figure 8.3 SOSC, MiME, and FOME curves for cases presenting A. a less or a B. more pronounced $\dot{V}O_2$SA without O$\dot{V}O_2$K, and C. a the coexistence of both the $\dot{V}O_2$SD and O$\dot{V}O_2$K with discreet magnitudes. See this chapter's text and Section *7.4.1 Curve characteristics and fitting aspects* (especially the legend for Figure 7.6) for more information.

8.3 General patterns in the SOSC curves

Considering the exposed SOSC model internal dynamics, and by analysing the typical patterns of CI and CII in the cases where the $O\dot{V}O_2K$ and/or the $\dot{V}O_2SA$ phenomena are present, some general rules may be inferred, namely:

- The greater the $\dot{V}O_2SA$, the greater the A_{CII};
- The greater the $O\dot{V}O_2K$ magnitude, the greater the CI_{Ovsht}'s overshoot;
- For cases of CI_{NOvsht}, no $O\dot{V}O_2K$ is manifested in the CR; and
- Not all of the CI_{Ovsht} cases will necessarily reflect an $O\dot{V}O_2K$ in the CR, since the deformation of CI_{NOvsht} into the CR shape caused by the CII may "transform" the $O\dot{V}O_2K$ into a plateau (Figure 8.1.A and Figure 8.3.A-B) or even into a continuously ascending curve (Figure 8.2).

Additionally, even if the influence of the CII is not important enough to eliminate the $O\dot{V}O_2K$ manifestation, it will still alter the CR shape by both attenuating the $O\dot{V}O_2K$'s perceptible amplitude (i.e., $O\dot{V}O_2K$ amplitude < CI_{Ovsht}'s amplitude) and positioning its peak a few instants after the CI_{Ovsht}'s overshoot peak. Moreover, because in the MiME model one single curve (FC_{Ovsht}, for $O\dot{V}O_2K$ cases) is responsible for the CR shape, and considering that the CRs of both MiME and SOSC models tend have their $O\dot{V}O_2K$ peaks matching the actual peak of the measured data, it is plausible that the overshoot peak will occur earlier in the CI_{Ovsht} than in the FC_{Ovsht} (see the difference between their peaks in Figure 8.3.C).

This difference implies greater values for the ω_{d_CI} than for the FC_{Ovsht}'s ω_d for the cases where an $O\dot{V}O_2K$ was present—at supra-LT intensities: $\omega_{d\_CI} = 0.053 \pm 0.007$ rad·s^{-1} > $\omega_d = 0.044 \pm 0.014$ rad·s^{-1} for the CONV group ($n = 2$), and $\omega_{d\_CI} = 0.058$ rad·s^{-1} > $\omega_d = 0.054$ rad·s^{-1} for the one case in the CONV+ group. For the $O\dot{V}O_2K$ cases at lower WRs, where the role of CII in the CR formation is less important, this effect is less evident but still present (see the smaller difference between peaks in Figure 8.1.B).

CHAPTER 9 GENERAL DISCUSSION

The specific contextualization and discussion of the results obtained by the models proposed in this study are presented in Chapters 5 to 8. In the present chapter, the main aspects of these previous discussions are resumed and combined with additional insights in a general, integrative overview.

9.1 The advantages of the second-order modeling for the $\dot{V}O_2$ kinetics

While the fitting advantages of the models using SOS-based curves is numerically demonstrated by the statistical testing results contained in Tables 5.3, 6.2, 7.2, and 8.1, and the curve shaping aspects leading to such greater performances are extensively discussed in Sections 5.3.2, 6.2.4, 7.4.1, 7.4.2, 8.1.2, and 8.2, the conceptual advantages involving the representation of the $\dot{V}O_2$ step responses in the entire WR spectrum by the MiME and SOSC models are revisited bellow.

9.1.1 The modeling of the O$\dot{V}O_2$K and $\dot{V}O_2$SA phenomena

One important implication of the second-order curves' ability to assume overshooting or nonovershooting shapes by solely altering the value of their parameter ζ [55, 56] is the incorporation of the O$\dot{V}O_2$K phenomenon to the $\dot{V}O_2$ step responses as an inherent feature of the human cardiorespiratory system [12, 46-48, 50]. This represents a change in paradigm that not only refutes the O$\dot{V}O_2$K representation by means of add-on terms of conditional existence incorporated to the first-order model [46, 48, 51], but also counters the concept that the O$\dot{V}O_2$K is an artifact caused by specific experimental conditions.

As presented in Section *5.1.2 Physiomechanical analogy*, both the SOS nature of a mechanical system and the manifestation of an overshoot in its step response are associated with the presence of an inertial element *M*, while its level of responsivity and the magnitude of its overshoot are dependent on the proportion between the *K*, *M*, and *D* elements. In the FOS context, or in the nonovershooting SOS, the proportion between *K* and *M* is also determinant of the system's responsivity [55, 56]. Thus, as may be inferred from the physiological contextualization of these elements presented in Section *5.1.2*, not only the occurrence of an O$\dot{V}O_2$K in the "$\dot{V}O_2$ system" response denotes its SOS nature, but the fact that well-trained individuals are those presenting the O$\dot{V}O_2$K phenomenon more often and more pronouncedly than their less trained counterparts [12, 46-48] are in complete coherence with the internal logic of an augmented "physiological *K*" in the

SOS representation. Moreover, like the responsivity of the $\dot{V}O_2$ response in the conventional FOS representation is known to be increased by means of endurance training or other manipulations (e.g., increasing the O_2 availability [165]), the O$\dot{V}O_2$K phenomenon has been proved to become more pronounced and to have its peak accelerated after a manipulation via endurance training [12].

In fact, in terms of exercise performance and tolerance, the occurrence of a large O$\dot{V}O_2$K is actually desirable and in accordance with an improved training status: not only because it will reflect a faster overall $\dot{V}O_2$ kinetics, but also because this "extra" O_2 uptake above the steady-state valued occurring already at the beginning of exercise may cause a diminution of the total O_2 deficit accumulated during a given exercise bout [46-48].

But while the reasoning behind the O$\dot{V}O_2$K occurrence and its relationship with the individual's fitness status is the same in both MiME and SOSC contexts (respectively occurring in the FC_{Ovsht} or in the CI_{Ovsht}), the possible explanation for the continuous reduction in its incidence and magnitude as the step WR increases, practically disappearing at supra-LT intensities [12, 47, 48], will find different versions in each one of these models.

In the context of in the MiME model, it is possible that a gradual loss in linearity is responsible for the reduction in the O$\dot{V}O_2$K magnitude, like the spring in the *physiomechanical analogy* eventually deviates from a linear behavior if excessively extended. However, since the O$\dot{V}O_2$K is nearly vanished around the WR_{LT}, thus still far from the system's operational limit represented by the $WR_{\dot{V}O2max}$, it seems more likely that this loss in linearity may be due to the additional recruitment of less efficient muscle fibers [54]. Although this explanation is in agreement with the hierarchy of fiber recruitment [54, 166] in response to the augmentation in the force/speed requirements, the general belief associated with the MiME and FOME models' dynamics is that this linearity is disrupted only at WRs above the WR_{LT} (see Figure 9.1 in Section 9.2), mostly due to additional recruitment of type II fibers attributed as the cause of the SC [39, 41, 42, 88, 96-99]. Nevertheless, not only the reduction in the O$\dot{V}O_2$K magnitude and incidence is observed at sub-LT intensities, where the $\dot{V}O_2$SA—the actual phenomenon represented by the SC in the FOME and MiME models—is not usually observable, but the O$\dot{V}O_2$K itself typically occurs in the first two minutes of the response [46], thus before the onset of the SC.

Moreover, while there is large agreement in associating the $\dot{V}O_2$SA phenomenon with the participation of type II fibers [39, 41, 42, 88, 96-99] and the loss in efficiency [158, 163, 164] in

the exercising muscles, $\dot{V}O_2$SA-like increases are observable at constant WR conditions where the additional fiber recruitment is not possible [53, 159]. This fact, confronted with the necessarily delayed nature of the SC imposed by the FOME and MiME models [1, 121] increases the controversy involving the additional type II fiber recruitment and its relationship with the $\dot{V}O_2$SA phenomenon [38, 52-54, 133, 158, 159].

As discussed bellow, a concealing solution for such debate is offered by the SOSC model's basic structure, where the observable pulmonary $\dot{V}O_2$ step response is mainly composed not of two differently delayed components, but of two simultaneous elements.

9.1.2 The comprehensive approach of the SOSC model internal dynamics

The great conceptual advantage of the SOSC model is its ability to represent all possibly observed shapes of $\dot{V}O_2$ step on-transient responses by simply varying the relative contribution of each of its two simultaneous components to the CR. Thus, the SOSC model presents one single qualitative structure for all cases, in opposition to the add-on components of conditional existence required by the FOME model to represent the O$\dot{V}O_2$K, and by both the FOME and MiME models to represent the $\dot{V}O_2$SA. Such structural simplicity provides four fundamental advantages in relation to the FOME and MiME models, one concerning the mathematical and computational aspects, and three regarding the physiological basis of the $\dot{V}O_2$ response composition.

In computational terms, the SOSC model requires a total of six curve parameters in order to represent any shape of CR, whereas the MiME supra-LT CR requires seven (Table 7.1). Additionally, although the FOME supra-LT CR also requires six parameters in the absence of the O$\dot{V}O_2$K, the presence of this phenomenon will require the addition of a three-parameter overshoot add-on term [46, 48, 51], which may lead to a nine-parameter model (Table 7.1). It is important to remark, however, that the shape flexibility and superior fitting performance allowed by the simultaneity of the SOSC models components is necessarily related with the SOS nature of these curves, for a previously tested model applying two FOS-based simultaneous components presented a worse fitting performance than that of the usual FOME model [91].

In physiological terms, at least three aspects regarding the modeling of the recruitment of different muscle fiber types during constant-WR exercise are allowed to be differently interpreted in the SOSC theory than in the FOME and MiME models:

First, the SOSC's combination of its two components—roughly associated with the pools of type I and II muscle fibers—allows the consideration, already from the beginning of the exercise, of the specificities regarding the mix of muscle fiber types required for different WR, force, and contraction speed requirements (See *9.2 General relationship between the FOME, MiME, and SOSC curves in the time domain* bellow).

Second, the SOSC's single natural frequency ω_S, common to its both components and possibly associated with the interaction between the different circulatory compartments of the body, and the concept of different ζ_{CI} and ζ_{CII} values, specific to the metabolic features of each muscle fiber pool (see Physiological coherence of the SOSC model) offer a rich physiological interpretation of the curve parameters. Such improved representative capacity may support compartmental models (e.g., Barstow et al. [161]) and other theories for "human $\dot{V}O_2$ mechanism" in a deeper manner than the single parameter τ from the FOS representation.

Third, while the additional type II fiber recruitment at the SC onset is mandatory in the FOME and MiME theories, the delayed recruitment of fibers is not a requirement of the SOSC model due to the synchronism of its components. At the same time, the additional recruitment of type II is not necessarily refuted by the SOSC theory. In fact, the slow ascending profile of the CII itself, when considered independently, may be explained by (i) the loss of efficiency of its originally recruited fibers; and/or (ii) a naturally slow response of the type II fibers; and/or (iii) the additional recruitment of type II fibers. In that last case, however, such additional recruitment would take place gradually throughout the exercise—due to fatigue of already recruited fibers and/or another triggering factor(s)—instead of initiating precisely at the beginning of a given SC.

9.1.3 The initial upward concavity of the SOS curves

Finally, another characteristic of SOS curves, namely the initial upward concavity (see, for example, the onset of the CR in Figures 5.7, 7.5, or 7.7, among others), is a feature naturally associated with presence of an inertia-like element [57]. Such "signature" of a higher-than-one order curve, however, is not noticeable in $\dot{V}O_2$ responses measured at the pulmonary level due to the presence of the CC at the initial instants of the response [74, 122]. Conveniently, it is more evident in the kinetics of $\dot{V}O_2$ (see [155], Figure 2) and [HHb] (see plots in [7] and [123]) measured at the muscle level, which corroborates the idea of an underlying SOS dynamics in the $\dot{V}O_2$ kinetics. The physiological coherence of this smooth initial increase of the SOS-based curves and

its role on the evaluation of the td_{FC} are discussed in Chapter 5 (see *Parameters, curve shaping, and underlying phenomena*, in Section *5.3.2*).

9.2 General relationship between the FOME, MiME, and SOSC curves in the time domain

The combined analysis of the content exposed specially in Sections 8.1.1 and 8.1.2 may provide interesting insights into the general relationship between the tested models throughout the WR spectrum, which may be summarized as:

- At lower exercise intensities, the mild participation of the CII in the SOSC's CR renders this model very similar to the MiME model and, for nonovershooting cases, to the FOME model as well. In fact, from this viewpoint, the FOME model may be seen as the first-order approximation of the nonovershooting MiME case; and
- At higher exercise intensities, where the $O\dot{V}O_2K$ is usually nonexistent or imperceptible in the CR [48, 57], both MiME and FOME models tend to be similar, for they rely on the same SC to represent the now rising $\dot{V}O_2SA$ phenomenon. Additionally, this need for comprising the $\dot{V}O_2SA$ at higher exercise intensities is also revealing of the advantages of the concomitant evaluation of the SOSC model's components, which outperforms the subjectivity and artificiality of the "break point" imposed at the beginning of the FOME and MiME's SC.

9.3 The profiles of the SOSC, MiME, and FOME models in the WR domain

In the FOME and MiME models, the general linear gain assumed for the A_{CR} evaluated in the moderate domain—where it is composed solely of the A_{FC} [36, 52, 54, 82, 118, 120]—is considered to be disrupted by the addition of the SC at supra-LT exercise intensities [36, 52], so the A_{CR} values will deviate from the line corresponding to the A_{FC} (Figure 9.1.A).

However, like it is evident in the case depicted in Figure 9.1.A, even the supra-LT A_{FC} values deviate from the extrapolated FC line obtained from the sub-LT A_{FC} values, which may indicate that a CII-like component is already present at the beginning of the step response, being thus erroneously attributed to the FC. Such spurious increment of the A_{FC} will be obviously accompanied by a proportional reduction in the expected A_{SC}, similarly to the effect caused by an increased WR in the baseline of the step on-transient (thus inducing a greater recruitment of higher-

order fibers already at the beginning of the exercise, i.e., a greater CII in reality) reported by Wilkerson and Jones [133].

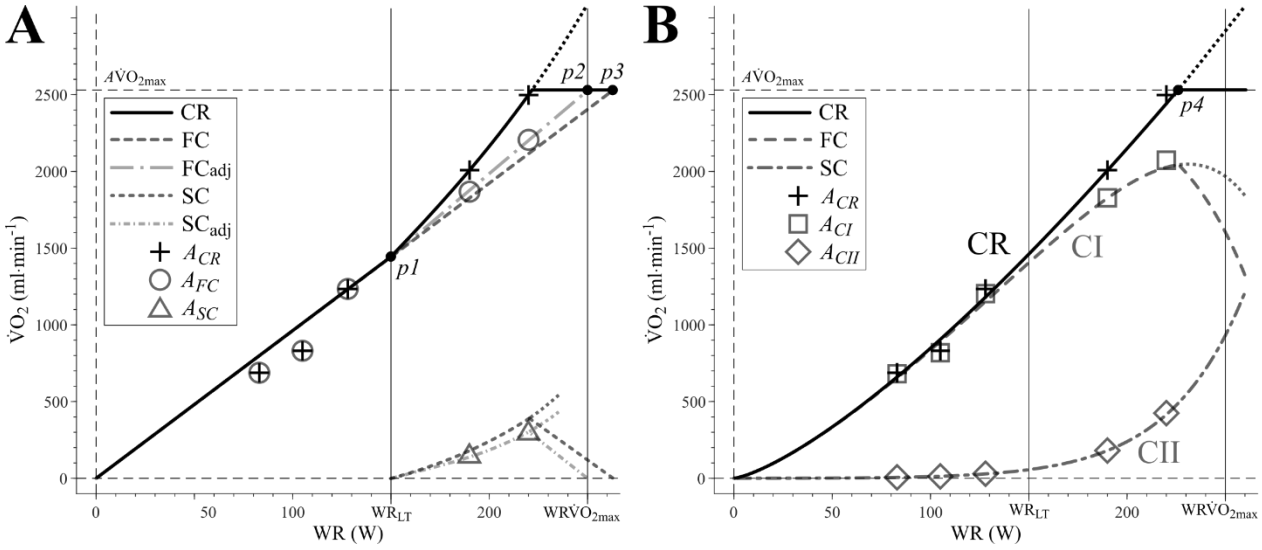

Figure 9.1 Profiles of the A. FOME and MiME models, and B. SOSC model throughout the WR spectrum evaluated for *subject 4*. In panel A, the FC line is obtained from the linear regression comprising only the sub-LT A_{FC} values (including the origin point [0 W,0 ml·min^{-1}]), and the "adjusted FC" (FC_{adj}) line is obtained by linking the points *p1* and *p2*, since the FC linear approximation will reach $\dot{V}O_{2max}$ only on point *p3*, at a WR greater than the $WR\dot{V}O_{2max}$. The supra-LT region of the CR is approximated with a generic "exponential" curve (adopting the "exponential-like" nature of the SC suggested in figure 1.12 from [1]) including both available supra-LT A_{CR} values. The SC and "adjusted SC" (SC_{adj}) curves are respectively obtained from the differences CR – FC and CR – FC_{adj}; In panel B, the power law (equation 9.1) describing the CR was obtained using only the sub-LT A_{CR} values.

Another incongruence is the fact that not even the sub-LT A_{FC} values (identical to the sub-LT A_{CR}, in the FOME and MiME context) seem to follow the linear fit actually obtained from themselves, which motivates the consideration of alternative functions such as the power law in (equation 9.1) for the modeling of the CR (Figure 9.1.B).

$$A_{CR}(\mathrm{WR}) = C_{CR} \cdot \mathrm{WR}^{\,D_{CR}} \qquad (9.1)$$

For WR < CP

Interestingly, although the parameters C_{CR} and D_{CR} in Figure 9.1.B are evaluated exclusively from the sub-LT A_{CR} values, the CR curve provides a very close approximation of the measured supra-

LT A_{CR} values. Moreover, this CR curve crosses the $A\dot{V}O_{2max}$ level at an WR corresponding, for this particular subject, to an intensity 13% above his 50%Δ (Figure 9.1.B; point *p4*). Assuming a rough approximation of the individual's CP as his 50%Δ value [167-169], the WR value of *p4* is in agreement with the results from de Lucas et al. [170], where the $\dot{V}O_{2max}$ was reached by trained cyclists when the constant WR exercise was performed not at the classically evaluated CP, but at an intensity 5% higher. In fact, such agreement may be improved by the fact that, for trained cyclists, the 50%Δ will probably represent an underestimation of CP.

Regardless of the pertinence of the specific formula proposed in equation 9.1, an important advantage of the SOSC model dynamics is that its CR may be expressed as a single continuous function of the WR from 0 Watt until some intensity slightly above the individual's CP, where physiological upper limit represented by the $\dot{V}O_{2max}$ is finally reached. Such a continuity is interrupted, by definition, by the onset of the SC at some point in the FOME and MiME's representation of the CR in the WR spectrum. Also by definition, possible cases of mild manifestations of the $\dot{V}O_2SA$ at sub-LT intensities threshold, like observed in Chapter 7 and in [160], are automatically discharged by the non-inclusion of the SC term in the FOME and MiME model.

In terms of the fiber recruitment pattern, the SOSC model offers a scenario where the portion of type II fibers pool responsible for the $\dot{V}O_2SA$ may start to be recruited already at the beginning of the exercise and already in the moderate domain, which is not allowed in the FOME and MiME context due to their necessarily delayed SC. As extensively discussed in Section *7.4.2 Physiological coherence of the SOSC model*, the exponential increase in the $A_{CII\%}$ in response to the WR augmentation is in perfect agreement with the predominance of type I and II fibers recruitment at respectively low and high power outputs found in the cortically stimulated muscle [162], and with the increased proportional contribution of the $\dot{V}O_2SA$ to the A_{CR} associated with (i) a higher percentage of type II fibers [39]; (ii) a higher blood lactate concentration [39, 41, 96, 98, 99]; (iii) a higher exercise intensities [88, 96]; and (iv) and higher pedalling cadences (i.e., higher contraction velocities) [42, 97, 98].

The balance between the magnitudes of CI and CII describe a logic according to which, at any given WR, the individual will recruit as few type II fibers as possible, in a trade-off between

avoiding the overuse of these powerful but less efficient contractile elements [94, 95] while still respecting the minimal requirements of speed and/or force of contraction dictated by the exercise.

Therefore, each A_{CI}:A_{CII} ratio established in the WR spectrum could be associated with a [Lac] dynamic, with the lactate production rate being somehow proportional to A_{CII} (i.e., to the anaerobic portion of the type II fibers metabolism) and its removal rate proportional to A_{CI} or to A_{CR} (thus, related with pyruvate oxidation). This could explain the WR_{LT} as the intensity where the A_{CI}:A_{CII} (or maybe the A_{CR}:A_{CII}) ratio becomes smaller than a given threshold, causing the [Lac] to increase. Moreover, the CP and/or the WR at the maximal lactate steady-state (WR_{MLSS}) could also be explained as the intensity where these ratios reach a minimum value still eliciting a stable [Lac], which would likely correspond to the maximal value of CI, where the slope of the CII surpasses that of the CR. In fact, although the CI maximal value for *subject 4* is placed slightly to the right of *p4* (Figure 9.1.B), in five of the other six subjects in the CONV+ group (see Section *7.3.1*) it was placed closer to the 50%Δ intensity than to *p4* itself—thus, to the left of *p4*) and in the expected region for CP and/or WR_{MLSS} [167-169].

In any case, these speculative theories offered by the SOSC model reflect a perspective that places such important physiological concepts no longer as a cause, but as a consequence of the $\dot{V}O_2$ response components' shape. In that sense, further studies comparing the profile of the A_{CI}:A_{CII} and A_{CR}:A_{CII} ratios and the WR at the intersection *p4* with the individually evaluated CP, WR_{LT}, and WR_{MLSS} values are required.

9.4 Detection and characterization of the O$\dot{V}O_2$K and $\dot{V}O_2$SA phenomena

The O$\dot{V}O_2$K phenomenon. In Chapter 5, some objective criteria are presented for the detection and characterization of the O$\dot{V}O_2$K occurrences with basis on the MiME model and its second-order representation of the FC (see Sections *5.2.4 Overshoot detection using the FCOvsht solution* and *5.3.1 Overshoot detection and quantification*). Because the O$\dot{V}O_2$K indicators proposed in this study, namely the tp_{ref}, Mp_{ref}, and $V_{O\dot{V}O2K}$, are obtained from the FC_{Ovsht}'s regression curve, thus representing an "averaged" behavior of the data set, the susceptibility of the O$\dot{V}O_2$K analysis to punctual data variations and to the data interval considered via the previously proposed *Peak-SS* and *IV* [47, 48] is reduced.

Nevertheless, not only the utility of these point-by-point indicators as preliminary O$\dot{V}O_2$K

assessment tool is recognizable, but also their complementary application in this study's $O\dot{V}O_2K$ occurrences served to indicate their coherence with those reported in the literature [46-48].

Because in the MIME model the FC is the only component participating in the CR composition during the period where the $O\dot{V}O_2K$ is considered to manifest (i.e., $t_0 < t < t_{FC}$), this detection via the FC_{Ovsht} solution becomes evident. However, the concomitant participation of CI and CII in the SOSC composition for any $t \geq td_S$ impose differences between any possible $O\dot{V}O_2K$ represented in the CR and the overshoot in its associated CI_{Ovsht} curve.

As already exposed, not only will some overshooting CI cases (i.e., using the CI_{Ovsht}) not cause a detectable $O\dot{V}O_2K$ in the CR, but even when the $O\dot{V}O_2K$ occurs, the influence of the CII will result in differences between the $O\dot{V}O_2K$ and the overshoot of its associated CI_{Ovsht}'s in terms of magnitude and peak instant.

In this case, a possibility is the establishment of two classes of CR, namely a class where the CI is better represented by its overshooting version (CI_{Ovsht}), and another where its nonovershooting version (CI_{NOvsht}) is the optimal one. However, such criterion would be, in some cases, dissociated from the actual manifestation of the $O\dot{V}O_2K$ phenomena in the CR (e.g., Figures 8.1.A and 8.3.A-B).

Another possibility, more aligned with the practicalities of the $\dot{V}O_2$ kinetics studies, is the use of the MiME's approach for the general detection of the $O\dot{V}O_2K$ phenomenon, leaving the actual—and more detailed—physiological characterization of the response to be performed via the SOSC model's parameters. In any case, unlike in the FOME and MiME methodologies, the "formalization" of the $O\dot{V}O_2K$ phenomenon occurrence is not fundamental to the implementation of the SOSC model.

In the MiME methodology, even if following very objective criteria (see Section *5.2.4 Overshoot detection using the FCOvsht solution*), the $O\dot{V}O_2K$ detection is required in order to define which second-order formula to implement (either FC_{Ovsht} or FC_{NOvsht}). In the FOME model, where an add-on term must be incorporated to the usual FC_{FOS} in order to comprise the $O\dot{V}O_2K$, two situations are presented in literature: (i) one where the add-on term is used only for the cases where the phenomenon is previously detected for positive *Peak-SS* values [48], and (ii) another where the add-on term may always be used, although a pre-defined "$O\dot{V}O_2K$ portion" of the data must be

preliminarily excluded from the data set during the fitting procedures [51], which is only justifiable once the O$\dot{V}O_2$K is actually present.

The $\dot{V}O_2$SA phenomenon. Unlike the O$\dot{V}O_2$K, the $\dot{V}O_2$SA in the FOME and MiME contexts is never the object of an actual detection, for it is considered *a priori* to be either absent or present at respectively sub- or supra-LT WRs. Instead, regardless of the correctness of this assumption, the methodological issue regarding these models where the $\dot{V}O_2$SA is represented by the SC is the definition of its onset instant td_{SC} (or, equivalently, t_{FC}; see Section *5.2.3 Curve-fitting procedures*). Such issue, however, does not concern the SOSC methodology, for the $\dot{V}O_2$SA is naturally represented in the CR in accordance with the data demands. Moreover, the $\dot{V}O_2$SA representation in the SOSC model is not conceptually restricted to any exercise intensity domain, being thus observable (or not) regardless of the sub- or supra-LT condition. Although very discreet, $\dot{V}O_2$SA-like rises are noticeable even in sub-LT SOSC curves (see the legend of Figure 7.7). These are examples of the SOSC conceptual flexibility (see Section *7.4.2 Physiological coherence of the* SOSC model

One strong aspect of the SOSC model is that, despite the possibility of assuming two independent ω values for CI and CII, significantly better fittings are obtained by adopting a common ωS shared by CI and CII. More than reducing the quantity of model parameters, this single ωS may suggest the concept of a natural frequency of the "human $\dot{V}$O2 mechanism" that could reflect the interaction between the respiratory and circulatory systems and/or between central and peripheral regions of the circulatory system alone—similarly to the computational model of "muscle and 'rest-of-body' compartments" proposed by Barstow et al. [161]. Such common ωS, that may vary from one intensity to another (e.g., due to differences in heart rate, muscle perfusion, or pulmonary gas exchange) would represent the time course of muscle oxygen supply, while the difference between ζCI and ζCII would be due to the intrinsic features (e.g. biochemical) of each muscle fiber type that affect the efficiency of oxygen utilization. The tight variation of ζCI values around the value of one (Table 7.3) agrees with fast and responsive CI that, due to the high oxidative capacity of type I fibers, is often overshooting or on the verge of doing so. Oppositely, the ζCII values consistently much greater than one are coherent with the slower CII mechanism, less specialized in the oxidative activity, but offering the advantages of force and/or speed generation from the type II fibers, even if at the expenses of the system's net efficiency (see *GCR* ascending values; Table 7.3).

This may be the underlying message from studies associating more pronounced V̇O2SA relative contributions in the V̇O2 net response with higher percentage of type II fibers in the working muscles [39], with higher blood lactate concentration situations [39, 41, 96, 98, 99], higher exercise intensities [88, 96], and higher pedalling cadences—thus, higher contraction velocity [42, 97, 98]. In studies applying step tests [97, 98], the increase of both *AFC* and *ASC* observed at the higher cadences for a same WR have been attributed to the augmented recruitment of fast-twitch fibers. While this expected increment in *ASC* alone does not affect the delayed SC theory, the increase in *AFC* suggests the presence of a type II fiber-related contribution manifesting before *tdFC*. This early contribution, that in the FOME model might be wrongly attributed to the FC, would be trivially explained by the SOSC dynamics of larger CIIs at higher cadences.

A similar perspective may explain the smaller *A*SC, and the larger gain and τ values of the fundamental phase obtained for heavy WR step transitions when initiating from a moderate rather than an unloaded cycling baseline [133], considered by the authors as a possible effect of the greater recruitment of higher-order fibers (i.e., approaching a type II) already "at (or close to)" the WR transition, and thus, refuting the relationship between the V̇O2SA and the progressive recruitment of these fibers.

In fact, the debate about whether type II fibers are recruited under a time-progressive regimen or already at the beginning of the exercise [38, 52-54, 133, 158, 159] becomes pointless if the aforementioned association between these fibers and the V̇O2SA is considered in the FOME model context, where the V̇O2SA is represented by the necessarily delayed SC.

Instead of assuming that type I fibers are initially stressed to their limit and an additional fast-twitch pool is only recruited after $t = tdSC$, the SOSC logic prioritizes the "original purpose" of each fiber type, using the efficient slow-twitch fibers for the main portion of the work generation and recruiting their stronger and faster type II counterparts "on demand," as required by the instantaneous WR. Such strategy has been recently corroborated by the predominance of type I and II fibers recruitment at respectively, low and high power outputs found in the model of the cortically stimulated muscle [162].

In terms of aerobic efficiency of force production, the use of a muscle pool composed of type II fibers—with both higher ATP cost of force generation [94], and higher V̇O2 cost per ATP resynthesis [95] than the type I—already at the beginning of the exercise may not seem appealing.

However, when a given WR must be delivered already at the first seconds of the exercise, with power generation requiring certain levels of speed and/or force of contraction, delaying the recruitment of eventually necessary type II fibers does not appear convenient.

A fundamental aspect of our model, however, is that it does not ignore the effect of fatigue nor its relationship with the loss in muscle efficiency and the V̇O2SA phenomenon [158, 163, 164]. Instead, it actually considers that such effect may take place within the CI and/or CII respective fiber pools, gradually starting already at the exercise onset and being more evident in the CII (e.g., causing a greater ζCII than ζCI) due to the greater susceptibility of type II fibers to fatigue. Corroborating this possibility, studies involving all-out cycling tests in humans [159], or electrically stimulated animal preparations [53] demonstrate that a same pool of fibers may manifest V̇O2SA-like increases for a constant WR independently of additional fiber recruitment.

SOSC curve shape formation), which allows this model to represent—and justify—occurrences such as the $\dot{V}O_2$SA-like drifts in step responses below the ventilatory threshold [160] and the coexistence of both O$\dot{V}O_2$K and $\dot{V}O_2$SA in the same response [57] (Figure 8.3.C).

9.5 Limitations and constraints

Amongst the main limitations or constraints identified in the application of the MiME and SOSC models, two issues intrinsic to the pulmonary measurement of $\dot{V}O_2$, thus also affecting the use of the FOME model, are identifiable:

- Like in the FOME model's FC, the very beginning of the MiME's FC, and SOSC's CI and CII must be predicted by means of the extrapolation of the curves obtained from data measured 15 to 25 seconds after the step transition onset, where the "disturbance" caused by the cardiodynamic phase—considered alien to the actual muscle O_2 uptake [50, 122]—can not be avoided; and
- Repeated trials must be performed for each experimental condition (e.g., for a given WR) in order to minimize the deleterious effects of the low signal-to-noise ratio characteristic of pulmonary $\dot{V}O_2$ data, especially at low exercise intensities.

Specifically regarding the models proposed in this work:

- The implementation of the SOSC model is largely facilitated by the occurrence of a noticeable, preferably pronounced $\dot{V}O_2$SA. However, larger $\dot{V}O_2$SAs are observed at higher exercises intensities, where the CR takes a longer time to reach its steady-state (see second item of Section *10.4 Recommendations*), which will often require step tests as long as 15 min or more; and

- Improvements must be made in the curve regression methods to overcome the shape similarity between some overdamped curves (FC_{NOvsht}, SC_{NOvsht}, CI_{NOvsht}, and CII_{NOvsht}) obtained with different combinations of ζ and ω values (i.e., ζ-ω pairs in the FC_{NOvsht} or SC_{NOvsht}; ζ_{CI}-ω_S pairs in the CI_{NOvsht}; and ζ_{CII}-ω_S pairs in the CII_{NOvsht}). This issue, intrinsic to regressions using SOS overdamped solutions, may contribute to (i) increase in the variability of some of MiME and SOSC models' parameters; and (ii) to reduce the assertiveness of the optimal A_{CII}% obtained in some SOSC implementations (nonCONV cases; see Section *7.3.1 Convergence analysis of the SOSC model at supra-LT intensities*).

9.6 Practical overview

Due to fundamental differences resulting from the curve-order and/or the synchronism of their components, it is difficult to synthesise one general relationship between the FOME, MiME, and SOSC models. In a simplistic sense, the FOME model may be seen as a first-order approximation of the MiME model, where the former's results will be as close to the latter's as the overshooting characteristics are less pronounced—or possibly, absent—in the $\dot{V}O_2$ response. Analogously, the MiME model may be interpreted as an approximation of the SOSC model that performs very similarly at low intensity WR transitions, where the influence of the CII is close to negligible and the $\dot{V}O_2$SA phenomenon imperceptible (see *Sub-LT intensities* in Section *7.2.4 Curve fitting procedures*).

However, while the assertion above addresses the practicality of overlapping these models in specific conditions, it is important to remark that the conceptual issues of using the wrong model to describe and analyse the human $\dot{V}O_2$ kinetics remains present in all cases, regardless of the WR and the presence of the O$\dot{V}O_2$K and/or the $\dot{V}O_2$SA phenomena. Even when the fit performances of these models' curves are very similar, their conceptual differences may still induce poor interpretation of data (e.g., spurious evaluations of A_{FC} [47], τ_{FC} [47, 48], and O_2 deficit [46-48] via

FOME model), which in turn, may jeopardize not only the practical usefulness of the $\dot{V}O_2$ kinetics analysis, but the understanding of the underlying physiological mechanism itself.

CHAPTER 10 CONCLUSION AND RECOMMENDATIONS

10.1 Objectives accomplishment and hypotheses testing

10.1.1 Specific objective 1

In Chapter 5, the implementation the MiME model was accomplished, with the second-order representation of the FC being proved viable at all tested WRs and its curve parameters being evaluated and compared to those from the usual first-order representation. Also in this chapter, the SOS family of curves was presented in the context of the $\dot{V}O_2$ kinetics (by means of a *physiomechanical analogy*), and its coherence with the possible advent of an overshoot and/or the initial upward concavity is remarked on.

One important characteristic the MiME model, the first-order representation of the SC (retained from the FOME model), was adopted in Chapter 5 without a formal comparison with the second-order alternative. The formalization of this comparison was added to this thesis in Chapter 6 in order to complement and support the accomplishment of the *specific objective 1*.

10.1.2 Specific objective 2

Because the implementation of the MiME model is oriented by the existence or absence of the O$\dot{V}O_2$K in the $\dot{V}O_2$ response, so that the FC_{Ovsht} or FC_{NOvsht} solution may be respectively applied, the definition and implementation of an objective methodology for detecting and quantifying this phenomenon also had to be accomplished in Chapter 5. Such O$\dot{V}O_2$K detection and quantifying methodology was once again applied in Chapter 6, this time in the context of the SC.

Although the proposed O$\dot{V}O_2$K detection and quantifying method is based upon the MiME's representation of the FC, it may be applied prior to the modeling via other models: (i) in the case of the FOME model, to test the level of inadequacy of the data to a first-order approximated solution; and (ii) in the SOSC model context, as a tool for "previewing" the CI, since, as described in Chapter 8, the existence of an O$\dot{V}O_2$K in the CR necessarily implies an overshooting CI (CI_{Ovsht}).

10.1.3 Specific objective 3

Chapter 7 comprises the implementation of the SOSC model, which is accompanied by a discussion regarding the physiological coherence of this model and its consequences to the theory of the delayed fiber recruitment during constant WR exercise. The automatic methodology applied to obtain the SOSC model's curve parameters is also described in this chapter, allowing its reproduction in further studies. Because the SOS family of curves is already introduced in Chapter 5, the SOSC model's presentation focused on its mechanistic basis; a simple variation in the proportional contributions of CI and CII to the CR—in response to variations in WR, force, or speed of movement—allows the modeling of all $\dot{V}O_2$ step on-transients responses observed in humans, whether manifesting or not the O$\dot{V}O_2$K and/or the $\dot{V}O_2$SA phenomena.

10.1.4 Specific objective 4

The comparison between the performances of the FOME, MiME, and SOSC models for fitting and describing human $\dot{V}O_2$ step on-transients at all WRs, and regardless of the presence of the O$\dot{V}O_2$K and/or the $\dot{V}O_2$SA phenomena, is performed in different chapters.

MiME vs. FOME models. In the direct statistical comparison of RMSE means performed in Chapter 5, the MiME model proves to be significantly superior to the FOME model for O$\dot{V}O_2$K cases, and equivalent for NO$\dot{V}O_2$K cases. Beyond the general RMSE analyses, the specific features of the second-order curves—which allow the representation of an overshooting behavior whenever required by the data characteristics—imply a different interpretation of the O$\dot{V}O_2$K: rather than an inconvenient artifact that only manifests in certain experimental conditions, this phenomenon may be an intrinsic manifestation of the $\dot{V}O_2$ response in humans.

SOSC vs. FOME models. In Chapter 7, the SOSC model's RMSE values, consistently smaller than those from the FOME model (with statistical significance in the majority of the tested conditions), denote the fitting superiority of the SOS-based representation. Additionally, due to the second-order nature of the curves composing the SOSC model, it shares the same conceptual and mathematical advantages as the MiME model over the FOME in regards to the O$\dot{V}O_2$K representation. Other advantages of the SOSC over the FOME model are also found in relation to the MiME model, and are commented on bellow and in Chapter 9.

SOSC vs. MiME vs. FOME models. The concomitant numerical comparison of the three models' fitting performances is presented in Chapter 8, demonstrating RMSE mean values consistently greater for the FOME and smaller for the SOSC model. However, due to the absence of the O$\dot{V}O_2$K at supra-LT intensities, the difference between the MiME and FOME models is not significant—like described above in the paired comparison between these models at sub-LT but for NO$\dot{V}O_2$K cases. The same lack of significant differences happens between the SOSC and MiME models at sub-LT WRs, since both of these SOS-based models are able to describe any O$\dot{V}O_2$K possibly observed. For supra-LT conditions, however, the superiority of the SOSC model observed in the paired comparison with FOME becomes evident also in the concomitant comparison to both FOME and MiME models.

Further differences in the conceptual structure and methodologies applied to each of these models are discussed in details in Chapters 5 to 9, with the general relationship between the curves of the three compared models (see Section *9.2 GENERAL relationship between the FOME, MiME, and SOSC curves in the time* domain) being summarized as follows:

- The SOSC and MiME curves tend to be similar at lower WRs;
- The MiME and FOME curves tend to be similar at higher WRs; and
  Note: the difference at lower WRs observed in the CR (Table 8.1) are likely conditioned to the manifestation of the O$\dot{V}O_2$K during *phase II* of the $\dot{V}O_2$ step response, since the separate analyses of O$\dot{V}O_2$K and NO$\dot{V}O_2$K groups demonstrated such dependence for the FC (Table 5.3), but not for the SC (Table 6.2).
- The SOSC model normally presents better fitting curves (usually significantly better) than the FOME model.

10.1.5 General objective

Arising from the accomplishment of the four *specific objectives* described above, the development and implementation a comprehensive model for the $\dot{V}O_2$ kinetics in humans capable of comprising none, either, or both of the O$\dot{V}O_2$K and/or $\dot{V}O_2$SA phenomena observed in response to the step on-transient at any exercise intensity, the matter of this thesis's *general objective*, has been achieved by both MiME and SOSC propositions, with the latter overcoming the former in terms of its comprehensiveness and physiological foundations.

10.1.6 Hypotheses 1 and 2

The *Hypothesis 1* and *2* were tested and confirmed in Chapters 5 and 7, respectively. Both MiME and SOSC models present a better overall performance than that of the FOME model in fitting $\dot{V}O_2$ step responses at all WRs, containing none, either, or both of the $O\dot{V}O_2K$ and/or $\dot{V}O_2SA$ phenomena. In the case of the *hypothesis 1*, the alternative of containing or not the $\dot{V}O_2SA$ phenomenon did not have to be included, for the tested data was only that comprising the FC before the beginning of the SC, with the representation of the $\dot{V}O_2SA$ being identical in both MiME and FOME models.

10.2 Contributions and benefits of this study

10.2.1 Benefits to clinical and physical activity related evaluations

From a pragmatical viewpoint, the formal documentation of the innovative models presented here will allow their incorporation to the roster of available tools for the analysis of respiratory data, either as a new *software package* or as *specialized suites* in already existent data treatment sets. Some practical benefits of the adoption of these models are listed bellow:

- The MIME and SOSC models can improve the assessments of fitness status via ergospirometry, especially in the cases where shapes of the $\dot{V}O_2$ responses are overshooting or close to it (i.e., significantly differing from a first-order behavior). For example, the replacement of τ with ω and ζ (and is derivations like τ_{App} and ω_d) may improve the evaluation of the speed of the $\dot{V}O_2$ augmentation, or the use of second-order solutions may provide a more accurate O_2 deficit estimative by considering the influence of the $V_{O\dot{V}O2K}$ and the V_{comp} (Figure 5.1);
- The SOSC model does not require a detection of the $O\dot{V}O_2K$ previous to its application, in opposition to the MiME or FOME[16] models;

[16] See *The phenomenon of the overshoot in the $\dot{V}O2$ kinetics* in Section *2.6.1* for commentary on the addition of the *overshoot term* (*curve III*) to the FOME model for $NO\dot{V}O_2K$ cases.

- The MiME model provides an objective detection and quantification method for the O$\dot{V}O_2$K phenomenon;
- The SOSC model does not require the previous detection of the individual's WR or $\dot{V}O_2$ at the LT or at the GET, in opposition to the FOME and MiME models, which use this information to include or not the SC in its configuration;
- Because the SOSC model does not require a previous definition of the beginning of the "slow component" (i.e., the td_{SC}), it may comprise responses where the $\dot{V}O_2$SA is imperceptible or where its beginning in not clearly identifiable; and
- As discussed in Section *9.3*, the SOSC model may provide alternative explanations for the WR_{LT}, the CP and the WR_{MLSS} that potentially allow their evaluation by means of simpler methods (e.g., shorter and/or less extenuating testing protocols);

10.2.2 Conceptual contributions to the $\dot{V}O_2$ kinetics knowledge

As important as the practical benefits brought by the models presented in this work are, it is noteworthy that they offer two alternative interpretations for the human $\dot{V}O_2$ kinetics that, despite diverging from a multi-exponential type of model adopted for nearly half a century (based on a first-order-like exponential shape suggested almost one century ago), are founded numerically and conceptually not only on experimental data collected in this study, but also on reports from the literature. The advent of such innovative theories has the power to encourage—and ultimately, allow—studies whose designs, experimental interventions, and results treatment and interpretations are guided by alternative hypotheses, which may enhance significantly the knowledge of the field.

- *The O$\dot{V}O_2$K.* Since the O$\dot{V}O_2$K phenomenon is itself a poorly covered subject, still considered 'unusual' or artifact by part of the exercise physiology community, the availability of models capable of describing it may encourage the propagation of the topic. This may lead researchers to recognize this phenomenon among their experimental data and/or to reproduce the adequate experimental conditions for the O$\dot{V}O_2$K manifestation in their new study designs.
- *The $\dot{V}O_2$SA.* By offering an alternative explanation for the $\dot{V}O_2$SA (widely know as the "slow component" phenomenon) that is *a priori* independent from the concepts of the LT and the

delayed fiber recruitment, the SOSC model has the potential to contribute to the full understanding of this still controversial phenomenon;

- *Response manipulation and prediction.* The knowledge of the real components of the CR, may allow the definition of the system's transfer function composition. This is valuable information for the prediction and manipulation of the systems output ($\dot{V}O_2$) in response to different and more complex input (WR) stimuli; and
- *Continuity and smoothness of the SOSC model.* The idea of a model that conserves the same composition for all the WR spectrum and that presents an internal dynamic between its components ruled by smooth and continuous functions releases the $\dot{V}O_2$ kinetics modeling from milestone concepts like the LT or the GET. At the same time, as discussed in Section *9.3*, these physiological reference values may be understood as a consequence of this dynamic, rather than as its cause.

10.3 Future work

Some possible future work aiming to either give continuity to this study or to improve some aspects of the already proposed models are listed bellow:

- A power law dependence between the A_{CII}% and the WR (equation 10.1), alternative to the exponential relationship depicted in the equation on Figure 7.3 could be tested for the SOSC model:

$$A_{CII}\%(\mathrm{WR}) = c \cdot \mathrm{WR}^{\,d} \tag{10.1}$$

  This would not only be in better accordance with the A_{CR}(WR) profile, but could also allow the CII curve to have its own parameters C_{CII} and D_{CII}, as follows from the multiplication of equations 10.1 and 9.1:

$$A_{CII}(\mathrm{WR}) = A_{CII}\%(\mathrm{WR}) \cdot A_{CR}(\mathrm{WR}) = c \cdot \mathrm{WR}^{\,d} \cdot C_{CR} \cdot \mathrm{WR}^{\,D_{CR}} = c \cdot C_{CR} \cdot \mathrm{WR}^{\,d+D_{CR}} = C_{CII} \cdot \mathrm{WR}^{\,D_{CII}} \tag{10.2}$$

- Instead of an overdamped second-order curve, a first-order approximation may be tested for the CII as a simpler alternative to the $CII_{NOvosht}$;

- A version of the SOSC model where independent ω values are evaluated for CI and CII may be compared with the original SOSC version with a single ω_S in order to test if (i) smaller RMSE values are obtained, and (ii) the two independent ω values are similar to each other and to the original ω_S;
- The EPOC values for overshooting and nonovershooting situations may be compared, since the $V_{O\dot{V}O2K}$ and V_{comp} could cause its reduction;
- As mentioned in Chapter 5, the td_{SC} evaluation and the whole MiME's CR fit (or even the FOME's) may benefit from the introduction of a $2 \cdot \rho$ tolerance range around the preliminarily determined t_{FC} (i.e., $t_{FC} - \rho \leq td_{SC} \leq t_{FC} + \rho$);
- The enhancement of the regression methods may avoid the aforementioned imprecisions caused in the situations with different ζ–ω pairs yielding similar overdamped curves;
- As suggested above, the newly proposed models may benefit from studies relating its parameters with the already known FOME variables. The establishment of such relationships for various populations and exercise conditions would be extremely valuable;
- The MiME and SOSC models may be applied to $\dot{V}O_2$ responses obtained at the muscular level. Under these conditions, some SOS features like such as the initial upward concavity and oscillatory patterns of decreasing amplitude (occurring after the conventional $O\dot{V}O_2K$) might be identified;
- Both the MiME and SOSC models may be implemented to $\dot{V}O_2$ responses to different input stimuli, such as the ramp, sinusoidal, amongst others, including some random profiles typical of training and racing conditions. In this case, comparative references could be provided by computational models comprising the variations caused in the MiME and SOSC's linearity and in the MiME's structure by a nonconstant WR; and
- As proposed in Section *9.3*, studies investigating possible relationships between the profiles of CI, CII, and CR (including the A_{CI}:A_{CII} and A_{CR}:A_{CII} ratios), and the individually evaluated $WR\dot{V}O_{2max}$, CP, WR_{LT}, and WR_{MLSS} values are required.

10.4 Recommendations

Some recommendations regarding the application of the models discussed in this thesis are:

- Even if the SOSC model is adopted, the $O\dot{V}O_2K$ observable in the measured data may be described by means of the MiME methodology of detection [convergent FC_{Ovsht} satisfying ($\zeta \in \mathbb{R} \mid 0 \leq \zeta < 1$) and $tp_{ref} \leq 5$] and quantification (Mp, Mp_{ref}, $V_{O\dot{V}O2K}$, $O\dot{V}O_2K_{peak}$, V_{comp}, tp, and tp_{ref});
- At supra-moderate exercise intensities, where the steady-state of the CR takes longer to be achieved, enough time at constant WR testing must be allowed to ensure stability in the $\dot{V}O_2$ response (i.e., full development of the $\dot{V}O_2SA$ or, for supra-CP intensities, the attainment of $\dot{V}O_{2max}$). This will avoid errors, for instance, in the A_{CII}% evaluation;
- When applying the MiME model, the O_2 deficit (obtained as the difference between the area below the A_{FC} asymptote and that under the FC_{Ovsht} curve) must be corrected by subtracting the $V_{O\dot{V}O2K}$ from it;
- Although a change of paradigms is intended, the use of MiME's indicators that establish a comparison to the already familiar FOME variables is still welcome (e.g., τ_{App}, MRT, and MRT_{App}), so that a gradual transition from one model to another—or even their coexistence—is facilitated; and
- Even if applying the MiME or FOME models at moderate intensities, perform the preliminary checking for any discernible $\dot{V}O_2SA$ (i.e., an identifiable td_{SC} or t_{FC}), since this phenomenon's occurrence might not be restricted to supra-LT or supra-GET conditions.

10.5 Final comments

While the innovative and enhancing aspect of the MiME and SOSC propositions are strongly remarked on in order to evidence their advantages over the FOME theory, it is also of great importance that the exponential nature of the $\dot{V}O_2$ response is retained by the essence of these models. First, because the shapes of the curves representing the MiME and SOSC's components are based on exponential expressions. Second, because the relative contributions of the SOSC model's components throughout the exercise intensity spectrum are ruled by an exponential relationship with the WR.

The retainment of this exponential essence is not only important for corroborating the pertinence of the proposed models: it is also a confirmation that the FOME model proposed by Whipp and

Wasserman [71], and even the early descriptions of the $\dot{V}O_2$ kinetics of Lupton and Hill [66] were not wrong in their basic principles. In fact, the present work relies on the pathway paved by these outstanding researchers and for all of those who adopted and tested their propositions throughout time.

Moreover, instead of a final description of the proposed models, this work represents merely the first description of some concepts that, like any other theory, will derive its robustness from the scrutiny of the scientific community, which will reveal its actual utility and appropriateness. Nevertheless, the answer to this study's research question posed at the end of Section *3.1* seems to be already oriented to a confirmation that "the oxygen uptake kinetics in humans is in better agreement with a second-order system model than with the currently adopted first-order system theory."

Finally, it is also important to mention that the increased complexity of the second-order curves represents one side of the trade-off between the complexity of a model and its representation capacity. *C'est la vie* of modeling: to find the model with the lowest order required to satisfy our data.

REFERENCES

[1] A. M. Jones and D. C. Poole, "Introduction to oxygen uptake kinetics," in *Oxygen uptake kinetics in sport, exercise and medicine*, vol. 1, A. M. Jones and D. C. Poole, Eds. New York, USA: Taylor & Francis, 2005, pp. 3-35.

[2] D. R. Basset, Jr. and E. T. Howley, "Limiting factors for maximum oxygen uptake and determinants of endurance performance," *Med Sci Spo Exerc*, vol. 1, no. 32, pp. 70-84, 2000.

[3] C. A. Kindig, B. J. Behnke, and D. C. Poole, "$\dot{V}O_2$ dynamics in different species," in *Oxygen uptake kinetics in sport, exercise and medicine*, vol. 1, A. M. Jones and D. C. Poole, Eds. New York, USA: Taylor & Francis, 2005, pp. 115-137.

[4] S. Koga, T. Shiojiri, and N. Kondo, "Measuring $\dot{V}O_2$ kinetics: The practicalities," in *Oxygen uptake kinetics in sport, exercise and medicine*, vol. 1, A. M. Jones and D. C. Poole, Eds. New York, USA: Taylor & Francis, 2005, pp. 39-61.

[5] J. Boone, K. Koppo, T. J. Barstow, and J. Bouckaert, "Aerobic fitness, muscle efficiency, and motor unit recruitment during ramp exercise," *Med Sci Sports Exerc*, vol. 42, no. 2, pp. 402-408, 2010.

[6] S. P. von Duvillard, L. M. LeMura, D. W. Bacharach, and P. Di Vico, "Determination of lactate threshold by respiratory gas exchange measures and blood lactate levels during incremental load work," *J Manipulative Physiol Ther*, vol. 16, no. 5, pp. 312-318, 19930907 DCOM-19930907, 1993.

[7] S. J. Bailey, D. P. Wilkerson, F. J. Dimenna, and A. M. Jones, "Influence of repeated sprint training on pulmonary O_2 uptake and muscle deoxygenation kinetics in humans," *J Appl Physiol*, vol. 106, no. 6, pp. 1875-1887, Jun 2009.

[8] J. R. Stirling, M. S. Zakynthinaki, and V. Billat, "Modeling and analysis of the effect of training on $\dot{V}O_2$ kinetics and anaerobic capacity," *Bulletin of Mathematical Biology*, no. 1522-9602 (Electronic), 20080714 DCOM-20081010, 2008.

[9] W. L. Beaver, K. Wasserman, and B. J. Whipp, "A new method for detecting anaerobic threshold by gas exchange," *J Appl Physiol*, vol. 60, no. 6, pp. 2020-2027, 1986.

[10] M. Burnley and A. M. Jones, "Oxygen uptake kinetics as a determinant of sports performance," *Eur J Sport Sci*, vol. 7, no. 2, pp. 63-79, 2007.

[11] Y.-Y. Zhang, M. Johnson, II, N. Chow, and K. Wasserman, "The role of fitness on $\dot{V}O_2$ and VCO_2 kinetics in response to proportional step increases in work rate," *Eur J Appl Physiol Occup Physiol*, vol. 63, no. 2, pp. 94-100, 1991.

[12] A. R. Hoogeveen, H. Kuipers, and H. A. Keizer, "The effect of endurance training on the $\dot{V}O_2$ overshoot and the submaximal $\dot{V}O_2$ during steady-state exercise in competitive cyclists," in *The lactate and ventilatory response to exercise in endurance athletes*. Netherlands: Thesis, Saint Joseph Hospital, Vcldhoven, 2001, pp. 73-84.

[13] S. R. Murgatroyd, C. Ferguson, S. A. Ward, B. J. Whipp, and H. B. Rossiter, "Pulmonary O_2 uptake kinetics as a determinant of high-intensity exercise tolerance in humans," *J Appl Physiol*, vol. 110, no. 6, pp. 1598-606, 2011.

[14] D. Maione et al., "Constant load exercise $\dot{V}O_2$ kinetics study in the evaluation of heart failure," *Am J Hypertens,* vol. 16, no. 5, p. A86, 2003.

[15] A. Cohen-Solal, D. Guichet, J. Benessiano, and M. C. Aumont, "Determination of the ventilatory threshold during the exercise test in patients with cardiac insufficiency. Relation of the lactate threshold," *Arch. Cardiovasc. Dis.,* vol. 83, no. 2, pp. 255 -260, 1990.

[16] L. Kern et al., "Oxygen kinetics during 6-minute walk tests in patients with cardiovascular and pulmonary disease," *BMC Pulm Med,* vol. 14, p. 167, 2014.

[17] P. Palange et al., "Oxygen effect on O_2 deficit and $\dot{V}O_2$ kinetics during exercise in obstructive pulmonary disease," *J Appl Physiol,* vol. 78, no. 6, pp. 2228 -2234, 1995.

[18] L. Puente-Maestu, M. L. Sanz, P. Sanz, J. M. R. de Ona, J. L. Rodriguez-Hermosa, and B. J. Whipp, "Effects of two types of training on pulmonary and cardiac responses to moderate exercise in patients with COPD," *Eur Respir J,* vol. 15, pp. 1026-1032, 2000.

[19] A. Somfay, J. Porszasz, L. Sang-Moo, and R. Casaburi, "Effect of hyperoxia on gas exchange and lactate kinetics following exercise onset in nonhypoxemic COPD patients," *Chest,* vol. 121, no. 2, pp. 393-400, 2002.

[20] G. Kusenbach, R. Wieching, M. Barker, U. Hoffmann, and D. Essfeld, "Effects of hyperoxia on oxygen uptake kinetics in cystic fibrosis patients as determined by pseudo-randomic binary sequence exercise," *Eur J Appl Physiol,* vol. 79, pp. 192-196, 1999.

[21] H. Adachi et al., "Percutaneous transluminal coronary angioplasty improves oxygen uptake kinetics during the onset of exercise in patients with coronary artery disease," *Chest,* vol. 118, no. 2, pp. 329-335, 2000.

[22] H.-Y. Lim et al., "Effects of percutaneous balloon mitral valvuloplasty and exercise training on the kinetics of recovery oxygen consumption after exercise in patients with mitral stenosis," *Eur Heart J,* vol. 19, pp. 1865-1871, 1998.

[23] A. McManus and M. Leung, "Maximising the clinical use of exercise gaseous exchange testing in children with repaired cyanotic congenital heart defects: the development of an appropriate test strategy," *Sports Med,* vol. 29, no. 4, pp. 229-244, 2000.

[24] R. T. Hepple, P. P. Liu, M. J. Plyley, and J. M. Goodman, "Oxygen uptake kinetics during exercise in chronic heart failure: influence of peripheral vascular reserve," *Clinical Science (London, England : 1979),* vol. 97, no. 5, pp. 569-77, 1999.

[25] N. S. Lok and C. P. Lau, "Oxygen uptake kinetics and cardiopulmonary performance in lone atrial fibrillation and the effects of sotalol," *Chest,* vol. 111, no. 4, pp. 934-940, 1997.

[26] P. de Groote, A. Millaire, E. Decoulx, O. Nugue, P. Guimier, and G. Ducloux, "Kinetics of oxygen consumption during and after exercise in patients with dilated cardiomyopathy. New markers of exercise intolerance with clinical implications," *J Am Coll Cardiol,* vol. 28, no. 1, pp. 168-175, 1996.

[27] M. S. Riley, J. Porszasz, M. P. Engelen, S. M. Shapiro, B. H. Brundage, and K. Wasserman, "Responses to constant work rate bicycle ergometry exercise in primary pulmonary hypertension: the effect of inhaled nitric oxide," *J Am Coll Cardiol,* vol. 36, no. 2, pp. 547-556, 2000.

[28] T. A. Bauer, J. G. Regensteiner, E. P. Brass, and W. R. Hiatt, "Oxygen uptake kinetics during exercise are slowed in patients with peripheral arterial disease," *J Appl Physiol,* vol. 87, no. 2, pp. 809-816, 1999.

[29] T. J. Barstow, A. M. Scremin, D. L. Mutton, C. F. Kunkel, T. G. Cagle, and B. J. Whipp, "Peak and kinetic cardiorespiratory responses during arm and leg exercise in patients with spinal cord injury," *Spinal cord,* vol. 38, no. 6, pp. 340-5, 2000.

[30] Y. Fukuoka, M. Endo, H. Kagawa, M. Itoh, and R. Nakanishi, "Kinetics and steady-state of $\dot{V}O_2$ responses to arm exercise in trained spinal cord injury humans," *Spinal Cord,* vol. 40, no. 12, pp. 631-638, 2002.

[31] O. Inbar, R. Dlin, A. Rotstein, and B. J. Whipp, "Physiological responses to incremental exercise in patients with chronic fatigue syndrome," *Med Sci Sports Exerc,* vol. 33, no. 9, pp. 1463-70, 2001.

[32] V. A. Convertino, D. J. Goldwater, and H. Sandler, "$\dot{V}O_2$ kinetics of constant-load exercise following bed-rest-induced deconditioning," *J Appl Physiol Respir Environ Exerc Physiol,* vol. 57, no. 5, pp. 1545-1550, 1984.

[33] A. Krogh and J. Lindhard, "The regulation of respiration and circulation during the initial stages of muscular work," *J Physiol,* vol. 47, no. 1-2, pp. 112-36, 1913.

[34] V. A. Hill, C. N. H. Long, and H. Lupton, "Muscular exercise, lactic acid and the supply and utilisation of oxygen.— Parts VII–VIII," in *Proceedings of the Royal Society of London. Series B, Containing Papers of a Biological Character*, 1924, vol. 97, no. 682: Royal Society, pp. 155-176.

[35] P.-O. Åstrand and B. Saltin, "Oxygen uptake during the first minutes of heavy muscular exercise," *J Appl Physiol,* vol. 16, no. 6, pp. 971-976, 1961.

[36] G. A. Gaesser and D. C. Poole, "The Slow Component of Oxygen Uptake Kinetics in Humans," *Exerc Sport Sci Rev,* vol. 24, no. 1, pp. 35-71, 1996.

[37] E. Tam et al., "Effect of Endurance and Strength Training on the Slow Component of O2 Kinetics in Elderly Humans," *Front Physiol,* vol. 9, no. 1353, 2018.

[38] F. Borrani, G. Candau, G. Y. Millet, S. Perrey, J. Fuchslocher, and J. D. Rouillon, "Is the $\dot{V}O_2$ slow component dependent on progressive recruitment of fast-twitch fibers in trained runners?," *J Appl Physiol,* vol. 90, pp. 2212-2220, 2001.

[39] T. J. Barstow, A. M. Jones, P. H. Nguyen, and R. Casaburi, "Influence of muscle fiber type and pedal frequency on oxygen uptake kinetics of heavy exercise," *J Appl Physiol,* vol. 81, no. 4, pp. 1642-1650, 1996.

[40] M. Burnley, J. H. Doust, and A. M. Jones, "Effects of prior heavy exercise, prior sprint exercise and passive warming on oxygen uptake kinetics during heavy exercise in humans," *Eur J Appl Physiol,* vol. 87, no. 4, pp. 424-432, 2002.

[41] C. J. Womack, S. E. Davis, J. L. Blumer, E. Barrett, A. L. Weltman, and G. A. Gaesser, "Slow component of O2 uptake during heavy exercise: adaptation to endurance training," *J Appl Physiol (1985),* vol. 79, no. 3, pp. 838-45, 1995.

[42] J. S. M. Pringle, J. H. Doust, H. Carter, K. Tolfrey, and A. M. Jones, "Effect of pedal rate on primary and slow-component oxygen uptake responses during heavy-cycle exercise," *J Appl Physiol,* vol. 94, pp. 1501–1507, 2003.

[43] D. C. Poole et al., "Contribution of excising legs to the slow component of oxygen uptake kinetics in humans," *J Appl Physiol,* vol. 71, no. 4, pp. 1245-1260, 1991.

[44] S. Perrey, "Comments on point: counterpoint: the kinetics of oxygen uptake during muscular exercise do/do not manifest time-delayed phases. Profiles of the muscle fiber recruitment and the time-delayed slow phase," *J Appl Physiol (1985),* vol. 107, no. 5, p. 1669, 2009.

[45] J. R. Stirling and M. Zakynthinaki, "Counterpoint: The kinetics of oxygen uptake during muscular exercise do not manifest time-delayed phases," *J Appl Physiol,* vol. 107, no. 5, pp. 1665-1667, 2009.

[46] A. R. Hoogeveen and H. A. Keizer, "The $\dot{V}O_2$ overshoot at the onset of constant-load exercise in elite cyclists: An undescribed phenomenon," *J Exerc Physiol Online,* vol. 6, no. 4, pp. 34-41, 2003.

[47] A. E. Kilding and A. M. Jones, "$\dot{V}O_2$ 'overshoot' during moderate-intensity exercise in endurance-trained athletes: The influence of exercise modality," *Respir Physiol Neurobiol,* vol. 160, no. 2, pp. 139-146, 2008.

[48] K. Koppo, B. J. Whipp, A. M. Jones, D. Aeyels, and J. Bouckaert, "Overshoot in $\dot{V}O_2$ following the onset of moderate-intensity cycle exercise in trained cyclists," *Eur J Appl Physiol,* vol. 93, no. 3, pp. 366-73, 2004.

[49] L. A. P. de Lima, "O overshoot na cinética do consumo de oxigênio," Baccalaureate, Sports Center, Federal University of Santa Catarina, Florianópolis, Brasil, 2013.

[50] A. E. Kilding, N. V. Challis, E. M. Winter, and M. Fysh, "Characterisation, asymmetry and reproducibility of on- and off-transient pulmonary oxygen uptake kinetics in endurance-trained runners," *Eur J Appl Physiol,* vol. 93, no. 5-6, pp. 588-597, 2005.

[51] J. Dale and M. Glaister, "Moderate-Intensity Oxygen Uptake Kinetics: Is a Mono-Exponential Function Always Appropriate to Model the Response?," *Res Q Exercise Sport,* vol. 89, no. 3, pp. 309-321, 2018.

[52] D. C. Poole and A. M. Jones, "Oxygen Uptake Kinetics," *Compr Physiology,* vol. 2, no. 2, pp. 933-996, 2012.

[53] J. A. Zoladz, L. B. Gladden, M. C. Hogan, Z. Nieckarz, and B. Grassi, "Progressive recruitment of muscle fibers is not necessary for the slow component of $\dot{V}O_2$ kinetics," *J Appl Physiol,* vol. 105, pp. 575-580, 2008.

[54] J. A. Zoladz, A. C. Rademaker, and A. J. Sargeant, "Non-linear relationship between O_2 uptake and power output at high intensities of exercise in humans," *J Physiol,* vol. 488, no. Pt 1, pp. 211-217, 1995.

[55] K. Ogata, "Transient and Steady-State Response Analyses," in *Modern Control Engineering,* K. Ogata, Ed., Fourth ed., Upper Saddle River, New Jersey: Prentice Hall, 2002, pp. 219-336.

[56] N. S. Nise, "Time Response," in *Control systems engineering*, N. S. Nise, Ed. Hoboken, New Jersey: J. Wiley & Sons, 2015, pp. 157-298.

[57] L. A. P. de Lima, M. Raison, S. Achiche, and R. D. de Lucas, "Second-order modeling for the pulmonary oxygen uptake on-kinetics: a comprehensive solution for overshooting and nonovershooting responses to exercise," *J Appl Physiol,* vol. 125, no. 4, pp. 1315-1328, 2018.

[58] J. B. West, "Ibn al-Nafis, the pulmonary circulation, and the Islamic Golden Age," *Journal Appl Physiol (1985),* vol. 105, no. 6, pp. 1877-1880, 2008.

[59] C. A. Singer, *Short History of Anatomy and Physiology from the Greeks to Harvey*. New York: Dover, 1957.

[60] A. Siddiquey, S. Husain, and S. Laila, "History of Anatomy," *Bangladesh Journal of Anatomy,* vol. 7, no. 1, pp. 1-3, 2009.

[61] N. Zuntz and C. Lehmann, "Remarks on the Chemistry of respiration in the Horse during Rest and Work," *The Journal of physiology,* vol. 11, no. 4-5, pp. 396-398, 1890.

[62] A. E. Fick, "Ueber die Messung dea Blutquantums in den Herzrentrike," in *Verhandlungen der Physikalisch-medizinische Gesellschaft zu Würzburg*, Würzburg, 1870: Verlag der Physik-med Gesellschaft [etc.]. p. XVI.

[63] C. G. Douglas, "A method for determining the total respiratory exchange in man," *Proceedings of the Physiological Society: March 18, 1911, J Physiol,* vol. 42 (suppl), pp. xvii-xviii, 1911.

[64] P. B. Raven, M. Kjaer, and Y. Hellsten, "Contributions from the Copenhagen Muscle Research Center," in *History of Exercise Physiology*, C. M. Tipton, Ed. Champaign, IL: Human Kinetics, 2014.

[65] W. J. O'Connor, *British physiologists 1885–1914: a biographical dictionary*, Manchester: Manchester University Press, 1991.

[66] A. V. Hill and H. Lupton, "Muscular Exercise, Lactic Acid, and the Supply and Utilization of Oxygen," *QJM-Int J Med,* vol. os-16, no. 62, pp. 135-171, 1923.

[67] H. Lupton and A. V. Hill, "An analysis of the effects of speed on the mechanical efficiency of human muscular movement," *J Physiol,* vol. 57, no. 6, pp. 337-353, 1923.

[68] H. B. Rossiter, F. A. Howe, and S. A. Ward, "Intramuscular phosphate and pulmonary $\dot{V}O_2$ kinetics during exercise: implications for control of skeletal muscle oxygen consumption," in *Oxygen uptake kinetics in sport, exercise and medicine,* vol. 1, A. M. Jones and D. C. Poole, Eds. New York, USA: Taylor & Francis, 2005, pp. 154-184.

[69] Y. Fukuba, J. M. Kowalchuk, and H. B. Rossiter, "Professor Brian J. Whipp: an obituary," *Eur J Appl Physiol,* vol. 113, no. 4, pp. 1099-1100, 2013/04/01 2013.

[70] P. Palange, R. Casaburi, and S. A. Ward, "Prof. Brian James Whipp, 1937–2011: a master in respiratory and exercise physiology," *Eur Respir J,* vol. 39, no. 1, p. 1, 2012.

[71] B. J. Whipp and K. Wasserman, "Oxygen uptake kinetics for various intensities of constant-load work," *J Appl Physiol,* vol. 33, no. 3, pp. 351-356, 1972.

[72] N. I. Volkov, V. N. Cheremisinov, and E. N. Ruzumovskii, "Oxygen exchange in man during muscular activity," presented at the Oxygen regime of the organism and its regulation (Symposyum, translated from Russian), Kiev, 1966.

[73] W. L. Beaver, K. Wasserman, and B. J. Whipp, "On-line computer analysis and breath-by-breath graphical display of exercise function tests," *J Appl Physiol,* vol. 34, no. 1, pp. 128-32, 1973.

[74] B. J. Whipp, S. A. Ward, N. Lamarra, J. A. Davis, and K. Wasserman, "Parameters of ventilatory and gas exchange dynamics during exercise," *J Appl Physiol,* vol. 52, no. 6, pp. 1506-1513, 1982.

[75] W. L. Beaver, N. Lamarra, and K. Wasserman, "Breath-by-breath measurement of true alveolar gas exchange," *J Appl Physiol Respir Environ Exerc Physiol,* vol. 51, no. 6, pp. 1662-75, 1981.

[76] J. Kelly et al., "Dietary nitrate supplementation: effects on plasma nitrite and pulmonary O_2 uptake dynamics during exercise in hypoxia and normoxia," *Am J Physiol Regul Integr Comp Physiol,* vol. 307, no. 7, pp. R920-R930, 2014.

[77] S. Ulrich, S. R. Schneider, and K. E. Bloch, "Effect of hypoxia and hyperoxia on exercise performance in healthy individuals and in patients with pulmonary hypertension: a systematic review," *J Appl Physiol,* vol. 123, no. 6, pp. 1657-1670, 2017.

[78] S. Perrey, C. Cleuziou, A. M. Lecoq, D. Courteix, and P. Obert, "Cardiorespiratory dynamics to hypoxia at the onset of cycling exercise in male endurance subjects.," *J Sports Med Phys Fitness,* vol. 45, no. 1, pp. 7-12, 2005.

[79] F. Lador et al., "Cardiac output, O_2 delivery and $\dot{V}O_2$ kinetics during step exercise in acute normobaric hypoxia," *Respir Physiol Neurobiol,* vol. 186, no. 2, pp. 206-213, 2013.

[80] H. C. Xing, J. E. Cochrane, Y. Yamamoto, and R. L. Hughson, "Frequency domain analysis of ventilation and gas exchange kinetics in hypoxic exercise," *J Appl Physiol,* vol. 71, no. 6, pp. 2394-2401, 1991.

[81] C. Bell, D. H. Paterson, J. M. Kowalchuk, and D. A. Cunningham, "Oxygen uptake kinetics of older humans are slowed with age but are unaffected by hyperoxia," *Exp Physiol,* vol. 84, no. 4, pp. 747-59, 1999.

[82] R. Casaburi, R. W. Stremel, B. J. Whipp, W. L. Beaver, and K. Wasserman, "Alteration by hyperoxia of ventilatory dynamics during sinusoidal work," *J Appl Physiol Respir Environ Exerc Physiol,* vol. 48, no. 6, pp. 1083-1091, 1980.

[83] H. B. Rossiter, S. A. Ward, J. M. Kowalchuk, F. A. Howe, J. R. Griffiths, and B. J. Whipp, "Effects of prior exercise on oxygen uptake and phosphocreatine kinetics during high-intensity knee-extension exercise in humans," *J Physiol,* vol. 537, no. 1, pp. 291-303, 2001.

[84] M. Burnley, J. H. Doust, and A. M. Jones, "Time required for the restoration of normal heavy exercise $\dot{V}o_2$ kinetics following prior heavy exercise," *J Appl Physiol,* vol. 101, no. 5, pp. 1320-1327, 2006.

[85] P. E. di Prampero, P. B. Mahler, D. Giezendanner, and P. Cerretelli, "Effects of priming exercise on $\dot{V}o_2$ kinetics and O_2 deficit at the onset of stepping and cycling," *J Appl Physiol,* vol. 66, no. 5, pp. 2023-2031, 1989.

[86] Y. Fukuoka et al., "Reduction of $\dot{V}O_2$ slow component by priming exercise: novel mechanistic insights from time-resolved near-infrared spectroscopy," *Physiol Rep,* vol. 3, no. 6, e12432, pp. 1-13, 2015.

[87] H. Carter, J. S. Pringle, L. Boobis, A. M. Jones, and J. H. Doust, "Muscle glycogen depletion alters oxygen uptake kinetics during heavy exercise," *Med Sci Sports Exerc,* vol. 36, no. 6, pp. 965-72, 2004.

[88] S. E. Bearden and R. J. Moffatt, "$\dot{V}O_2$ kinetics and the O_2 deficit in heavy exercise," *J Appl Physiol,* vol. 88, no. 4, pp. 1407–1412, 2000.

[89] E. J. Tisdell, "Evaluation of the relationship between venous function and post exercise oxygen consumption recovery kinetics," Master Master thesis, Department of Kinesiology, Louisiana State University and Agricultural and Mechanical College, Louisiana, United States of America, 2004.

[90] P. C. do Nascimento Salvador et al., "Are the oxygen uptake and heart rate off-kinetics influenced by the intensity of prior exercise?" *Respir Physiol Neurobiol,* vol. 230, pp. 60-67, 2016.

[91] T. J. Barstow and P. A. Molé, "Linear and nonlinear characteristics of oxygen uptake kinetics during heavy exercise," *J Appl Physiol,* vol. 71, no. 6, pp. 2099-2106, 1991.

[92] Y. Miyamoto, "Kinetics of respiratory and circulatory responses to step, impulse, sinusoidal and ramp forcings of exercise load in humans," *Front Med Biol Eng,* vol. 4, no. 1, pp. 3-18, 1992.

[93] A. M. Jones, J. S. M. Pringle, and H. Carter, "Influence of muscle fibre type and motor unit recruitment on $\dot{V}O_2$ kinetics," in *Oxygen uptake kinetics in sport, exercise and medicine*, vol. 1, A. M. Jones and D. C. Poole, Eds. New York, USA: Taylor & Francis, pp. 261-293, 2005.

[94] G. J. Stienen, J. L. Kiers, R. Bottinelli, and C. Reggiani, "Myofibrillar ATPase activity in skinned human skeletal muscle fibres: fibre type and temperature dependence," *J Physiol,* vol. 493, no. 2, pp. 299-307, 1996.

[95] W. T. Willis and M. R. Jackman, "Mitochondrial function during heavy exercise," *Med Sci Sports Exerc,* vol. 26, no. 11, pp. 1347-53, 1994.

[96] H. Carter, A. M. Jones, T. J. Barstow, M. Burnley, C. A. Williams, and J. H. Doust, "Oxygen uptake kinetics in treadmill running and cycle ergometry: a comparison," *J Appl Physiol,* vol. 89, no. 3, pp. 899-907, 2000.

[97] T. Migita and K. Hirakoba, "Effect of different pedal rates on oxygen uptake slow component during constant-load cycling exercise," *J Sports Med Phys Fitness,* vol. 46, no. 2, pp. 189-196, 2006.

[98] D. M. Hirai et al., "Effects of altering pedal frequency on the slow component of pulmonary $\dot{V}O_2$ kinetics and EMG activity," *Int J Sports Med,* vol. 31, no. 8, pp. 529-536, 2010.

[99] W. L. Roston, B. J. Whipp, J. A. Davis, D. A. Cunningham, R. M. Effros, and K. Wasserman, "Oxygen uptake kinetics and lactate concentration during exercise in humans," *Am Rev Respir Dis,* vol. 135, no. 5, pp. 1080-1084, 1987.

[100] G. Solberg, B. Robstad, O. H. Skjønsberg, and F. Borchsenius, "Respiratory gas exchange indices for estimating the anaerobic threshold," *Journal of Sports Science & Medicine,* vol. 4, no. 1, pp. 29-36, 2005.

[101] B. J. Whipp and H. B. Rossiter, "The kinetics of oxygen uptake: physiological inferences from the parameters," in *Oxygen uptake kinetics in sport, exercise and medicine*, vol. 1, A. M. Jones and D. C. Poole, Eds. New York, USA: Taylor & Francis, 2005, pp. 62-94.

[102] A. R. Hoogeveen and H. A. Keizer, "The $\dot{V}O_2$ overshoot at the onset of constant-load exercise in elite cyclists: an undescribed phenomenon," in *The lactate and ventilatory response to exercise in endurance athletes*. Netherlands: Thesis, Saint Joseph Hospital, Vcldhoven, 2001, pp. 63-72.

[103] W. W. Stringer, "Mechanisms of exercise limitation in HIV+ individuals," *Med Sci Sports Exerc,* vol. 32, no. 7 Suppl, pp. S412-S421, 2000.

[104] A. Rocha et al., "Exercise intolerance in comorbid COPD and heart failure: the role of impaired aerobic function," *Eur Respir J,* vol. 53, no. 4, p. 1802386, 2019.

[105] F. Baty, A. J. R. van Gestel, L. Kern, and M. H. Brutsche, "Oxygen uptake recovery kinetics after the 6-minute walk test in patients with chronic obstructive pulmonary disease," *Respiration,* vol. 92, no. 6, pp. 371-379, 2016.

[106] P. Pornsuriyasak, M. Rambod, R. M. Effros, R. Casaburi, and J. Porszasz, "Oxygen uptake and lactate kinetics in patients with chronic obstructive pulmonary disease during heavy intensity exercise: role of pedaling cadence," *COPD,* vol. 15, no. 3, pp. 283-293, 2018.

[107] A. Wolpat et al., "Association between inspiratory muscle weakness and slowed oxygen uptake kinetics in patients with chronic obstructive pulmonary disease," *Appl Physiol Nutr Metab,* vol. 42, no. 12, pp. 1239-1246, 2017.

[108] C. Kiely, J. Rocha, E. O'Connor, D. O'Shea, S. Green, and M. Egaña, "Influence of menopause and Type 2 diabetes on pulmonary oxygen uptake kinetics and peak exercise performance during cycling," *Am J Physiol Regul Integr Comp Physiol,* vol. 309, no. 8, pp. R875-R883, 2015.

[109] M. Greutmann, D. Rozenberg, T. L. Le, C. K. Silversides, and J. T. Granton, "Recovery of respiratory gas exchange after exercise in adults with congenital heart disease," *Int J Cardiol,* vol. 176, no. 2, pp. 333-339, 2014.

[110] R. L. Hughson, D. L. Sherrill, and G. D. Swanson, "Kinetics of $\dot{V}O_2$ with impulse and step exercise in humans," *J Appl Physiol,* no. 64, pp. 451-459, 1988.

[111] A. M. Jones, I. T. Campbell, and J. S. M. Pringle, "Influence of muscle fibre type and pedal rate on the $\dot{V}O_2$-work rate slope during ramp exercise," *Eur J Appl Physiol,* vol. 91, no. 2-3, pp. 238-245, 2004.

[112] J. M. Zuniga et al., "Metabolic parameters for ramp versus step incremental cycle ergometer tests," *Appl Physiol Nutr Metab,* vol. 37, no. 6, pp. 1110-1117, 2012.

[113] Y. Miyamoto and K. Niizeki, "Dynamics of ventilation, circulation, ans gas-exchange to incremental and decremental ramp exercise," *J Appl Physiol,* vol. 72, no. 6, pp. 2244-2254, 1992.

[114] R. L. Hughson et al., "Time domain analysis of oxygen uptake during pseudorandom binary sequence exercise tests," *J Appl Physiol,* vol. 71, no. 4, pp. 1620-1626, 1991.

[115] R. L. Hughson, D. A. Winter, A. E. Patla, G. D. Swanson, and L. A. Cuervo, "Investigation of $\dot{V}o_2$ kinetics in humans with pseudorandom binary sequence work rate change," *J Appl Physiol,* vol. 68, no. 2, pp. 796-801, 1990.

[116] A. M. Edwards, D. B. Claxton, and M. L. Fysh, "A comparison of two time-domain analysis procedures in the determination of $\dot{V}O_2$ kinetics by pseudorandom binary sequence exercise testing," *Eur J Appl Physiol,* vol. 88, no. 4-5, pp. 411-416, 2003.

[117] D. A. Cunningham, J. E. Himann, D. H. Paterson, and J. R. Dickinson, "Gas exchange dynamics with sinusoidal work in young and elderly women," *Respir Physiol,* vol. 91, no. 1, pp. 43-56, 1993.

[118] R. Casaburi, B. J. Whipp, K. Wasserman, W. L. Beaver, and S. N. Koyal, "Ventilatory and gas exchange dynamics in response to sinusoidal work," *J Appl Physiol Respir Environ Exerc Physiol,* vol. 42, no. 2, pp. 300-1, 1977.

[119] R. L. Hughson, H. C. Xing, G. C. Butler, and D. R. Northey, "Effect of hypoxia on $\dot{V}O_2$ kinetics during pseudorandom binary sequence exercise," *Aviat Space Environ Med,* vol. 61, no. 3, pp. 236-9, 1990.

[120] Y. Miyamoto, Y. Nakazono, T. Hiura, and Y. Abe, "Cardiorespiratory dynamics during sinusoidal and impulse exercise in man," *Jpn J Physiol,* vol. 33, no. 6, pp. 971-986, 1983.

[121] D. P. Wilkerson, K. Koppo, T. J. Barstow, and A. M. Jones, "Effect of work rate on the functional 'gain' of Phase II pulmonary O_2 uptake response to exercise," *Respir Physiol Neurobiol,* vol. 142, no. 2, pp. 211-223, 2004.

[122] B. J. Behnke, T. J. Barstow, and D. C. Poole, "Relationship between $\dot{V}O_2$ responses at the mouth and across the exercising muscles," in *Oxygen uptake kinetics in sport, exercise and medicine,* vol. 1, A. M. Jones and D. C. Poole, Eds. New York, USA: Taylor & Francis, 2005, pp. 141-153.

[123] D. P. Wilkerson et al., "Older Type 2 diabetic males do not exhibit abnormal pulmonary oxygen uptake and muscle oxygen utilization dynamics during submaximal cycling exercise," *Am J Physiol Regul Integr Comp Physiol,* vol. 300, no. 3, pp. R685-R692, 2011.

[124] D. W. Hill, D. C. Poole, and J. C. Smith, "The relationship between power and time to achieve $\dot{V}O_{2max}$," *Med Sci Sports Exerc,* vol. 34, pp. 709-714, 2002.

[125] F. Caputo and B. S. Denadai, "The highest intensity and the shortest duration permitting attainment of maximal oxygen uptake during cycling: effects of different methods and aerobic fitness level," *Eur J Appl Physiol,* vol. 103, pp. 47-57, 2008.

[126] T. Moritani, A. Nagata, H. A. deVries, and M. Muro, "Critical power as a measure of physical work capacity and anaerobic threshold," *Ergonomics,* vol. 24, no. 5, pp. 339-50, 1981.

[127] E. Doebelin, *System Dynamics: Modeling, Analysis, Simulation, Design*. Taylor & Francis, 1998.

[128] J. Boone, "Response," *Medicine & Science in Sports & Exercise,* vol. 42, no. 7, p. 1428, 2010.

[129] J. K. Kalis, B. J. Freund, M. J. Joyner, S. M. Jilka, J. Nittolo, and J. H. Wilmore, "Effect of beta-blockade on the drift in O_2 consumption during prolonged exercise," *J Appl Physiol,* vol. 64, no. 2, pp. 753-758, 1988.

[130] M. T. Hamilton, J. Gonzalez-Alonso, S. J. Montain, and E. F. Coyle, "Fluid replacement and glucose infusion during exercise prevent cardiovascular drift," *J Appl Physiol (1985),* vol. 71, no. 3, pp. 871-7, 1991.

[131] B. W. Scheuermann, B. D. Hoelting, M. L. Noble, and T. J. Barstow, "The slow component of O_2 uptake is not accompanied by changes in muscle EMG during repeated bouts of heavy exercise in humans," *J Physiol,* vol. 531, no. Pt 1, pp. 245-56, 2001.

[132] K. Sahlin, J. B. Sorensen, L. B. Gladden, H. B. Rossiter, and P. K. Pedersen, "Prior heavy exercise eliminates $\dot{V}O_2$ slow component and reduces efficiency during submaximal exercise in humans," *J Physiol,* vol. 564, no. 3, pp. 765-73, 2005.

[133] D. P. Wilkerson and A. M. Jones, "Effects of baseline metabolic rate on pulmonary O_2 uptake on-kinetics during heavy-intensity exercise in humans," *Respir Physiol Neurobiol,* vol. 156, no. 2, pp. 203-211, 2007.

[134] J. R. Stirling and M. Zakynthinaki, "Last word on point/counterpoint: the kinetics of oxygen uptake during muscular exercise do/do not manifest time-delayed phases," *J Appl Physiol,* vol. 107, no. 5, pp. 1676-1676, 2009.

[135] V. L. Billat, H. Petot, G. Sarre, and L. Hamard, "Comments on point/counterpoint: the kinetics of oxygen uptake during muscular exercise do/do not manifest time-delayed phases. The real appropriate model is the one for $\dot{V}o_2$ (T) variation and not for $\dot{V}o_2$ (T)," *J Appl Physiol (1985),* vol. 107, no. 5, p. 1675, 2009.

[136] J. R. Stirling, M. S. Zakynthinaki, and B. Saltin, "A model of oxygen uptake kinetics in response to exercise: including a means of calculating oxygen demand/deficit/debt," *Bull Math Biol,* vol. 67, no. 5, pp. 989-1015, 2005.

[137] Lode, "Lode Excalibur Sport brochure," ed, [Online]. Available: www.lode.nl/en/product/excalibur-sport/3/id_segment/8#, dowloaded in 2/14/2019.

[138] Cosmed. [Online]. Available: www.cosmed.com/en/products/cardio-pulmonary-exercise-test, accessed in 2/15/2019.

[139] G. McFadyen, "Respiratory gas analysis," *Update in anaesthesia,* pp. 170-73, 2008.

[140] YSI. [Online]. Available: www.ysi.com, accessed in 2/16/2019.

[141] Polar. [Online]. Available: support.polar.com/ca-en/support/datalink, accessed in 2/15/2019.

[142] Sanny. [Online]. Available: www.sanny.com.br/avaliacao-fisica/estadiometros/estadiometro-profissional-sanny.html, accessed in 2/18/2019.

[143] Soehnle. [Online]. Available: [Online]. Available: www.soehnle.de/en/personal-scales, accessed in 2/18/2019.

[144] K. Wasserman, W. L. Beaver, and B. J. Whipp, "Mechanisms and patterns of blood lactate increase during exercise in man," *Med Sci Sports Exerc,* vol. 18, no. 3, pp. 344-52, 1986.

[145] Eppendorf. [Online]. Available: online-shop.eppendorf.ca/CA-en/Laboratory-Consumables-44512/Tubes-44515, accessed in 2/16/2019.

[146] A. R. Hoogeveen and G. Schep, "The plasma lactate response to exercise and endurance performance: relationships in elite triathletes," *Int J Sports Med,* vol. 18, no. 7, pp. 526 - 530, 1997.

[147] O. Wigertz, "Dynamics of ventilation and heart rate in response to sinusoidal work load in man," *J Appl Physiol,* vol. 29, no. 2, pp. 208-18, 1970.

[148] K. Ogata, "Frequency-Response Analysis," in *Modern Control Engineering*, K. Ogata, Ed. Fourth ed. Upper Saddle River, New Jersey: Prentice Hall, 2002, pp. 492-617.

[149] N. S. Nise, "Frequency response techniques," in *Control systems engineering*, N. S. Nise, Ed. Hoboken, New Jersey: J. Wiley & Sons, 2015, pp. 525-612.

[150] S. Ma, H. B. Rossiter, T. J. Barstow, R. Casaburi, and J. Porszasz, "Clarifying the equation for modeling of $\dot{V}O_2$ kinetics above the lactate threshold," *J Appl Physiol,* vol. 109, no. 4, pp. 1283-4, 2010.

[151] M. Burnley, A. M. Jones, H. Carter, and J. H. Doust, "Effects of prior heavy exercise on phase II pulmonary oxygen uptake kinetics during heavy exercise," *J Appl Physiol,* vol. 89, no. 4, pp. 1387-1396, 2000.

[152] A. Gerbino, S. A. Ward, and B. J. Whipp, "Effects of prior exercise on pulmonary gas-exchange kinetics during high-intensity exercise in humans," *J Appl Physiol,* vol. 80, no. 1, pp. 99-107, 1996.

[153] D. A. Keir, A. P. Benson, L. K. Love, T. C. Robertson, H. B. Rossiter, and J. M. Kowalchuk, "Influence of muscle metabolic heterogeneity in determining the $\dot{V}o_{2p}$ kinetic response to ramp-incremental exercise," *J Appl Physiol,* vol. 120, no. 5, pp. 503-513, 2016.

[154] B. Grassi, "Limitation of muscle $\dot{V}O_2$ by cellular respiration," in *Oxygen uptake kinetics in sport, exercise and medicine*, vol. 1, A. M. Jones and D. C. Poole, Eds. New York, USA: Taylor & Francis, 2005, pp. 212-229.

[155] B. Grassi, "Oxygen uptake kinetics: old and recent lessons from experiments on isolated muscle in situ," *Eur J Appl Physiol,* vol. 90, no. 3, pp. 242-249, 2003/10/01 2003.

[156] T. A. Bauer, J. E. B. Reusch, M. Levi, and J. G. Regensteiner, "Skeletal muscle deoxygenation after the onset of moderate exercise suggests slowed microvascular blood flow kinetics in Type 2 diabetes," *Diabetes Care,* vol. 30, no. 11, pp. 2880-2885, 2007.

[157] D. J. Padilla et al., "Effects of Type II diabetes on muscle microvascular oxygen pressures," *Respir Physiol Neurobiol,* vol. 156, no. 2, pp. 187-195, 2007.

[158] D. T. Cannon, A. C. White, M. F. Andriano, F. W. Kolkhorst, and H. B. Rossiter, "Skeletal muscle fatigue precedes the slow component of oxygen uptake kinetics during exercise in humans," *J Physiol,* vol. 589, no. 3, pp. 727-739, 2011.

[159] A. Vanhatalo, D. C. Poole, F. J. DiMenna, S. J. Bailey, and A. M. Jones, "Muscle fiber recruitment and the slow component of O2 uptake: constant work rate vs. all-out sprint exercise," *Am J Physiol Regul Integr Comp Physiol,* vol. 300, no. 3, pp. R700-R707, 2011.

[160] J. E. Cochrane and R. L. Hughson, "Evidence for a slow drift component in oxygen uptake ($\dot{V}O_2$) kinetics below the ventilatory threshold (VT)," *Med Sci Sports Exerc,* vol. 22, no. 2, p. S54, 1990.

[161] T. J. Barstow, N. Lamarra, and B. J. Whipp, "Modulation of muscle and pulmonary O2 uptakes by circulatory dynamics during exercise," *J Appl Physiol,* vol. 68, no. 3, pp. 979-989, 1990.

[162] B. Korzeniewski, "Regulation of oxidative phosphorylation is different in electrically- and cortically-stimulated skeletal muscle," *PloS one,* vol. 13, no. 4, e0195620, pp. 1-28, 2018.

[163] D. A. Keir, D. B. Copithorne, M. D. Hodgson, S. Pogliaghi, C. L. Rice, and J. M. Kowalchuk, "The slow component of pulmonary O_2 uptake accompanies peripheral muscle fatigue during high intensity exercise," *J Appl Physiol,* vol. 121, pp. 493–502, 2016.

[164] P. C. do Nascimento Salvador, K. M. d. Souza, R. D. De Lucas, L. G. A. Guglielmo, and B. S. Denadai, "The effects of priming exercise on the ṾO2 slow component and the time-course of muscle fatigue during very-heavy-intensity exercise in humans," *Appl Physiol Nutr Metab,* vol. 43, no. 9, pp. 909-919, 2018.

[165] R. L. Hughson, "Regulation of $\dot{V}O_2$ by O_2 delivery," in *Oxygen uptake kinetics in sport, exercise and medicine,* vol. 1, A. M. Jones and D. C. Poole, Eds. New York, USA: Taylor & Francis, 2005, pp. 185-211.

[166] A. J. Sargeant, "Human Power Output and Muscle Fatigue," *Int J Sports Med,* vol. 15, no. 3, pp. 116-121, 1994.

[167] K. M. d. Souza et al., "Agreement analysis between critical power and intensity corresponding to 50% in cycling exercise," *Rev Bras Cineantropom Desempenho Hum,* vol. 18, pp. 197-206, 2016.

[168] J. S. Pringle and A. M. Jones, "Maximal lactate steady state, critical power and EMG during cycling," *Eur J Appl Physiol,* vol. 88, no. 3, pp. 214-26, 2002.

[169] C. G. Smith and A. M. Jones, "The relationship between critical velocity, maximal lactate steady-state velocity and lactate turnpoint velocity in runners," *Eur J Appl Physiol,* vol. 85, no. 1-2, pp. 19-26, 2001.

[170] R. D. de Lucas, K. M. de Souza, V. P. Costa, T. Grossl, and L. G. A. Guglielmo, "Time to exhaustion at and above critical power in trained cyclists: The relationship between heavy and severe intensity domains," *Sci Sport,* vol. 28, no. 1, pp. e9-e14, 2013.

APPENDIX A ALTERNATIVE REPRESENTATION OF THE FOME MODEL'S FC

The concept of a three-phase $\dot{V}O_2$ response to the constant work rate transition (i.e., step on-transient) is found in literature under slightly different mathematical representations, even if the first-order exponential nature of their basic components remains untouched. The two most common variants of these representations are depicted by Figures 2.6 and A.1 (and, respectively, equations 2.3 and A.1).

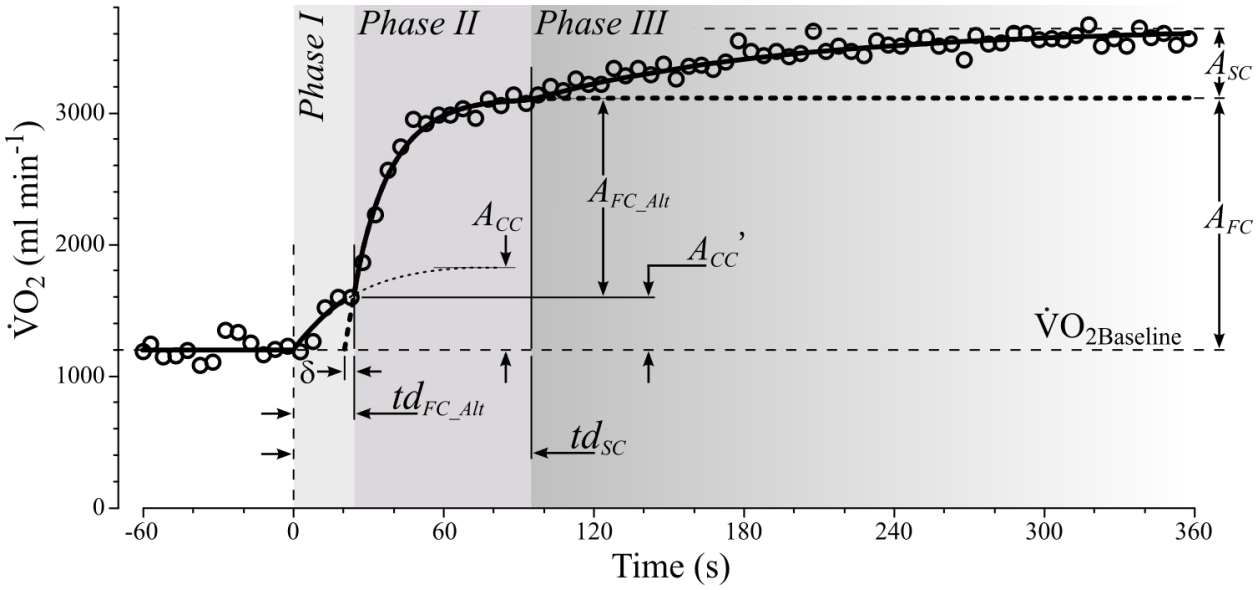

Figure A.1 Alternative representation of the FOME model's combined response to the exercise step on-transient.

$$\dot{V}O_2(t) = \dot{V}O_{2Baseline} + A_{CC}\left\{1-\exp\left[\frac{-t}{\tau_{CC}}\right]\right\}_{0 \le t < td_{FC\_Alt}} + \left\{A_{CC}'\right\}_{t \ge td_{FC\_Alt}} + A_{FC\_Alt}\left\{1-\exp\left[\frac{-(t-td_{FC\_Alt})}{\tau_{FC}}\right]\right\}_{t \ge td_{FC\_Alt}} + A_{SC}\left\{1-\exp\left[\frac{-(t-td_{SC})}{\tau_{SC}}\right]\right\}_{t \ge td_{SC} > td_{FC}} \quad , \quad (A.1)$$

In this alternative representation, noteworthy for its recurrence in the literature (e.g., [1, 4, 101, 131]), the term referred to as the "fundamental component" (FC)—here renamed as FC_Alt, for differentiation purposes—has an amplitude $A_{FC\_Alt} \neq A_{FC}$, and starts at an onset time delay $td_{FC\_Alt} \neq td_{FC}$ (see Figure A.1). Although this representation locates the transition from *phase I* to *phase*

II at the instant $t = td_{FC\_Alt}$, which is not essential for the evaluation of the model's parameters, it imposes an amplitude for the FC that does not assume the $\dot{V}O_{2Baseline}$ value as its lower limit. Moreover, instead of considering the CC inactive from $t = td_{FC\_Alt} + \delta$ on, when the FC starts to impose the shape of the combined response, this alternative representation truncates the CC at $t = td_{FC\_Alt}$ and considers its value constant at A_{CC}' from this instant until the end of the exercise (see equation A.1).

Finally, the "physiologically relevant increase in $\dot{V}O_2$" (A_{FC_Alt}'), as described by Scheuermann et al. [131], must be evaluated as the sum $A_{CC}' + A_{FC\_Alt}$ (Figure A.1) and, consequently, the gain of the *phase II* must be evaluated as $A_{FC\_Alt}'/\Delta WR$ [131], instead of $A_{FC}/\Delta WR$, like in the representation of Figure 2.6.

Nevertheless, despite conceptual or mathematical convenience differences, both representations present the same shape for the *phase II* of the response. As long as both the FC and FC_Alt mono-exponentials are estimated from the same data points, the estimate of τ will be the same (i.e., $\tau_{FC\_Alt} = \tau_{FC}$) in both curve representations. This is usually the case, since the data sets used in the *phase I* evaluation are obtained by excluding the first 20 s or so of the response, and by considering points until $t = td_{SC}$, when the SC is present, or until the end of the step, otherwise (e.g., the ascending part of Figure 2.5). Consequently, the FC is the same as the FC_Alt curve extrapolated backwards from $t = td_{FC\_Alt}$ until $t = td_{FC\_Alt} - \delta$ (Figure 2.6), and δ may be inferred from the parameters of FC and FC_Alt, as follows:

From Figure 2.6 and Figure A.1,

$$td_{FC\_Alt} = td_{FC} + \delta \tag{A.2}$$

$$A_{FC} = A_{FC\_Alt}' = A_{CC}' + A_{FC\_Alt} \tag{A.3}$$

For $td_{FC\_Alt} \leq t < td_{FC}$ (*phase II*), the $\dot{V}O_2(t)$ expressions on equations 2.3 and A.1 become respectively,

$$\dot{V}O_2(t) = \dot{V}O_{2Baseline} + A_{FC}\left\{1 - \exp\left[\frac{-(t - td_{FC})}{\tau_{FC}}\right]\right\} \tag{A.4}$$

and

$$\dot{V}O_2(t) = \dot{V}O_{2Baseline} + A_{CC}' + A_{FC\_Alt}\left\{1 - \exp\left[\frac{-(t - td_{FC\_Alt})}{\tau_{FC}}\right]\right\} \tag{A.5}$$

After applying A.2 to A.5, the equality A.4 = A.5 gives

$$A_{FC}\left\{1-\exp\left[\frac{-(t-td_{FC})}{\tau_{FC}}\right]\right\}=A_{CC}{}'+A_{FC\_Alt}\left\{1-\exp\left[\frac{-(t-td_{FC}-\delta)}{\tau_{FC}}\right]\right\} \tag{A.6}$$

Defining the ratio $K_{\_Alt}$ as

$$K_{\_Alt}=\frac{A_{FC\_Alt}}{A_{FC}}=\frac{A_{FC\_Alt}}{A_{FC\_Alt}}, \qquad , \tag{A.7}$$

and applying A.7 and A.3 to A.6, the value of the δ term is finally obtained:

$$A_{FC}\left\{1-\exp\left[\frac{-(t-td_{FC})}{\tau_{FC}}\right]\right\}=A_{FC}(1-K_{\_Alt})+K_{\_Alt}\ A_{FC}\left\{1-\exp\left[\frac{-(t-td_{FC}-\delta)}{\tau_{FC}}\right]\right\}$$

$$K_{\_Alt}=\exp\left(\frac{-\delta}{\tau_{FC}}\right) \tag{A.8}$$

$$\delta=-\tau_{FC}\cdot\ln K_{\_Alt}=-\tau_{FC}\cdot\ln\left(\frac{A_{FC\_Alt}}{A_{FC}}\right) \tag{A.9}$$

APPENDIX B MATHEMATICAL PROOF OF THE NEED FOR A LONGER SC'S DELAY IN THE FOS REPRESENTATION OF THE $\dot{V}O_2SA$

Equation B.1 presents the formulation for the generic combined response depicted in Figure 2.11.B, where the common onset time delay $td = td_{FC} = td_{SC}$ marks the simultaneous activation of both FC and SC:

$$\dot{V}O_2(t) = \dot{V}O_{2Baseline} + A_{FC}\left\{1 - \exp\left[\frac{-(t-td)}{\tau_{FC}}\right]\right\}_{t \geq td} + A_{SC}\left\{1 - \exp\left[\frac{-(t-td)}{\tau_{SC}}\right]\right\}_{t \geq td} \quad \text{(B.1)}$$

Thus, the expression for the slope of $\dot{V}O_2(t)$ at any instant t (Figure B.1) is given by:

$$\frac{\partial \dot{V}O_2(t)}{\partial t} = \ddot{V}O_2(t) = (1-td)\left\{\frac{A_{FC}}{\tau_{FC}}\exp\left[\frac{-(t-td)}{\tau_{FC}}\right] + \frac{A_{SC}}{\tau_{SC}}\exp\left[\frac{-(t-td)}{\tau_{SC}}\right]\right\}_{t \geq td} \quad \text{(B.2)}$$

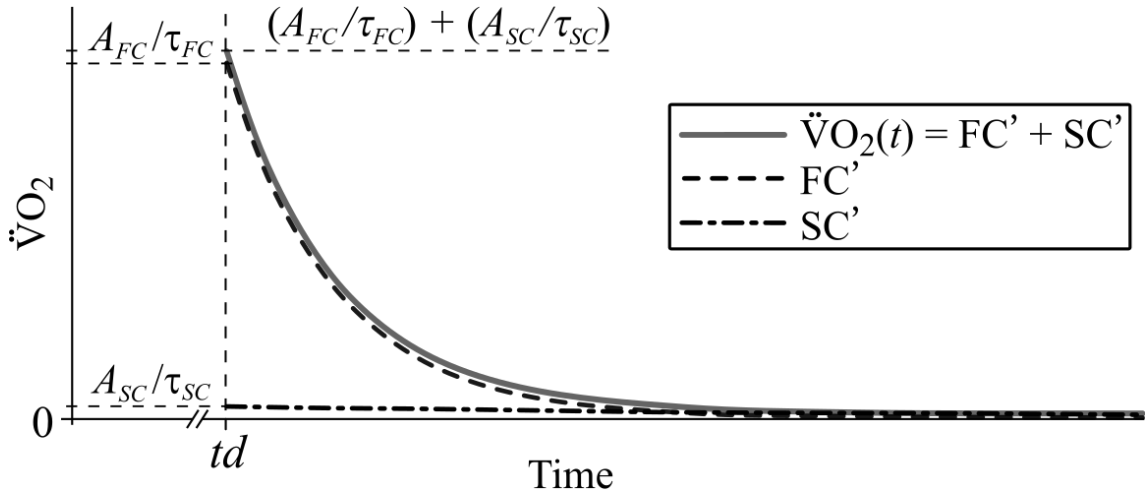

Figure B.1 Slope of the $\dot{V}O_2(t)$ curve formed by two first-order components starting at $t = td$.

The existence of a bump in the $\dot{V}O_2(t)$ combined response curve would represent an augmentation in the local slope of $\dot{V}O_2(t)$ at some time point, i.e., a disruption in the descending exponential pattern of any of the two terms FC' and SC' (Figure B.1) composing $\ddot{V}O_2(t)$. This would also mean that the derivative of $\ddot{V}O_2(t)$ with respect to time (equation B.3) would have to be positive at some given instant, which is not possible due to the negative sign multiplying the right term of expression B.3 below:

$$\frac{\partial \ddot{V}O_2(t)}{\partial t} = -(1-td)^2\left\{\frac{A_{FC}}{{\tau_{FC}}^2}\exp\left[\frac{-(t-td)}{\tau_{FC}}\right] + \frac{A_{SC}}{{\tau_{SC}}^2}\exp\left[\frac{-(t-td)}{\tau_{SC}}\right]\right\}_{t \geq td} \quad \text{(B.3)}$$

APPENDIX C EXAMPLE OF INDIVIDUAL REPORT FROM THE INCREMENTAL STEP TEST (ORIGINAL VERSION: PORTUGUESE)

UNIVERSIDADE FEDERAL DE SANTA CATARINA

CENTRO DE DESPORTOS

DEPARTAMENTO DE EDUCAÇÃO FÍSICA

RELATÓRIO RESUMIDO DE

AVALIAÇÃO AERÓBIA EM CICLISMO

Prof. Dr. Ricardo Dantas de Lucas

Coordenador de Avaliação Física

ricardo.dantas@ufsc.br

Luis Antonio Pereira de Lima

Doutorando

luisdelima.mail@gmail.com

LABORATÓRIO DE ESFORÇO FÍSICO

MARÇO / 2016

Atleta: [redacted]

Idade: [redacted] **anos** **Estatura:** [redacted] **cm**

Massa corporal: [redacted] **kg** **Modalidade:** [redacted]

Valores de potência (P), consumo de oxigênio ($\dot{V}O_2$) e frequência cardíaca (FC) estimados para os limiares de lactato e para o consumo máximo de oxigênio ($\dot{V}O_{2máx}$).

Resultados para o TESTE INCREMENTAL com início a 100 W e incrementos de 25 W a estágios de 3 minutos
1º LIMIAR DE LACTATO (Estimado em múltiplos inteiros de 25 W) **P = 175 W (≈ 53% $P_{máx}$)** $\dot{V}O_2$ = 35,5 ml·kg^{-1}·min^{-1} (≈ 58% $\dot{V}O_{2máx}$) **FC ≈ 124 bpm* (≈ 77% $FC_{máx}$)**
2º LIMIAR DE LACTATO **P = 251 W (≈ 77% Pmáx)** $\dot{V}O_2$ = 44,2 ml·kg^{-1}·min^{-1} (≈ 73% $\dot{V}O_{2máx}$) **FC ≈ 136 bpm (≈ 84% $FC_{máx}$)**
$\dot{V}O_{2máx}$ (CONSUMO MÁXIMO DE OXIGÊNIO) **P = 325 W (4,7 W·kg^{-1}) (≈ 99% Pmáx)** **$\dot{V}O_{2max}$ = 61,0 ml·kg^{-1}·min^{-1}** **FC ≈ 158 bpm (≈ 98% $FC_{máx}$)**
$P_{máx}$ (P máxima, proporcional ao tempo no estágio final) = 328 W (4,7 W·kg^{-1}) **$FC_{máx}$ = FC máxima atingida durante o teste = 162 bpm** ***bpm = batimentos por minuto**

Equipamentos utilizados:

Analizador de Gases Cosmed® Quark PFT
Lactímetro YSI® 2700 Select
Cicloergômetro Lode® Excalibur

$\dot{V}O_2$ e FC durante o teste incremental (Dados brutos)

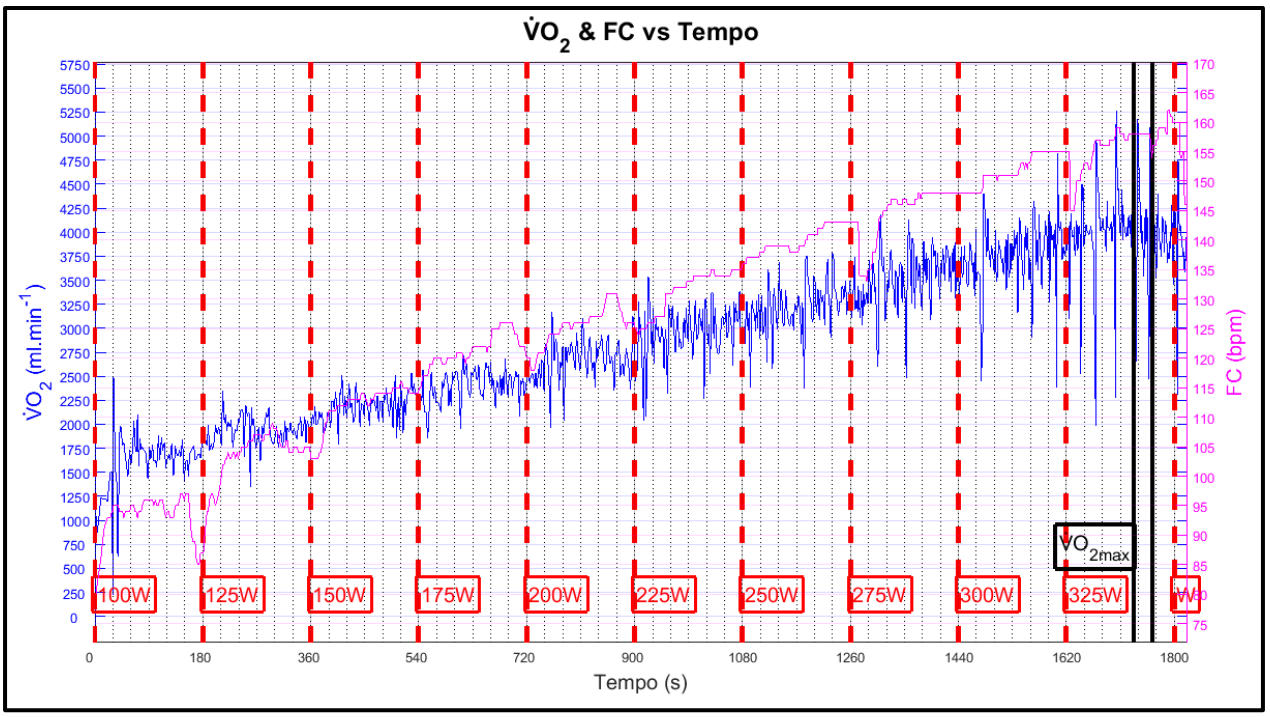

Concentração do lactato sanguíneo ([Lac]) durante o teste incremental

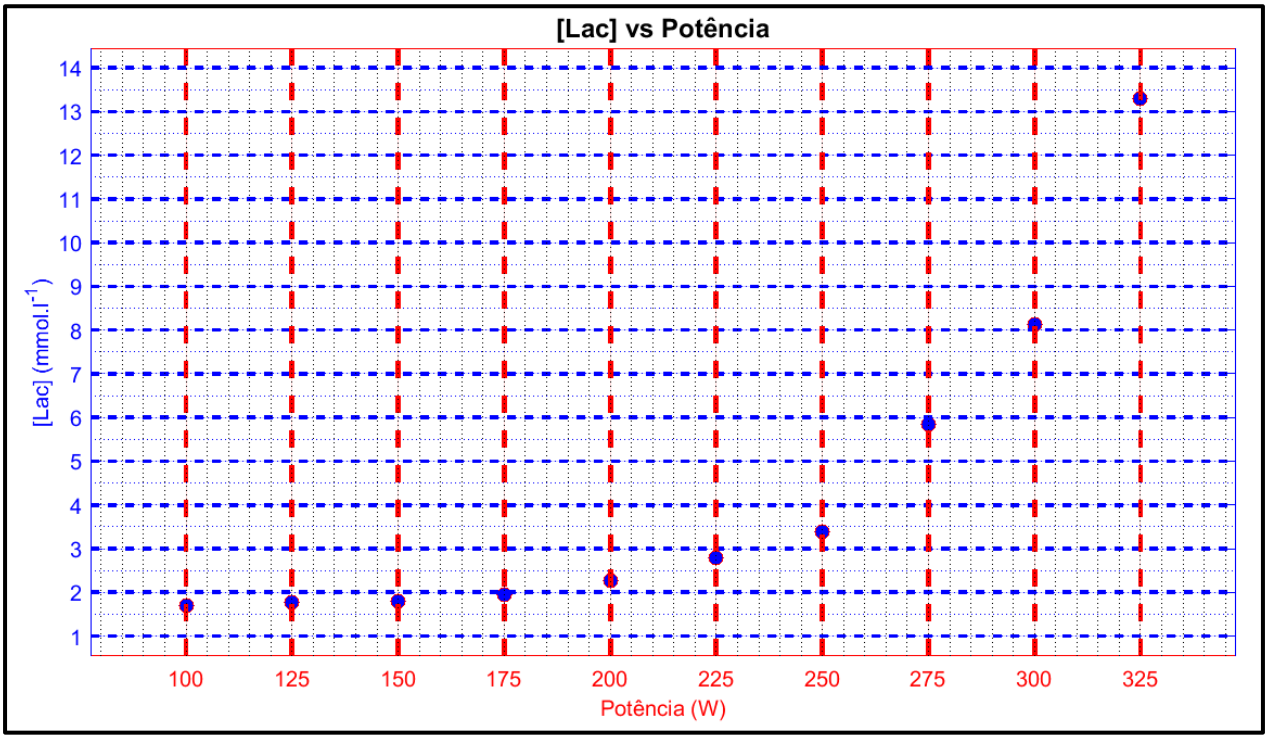

APPENDIX D EXAMPLE OF INDIVIDUAL REPORT FROM THE INCREMENTAL STEP TEST (TRANSLATED VERSION: ENGLISH)

FERERAL UNIVERSITY OFSANTA CATARINA

SPORTS CENTRE

PHYSICAL EDUCATION DEPARTMENT

SUMMARY REPORT OF AEROBIC EVALUATION IN CYCLING

Prof. Dr. Ricardo Dantas de Lucas

Physical Evaluation Coordinator

ricardo.dantas@ufsc.br

Luis Antonio Pereira de Lima

Doctorate student

luisdelima.mail@gmail.com

LABORATÓRIO DE ESFORÇO FÍSICO

MARCH / 2016

Athlete: [redacted]

Age: [redacted] **years** **Stature:** [redacted] **cm**

Body mass: [redacted] **kg** **Modality:** [redacted]

Values of power output (P), oxygen uptake ($\dot{V}O_2$) and heart rate (FC) estimated for the lactate thresholds and for the maximal oxygen uptake ($\dot{V}O_{2max}$).

Results from the INCREMENTAL TEST initiating at 100 W with a 25-W increment every third minute
1st LACTATE THRESHOLD (Estimated in entire multiples of 25 W) **P = 175 W (≈ 53% P_{max})** $\dot{V}O_2$ = 35.5 ml·kg^{-1}·min^{-1} (≈ 58% $\dot{V}O_{2max}$) **HR ≈ 124 bpm* (≈ 77% $FC_{máx}$)**
2nd LACTATE THRESHOLD **P = 251 W (≈ 77% Pmax)** $\dot{V}O_2$ = 44.2 ml·kg^{-1}·min^{-1} (≈ 73% $\dot{V}O_{2max}$) **FC ≈ 136 bpm (≈ 84% FC_{max})**
$\dot{V}O_{2max}$ (MAXIMAL OXYGEN UPTAKE) **P = 325 W (4.7 W·kg^{-1}) (≈ 99% Pmax)** **$\dot{V}O_{2max}$ = 61.0 ml·kg^{-1}·min^{-1}** **FC ≈ 158 bpm (≈ 98% FC_{max})**
P_{max} (Maximal P, proportional to time spent at the final stage) = 328 W (4.7 W·kg^{-1}) **FC_{max} = Maximal FC attained during the test = 162 bpm** ***bpm = beats per minute**

Equipment used:

Gas Analyzer Cosmed® Quark PFT
Lactate analyzer YSI® 2700 Select
Cycle ergometer Lode® Excalibur

$\dot{V}O_2$ and HR during the incremental test (Raw data)

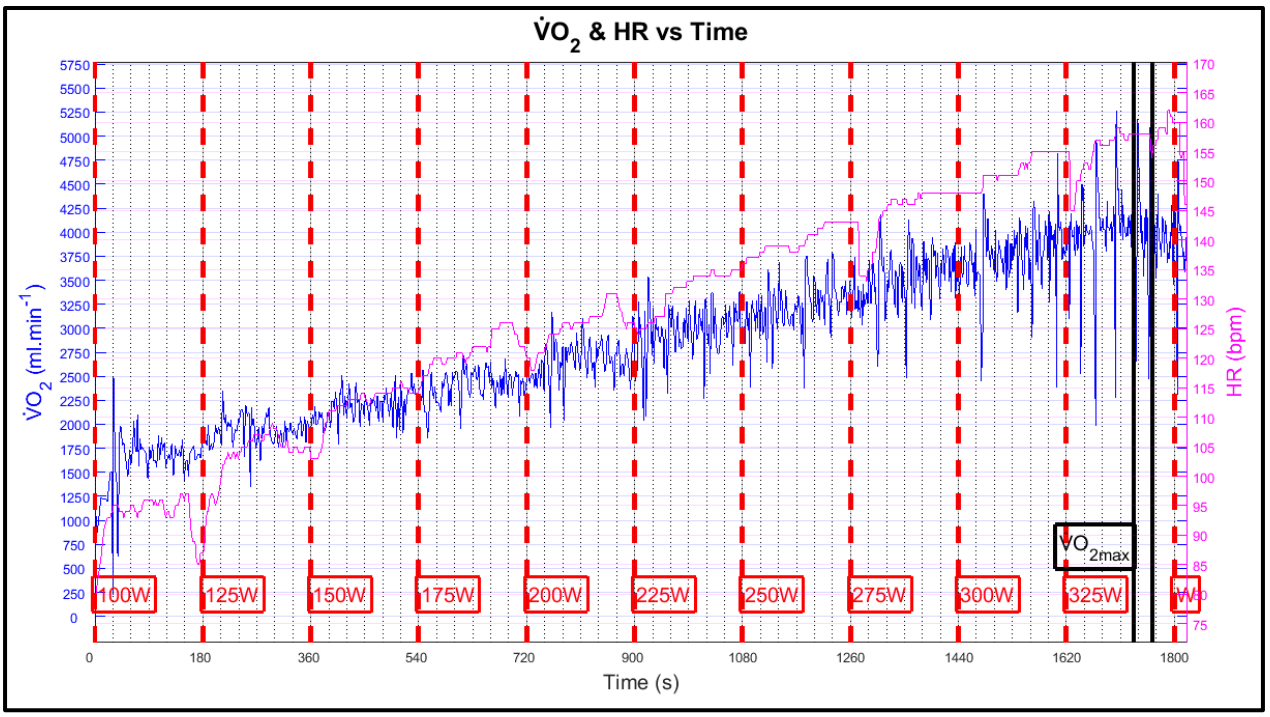

Blood lactate concentration ([Lac]) during the incremental test

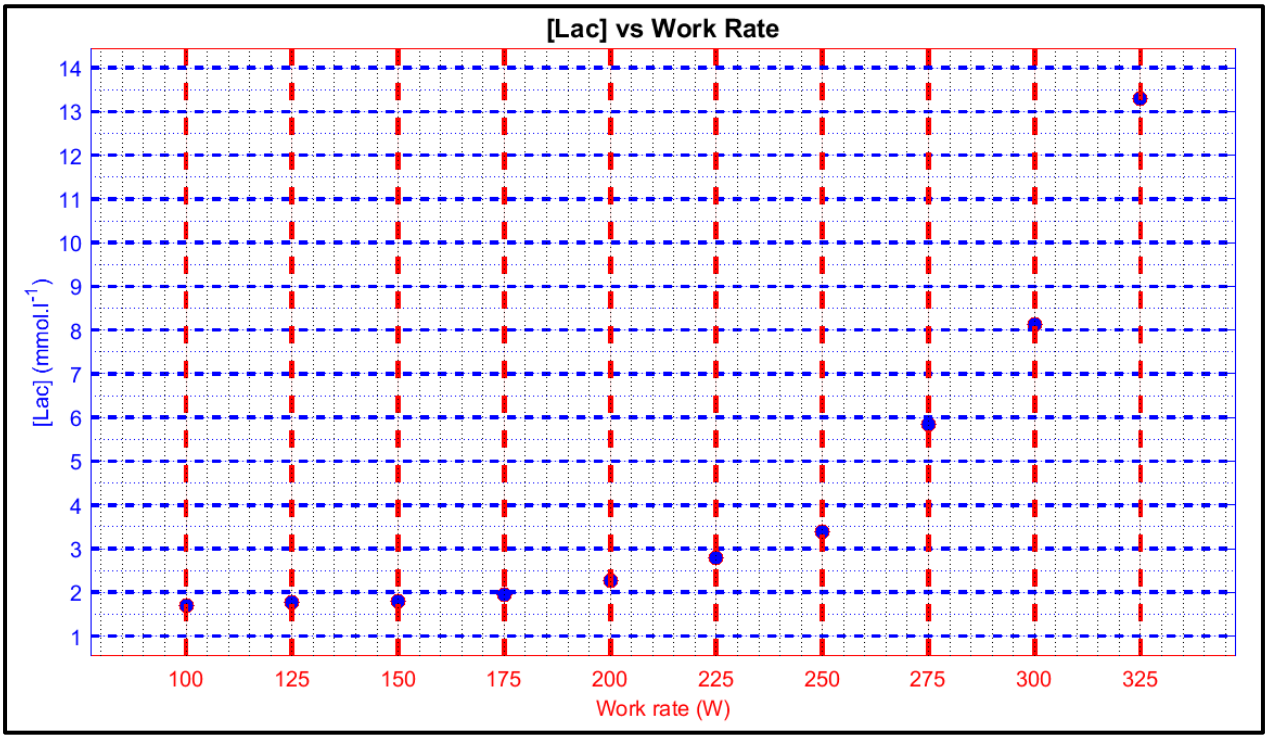

APPENDIX E APPENDIX FOR ARTICLE 1

To define an objective criterion for the classification of a given data set as either an O$\dot{V}O_2$K or a NO$\dot{V}O_2$K case, we analyzed the patterns followed by the whole sample's tp_{ref} and Mp_{ref} values. Additionally, the RMSE values obtained by the least squares regressions of data sets were used for performance comparison between the FC_{Ovsht} solution (equation 5.3; considered the only one suitable for overshooting cases), and both the FC_{FOS} and the FC_{NOvsht} formulas (respectively equations 5.2 and 5.5, the classic and the innovative solutions for NO$\dot{V}O_2$K cases). Table E.1 brings the Mp_{ref} and RMSE related results for all data sets (all subjects, at all WRs) organized in ascending order of their respective tp_{ref} values.

Data patterns on Table E.1 (visually represented by the plot on Figure E.1) suggest the adoption of a tp_{ref}-based criterion, according to which a threshold value for tp_{ref} ($tp_{ref}T$) may be used as a divisor between two groups of data, namely the O$\dot{V}O_2$K ($tp_{ref} \leq tp_{ref}T$) and the NO$\dot{V}O_2$K ($tp_{ref} > tp_{ref}T$) groups. When well defined by a proper $tp_{ref}T$, the O$\dot{V}O_2$K group should present smaller RMSE values for the FC_{Ovsht} than for the FC_{FOS} or the FC_{NOvsht} (thus, presenting positive RMSE differences; Figure E.1), with this pattern being inverted in the NO$\dot{V}O_2$K group.

On the basis of this premise, a reasonable reference for $tp_{ref}T$ may be set between the measured tp_{ref} values of 4.82 and 5.14 (Table E.1, first column). In fact, for observed tp_{ref} values greater than 4.82, the RMSE differences between FC_{NOvsht} and FC_{Ovsht} solutions become consistently smaller than 1 $ml \cdot min^{-1} \cdot kg^{-1}$, eventually assuming constantly negative values (Table E.1, seventh column; and Figure E.1, squares). In the case of the difference between FC_{FOS} and FC_{Ovsht}, a similar pattern is observed (Table E.1, sixth column; and Figure E.1, black triangles), with the exception of a few outlying points.

A congruent condition is observed for Mp_{ref} (Table E.1, second column; Figure E.1, hollow triangles), which represents the O$\dot{V}O_2$K's magnitude. At $tp_{ref} = 5.14$, it becomes consistently small, remaining under 0.001 (i.e., less than 0.1% of A_{ref}) for all subsequent tp_{ref} values.

Additionally, the suggested $tp_{ref}T$ value around five is supported by the distribution of tp_{ref} values themselves throughout the whole sample. Whereas the 39 tp_{ref} values below 5.14 ($3.63 \leq tp_{ref} \leq 4.82$ interval) on Figure E.1 are separated by minute line-to-line differences (mean ± SD = 0.03 ± 0.04; maximum of 0.14), the subsequent increments of the next 23 valid results demonstrate a 'rapid' line-to-line increase (mean ± SD = 12.09 ± 35.30; minimum of 0.32) towards an

unrealistically late instant of $O\dot{V}O_2K_{peak}$ occurrence.

Table E.1 RMSE (FC_{FOS}, FC_{NOvsht} and FC_{Ovsht}), tp_{ref} and Mp_{ref} values from all subjects at all WRs

		RMSE				
tp_{ref}*	Mp_{ref}	FC_{FOS}	FC_{NOvsht}	FC_{Ovsht}	FC_{FOS} - FC_{Ovsht}	FC_{NOvsht} - FC_{Ovsht}
3.63	0.031	67.7	66.1	63.2	4.5	2.9
3.64	0.055	106.2	106.0	102.3	3.9	3.6
3.65	0.107	119.4	116.0	99.9	19.4	16.1
3.77	0.056	79.6	79.1	77.4	2.2	1.7
3.83	0.101	61.9	58.8	43.5	18.4	15.3
3.83	0.030	73.7	71.7	67.6	6.1	4.1
3.86	0.019	58.4	55.5	52.9	5.5	2.6
3.88	0.025	59.5	58.0	55.4	4.1	2.6
3.91	0.037	133.0	128.5	118.8	14.3	9.7
3.93	0.066	59.6	56.1	43.1	16.4	13.0
3.96	0.036	72.8	70.5	63.0	9.7	7.4
4.00	0.017	82.4	81.9	80.0	2.4	1.9
4.06	0.053	71.4	71.4	67.9	3.5	3.5
4.07	0.053	95.3	94.9	88.3	7.0	6.5
4.08	0.074	77.7	76.1	64.7	12.9	11.4
4.10	0.012	121.7	122.0	120.5	1.3	1.6
4.13	0.048	143.8	139.7	131.3	12.5	8.4
4.139	0.013	61.4	58.1	55.5	5.9	2.6
4.147	0.019	82.8	81.9	79.2	3.6	2.6
4.149	0.034	88.7	87.8	83.4	5.3	4.4
4.154	0.089	78.2	78.1	72.0	6.1	6.0
4.17	0.050	116.0	116.6	114.6	1.3	2.0
4.17	0.009	93.4	89.5	86.4	7.0	3.1
4.17	0.071	54.4	53.2	44.8	9.6	8.5
4.21	0.018	71.1	69.9	67.2	3.9	2.7
4.23	0.053	123.0	122.1	116.0	7.0	6.0
4.25	0.043	92.1	91.5	85.7	6.3	5.7
4.25	0.007	63.8	57.8	55.0	8.8	2.8
4.26	0.003	97.0	94.2	93.1	3.9	1.1
4.28	0.006	80.4	78.7	77.4	3.0	1.2
4.35	0.010	102.8	101.4	99.1	3.7	2.3
4.44	0.048	155.3	156.0	151.8	3.6	4.2
4.46	0.028	67.4	67.2	65.1	2.3	2.0
4.46	0.028	66.0	66.4	65.2	0.8	1.1
4.47	0.006	99.9	97.5	95.3	4.6	2.2

Continues on the next page

*Some values are represented with an additional digit for the purpose of clarity. RMSE, root mean squared error.

Table E.1 RMSE (FC_{FOS}, FC_{NOvsht} and FC_{Ovsht}), tp_{ref} and Mp_{ref} values from all subjects at all WRs (cont'd)

		RMSE				
tp_{ref}	Mp_{ref}	FC_{FOS}	FC_{NOvsht}	FC_{Ovsht}	FC_{FOS} - FC_{Ovsht}	FC_{NOvsht} - FC_{Ovsht}
4.47	0.003	102.1	91.5	87.1	15.1	4.5
4.58	0.068	155.9	156.5	153.5	2.4	3.0
4.68	0.008	122.4	123.5	122.9	-0.6	0.6
4.82	0.076	87.0	87.6	82.4	4.6	5.2
5.14	0.002	56.2	56.1	55.9	0.3	0.3
5.92	<0.001	79.6	79.0	78.7	0.8	0.2
7.83	<0.001	98.5	90.4	89.5	9.0	0.8
9.43	<0.001	47.4	45.0	44.9	2.5	0.1
22.61	<0.001	66.0	59.0	60.3	5.8	-1.2
31.79	<0.001	72.9	73.9	74.8	-1.9	-0.9
33.76	<0.001	46.5	46.9	47.4	-0.8	-0.5
38.34	<0.001	66.0	66.7	75.4	-9.4	-8.7
39.95	<0.001	69.1	64.9	65.7	3.4	-0.8
42.22	<0.001	71.7	72.3	76.6	-4.9	-4.2
44.39	<0.001	121.5	121.1	121.9	-0.4	-0.8
47.97	<0.001	81.8	82.8	84.0	-2.2	-1.2
50.80	<0.001	113.4	114.5	124.7	-11.3	-10.1
54.49	<0.001	146.7	146.8	147.3	-0.5	-0.5
56.02	<0.001	113.0	115.6	118.0	-5.0	-2.4
69.43	<0.001	82.0	83.7	90.6	-8.6	-6.9
75.24	<0.001	120.5	123.1	126.9	-6.3	-3.8
79.88	<0.001	79.3	80.4	94.2	-15.0	-13.8
95.89	<0.001	84.4	85.7	106.3	-21.9	-20.6
96.37	<0.001	112.8	111.6	114.6	-1.8	-3.0
102.49	<0.001	152.1	155.5	158.1	-6.1	-2.6
110.12	<0.001	89.3	88.8	91.0	-1.7	-2.2
282.86	<0.001	102.9	105.9	118.7	-15.8	-12.8
N-C	N-C	87.1	88.5	N-C	N-C	N-C
N-C	N-C	92.4	93.2	N-C	N-C	N-C
N-C	N-C	117.1	118.5	N-C	N-C	N-C
N-C	N-C	93.8	94.9	N-C	N-C	N-C
N-C	N-C	147.7	149.5	N-C	N-C	N-C
N-C	N-C	67.6	68.6	N-C	N-C	N-C
N-C	N-C	105.4	105.8	N-C	N-C	N-C
N-C	N-C	96.5	97.7	N-C	N-C	N-C

N-C: No convergent solution satisfying ζ's requirements ($\zeta \in \mathbb{R} \mid 0 \leq \zeta < 1$) was found. RMSE, root mean squared error.

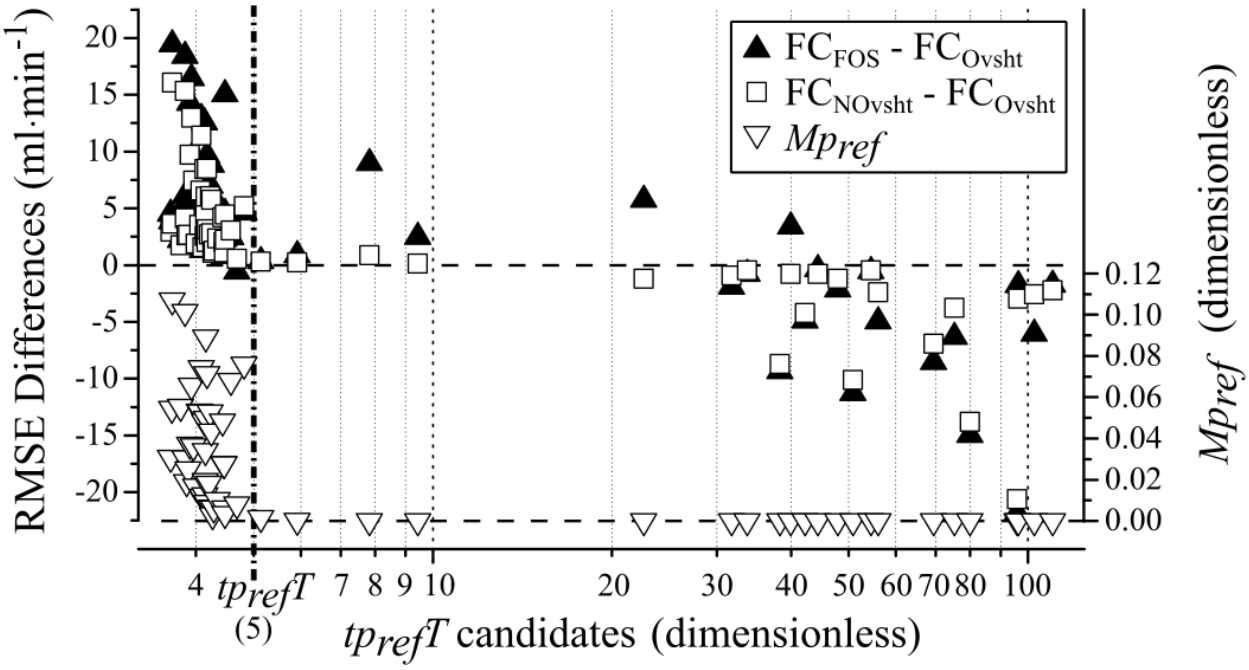

Figure E.1 *Left vertical axis:* values of root mean squared error (RMSE) differences between fittings from FC_{Ovsht}, and either FC_{FOS} or FC_{NOvsht} solutions (respectively FC_{FOS} - FC_{Ovsht} or FC_{NOvsht} - FC_{Ovsht}). Positive values denote a better fitting performance of the FC_{Ovsht} formula, and vice-versa; *Right vertical axis:* values of Mp_{ref}; *Horizontal axis:* values of candidates for tp_{ref} threshold ($tp_{ref}T$) in logarithmic scale for better visualization (highest value omitted; see tp_{ref} = 282.86 on Table E.1). Dot-dashed line indicates the suggested $tp_{ref}T$ = 5.

Furthermore, the combination of negligible Mp_{ref} values with clearly late tp_{ref} values obtained above the suggested $tp_{ref}T$ of nearly five denote the inability of the FC_{Ovsht} formula in fitting data where the $O\dot{V}O_2K$ phenomenon is likely absent. Eventually (at $tp_{ref} > 282.86$), the FC_{Ovsht} formula becomes so inappropriate that not even a convergent solution may be found.

Considering the information provided by the profiles of tp_{ref}, Mp_{ref}, and RMSE differences altogether, our analysis points towards a transition region (roughly situated around $tp_{ref}T$ candidate = 5) rather than to a sharp threshold value for tp_{ref}.

However, motivated by the need of a general yet objective criterion for the $O\dot{V}O_2K$ phenomenon's detection, we recommend the confirmation of an $O\dot{V}O_2K$ occurrence in $\dot{V}O_2$ responses to the step stimulus every time the FC_{Ovsht} solution finds a convergent solution with a real, nonnegative ζ smaller than one ($\zeta \in \mathbb{R} \mid 0 \leq \zeta < 1$), combined with a $tp_{ref} \leq 5$.

APPENDIX F COMPLETE VERSION OF COMPARATIVE TABLE 7.3

Table F.2 $\dot{V}O_2$ on-kinetics parameters from SOSC, MiME, and FOME models at all tested intensities (CONV+ and CONV groups)

Group	CONV+					CONV	
WR	55%LT	70%LT	85%LT	40%Δ	70%Δ	40%Δ	70%Δ
FOME							
td_{FC}, s	17.7 ± 2.8	18.6 ± 3.4	18.2 ± 3.2	16.0 ± 3.7	16.7 ± 2.7	16.8 ± 3.4	16.8 ± 2.8
τ_{FC}, s	16.6 ± 5.2	16.2 ± 4.6	17.6 ± 3.8	23.2 ± 7.2[ab]	23.3 ± 7.2[ab]	21.5 ± 6.5	23.0 ± 6.9
MiME							
td_{FC}, s	7.2 ± 4.9	8.7 ± 5.6	10.1 ± 5.9	11.7 ± 2.2	13.3 ± 6.0	12.5 ± 3.2	13.7 ± 4.5
ω, rad·s^{-1}	0.062 ± 0.010	0.068 ± 0.016	0.082 ± 0.034	0.144 ± 0.100	0.231 ± 0.224[ab]	0.173 ± 0.158	0.224 ± 0.187
ω_d, rad·s^{-1} [f]	0.047 ± 0.011 (6)	0.047 ± 0.011 (6)	0.042 ± 0.011 (5)	0.054 (1)	(0)	0.044 ± 0.014 (2)	(0)
ζ, (dimensionless)	0.71 ± 0.16	0.76 ± 0.12	0.92 ± 0.24	1.89 ± 1.42[b]	2.27 ± 1.44[abc]	1.99 ± 1.53	2.57 ± 1.95
FOME and MiME							
td_{SC}, s	—	—	—	210.0 ± 46.5	167.9 ± 35.5[e]	190.0 ± 51.4	171.9 ± 51.9[e]
τ_{SC}, s	—	—	—	176.4 ± 116.5	152.1 ± 103.1	143.8 ± 111.2	134.6 ± 84.1
A_{FC}, ml·min^{-1}	777 ± 176	1037 ± 267[a]	1342 ± 267[ab]	2189 ± 411[abc]	2458 ± 355[abcd]	2126 ± 372	2502 ± 362[e]
A_{SC}, ml·min^{-1}	—	—	—	174 ± 56	312 ± 115[e]	184 ± 53	323 ± 136[e]
A_{SC}%, % of A_{CR}	—	—	—	7.3 ± 1.4	11.1 ± 3.1[e]	8.0 ± 2.2	11.5 ± 4.7[e]
G_{FC}, ml·min^{-1}·W^{-1}	7.90 ± 0.66	8.26 ± 0.75	8.87 ± 0.55[a]	9.58 ± 1.72[ab]	9.09 ± 1.30[ab]	9.26 ± 1.75	9.46 ± 1.87[e]
G_{SC}, ml·min^{-1}·W^{-1}	—	—	—	0.77 ± 0.26	1.16 ± 0.47[e]	0.80 ± 0.23	1.20 ± 0.49[e]

Continues on the next page

Values are mean ± SD; CONV+ group: n = 7 for each tested WR, except where indicated between parenthesis; CONV group: n = 10 and 13, respectively for 40%Δ and 70%Δ, except where indicated between parenthesis; [a,b,c,d] Significantly different from 55%LT, 70%LT, 85%LT and 40%Δ, respectively, in the CONV+ group (Post hoc test); [e] Significantly different from 40%Δ (Paired tests), within either the SOSC+ or SOSC group; [f] Values between parenthesis indicate the quantity of CI_{Ovsht} cases, since the concept of ω_d do not apply to the *overdamped* solution, i.e., when CI is represented by CI_{NOvsht} (*Equation 5*).

Table F.3 $\dot{V}O_2$ on-kinetics parameters from SOSC, MiME, and FOME models at all tested intensities (CONV+ and CONV groups) (cont'd)

Group	CONV+					CONV	
WR	55%LT	70%LT	85%LT	40%Δ	70%Δ	40%Δ	70%Δ
SOSC							
td_S, s	5.7 ± 4.6	7.8 ± 5.7	9.2 ± 6.0	12.0 ± 2.5[a]	11.5 ± 5.4[a]	12.2 ± 3.7	11.5 ± 4.6
ω_S, rad·s^{-1}	0.057 ± 0.010	0.064 ± 0.017	0.075 ± 0.031	0.116 ± 0.079[ab]	0.099 ± 0.036[ab]	0.115 ± 0.075	0.094 ± 0.029
ζ_{CI} (dimensionless)	0.62 ± 0.12	0.67 ± 0.13	0.79 ± 0.22[a]	1.13 ± 0.40[ab]	1.02 ± 0.43[ab]	1.00 ± 0.39	0.98 ± 0.35
ω_{d_CI}, rad·s^{-1} [f]	0.044 ± 0.011	0.046 ± 0.012	0.045 ± 0.012 (6)	0.046 ± 0.011 (3)	0.049 ± 0.023 (5)	0.060 ± 0.030 (6)	0.050 ± 0.021 (9)
ζ_{CII} (dimensionless)	72.44 ± 88.68	32.12 ± 46.83	4.25 ± 3.17[ab]	11.70 ± 6.00[c]	9.78 ± 8.93	9.42 ± 6.15	8.10 ± 6.70
A_{CI}, ml·min^{-1}	745 ± 198	981 ± 295[a]	1245 ± 317[ab]	1927 ± 532[abc]	1921 ± 552[abc]	1767 ± 537	1999 ± 464
A_{CII}, ml·min^{-1}	32 ± 41	56 ± 62[a]	97 ± 93[ab]	436 ± 235[abc]	848 ± 342[abcd]	544 ± 278	826 ± 273[e]
A_{CII}%, % of A_{CR}	4.9 ± 7.5	6.2 ± 8.3[a]	8.0 ± 9.2[ab]	19.3 ± 12.9[abc]	31.4 ± 15.2[abcd]	24.6 ± 14.9	29.8 ± 12.0
G_{CI}, ml·min^{-1}·W^{-1}	7.54 ± 1.08	7.77 ± 1.18	8.19 ± 1.18	8.29 ± 1.71	7.12 ± 1.99[d]	7.80 ± 1.76	7.43 ± 1.54
G_{CII}, ml·min^{-1}·W^{-1}	0.36 ± 0.50	0.48 ± 0.60[a]	0.68 ± 0.75[ab]	1.90 ± 1.09[abc]	3.12 ± 1.23[abcd]	2.50 ± 1.47	3.09 ± 1.07
All models							
$\dot{V}o_{2Baseline}$, ml·min^{-1}	1108 ± 81	1110 ± 74	1098 ± 88	1133 ± 61	1145 ± 102	1157 ± 65	1169 ± 108
A_{CR}, ml·min^{-1}	777 ± 176	1037 ± 267[a]	1342 ± 267[ab]	2363 ± 454[abc]	2770 ± 423[abcd]	2311 ± 395	2825 ± 373[e]
G_{CR}, ml·min^{-1}·W^{-1}	7.90 ± 0.66	8.26 ± 0.75	8.87 ± 0.55[a]	10.19 ± 0.75[abc]	10.24 ± 0.94[abc]	10.30 ± 0.78	10.52 ± 0.87
WR, W	98 ± 16	124 ± 21[a]	151 ± 25[ab]	231 ± 35[abc]	271 ± 41[abcd]	224 ± 32	269 ± 34[e]

Values are mean ± SD; CONV+ group: n = 7 for each tested WR, except where indicated between parenthesis; CONV group: n = 10 and 13, respectively for 40%Δ and 70%Δ, except where indicated between parenthesis; [a,b,c,d] Significantly different from 55%LT, 70%LT, 85%LT and 40%Δ, respectively, in the CONV+ group (Post hoc test); [e] Significantly different from 40%Δ (Paired tests), within either the SOSC+ or SOSC group; [f] Values between parenthesis indicate the quantity of CI_{Ovsht} cases, since the concept of ω_d do not apply to the *overdamped* solution, i.e., when CI is represented by CI_{NOvsht} (Equation 7.5).